



Preparation of well-defined Ir(I)-NHC based catalytic material for the hydrogenation of functional olefins

Iuliia Romanenko

► To cite this version:

Iuliia Romanenko. Preparation of well-defined Ir(I)-NHC based catalytic material for the hydrogenation of functional olefins. Material chemistry. Université Claude Bernard - Lyon I, 2015. English. NNT : 2015LYO10262 . tel-01626512

HAL Id: tel-01626512

<https://theses.hal.science/tel-01626512>

Submitted on 30 Oct 2017

HAL is a multi-disciplinary open access archive for the deposit and dissemination of scientific research documents, whether they are published or not. The documents may come from teaching and research institutions in France or abroad, or from public or private research centers.

L'archive ouverte pluridisciplinaire **HAL**, est destinée au dépôt et à la diffusion de documents scientifiques de niveau recherche, publiés ou non, émanant des établissements d'enseignement et de recherche français ou étrangers, des laboratoires publics ou privés.

N° d'ordre

Année 2015

THESE DE L'UNIVERSITE DE LYON
Délivrée par
L'UNIVERSITE CLAUDE BERNARD LYON 1
ECOLE DOCTORALE

DIPLOME DE DOCTORAT

(arrêté du 7 août 2006)

soutenue publiquement le 30 Novembre 2015

par

Mlle Iuliia ROMANENKO

**Preparation of well-defined Ir(I)-NHC based catalytic material for the
hydrogenation of functional olefins**

Directeur de thèse : M. Emmanuel Lacôte

Co-Directeur de thèse : Mme. Chloé Thieuleux

Jury:

M. Laurent Lefort	Rapporteur
M. Matthieu Sollogoub	Rapporteur
M. Eric Besson	Membre du jury
M. Stéphane Daniele	Membre du jury
Mme. Chloé Thieuleux	Membre du jury
M. Emmanuel Lacôte	Membre du jury

UNIVERSITE CLAUDE BERNARD - LYON 1

Président de l'Université

M. François-Noël GILLY

Vice-président du Conseil d'Administration

M. le Professeur Hamda BEN HADID

Vice-président du Conseil des Etudes et de la Vie Universitaire

M. le Professeur Philippe LALLE

Vice-président du Conseil Scientifique

M. le Professeur Germain GILLET

Directeur Général des Services

M. Alain HELLEU

COMPOSANTES SANTE

Faculté de Médecine Lyon Est – Claude Bernard

Directeur : M. le Professeur J. ETIENNE

Faculté de Médecine et de Maïeutique Lyon Sud – Charles Mérieux

Directeur : Mme la Professeure C. BURILLON

Faculté d'Odontologie

Directeur : M. le Professeur D. BOURGEOIS

Institut des Sciences Pharmaceutiques et Biologiques

Directeur : Mme la Professeure C. VINCIGUERRA

Institut des Sciences et Techniques de la Réadaptation

Directeur : M. le Professeur Y. MATILLON

Département de formation et Centre de Recherche en Biologie Humaine

Directeur : Mme. la Professeure A-M. SCHOTT

COMPOSANTES ET DEPARTEMENTS DE SCIENCES ET TECHNOLOGIE

Faculté des Sciences et Technologies

Directeur : M. F. DE MARCHI

Département Biologie

Directeur : M. le Professeur F. FLEURY

Département Chimie Biochimie

Directeur : Mme Caroline FELIX

Département GEP

Directeur : M. Hassan HAMMOURI

Département Informatique

Directeur : M. le Professeur S. AKKOUCHE

Département Mathématiques

Directeur : M. le Professeur Georges TOMANOV

Département Mécanique

Directeur : M. le Professeur H. BEN HADID

Département Physique

Directeur : M. Jean-Claude PLENET

UFR Sciences et Techniques des Activités Physiques et Sportives

Directeur : M. Y. VANPOULLE

Observatoire des Sciences de l'Univers de Lyon

Directeur : M. B. GUIDERDONI

Polytech Lyon

Directeur : M. P. FOURNIER

Ecole Supérieure de Chimie Physique Electronique

Directeur : M. G. PIGNAULT

Institut Universitaire de Technologie de Lyon 1

Directeur : M. le Professeur C. VITON

Ecole Supérieure du Professorat et de l'Education

Directeur : M. le Professeur A. MOUGNIOTTE

Institut de Science Financière et d'Assurances

Directeur : M. N. LEBOISNE

Acknowledgement

This work was done in the laboratory of Organometallic Surface Chemistry (C2P2-LCOMS), one of the most well-equipped laboratories I had a chance to work at. For this outstanding opportunity I would like to thank my supervisors: Dr. Emmanuel Lacote and Dr. Chloé Thieuleux. I deeply appreciate your assistance, useful critiques and patient guiding. The combination of freedom and control together with scientific discussions I value the most in our work.

However this work would not be possible without support of many people. First of all I would like to express my deep gratitude to Dr. Reine Sayah for her advices, support and assistance in the laboratory. My special thanks go to Dr. Crisstoph Boisson for his idea to work with polyethylenes that finally led to the creation of a new project. I would also thank Dr. Jean Raynaud, Dr. Franck D'Agosto and Sebastien Norsic for scientific assistance in the polymer project.

The good quality research in chemistry is not possible without advanced characterization methods. For this reason I would like to thank Dr. Davide Gajan and our collaborators Prof. Lyndon Emsley and Dr. Anne Lesage from the NMR center for the possibility to investigate my materials. The advanced NMR experiments conducted by Dr. Gajan were crucial for understanding the catalytic behavior of material obtained. I would like also to show my greatest appreciation to Laurent Veyre for TEM and EDX measurements and to Dr. Erwann Jeanneau and Dr. Ruben Vera for XRD measurements. Your professionalism deserves a respect. For technical support I would like to thank Dr. Kai Szeto, Dr. Nicolas Merle, Dr. Nesrin Queslati, Cristine Lucas, Francois Bayard.

For the moral support and encouraging I would like to thank my colleagues Alina Moscu, Giulliana Rubulotta, Audrey Ledoux, Ewelina Bolimowska, Bishoy Marcos, Walid Darwich, David Baudouin, Thibault Alphazan and Henri van Kalker. I would like also to thank all LCOMS group members past and present for their help and friendship.

And finally I would like to thank my parents that always believed in me: nothing of this would be possible without you.

Table of content

General introduction	1
Chapter 1: Bibliography	5
Chapter 2: Synthesis and characterization of Ir(I)-NHC based hybrid material	43
Chapter 3: Catalytic performance of the Ir(I)-NHC based material and its homogeneous analogues. Application to alkene hydrogenation reactions.....	91
Chapter 4: Functionalized polyethylene as a new support for organometallic complexes.....	129
General conclusions and perspectives	177

List of Abbreviations

BET	Brunauer-Emmett-teller
CP	Cross-Polarization
COD	1,5-cyclooctadiene
Im	Imidazole
KHMDS	Potassium hexamethyldisilazide
MAS	Magic Angle Spinning
MCM	Mobil Catalytic Material
Mes	Mesityl
NHC	N-Heterocyclic Carbene
NMR	Nuclear Magnetic Resonance
P123	Pluronic 123
PE-I	Polyethylene iodide
ppm	Parts per million
SBA	Santa Barbara
TEOS	Tetra ethyl orthosilicate
TMSBr	Trimethylsilylbromide
TOF	Turnover Frequency
TON	Turnover Number
XRD	X-Ray Diffraction
PHOX	Phosphine-oxazoline
PE	Polyethylene
Cp*	Pentamethylcyclopentadienyl anion
RCM	Ring closing metathesis
BBN	9-Borabicyclo(3.3.1)nonane
CAAC	cyclic (alkyl)(amino)carbenes

Résumé

L'hydrogénation catalytique est l'une des réactions les plus importantes pour la production de produits de commodité ou de spécialité.¹ Parmi les catalyseurs de choix, de nombreux complexes de métaux de transition (groupe 8 à 10) ont été développés afin d'adresser des problèmes de sélectivités, d'activité voire d'énantiosélectivité. Cela est particulièrement vrai pour l'iridium, l'un des métaux les plus actifs pour les réactions d'hydrogénation catalytiques.² Cependant, en solution sous hydrogène, ces complexes ont tendance à former rapidement des clusters d'hydrures polymétalliques inactifs, par processus bimoléculaires.³

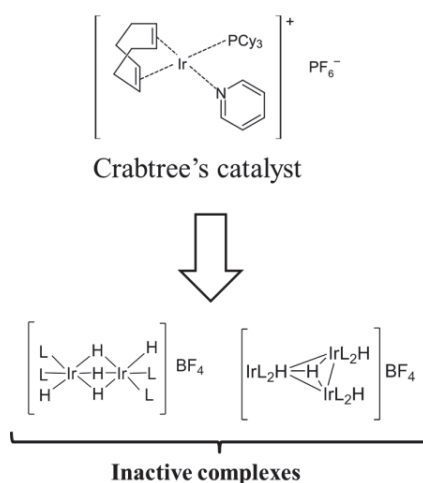


Figure 1.Degradation de catalyseur de Crabtree

Pour éviter ce mode de désactivation, nous avons choisi d'élaborer des catalyseurs contenant des complexes d'Ir isolés à la surface d'une charpente silicique mésostructurée. Le design du catalyseur a été réalisé en fonction des critères suivants :

- 1) un métal de transition connu pour être efficace en hydrogénation (Ir (I)) ;
- 2) un support solide pour isoler les sites Ir (I) et empêcher la formation de clusters ;
- 3) un ligand attaché de façon covalente au support d'oxyde et capable de coordonner fortement le

¹ a) The Handbook of Hydrogenation (Eds: J.G. de Vries, C.J. Elsevier), WILEY-VCH Verlag GmbH & Co, 2007. b) W. S. Knowles *Angew. Chem. Int. Ed.* 2002, 41(12), 1998-2007; c) W. Bonrath, J. Medlock, J. Shütz, B. Wüstenberg, T. Netscher in *Hydrogenation* (Eds.: I. Karame), InTech, 2012, pp. 69-90.

² a) Iridium complexes in organic synthesis (Eds: L. Oro, C. Claver), WILEY-VCH Verlag GmbH & Co, **2008**. b) *Iridium Catalysis, Topics in Organometallic Chemistry Vol. 34* (Ed.: P.G. Andersson), Springer-Verlag Berlin Heidelberg, **2011**, pp. 1-76; c) R. Crabtree, *Acc. Chem. Res.* **1979**, 12, 331-337

³ a) Y. Xu, M. A. Celik, A. L. Thompson, H. Cai, M. Yurtsever, B. Odell, J. C. Green, D. M. P. Mingos, J. M. Brown, *Angew. Chem. Int. Ed.* 2009, 48, 582-593; b) S. P. Smidt, A. Pfaltz, E. Martínez-Viviente, P. S. Pregosin, A. Albinati, *Organometallics* 2003, 22, 1000-1009; c) X. Cui, Y. Fan, M. B. Hall, K. Burgess, *Chem. Eur. J.* 2005, 11, 6859-6868; d) L. D. Vazquez-Serrano, B. T. Owens, J. M. Buriak, *Chem. Commun.* 2002, 2518-2519; e) J. Campos, L. S. Sharninghausen, R. H. Crabtree, D. Balcells, *Angew. Chem. Int. Ed.* 2014, 53, 12808-12811; f) *Homogeneous Catalysts: Activity – Stability – Deactivation, First Edition* (Eds: P.W.N.M. van Leeuwen, J.C. Chadwick), Wiley- VCH Verlag GmbH & Co, 2011

centre métallique (NHC) afin d'éviter des problèmes de lixiviation en procédé catalytique

- 4) un ligand labile permettant de libérer facilement des sites de coordination pour l'hydrogénation (COD dans notre cas) ;
- 5) un ligand X ou L permettant de compléter la sphère de coordination de l'Iridium
- 6) un espaceur flexible entre le support et le complexe actif, afin de permettre des interactions entre la surface d'oxyde et l'espèce métallique catalytiquement active (propyle dans notre cas).

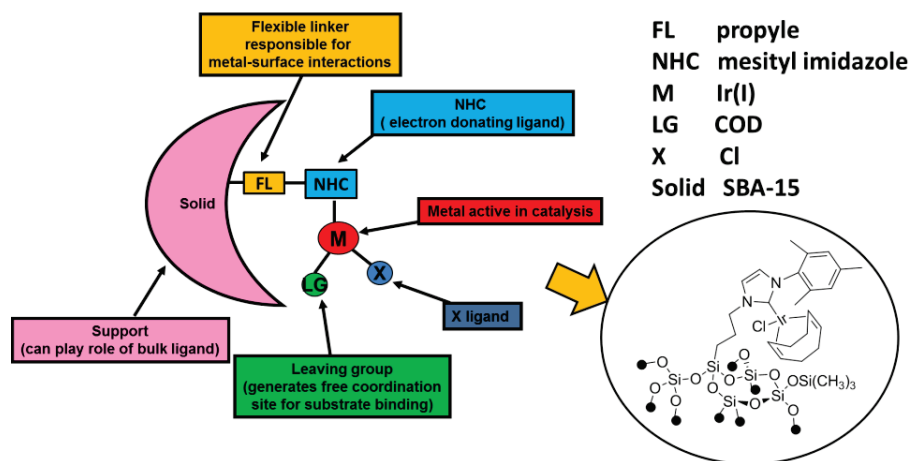


Figure 2. Stratégie employée pour le design de catalyseur.

Notre stratégie pour la préparation des matériaux catalytiques repose sur une approche en deux étapes.⁴ La première étape est la préparation de matrices hybrides de silice mésostructurées contenant des fonctionnalités organiques régulièrement espacés au moyen d'un procédé sol-gel utilisant un agent structurant de type tensioactif, puis transformation in-situ de ces fonctionnalités de surface en complexes d'Iridium supportés.^{5,6}

La préparation des matériaux catalytiques **M-Ir** a donc été réalisée à partir d'un matériau plateforme contenant des fonctionnalités iodopropyles. Ces fonctionnalités iodopropyles ont été transformées en groupements imidazoliums puis en complexes carbéniques N-hétérocycliques

⁴ a) M. P. Conley, C. Copéret, C. Thieuleux, ACS Catal. 2014, 4, 1458-1469; b) T. K. Maishal, J. Alauzun, J.-M. Basset, C. Copéret, R. J. P. Corriu, E. Jeanneau, A. Mehdi, C. Reyé, L. Veyre, C. Thieuleux, Angew. Chem. Int. Ed. 2008, 47, 8654-8656; c) M. P. Conley, R. M. Drost, M. Baffert, D. Gajan, C. Elsevier, W. T. Franks, H. Oschkinat, L. Veyre, A. Zagdoun, A. Rossini, M. Lelli, A. Lesage, G. Casano, O. Ouari, P. Tordo, L. Emsley, C. Copéret, C. Thieuleux, Chem. Eur. J. 2013, 19, 12234-12238; d) I. Karamé, M. Boualleg, J.-M. Camus, T. K. Maishal, J. Alauzun, J.-M. Basset, C. Copéret, R. J. P. Corriu, E. Jeanneau, A. Mehdi, C. Reyé, L. Veyre, C. Thieuleux, Chem. Eur. J. 2009, 15, 11820-11823; e) M. K. Samantaray, J. Alauzun, D. Gajan, S. Kavithake, A. Mehdi, L. Veyre, M. Lelli, A. Lesage, L. Emsley, C. Copéret, C. Thieuleux, J. Am. Chem. Soc. 2013, 135, 3193-3199.

⁵ a) S. L. Burkett, S. D. Sims, S. Mann, Chem. Commun. 1996, 1367-1368; b) D. J. Macquarrie, Chem. Commun. 1996, 1961-1962; c) D. Margolese, J. A. Melero, S. C. Christiansen, B. F. Chmelka, and G. D. Stucky, Chem. Mater. 2000, 12, 2448-2459; d) L. Mercier, T. J. Pinnavaia, Chem. Mater. 2000, 12, 188-196; For a review, see: e) F. Hoffmann, M. Cornelius, J. Morell, M. Fröba, Angew. Chem. Int. Ed. 2006, 45, 3216-3251.

⁶ C. Copéret, M. Chabanas, R. Petroff Saint-Arroman, J.-M. Basset, Angew. Chem. Int. Ed. 2003, 42, 156-181.

d'argent (I). Les complexes d'Iridium ont ensuite été formés par transmétallation en utilisant le précurseur $[\text{Ir}(\text{COD})\text{Cl}]_2$ (Schéma 1)

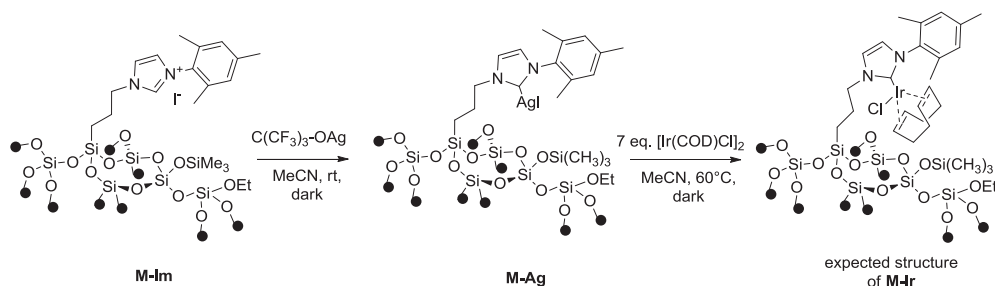


Schéma 1. Préparation du catalyseur hétérogène **M-Ir**

Ce matériau a été entièrement caractérisé par différentes techniques et notamment par des techniques de RMN sophistiquées telles que la RMN de l'état solide utilisant la polarisation nucléaire dynamique du ^{13}C et du ^{29}Si . L'analyse élémentaire de **M-Ir** indique qu'il contient 2,57% d'Iridium soit un rendement de transmétallation de 49%. L'ensemble des analyses réalisées indiquent qu'il n'y a pas de COD coordonné aux sites Ir de surface. La faible différence entre le déplacement chimique du carbène d'Argent de départ et celui du carbène d'Iridium permet difficilement de mettre en évidence la réussite du procédé de transmétallation par RMN ^{13}C de l'état solide. Seuls des spectres RMN-2D réalisés à haut champs ont permis de mettre en évidence deux taches de corrélation dans la zone de déplacement chimique des carbènes métalliques. L'absence de nanoparticules d'Iridium sur les images TEM suggère également que le processus de transmétallation a eu lieu et que l'iridium du matériau est lié au ligand NHC. Étonnamment, il a été constaté que seulement 8% des atomes d'Ir contenaient un ligand COD dans leur sphère de coordination ; celui-ci ayant été éliminé lors de l'étape de transmétallation. L'élimination de COD devrait conduire à des espèces d'Iridium en interaction avec la surface de silice. Ceci a pu être mis en évidence par spectroscopie RMN DNP 2D ^{29}Si - ^1H . Nous avons déjà émis l'hypothèse que ce genre d'interaction pouvait expliquer la stabilité de certains catalyseurs de métathèse d'oléfines à base de ruthénium mais nous n'avons pu acquérir de preuves spectroscopiques directes comme c'est le cas ici.

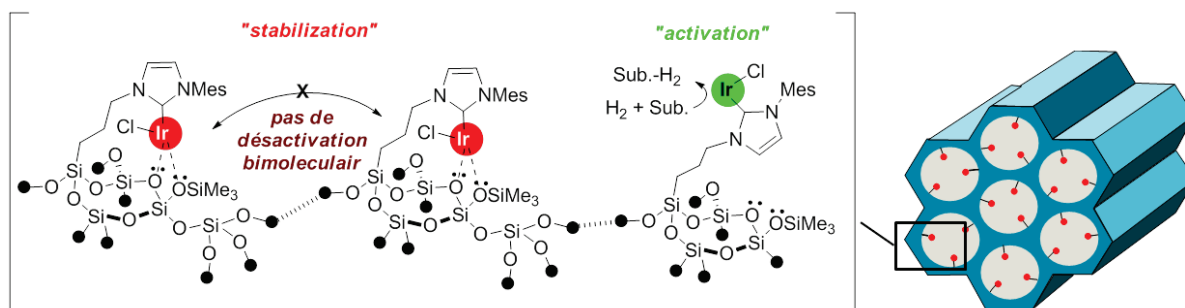


Figure 1. Structure définie de **M-Ir**

Les performances catalytiques de matériau **M-Ir** et de ses homologues moléculaires neutre $[\text{IrCl}(\text{COD})(\text{MesImPr})]$ et cationique $[\text{Ir}(\text{COD})(\text{MesImPr})]\text{BF}_4$ (en solution) ont été testés en réaction d'hydrogénation du trans-stilbène dans des conditions douces (0,1 mol% du catalyseur, 3 bars de H_2 , $T = 40^\circ\text{C}$). De manière surprenante, **M-Ir** a montré une activité 50 fois supérieure à celle du complexe neutre $[\text{IrCl}(\text{MesImPr})(\text{COD})]$ et 15-20 fois supérieure à celle du complexe cationique $[\text{Ir}(\text{MesImPr})(\text{COD})]\text{BF}_4$. Pour **M-Ir**, une conversion complète a été observée après 18 h de réaction. Le même test utilisant $[\text{IrCl}(\text{MesImPr})(\text{COD})]$ en solution montrent l'incapacité du catalyseur à atteindre une conversion complète, même après plus de 80 jours! L'espèce cationique $[\text{Ir}(\text{COD})(\text{MesImPr})]\text{BF}_4$ est quant à elle plus rapide mais la réaction n'est pas complète même après 60 jours. Le TOF calculé après 5h de réaction pour **M-Ir** est 38h^{-1} , tandis qu'il est d'environ $1,8\text{h}^{-1}$ et $0,75\text{h}^{-1}$ pour $[\text{IrCl}(\text{MesImPr})(\text{COD})]$ et $[\text{Ir}(\text{MesImPr})(\text{COD})]\text{BF}_4$ respectivement (Fig.3).

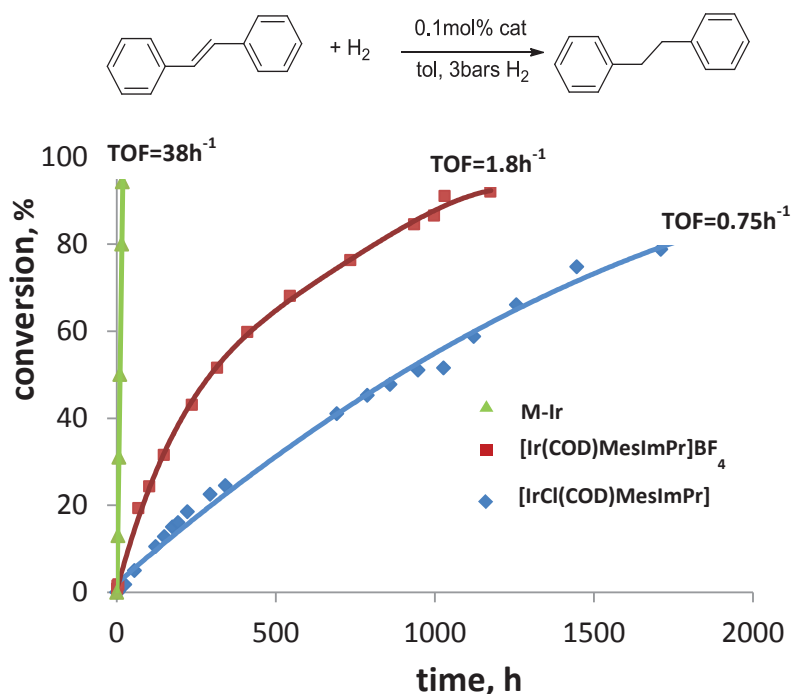


Figure 3. Performances catalytiques du complexe neutre $[\text{IrCl}(\text{COD})\text{MesImPr}]$, du complexe cationique $[\text{Ir}(\text{COD})(\text{MesImPr})]\text{BF}_4$ et du matériau **M-Ir** en hydrogénation du trans-stilbène. Les expériences d'hydrogénation ont été réalisées dans le toluène à 40°C sous 3 bars de H_2 (0,1% en mole d'Ir)

Le catalyseur **M-Ir** obtenu est donc très productif, atteignant un TON de plus de 8000, tandis que les deux catalyseurs homogènes parviennent difficilement à atteindre un TON de 1000. Nous n'avons cependant pas été capable de déterminer la productivité maximale de ce matériau **M-Ir** (TON max.) car sites actifs d'Ir sont empoisonnés par les traces d'impureté présentes dans le solvant et le substrat nécessaire pour ce test même après purification. L'augmentation de la productivité de **M-Ir** par rapport à celle de ses analogues moléculaires, ainsi que le profil linéaire des courbes d'hydrogénation suggère l'absence de processus de désactivation bimoléculaire. De

plus, les clichés de microscopie (MET) du catalyseur après catalyse montrent l'absence de nanoparticule d'Iridium. Enfin, aucune lixiviation d'Iridium n'a été détectée dans les produits de réaction. Une étude plus détaillée de la stabilité de **M-Ir** montre également que le catalyseur peut se dégrader sous pression d'H₂ en l'absence de substrat par clivage de la liaison Ir-carbène, avec formation de petites nanoparticules d'Iridium. Ces petites particules ont été détectées par HRTEM.

Nos résultats suggèrent que cette amélioration significative de l'activité catalytique du matériau **M-Ir** par rapport aux homologues homogènes est due à deux raisons principales: 1) l'isolation des espèces d'Ir sur le support qui supprime des processus de désactivation bimoléculaire; 2) l'absence de ligand COD dans **M-Ir** qui conduit à une activation extrêmement rapide du pré-catalyseur en catalyseur alors que les complexes homogènes nécessitent une période d'initiation (décoordination du ligand COD).

Nous avons également étudié le comportement du matériau **M-Ir** et du complexe neutre [IrCl(MesImPr)(COD)] lors de l'hydrogénation diastéréosélective du terpinène-4-ol, qui est connue pour être un point fort du catalyseur de Crabtree. Malgré une faible activité catalytique de **M-Ir** (35% en conversion en 500h), un haut degré de diastéréosélectivité (95%) est observé. Cette diastéréosélectivité est constante tout au long de la réaction catalytique.

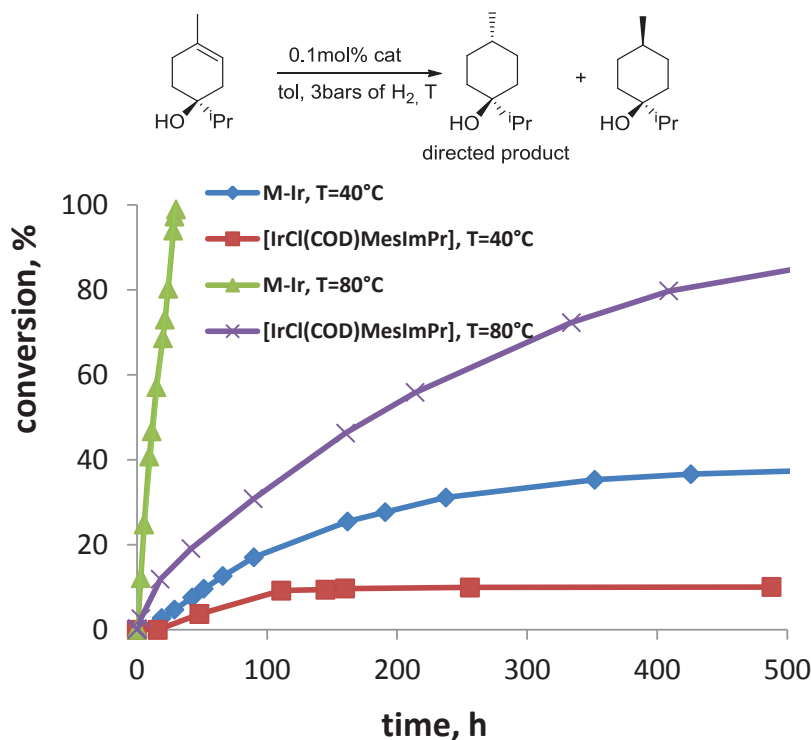
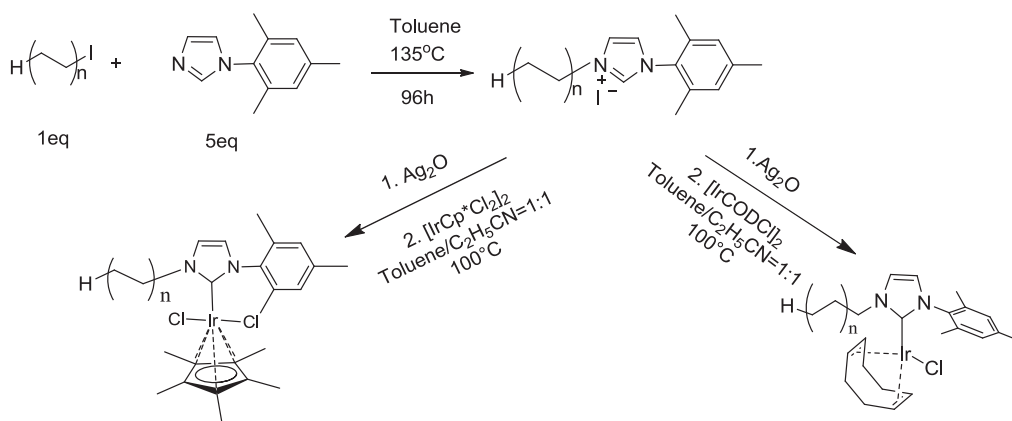


Figure 4. Performances catalytiques du complexe [IrCl(COD)MesImPr] et du matériau **M-Ir** en hydrogénation du terpinène-4-ol. Les expériences d'hydrogénation ont été réalisées dans le toluène à 40 ° C et 80 ° C sous 3 bars de H₂

Nous avons également entrepris dans ce projet de thèse, la préparation d'un catalyseur Ir-NHC supporté sur polymère comme alternatif au matériau silicique précédemment décrit ci-dessus. Nous avons choisi comme support un polyéthylène pour ses propriétés thermomorphiques. Les composés thermomorphiques sont des composés qui présentent une grande différence de solubilité à des gammes de températures proches. Ainsi, le polyéthylène est entièrement soluble dans des solvants non polaires à chaud (à $T > 80^\circ\text{C}$) mais est totalement insoluble dans ces mêmes solvants à température ambiante. Cette propriété permet de réaliser la réaction catalytique en phase homogène à haute température et de séparer facilement le solide des produits de réaction à froid.

La même méthodologie que celle utilisée précédemment a été réalisée ici en utilisant comme support de départ un polyéthylène téléchélifique présentant des fonctionnalités iodées (Schéma 2). Le complexe PE-IrCODCl obtenu n'est malheureusement que faiblement actif en l'hydrogénation du trans-stilbène à 40°C ou 80°C . À température élevée, on remarque la formation d'un dépôt noir, suggérant la désactivation du complexe par formation d'agrégats métalliques. Cela est en accord avec les spectres MALDI où la population majeure observée est liée aux dérivés de polyéthylène ayant pas d'Iridium.



Scheme2. Préparation de PE-IrCODCl and PE-IrCp*Cl₂

Malgré la faible activité catalytique de PE-IrCODCl en hydrogenation, son analogue Ir(III) PEIrCp*Cl₂ a été préparé et a montré une forte activité catalytique en réaction d'échange H-D de l'acétophénone à 100°C . Le PEIrCp*Cl₂ est également très stable et il a pu être facilement recyclé (au moins 3 fois) sans perte d'activité. Ce dernier résultat est intéressant car seuls quelques exemples de catalyseurs thermomorphiques très actifs et recyclables sont connus dans la littérature à ce jour.⁷

⁷ . a) Bergbreiter, D.E.; Cristopher, H.; Hongfa C. J.Org.Chem. 2011, 76, 523–533; b) Hobbs, C.; Yang, Y.-C.; Ling, J.; Nicola, S.; Su, H.-L.; Bazzi, H.S.; Bergbreiter, D.E. Org. Lett. 2011, 13, 3904–3907; c) Bergbreiter, D.E. ACS Macro Lett. 2014, 3, 260–265; d) Older, C.M.; Kristjansdottir, S.; Ritter, J.C.; Tam, W.; Grady, M.C. Chem.Ind. 2009, 123, 319–328.

General Introduction

Introduction

The main objective of this PhD project was to elaborate highly active and well-defined supported Ir(I)-NHC complexes for alkene hydrogenation reactions. The targeted Ir(I)-NHC catalytic materials were designed in order to prevent bimolecular decomposition processes known that lead to Ir-NHC complexes deactivation in solution. The supported Ir-NHC complexes were in-situ generated in an hybrid organic-inorganic material containing regularly distributed imidazolium units along the pore-channels of the silica framework. Beside the Ir-site isolation on the silica support, this catalytic system was also expected to ease the products purification and recovery at the end of the hydrogenation reaction.

Chapter1 reviews the use of Ir-based catalysts in alkene hydrogenation. It describes relevant scientific results encountered in this field, from the well-known Iridium based Crabtree's complex to recent promising Ir(I)-NHC complexes as potential alternatives. Finally, this chapter discusses different pathways for the introduction of organometallic complexes onto silica surfaces to yield appropriate supported complexes.

Chapter2 describes the preparation of Iridium(I)-NHC supported complexes and Ir-NHC complexes of identical molecular structure in solution. The full characterization of the catalytic systems using several techniques (N_2 adsorption/desorption, TEM, solid state NMR...) is also shown. A particular effort was directed here towards the elucidation of the Ir-NHC surface sites molecular structures using advanced NMR techniques such as the 2D DNP MAS NMR

Chapter3 presents the application of the as-obtained Ir(I)-NHC based material as catalyst for alkene hydrogenation. The catalytic performances of the supported Ir-NHC complex was also compared to those of neutral and cationic homogeneous analogues. Different olefinic substrates were used to compare the different catalytic systems. Of such substrates, the diastereoselective hydrogenation of terpinen-4-ol was undertaken.

Chapter4 depicts the preparation and the characterisation of alternative polymer-supported Ir-NHC complexes. Two Ir-NHC complexes [Ir(I) and Ir(III)] were covalently introduced in a polyethylene matrix and their catalytic performances in alkene hydrogenation (for Ir(I)) and H/D exchange reactions (for Ir(III)) were studied. Their catalytic performances were also compared to those of silica supported catalysts and to molecular homologues.

A general conclusion and possible perspectives are also given at the end of the manuscript.

Chapter 1

Bibliography

Table of content

I-1. Introduction.....	11
I-2. Alkenes hydrogenation by Iridium organometallic complexes	12
2.1. Introduction	12
2.2. Crabtree's catalyst	13
2.2.1. Discovery	13
2.2.2. Directing effects	15
2.2.3. Deactivation	15
2.2.4. Hydrogenation mechanism.....	16
2.3. N-Heterocyclic carbenes	17
2.3.1. Discovery and isolation.....	17
2.3.2. Synthesis	18
2.3.2. Electronic properties	18
2.3.3. Metallo-NHC catalysts.....	19
2.4. Ir-NHC	21
2.4.1. The most active hydrogenation catalysts	21
2.4.2. Chiral Ir(I) catalysts	24
I-3. Mesostructured hybrid materials for catalysis.....	27
3.1. Introduction	27
3.2. Porous materials	27
3.3. Sol-gel process	28
3.3.1. Introduction	28
3.3.2. Sol formation.....	28
3.3.3. Gel formation	29
3.3.4. Aging.....	29
3.3.5. Drying.....	30
3.4. Mesoporous materials	30

Chapter 1

3.5.	Strategies of preparation hybrid organic-inorganic materials	32
3.5.1.	Grafting	32
3.5.2.	Direct synthesis	33
3.5.3.	Periodic Mesoporous Organosilica	35
3.6.	Supported Iridium catalysts.....	35
I-4.	Strategy	40
4.1.	Objectives.....	40
4.2.	Formation of the Ir-NHC catalytic material.....	41

List of Figures

Figure 1. Relative reactivities of alkenes for hydrogenation by Wilkinson's catalyst.....	12
Figure 2. Directing effects for $[\text{Ir}(\text{cod})(\text{PCy})_3(\text{py})]\text{BF}_4$	15
Figure 3. Inactive hydride-bridged polynuclear iridium complexes	16
Figure 4 Alkene hydrogenation mechanism mediated Iridium phosphine oxazoline catalyst	17
Figure 5. Electronic configurations of imidazolium based carbenes	19
Figure 6. Families of ligands for Chiral Iridium based catalysts.	26
Figure 7. Main reactions involved in sol-gel process.....	29
Figure 8. Structures of Mesoporous M41S materials: MCM-41(hexagonal), MCM-48 (cubic) and MCM-50 (lamellar)	31
Figure 9. Formation of Mesoporous materials by structure-directing agents true liquid-crystal template mechanism	32
Figure 10. Strategies of preparation hybrid organic-inorganic materials.....	34
Figure 11. Hydrogenation strategies realized by grafting approach.....	36
Figure 12. Examples of iridium supported complexes that shows higher catalytic activity in comparison to homogeneous analogues	38
Figure 13. Preparation of Ir(III)-NHC based well-defined material	39
Figure 14. Strategy of hydrogenation catalyst design	42

List of Tables

Table1. Comparison of the most active homogeneous hydrogenation catalyst.....	14
Table2. Comparison of the most active Ir-NHC homogeneous hydrogenation catalysts.....	23

I-1. Introduction

Direct hydrogen addition to alkenes is forbidden according to orbital symmetry rules and therefore this reaction presents a high activation energy barrier. As a consequence, the hydrogenation of alkenes requires catalysts to proceed because transition metals have appropriate orbitals to interact with molecular hydrogen, forming metal hydride species, allowing the transfer of the hydride to the coordinated alkene.

The catalytic hydrogenation was first described in the pioneer report of P. Sabatier *et al.* in early 1900's in which the reduction of organic compounds under hydrogen flow was performed using nickel catalysts at 100-300°C. This discovery was of great importance for industrial processes development and P. Sabatier was awarded Nobel Prize (along with V. Grignard) in chemistry in 1912.

100 years after these literature precedents, Ni catalysts are still widely used in routine laboratory practice due to their low cost, despite their low catalytic activity and selectivity. These poor catalytic performances prompted researchers to investigate other catalytic systems based on metal particles and organometallic complexes. In the field of homogeneous catalysis, highly promising organometallic complexes of Rhodium, Iridium, Ruthenium, Platinum and Palladium were therefore developed, but one of the major achievement being the preparation of the Ir(I) based Crabtree's catalyst, $[\text{Ir}(\text{cod})(\text{PCy}_3)_3(\text{py})]\text{BF}_4$. This hydrogenation catalyst showed high catalytic activity and selectivity for a wide range of alkene substrates (*vide infra*). Based on Crabtree's catalyst, other Ir(I) based catalysts, among which Ir-NHC and chiral Ir-PHOX, were elaborated to hydrogenate functional substrates or to address selectivity issues in asymmetric hydrogenation. Despite numerous merits of Ir(I) based catalysts, their daily use is still limited due to fast bimolecular deactivation. We therefore tried in the present project to prevent deactivation processes by isolating Ir(I) active species onto oxide supports.

We therefore developed Ir(I)-NHC based heterogeneous catalyst and studied its catalytic performances.

I-2. Alkenes hydrogenation by Iridium organometallic complexes

2.1. Introduction

The application of Iridium complexes in olefin hydrogenation was assisted by the discovery of highly active Rhodium containing catalyst by Wilkinson in 1966. The complex $[\text{Rh}(\text{PPh}_3)_3\text{Cl}]$ was able to reduce easily monosubstituted and cis-disubstituted alkenes like cyclohexene. The hydrogenation was found to proceed at ambient temperature in benzene in the presence of a polar co-solvent such as ethanol under a low pressure of di-hydrogen. The relative rates of hydrogenation differ with the nature of the alkene double bond and cover a range of about 50-folds (Figure1). Such a difference in rate can be explained by difference in olefin binding constants; olefins binding strongly to the metal (as for instance terminal alkenes) being more easily hydrogenated. However, some olefins that bind too strongly, such as ethylene undergo hydrogenation very slow. In this particular case, the alkene binds tightly enough to withdraw (subtract) the catalyst from the cycle and alter the mechanism.⁸

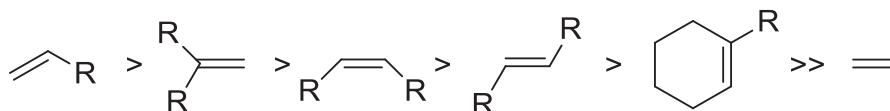


Figure 1. Relative reactivity of alkenes for hydrogenation by Wilkinson's catalyst⁹

The Wilkinson's catalyst is routinely used for synthetic applications due to its selectivity and catalytic efficiency but Rh catalysts were really considered as highly promising systems when their structures were optimized to insure asymmetric hydrogenation with very important e.e. In this context, Knowles and Noyori were awarded a Nobel prize in 2001 for the discovery of an enantioselective Rh complex: $[\text{Rh}(\text{R,R})\text{-DiPAMP}]\text{COD}]^+\text{BF}_4^-$. Nowadays, this catalyst is used industrially for the production of an enantiopure drug (95% of purity), namely the L-DOPA, which is used for Parkinson disease treatment.¹⁰⁻¹¹ In order to reduce the Rh catalyst cost,

⁸ Osborn, J. A.; Jardine, F. H.; Young, J. F.; Wilkinson, G., *J. Am. Chem. Soc. A* **1966**, 1711-1732.

⁹ The Handbook of Homogeneous Hydrogenation-Wiley-VCH (2007). Johannes G. de Vries, Elsevier C.J., Ed. Wiley-VCH: Weinheim, 2007; p. 1641.

¹⁰ Knowles, S. W.; Sabacky, M.J., *Chem. Commun.* **1968**, 1445-1446.

¹¹ Noyori, R., *Angew. Chem. Int. Ed.* **2002**, 41, 2008-2022.

Chapter 1

research efforts were directed towards the substitution of Rh by other metals such as Ru.¹² This led to the fast development of interesting Ru catalysts which are now extremely used for alkene hydrogenation.¹³ As an example, one of the first Ru complexes to be developed was $\text{HRuCl(PPh}_3)_3$, which was found to be much more active in hydrogenation of terminal double bond but less efficient for the reduction of cis-disubstituted alkenes than Rh derivatives (Table.1).

2.2. Crabtree's catalyst

2.2.1. Discovery

In the same time, Ir based catalysts as alternatives to Ru systems were also investigated. The first Ir catalyst was prepared by Vaska et al.¹⁴ This complex, $[\text{Ir(PPh}_3)_2\text{ClCO}]$, allowed the efficient di-hydrogen oxidative addition, the key step in alkene hydrogenation, however its overall catalytic performances were found disappointing. The reason for such a low activity is due to the absence of free coordination sites available for substrate binding. At the reverse, on the Wilkinson's catalyst, the phosphine ligands could easily dissociate leading to free coordination sites available for alkene coordination. The Iridium analogue of the Wilkinson catalyst, $[\text{IrH}_2\text{Cl(PPh}_3)_3]$, was therefore prepared but in contrary to Rhodium complex no phosphine dissociation occurred. In order to facilitate the dissociation step J. Osborn and R. Shrock¹⁵ decided to replace one phosphine by a weakly coordinated norbornadiene (nbd) ligand. The Osborn-Shrock complex, $[(\text{nbd})\text{Rh(PPh}_3)_2]\text{BF}_4$, was found to be highly active in hydrogenation with the generation of the following complex in methanol: $[\text{Rh(MeOH)}_2\text{L}_2]\text{BF}_4$ which undergoes methanol decoordination allowing the coordination of the alkene substrate. With the same idea, Ir complexes containing diene ligands were developed as for examples, $[\text{Ir(nbd)(PPh}_3)_2]^+$, $[\text{Ir(cod)(PPh}_3)_2]^+$ and $[\text{Ir(cod)(py)(PPh}_3)]^+$. However, such Ir complexes were found less active than Rh analogues.¹⁶⁻¹⁷

¹² Evans, D.; Osborn, J.A.; Jardine, F.H.; Wilkinson, G., *Nature* **1965**, 208, 1203-1204.

¹³ Hallman, P.S.; McGarvey, B. R.; Wilkinson, G., *J. Am. Chem. Soc. A* **1968**, 31430-3150.

¹⁴ Vaska, L.; Rhodes, R. E., *J. Am. Chem. Soc* **1965**, 83, 2784-2785.

¹⁵ Shapley, J.R.; Schrock, R.R.; Osborn, J.A., *J. Am. Chem. Soc* **1969**, 91, 2816-2817.


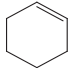
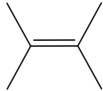
¹⁶ Schrock, R. R.; Osborn, J. A., *J. Am. Chem. Soc* **1976**, 98(8), 2134-2143.

¹⁷ Schrock, R. R.; Osborn, J. A., *J. Am. Chem. Soc* **1976**, 98(15), 4450-4455.

Chapter 1

Following these results, the development of Ir complexes declined till Crabtree described a complete study concerning the influence of solvents in hydrogenation reactions.¹⁸ Before this literature report, hydrogenation reactions were performed in coordinative solvents and Crabtree was the first to investigate hydrogenation reactions in dichloromethane; the use of halogenated solvents being avoided because of potential reactivity between the Rh and the C-X bond leading to the formation of a Rh-X bond (X = halogen). Interestingly, Ir complexes were found to be stable in dichloromethane. Overall, the change of solvent played a crucial role in hydrogenation processes and the iridium analogue to the Osborn-Shrock catalyst was found more active in alkene hydrogenation, even for difficult alkene substrates. The most active catalyst from this series is [Ir(cod)(PCy)₃(py)]BF₄, refereed as the Crabtree's catalyst. This complex is able to hydrogenate highly hindered tetrasubstituted olefins (Table1).¹⁹ High rates (TOF) were measured for the reduction of various hindered alkenes as for examples : t-BuCH=CH₂, 8300 h⁻¹; 1-hexene, 6400 h⁻¹; cyclohexene, 4500 h⁻¹; 1-methylcyclohexene, 3800 h⁻¹; Me₂C=CMe₂, 4000 h⁻¹.²⁰⁻²¹ This capability to hydrogenate sterically hindered substrates is still quite rare.

Table 1. Comparison of the most active homogeneous hydrogenation catalyst

Catalyst	Temperature	Solvent	TOF, h ⁻¹		
					
[Ir(cod)(PCy) ₃ (py)] ⁺	0	CH ₂ Cl ₂	6,400	4,500	4,000
RhCl(PPh ₃) ₃	0	C ₆ H ₆ /EtOH	60	70	0
HRuCl(PPh ₃) ₃	25	C ₆ H ₆	9,000	7	0

¹⁸ Crabtree R. H.; Felkin H.; Morris, G. E., *J. Organomet. Chem.* **1977**, 141, 205-215.

¹⁹ Suggs, W.; Cox, S. D.; Crabtree, R. H.; Quirk, J.M., *Tetrahedron Lett.* **1981**, 22, 303-306.

²⁰ Crabtree, R. H, *J. Am.Chem. Soc* **1979**, 101, 331-337

²¹ Crabtree, R. H.; Felkin, H.; Feillebeen-Khan, T.; Morris, G.E *J. Organomet. Chem.* **1979**, 168, 183-195.

Chapter 1

2.2.2. Directing effects

Crabtree's catalyst is interesting not only because of the possibility to hydrogenate sterically hindered substrates but also because of strong directing effects as discovered by M. Davis et al.²² The directing effect refers to a hydride transfer selectively on a face of a functional organic alkene that contains a ligating nucleophilic group (OH, OMe, NH₂, C=O etc) binding the catalyst. Later, Crabtree studied directing effects in reduction of terpinen-4-ol with [Ir(cod)(PCy)₃(py)]BF₄ in dichloromethane. The same reaction performed with Pd/C heterogeneous catalyst in ethanol results in formation of just 20% of directed product. The quantity of directed product can be increased till 53% in case of using the cyclohexane as a solvent.(Fig3).²³

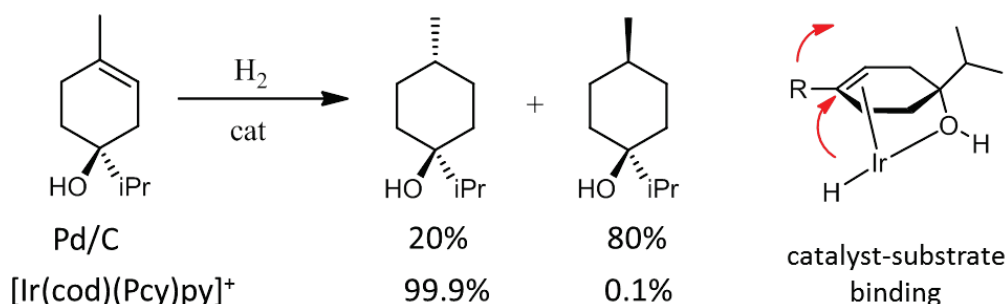


Figure 2. Directing effects for [Ir(cod)(PCy)₃(py)]BF₄

2.2.3. Deactivation

The industrial use of the Crabtree catalyst was however limited by its tendency to deactivate rapidly (within some hours) *via* the formation of highly stable polynuclear iridium hydride-bridged complexes (Fig3). The deactivation *via* bimolecular processes was also found to accelerate when increasing the reaction temperature, thus limiting the use of the Crabtree catalyst to low temperature (generally from 0°C to 40°C). Moreover, when full hydrogenation of the alkene was desired, multiple additions of fresh catalyst precursor were required. As an example,

¹⁵ Crabtree, R. H.; Davis, M. W., *Organometallics* **1983**, 2, 681-682;

²³ Crabtree., R. H.; Davis, M. W., *J. Org. Chem.* **1986**, 51 (14),2655-2661

Chapter 1

the reduction of $\text{Me}_2\text{C}=\text{CMe}_2$ needs an overall 0.1wt% loading of catalyst with a maximum TON of 400.²⁴

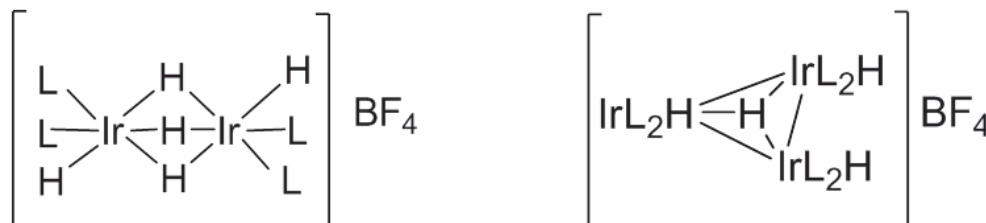


Figure 3. Inactive hydride-bridged polynuclear iridium complexes

Attempts to increase the stability of Crabtree's catalyst were undertaken through the tuning of the ligands (bulkiness of the phosphine and/or nitrogen ligands) which resulted in a slight improvement of catalyst stability. However, cluster formation was not fully prevented.²⁵⁻²⁶

2.2.4. Mechanism

Hydrogenation using the Wilkinson's catalyst proceeds *via* the formation of the Rh(III) species after oxidative addition of di-hydrogen on the starting Rh(I) complex and further reductive elimination of the σ -alkyl and hydride ligands.²⁷ Things were found different for Ir because of a major difference between Rh and Ir: the much easier access to M(V) oxidation state for Ir. A typical evidence of this is the existence $\text{IrH}_5(\text{PPh}_3)_2$ while Rh analogue had never been reported. DFT calculations with kinetic studies led to the conclusion that for Ir phosphine oxazoline complexes (closest analogues to the Crabtree's catalyst) hydrogenation proceeds through Ir(III) and Ir(V) intermediates. The most probable mechanism goes through the loss of COD ligand, coordination of alkene and oxidative addition of two molecules of dihydrogen and hydride

²⁴ Chodosh, D. F.; Crabtree, R. H *Organomet. Chem.* **1978**, 161, 67-70.

²⁵ Xu, Y.; Mingos, D. M.; Brown, J. M., *Chem. Commun.* **2008**, (2), 199-201.

²⁶ Xu, Y.; Celik, M. A.; Thompson, A. L.; Cai, H.; Yurtsever, M.; Odell, B.; Green, J. C.; Mingos, D. M.; Brown, J. M., *Angew. Chem. Int. Ed.* **2009**, 48 (3), 582-585.

²⁷ Gridnev, I. D.; Imamoto, T., *Acc. Chem. Res.* **2004**, 37 (9), 633-644.

Chapter 1

transfer to the coordinated alkene is considered as the rate limiting step. It can occur by dihydrogen metathesis or by migratory insertion of the alkene into Ir-H bond.^{28,29}

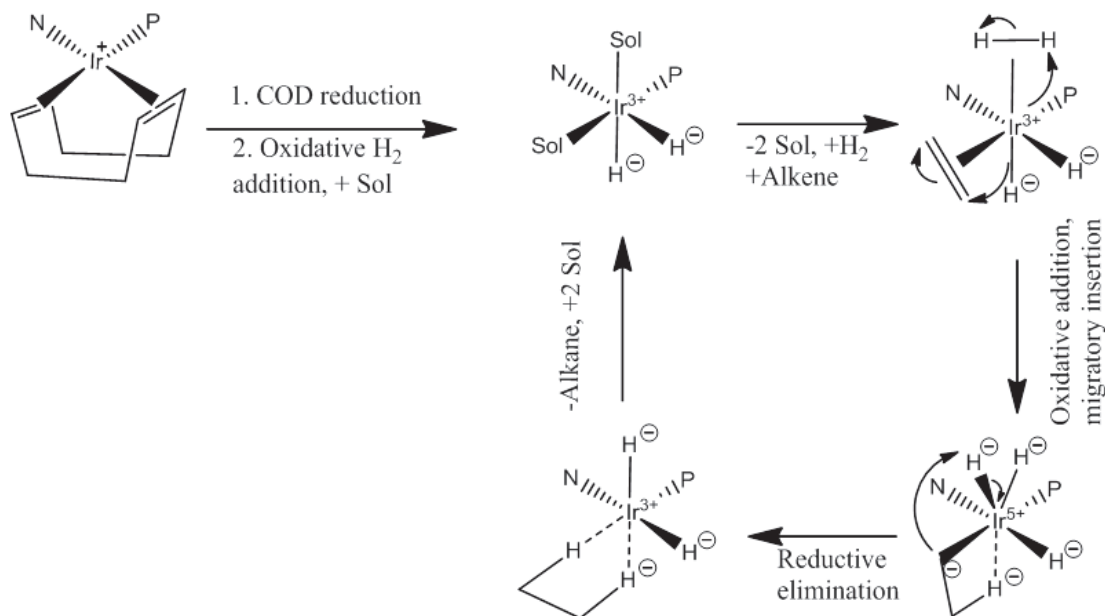


Figure 4 alkene hydrogenation mechanism mediated Iridium phosphine oxazoline catalyst³⁰

However for the gas phase reactions with $[(\text{PHOX})\text{Ir}(\text{COD})]^+\text{X}^-$, the hydrogenation was estimated to proceed via an oxidation of Ir(I) to Ir(III) species. Indeed, in the gas phase (no solvent) the Ir(V) species, $[\text{Ir}(\text{PHOX})(\text{Sub})(\text{H}_2)_2]$, were found to be unstable due to loss of hydrogen and thus could not be detected by spectroscopic studies. In contrast it was easy to detect the Ir(I) and Ir(III) species in the gas phase.³¹

2.3. N-Heterocyclic carbenes

2.3.1. Discovery and isolation

N-heterocyclic carbenes are heterocycles molecules bearing at least one nitrogen atom and a divalent carbon atom having six valence electrons. The first NHC carbene was isolated in 1991 by Arduengo and coworkers³² by deprotonation of 1,3-bis(adamantly)imidazolium chloride by

²⁸ Zhu, Y.; Burgess, K., *Acc. Chem. Res.* **2012**, 45 (10), 1623-1636.

²⁹ Sparta, M.; Riplinger, C.; Neese, F., *J. Chem. Theory Comput.* **2014**, 10 (3), 1099-1108.

³⁰ Hopmann, K. H.; Bayer, A., *Organometallics* **2011**, 30 (9), 2483-2497.

³¹ Dietiker, R.; Chen, P., *Angew. Chem. Int. Ed.* **2004**, 43 (41), 5513-5516.

³² Arduengo A. J.; Harlow R. L.; Kline, M J. *Am.Chem. Soc* **1991**, 113, 361-363.

Chapter 1

sodium hydride in THF in presence of a catalytic amount of DMF or t-BuOK. The carbene formation was proved by its structure elucidation using by X-Ray spectroscopy on a monocrystal and by ^{13}C liquid state RMN (presence of low field carbene peak at 211 ppm). The isolation of a free carbene was possible due to the presence of bulky adamantyl substituents that prevent carbene dimerization. Since this first Arduengo discovery, the interest towards the development of NHC carbenes increased drastically and families of carbenes were synthesized during the last decades.

2.3.2. Synthesis

Carbenes can be synthesized by simple deprotonation of the corresponding imidazolium salt by strong bases like potassium or sodium hydrides with a catalytic amount of tert-butoxide, lithium aluminium hydride, n-butyllithium, potassium hexamethyldisilazide, 1,8-diazabicyclo[5.4.0]undec-7-ene (DBU). The reaction of deprotonation is carried out in dry condition with the use of aprotic solvents such as THF or ethers.³³ In some cases (when the naked carbene is too instable), a transient silver carbene can be prepared by contacting the imidazolium salt with silver oxide (which acts as the deprotonating agent and the silver carbene promoter).

Numerous strategies were developed for the synthesis of symmetrical and unsymmetrical carbenes.³⁴

2.3.3. Electronic properties

N-Heterocyclic carbenes are singlet carbenes with excellent stability.^{35,36} The stabilization of NHC is provided by preserving carbene electroneutrality through a combination of inductive and mesomeric substituents effects. The carbene carbon atom is sp^2 -hybridised featuring two σ -bonds to the adjacent nitrogen atoms (“pull” stabilization due to the large electronegativity of nitrogen) and an electron lone pair in the remaining sp^2 -hybrid orbital. Two $\pi_{\text{N}} \rightarrow \pi_{\text{C}}$ donor interactions from the electron lone pairs of nitrogen into the “empty” p-orbital of the carbene carbon atom complete the electron configuration on the carbene carbon atom (“push” stabilization) and are responsible

³³ N-Heterocyclic Carbenes: Effective Tools for Organometallic Synthesis. Wiley-VCH Verlag GmbH & Co. KGaA: Boschstr. 12, 69469 Weinheim, Germany, 2014; p 568.

³⁴ Benhamou, L.; Chardon, E.; Lavigne, G.; Bellemin-Lapponnaz, S.; Cesar, V., *Chem. Rev.* **2011**, 111 (4), 2705-2733.

³⁵ Herrmann, W. A. ; Kocher, C., *Angew.Chem.Int.Ed.* **1997**, **36**, 2162-2187

³⁶ Bourissou, D.; Guerret, O.; Gabbai, F. P.; Bertrand, G., *Chem. Rev.* **2000**, 100, 39-91.

Chapter 1

for NHC stability (Figure 5). Due to their electronic structure, NHC are strong σ -donor but only very weak π -acceptor ligands.

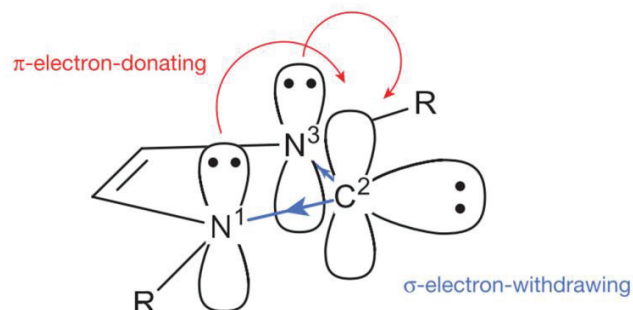


Figure 5. Electronic effects of the substituents in imidazolium based NHC

Of the huge variety of NHCs, imidazol-2-ylidenes were found extremely stable. Besides the stabilization related to electronic effects of the substituents, π -conjugation was also key for enhancing the stability.³⁷ Thus it was found that imidazole-2-ylidenes were more stable than dihydroimidazol-2-ylidene counterparts which were themselves more stable than their acyclic analogues. There are, however, many stable carbenes that do not benefit from aromaticity, as for example, 1,3-di(mesityl)-4,5dihydro-imidazol-2-ylidene reported by Arduengo and co-workers in 1995.

The stability of NHC can be increased by incorporation of bulky substituents like mesityl or adamantyl that can prevent the carbene dimerization (Wanzlick equilibrium). Additional steric protection of the carbene can compensate the lower electronic stabilization calculated for dihydro-imidazol-2-ylidene, which explains the successful isolation of the N-mesityl derivative of dihydroimidazol-2-ylidene.

Concerning electronic effects, the high π -conjugation encountered for unsaturated NHC is also important for stability and allows the use of less bulky substituents as the simple methyl-substituted NHC [1,3-di(methyl)imidazol-2-ylidene] exist in solution in monomeric form.³⁸

2.3.4. Metallo-NHC complexes (M-NHC)

³⁷ Denk, M. K.; Rodezno, J. M.; Gupta, S.; Lough, A. J., *Organomet.Chem.* **2001**, 617-618, 242-253

³⁸ Hopkinson, M. N.; Richter, C.; Schedler, M.; Glorius, F., *Nature* **2014**, 510 (7506), 485-496.

Chapter 1

First M-NHC was discovered 20 years before isolation of first free carbene by Arduengo. Wanzlick³⁹ and Ofele⁴⁰ independently synthesized mercury(II) and chromium(0) species bearing a imidazol-2-ylidene ligand respectively, in 1968.

From electronic structure of NHC, one can see that σ -donating property of the carbene lone electron pair ideally suits for σ -acceptor d_z^2 transition metal orbitals. This explains why carbene are very appropriate ligands for many metals. Even if the σ -donation is the main component in metal-NHC binding there is also an input coming from π donation and the π -backbonding between the π system localized on the NHC and the d_{xz} (or d_{yz} orbitals) of the metal. Frenkin and coworkers calculated that the π -contribution accounts for 20% from all the bond energy in group-11 metal-imidazol-2-ylidene and imidazolin-2-ylidene complexes.⁴¹ Strong σ -donating and weak π -acceptor properties of NHC make them similar to phosphines, however there is a number of difference between both classes of ligands.

First, significant difference lies on σ -donation. NHC were found more electron donating than phosphines, providing stronger binding with the metal. This was proved by measuring M-NHC bond distances and dissociation energy. As a result, M-NHC complexes are more thermally and oxidatively stable than phosphine homologues.¹⁸

Another difference relies on steric properties. Whereas sp^3 hybridized phosphines have a cone-shaped spatial arrangement, imidazol-2-ylidenes and dihydroimidazol-2-ylidenes mostly have a fan- or umbrella-shape, where the nitrogen-substituents are more oriented towards the metal. Therefore NHCs are bulky ligands which structure has a direct influence on the metal center and on the strength of the M-NHC bond. Using $[Cp^*Ru(NHC)Cl]$ complex as a model compound, A. Hillier showed that the energy of M-NHC bond decreases with increase of the ligand steric bulkiness. But even for more hindered NHC (as for example adamantly-NHC) the strength of M-NHC bond is still bigger those of phosphine complexes.⁴²

The main advantage of NHCs with respect to phosphines is the possibility to control more easily steric and electronic features by modifying the nitrogen substituents, the functional groups at the

³⁹ Wanzlick, H.-W.; Schonherr, H.J., *Angew. Chem. Int. Ed.* **1968**, 7 (2), 141-142.

⁴⁰ Öfele, K.; Herberhold, M., *Angew. Chem. Int. Ed.* **1970**, 9 (9), 739-740.

⁴¹ Nemcsok, D.; Wichmann, K.; Frenking, G., T, *Organometallics* **2004**, 3640-3646.

⁴² Hillier, A.C.; Sommer, W. J.; Yong, B.S.; Petersen, J.L.; Cavallo, L.; Nolan, S. P., *Organometallics* **2003**, 22, 4322-4326.

Chapter 1

NHC backbone and NHC itself (saturated, insaturated, CAAC...) allows for more independent variation of their steric and electronic parameters.

All these advantages therefore favored the impetuous development of M-NHC complexes. M-NHC complexes are usually synthesized by *in situ* deprotonation of appropriate azolium salt in presence of the desired metal precursor. Another method is transmetallation through the formation of a transient NHC-silver(I) complex.^{43,44,45} In the presence of more electronegative metal than silver, the silver-carbene bond is cleaved and carbene transfer occurs. This reaction is thermodynamically favored by precipitation of the solid silver (I) halide. Using this strategy, different complexes of Ru (IV), Rh (I), Pt (II), Pd (II) and Ir (I, III) were synthesized in excellent yields.⁴⁶

2.4. Ir-NHC complexes

2.4.1. The most active hydrogenation catalysts

After NHC discovery, numerous attempts were performed to replace the pyridine and the phosphine ligands in the Crabtree's catalyst $[\text{Ir}(\text{COD})(\text{PCy}_3)(\text{py})]\text{PF}_6$ by bulky NHC ligands to in order to increase its stability and avoid cluster formation. The first NHC-based analogue of the Crabtree's catalyst, $[\text{Ir}(\text{COD})(\text{SIMes})(\text{py})]\text{PF}_6$ (SIMes-1,3-dimesityl-4,5-dihydroimidazol-2-ylidene), was synthesized by S. Nolan and co-workers in 2001. The catalyst was tested in hydrogenation of cyclohexene derivatives. The catalytic activity was lower than that of the parent Crabtree's catalyst, but this new catalyst was found to be more thermally stable. Thus, the hydrogenation of 1-methyl-1-cyclohexene with 1mol% Crabtree's catalyst under 4bars of H_2 at 50°C resulted in a poor conversion (34%) after 7h of reaction whereas the Nolan's NHC analogue gave full conversion at the same reaction time (entry 1-2 Table2).⁴⁷

A second series of Ir-NHC complexes was prepared by J. Buriak and co-workers⁴⁸ by replacement of the pyridine ligand, resulting in the formation of complexes having the following

⁴³ Wang, H.; Lin, I., *Organometallics* **1998**, 972-975.

⁴⁴ Garrison, J. C.; Youngs, W. *Chem. Rev.* **2005**, 105, 3978-4008.

⁴⁵ Maishal, T. K.; Basset, J.-M.; Boualleg, M.; Coperet, C.; Veyre, L.; Thieuleux, C., *DaltonTrans.* **2009**, 6956–6959.

⁴⁶ N-Heterocyclic Carbenes in Synthesis. WILEY-VCH Verlag GmbH & Co. KGaA: Weinheim, Germany, 2006.

⁴⁷ LeeH. M.; Jiang T.;Nolan S.P., *Organometallics* **2001**, 20, 1255-1258.

⁴⁸ Vazquez-Serrano, L. D.; Owens, B. T.; Buriak, J. M., *Chem.Comm.* **2002**, (21), 2518-2519

Chapter 1

general formula: $[\text{Ir}(\text{COD})(\text{phosphine})(\text{NHC})]\text{PF}_6$. After detailed screening of available phosphines and NHC ligands, the most active complex was $[\text{Ir}(\text{COD})(\text{IMe})(\text{P}(\text{n-Bu})_3)]\text{PF}_6$, which was able to hydrogenate even tetra-substituted substrates at 1 mol% of catalyst loading under 1 bar of H_2 at room temperature. However at smaller catalyst loading 0.1 mol%, Crabtree's catalyst was superior, reaching 49% conversion before deactivation, while Buriak's catalyst barely reached 5% conversion (entry 6-7 Table2). Therefore the $[\text{Ir}(\text{COD})(\text{IMe})(\text{P}(\text{n-Bu})_3)]\text{PF}_6$ seemed to have the same stability problems as a parent Crabtree catalyst

A breakthrough was achieved by the replacement of the PF_6 counter-anion by the non-coordinating bulk tetrakis[3,5-bis(trifluoromethyl)phenyl]borate (BARF). A. Pfaltz and K. Burgess reported that phosphine-oxazoline iridium complexes were more active with BARF counter-anion than the traditional PF_6 or BF_4 .⁴⁹⁻⁵⁰ A significant enhancement in catalytic rates was observed even for the Crabtree's catalyst $[\text{Ir}(\text{COD})(\text{PCy}_3)(\text{py})]\text{BARF}$ (entry 1 and 4, Table2).⁵¹ From all the series, $[\text{Ir}(\text{COD})(\text{IMe})(\text{P}(\text{n-Bu})_3)]\text{BARF}$ was the only catalyst able to hydrogenate very difficult substrates such as 2,3-dimethylbut-2-ene with a quantitative yield and a catalyst loading of 0.1 mol%. When BARF was used as the counter-anion, it became possible to carry out the hydrogenation in non-dry conditions, using solvents straight from open under air bottle, however the rates were a bit lower even if the reaction still led to full hydrogenation of the substrate. Moreover $[\text{Ir}(\text{COD})(\text{PCy}_3)(\text{py})]\text{BARF}$ is an efficient catalyst even at 0.01 mol% catalyst loading, giving more than 90% of conversion (entry 8 Table2).⁵²

Further developments in Iridium-NHC chemistry were achieved, as for example the preparation of pyrazol-N-heterocyclic carbene iridium(I) complexes by P. Turner and coworkers. This complex was used as catalyst for styrene hydrogenation. The full conversion of styrene into ethyl-benzene was achieved in 35 min. under 8 bars of H_2 , with 1 mol% of catalyst; THF being used as a solvent.⁵³

⁴⁹ Lightfoot, A.; Schnider, P.; Pfaltz, A., *Angew.Chem.Int.Ed.* **1998**, 37, 2897-2899.

⁵⁰ Hou, D.R.; Reibenspies, J.; Colacot, T. J.; Burgess, K., *Chem.Eur.J.* **2001**, 7, 5391-5400.

⁵¹ Wüstenberg, B.; Pfaltz, A., *Adv. Synth. Catal* **2008**, 350 (1), 174-178.

⁵² Vazquez-Serrano, L. D.; Owens, B. T.; Buriak, J. M, *Inorg. Chim. Acta* **2006**, 359 (9), 2786-2797.

⁵³ Messerle, B. A.; Page, M. J.; Turner, P., *Dalton Trans.* **2006**, (32), 3927-33.

Chapter 1

Table2. Comparison the most active Ir-NHC alkene hydrogenation catalysts

Entry	Catalyst	Substrate	Cat. (mol%)	Time (min)	Yield (%)	Rate h ⁻¹
1	Crabtree's catalyst	1-Methylcyclohex-1-ene	1	16	99	516
			0.1	60	70	1496
2	[Ir(COD)(SIme)(py)]PF ₆	1-Methylcyclohex-1-ene	1	210	42	–
3	[Ir(COD)(Ime)(P(n-Bu) ₃)]PF ₆	1-Methylcyclohex-1-ene	1	21	100	278
			0.1	130	71	649
4	Crabtree's catalyst (BARF)	1-Methylcyclohex-1-ene	1	13	100	753
			0.1	60	78	1396
5	[Ir(COD)(Ime)(P(n-Bu) ₃)]BARF	1-Methylcyclohex-1-ene	1	16	100	375
			1(air)	23	100	279
			0.1	86	100	850
6	Crabtree's catalyst	2,3-Dimethylbut-2-ene	1	40	95	208
			0.1	50	49	1057
7	[Ir(COD)(Ime)(P(n-Bu) ₃)]PF ₆	2,3-Dimethylbut-2-ene	1	39	99	165
			0.1	30	5	70
8	[Ir(COD)(Ime)(P(n-Bu) ₃)]BARF	2,3-Dimethylbut-2-ene	1	25	100	217
			1(air)	32	100	157
			0.1	120	100	493

Interesting investigation was also performed by B. Marciniec and coworkers, who synthesized the first [Ir(COD)(IMes)(OSiMe₃)] complex as a model compound for Ir complexes immobilized on silica. The catalytic activity of the siloxide complex was compared with that of

Chapter 1

[Ir(COD)(IMes)Cl] in hydrogenation reactions. The activities of both complexes were found similar, however still much lower than that of the Crabtree's catalyst.⁵⁴

In the last decades, the bigger attention was driven toward selectivity issues and substrates scope broadening. In this context, G. Nilsson and co-workers tested [Ir(COD)(PR₃)(IMes)]PF₆ in hydrogenation of several substrates, containing potentially sensitive functional group such as halogeno, nito or benzyl fragments. The functional groups remained intact in hydrogenation with [Ir(COD)(PR₃)(IMes)]PF₆ as like with Crabtree's catalyst, however for some substrates Crabtree's catalyst showed lower rates.⁵⁵

The hydrogenation mechanism mediated by Ir-NHC was found to be similar to that previously mentioned for N,P-systems.⁵⁶ As it was reported by K. Burgess, strong σ -donating abilities of NHC can better stabilize Ir(V) species than phosphine ligand thus Ir(III)/Ir(V) cycle is expected.⁵⁷

2.4.2. Chiral Ir(I) catalysts

Rh(I)⁵⁸ and Ru(II)⁵⁹ diphosphine complexes are known to be highly active for the reduction of functionalized olefins containing amido- and carboxylic acid-groups in close vicinity to the double bond. Here, the functional group on the olefin is crucial for high enantiomeric excess since it coordinates to the metal and further influences the coordination of the substrate, leading to high stereoselectivity. In contrast, development of enantioselective catalysts for the hydrogenation of unfunctionalised olefins is difficult, since stereodifferentiation of the prochiral faces is mainly achieved via non-bonding, sterically-based interactions.¹⁹ From this point of view, during the last 20 years, a considerable attention was directed toward the elaboration of Ir(I) based catalysts for enantioselective reduction of prochiral unfunctionalized alkenes.⁶⁰

⁵⁴ Kownacki, I.; Kubicki, M.; Szubert, K.; Marciniak, B., *J. Organomet. Chem.* **2008**, 693 (2), 321-328.

⁵⁵ Bennie, L. S.; Fraser, C. J.; Irvine, S.; Kerr, W. J.; Andersson, S.; Nilsson, G. N., *Chem. Commun.* **2011**, 47 (42), 11653-11655.

⁵⁶ Cui, X.; Fan, Y.; Hall, M. B.; Burgess, K., *Chem. Eur. J.* **2005**, 11 (23), 6859-6868.

⁵⁷ Zhu, Y.; Fan, Y.; Burgess, K., *J. Am. Chem. Soc.* **2010**, 132, 6249-6253.

⁵⁸ Chi, Y.; Tang, W.; Zhang, X. In *Modern Rhodium-Catalyzed Organic Reactions*; Evans, P.A., Ed.; Wiley-VCH: Weinheim, 2004.

⁵⁹ Kitamura, M.; Noyori, R. In *Ruthenium in Organic Synthesis*; Murahashi, S.-I., Ed.; Wiley-VCH: Weinheim, 2004.

⁶⁰ Verendel, J. J.; Pamies, O.; Dieguez, M.; Andersson, P. G., *Chem. Rev.* **2014**, 114 (4), 2130-2169.

Chapter 1

A series of phosphinooxazoline (PHOX) ligands were thus synthesized to mimic the P,N binding motif of the Crabtree's catalyst.³⁸ The PHOX-Ir catalysts were able to hydrogenate simple, unfunctionalized alkenes with moderate to high enantioselectivities, however high pressure of H₂ (up to 50 bars) was required.³⁹ In order to broaden the scope to sterically bulk substrates, search for new P,N-binding motifs in ligand design was spread out. Thus new series of N-phosphine-oxazoline, phosphinite-oxazoline, phosphoroamidite/phosphite-oxazoline and a lot of others ligands were synthesized and found applications in asymmetric alkene hydrogenation (Figure 6). However the activity of these new families of complexes was not far from that of Ir-PHOX derivatives and enantioselectivities were mostly dependent on the nature of the substrate.⁴⁷

With the goal to decrease the required hydrogen pressure and the catalyst loading, K. Burgess undertaken the substitution of the phosphine ligand of the PHOX by a chiral NHC.⁶¹ The new Pfaltz-Burgess' catalyst was highly active and capable to efficiently hydrogenate primary, secondary and tertiary olefins with high enantioselectivities sometimes under just 1 bar of H₂.^{62,63} The highest level of selectivity was achieved with the ligand bearing an adamantyl group in the oxazoline ligand and an *ortho*-disubstituted aryl group in the carbene moiety. Such promising results prompted the screening of other carbene catalysts and high catalytic activity and selectivity were found for Iridium complexes with chelating N, NHC ligands (see fig. 6).

In summary, chiral analogues of Crabtree's catalyst were designed and found suitable for asymmetric hydrogenation of unfunctionalized trisubstituted alkenes whereas chiral metal diphosphine complexes were not able to reduce such hindered substrate with significant rate.

⁶¹ Powell, M.T.; Hou, D.R.; Perry, M.; Cui, X.; Burgess, K., *J. Am. Chem. Soc.* **2001**, 123, 8878-8879.

⁶² Perry, M. C.; Burgess, K., *Tetrahedron: Asymmetry* **2003**, 14 (8), 951-961.

⁶³ Gruber, S.; Neuburger, M.; Pfaltz, A., *Organometallics* **2013**, 32 (16), 4702-4711.

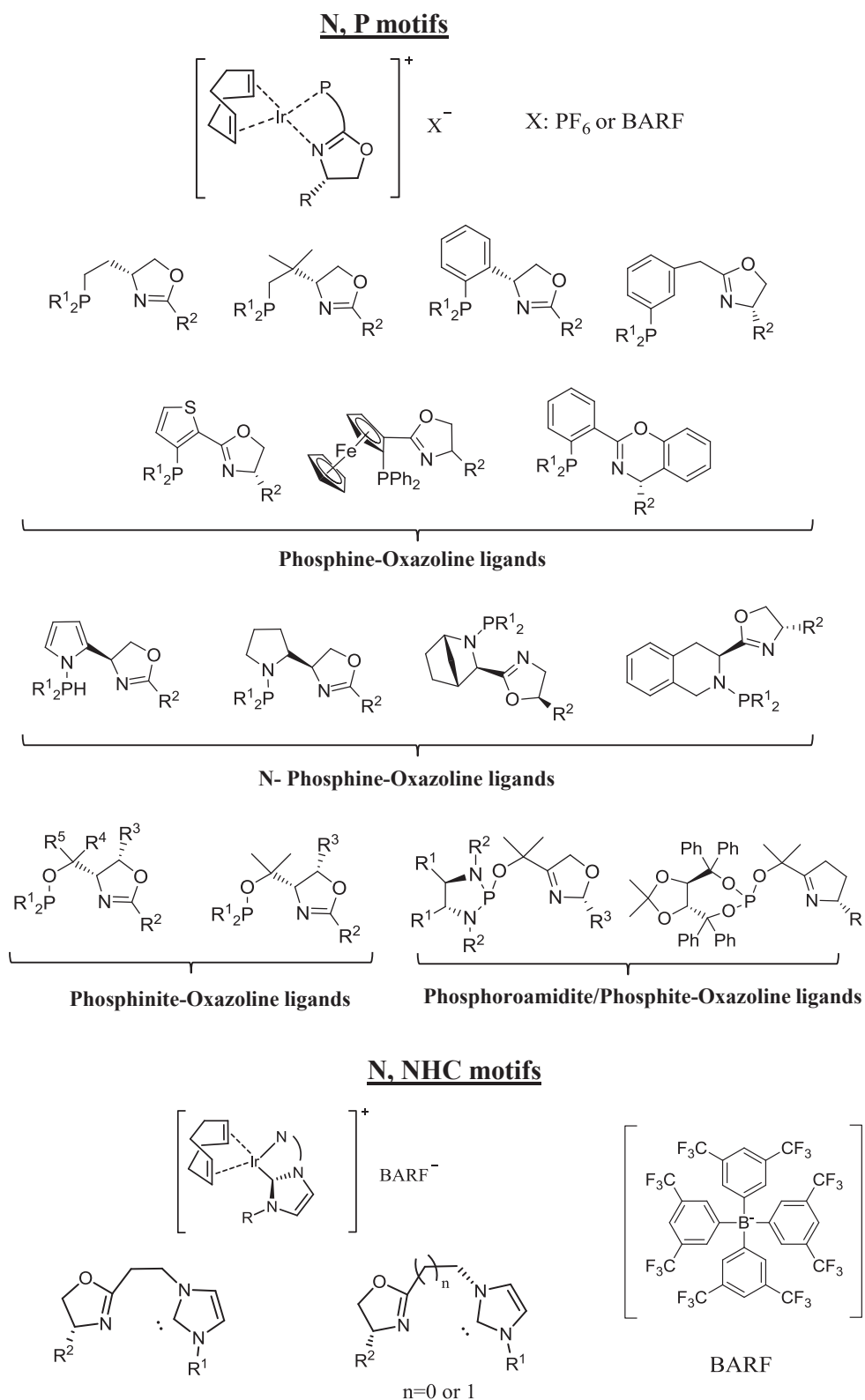


Figure 6. Families of ligands for Chiral Iridium based catalysts.

I-3. Mesostructured hybrid materials

3.1. Introduction

Despite the high activity and selectivity of homogeneous catalyst, heterogeneous catalysts which are often ill-defined systems (many surface species) are often preferred for the industrial processes (except some examples) due to their easier separation from the reaction products and their easier recycling and recovery.⁶⁴ In this context, in order to combine advantages of both heterogeneous and homogeneous catalysts, research efforts were directed towards the preparation of homogeneous supported catalysts on oxide supports (mainly silica and polymers). In this area of research, the development of porous hybrid organic inorganic materials as supports for organometallic complexes was studied.⁶⁵ A hybrid material is defined here as a material which contains two different components at the molecular level: organic groups used as ligands for the targeted complex and an oxide matrix. In this work, we will focus on this class of solids as supports for Ir-NHC complexes.

3.2. Porous materials

According to IUPAC classification all porous materials can be divided into three main classes dependent on the pore diameter (d)⁶⁶:

- 1) Microporous materials ($d < 2\text{nm}$)
- 2) Mesoporous materials ($2\text{nm} < d < 50\text{nm}$)
- 3) Macroporous materials ($d > 50\text{nm}$)

The well-known examples of microporous materials are zeolites that are crystalline aluminosilicates. Due to their crystalline framework, zeolites exhibit high surface area with a combination of narrow size pore distribution that allows their successful use in catalysis. Despite these positive features, zeolites have one significant drawback connected with their limited pore sizes

⁶⁴ Diaz, U.; Boronat, M.; Corma, A., *Proc. R. Soc. A* **2012**, 468 (2143), 1927-1954.

⁶⁵ Thomas, J. M.; Raja, R.; Lewis, D. W., *Angew. Chem. Int. Ed.* **2005**, 44 (40), 6456-82.

⁶⁶ Sing, K. S. W.; Everett, D. H.; Haul, R. A. W.; Moscou, L.; Pierotti, R. A.; Rouquerol, J.; Siemieniowska, T., *Pure Appl. Chem.* **1985**, 57, 603-619

Chapter 1

(<1.5nm), which exclude the transformation of bulky molecules. Another point is mass transfer limitations that occurs in case of liquid phase catalysis. The elaboration of new materials with bigger pore size and still with narrow size distribution became an important challenge.⁶⁷

The prerequisite for porous material discovery was the development of sol-gel process that allowed the preparation of amorphous silica gels with high surface area. This method comparing to high thermal methods allowed better control of morphology of the final material with lower energy costs.

3.3. Sol-gel process

3.3.1. Introduction

The term “sol-gel” corresponds to the abbreviation of “solution-gelification”. Sol-gel process refers to the transformation of liquid precursor (alkoxides) into the solid due to hydrolysis and condensation reactions. In the particular case of Silicon, tetraalkoxysilanes with the general formula $\text{Si}(\text{OR})_4$ where $\text{R}=\text{Me}$, Et , iPr are used as precursors. This reaction can be catalyzed by acids, bases or nucleophiles (Rh complexes can also be used) and lead to the formation of a silica gel or precipitate. The formation of the final oxide material proceeds through the four main steps, starting from sol formation, then gel formation, followed by the aging process and by drying. The experimental conditions implied in all of these steps influence the final morphology of the final oxide.⁶⁸

Non- hydrolytic processes also exist, and it involves the condensation of a metal alkoxide with metallic chlorides.⁶⁹

3.3.2. Sol formation

Sol is a dispersion of colloid particles (diameter 1-100nm) in solution. Colloidal particles are formed due to hydrolysis and condensation reactions that occurs after mixing $\text{Si}(\text{OR})_4$ with water. Hydrolysis is the reaction of silicon alkoxide with water resulting in formation of silanol groups that further condense with other silanols or alkoxides to generate Si-O-Si bonds. The reaction

⁶⁷ Taguchi, A.; Schüth, F., *Microporous Mesoporous Mater.* **2005**, 77 (1), 1-45.

⁶⁸ Hench, L. L.; West, J. K., *Chem.Rev.* **1990**, 90, 33-72

⁶⁹ R. J. P. Corriu; D. Leclercq; P. Lefevre; P. H. Mutin; A. Vioux *J. Mater. Chem.* **1992**, 2, 673-674.

Chapter 1

conditions (pH, temperature, H₂O/alkoxide ratio, presence of co-solvents...) has a great influence onto the particles size and structure of the final oxide.

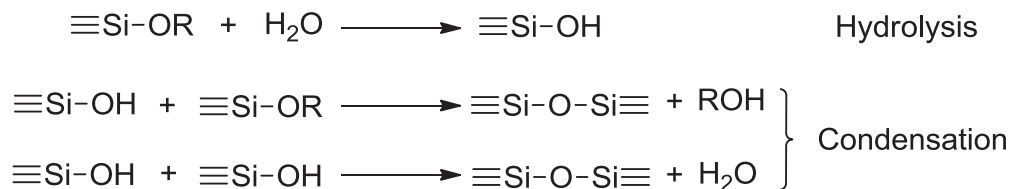


Figure7.Main reactions involved in the sol-gel process

3.3.3. Gel formation

With time, the colloidal particles and condensed silica species start to aggregate through condensation reactions that finally result in the formation of an interconnected tree-dimensional network, called gel. in a gel formation. The physical characteristics of the gel network depend greatly upon the size of particles and extent of cross linking prior to gelation. Moreover the relative rate of hydrolysis and condensation determine the structure of gel. At gelation, the viscosity of the solution sharply increases (also called the the gel point), loses it fluidity and takes the appearance of an elastic solid.

3.3.4. Aging

The condensation reactions that cause gelation continue after the gel point, producing strengthening, stiffening and shrinkage of the network. During the aging process, three main phenomena can occur: condensation, coarsening or ripening and phase transformation (only for transition metal oxides). The condensation reactions increase the connectivity of the network. Coarsening or ripening is a process of dissolution and re-precipitation driven by differences in solubility between surfaces. During this step, small particles disappear and small pores are filled in, so the interfacial area decreases and the average pore size increases. during aging, syneresis occurs and it corresponds to the spontaneous and irreversible shrinkage of the gel network, resulting in expulsion of liquid from the pores

3.3.5. Drying

The conventional drying of wet gels can be performed by temperature increase or by pressure decrease. Three stages occur:

1)- The gel shrinks by the volume of liquid present in the pores. The liquid flows from the interior of the gel body to the surface. Upon shrinkage, OH groups at the inner surface approach each other and can react with each other and new Si-O-Si bridges are formed. Upon drying, the network becomes increasingly stiffer and the surface tension in the liquid rises correspondingly because the pore radii become smaller.

2)- This “true drying” begins when the surface tension is no longer capable of deforming the network and the gel body becomes too stiff for further shrinkage. The tension in the gel becomes so large that the probability of cracking is high. In this stage of drying, the liquid/gas interface retreats into the gel body. Nevertheless, a contiguous funicular liquid film remains at the pore walls; that is, most of the liquid still evaporates from the exterior surface of the gel body.

3)- In this stage, the liquid film is disrupted. Eventually, liquid is only in isolated pockets and can leave the network only by diffusion via the gas phase.

Two processes are important for the collapse of the network. First, the slower shrinkage of the network in the interior of the gel body results in a pressure gradient that causes cracks. Second, larger pores will empty faster than smaller pores during drying. The walls between pores of different size are therefore subjected to uneven stress and crack. For these reasons, xerogel powders are usually obtained when wet gel bodies are conventionally dried.

Drying with supercritical fluids was therefore developed in order to retain the porous network structure. The obtained materials are called aerogels.

3.4. Mesoporous materials

The first mesoporous material was synthesized by C.Kato and co-workers who performed hydrolysis and co-condensation of kanemite ($\text{NaHSi}_2\text{O}_5 \cdot 3\text{H}_2\text{O}$) in the presence of alkyltrimethylammonium chloride (SDA) in basic medium ($\text{pH}=8-9$). The-obtained material had a large surface area $\sim 900\text{m}^2/\text{g}$ with the pore size distribution ranged from 2 to 4nm depending on

Chapter 1

the alkali precursor.⁷⁰ In 1992, researchers from Mobil Oil corporation re-investigated this type of synthesis and discovered a new class of porous materials, called M41S.⁷¹ These materials exhibit high surface areas, calibrated pores and a structuration of the porous network. The synthesis of such ordered systems became possible by introduction of a structure directing agents (SDA) during the sol-gel process. SDA are surfactants that self-organized in the liquid phase and play the role of template around which the polycondensation of organosilanes occurs. By changing the experimental conditions and the surfactant nature, different mesophases can be formed leading to a variety of mesoporous structures. As an example, hexagonal (p6mm ; MCM-41 solids), cubic (Ia3d ; MCM-48 solids), and laminar structures (p2 ; MCM-50 solids) can be easily obtained (Figure 8).

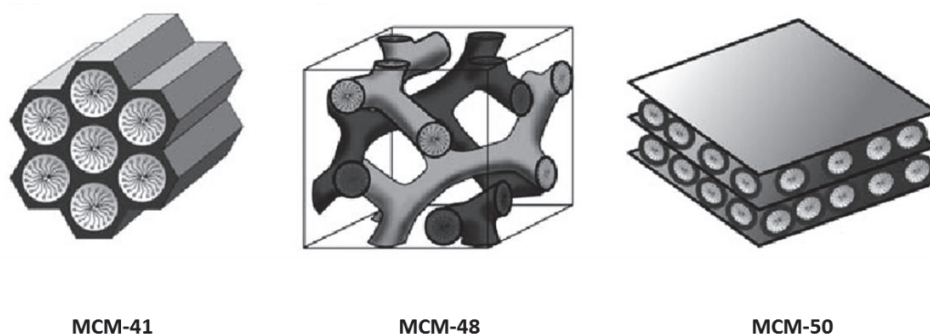


Figure 8. Structures of Mesoporous M41S materials: MCM-41(hexagonal), MCM-48 (cubic) and MCM-50 (lamellar).

Three main mechanisms were found to be involved in the formation of the final porous solids: the True Liquid-Crystal Templating (TLCT), the Cooperative Self-Assembly (CSA)⁷² and the Hard Sphere Packing (HSP).⁷³ For TLCT (Figure9). the liotropic phase is formed before adding organosiloxide precursor (an “assembly before condensation”), whereas for CSA , the liotropic phase and condensation processes occurs in the same time (an“assembly during condensation”).

⁷⁰ Yanagisawa, T.; Shimizu, T.; Kuroda, K.; Kato, C., *Bull. Chem. Soc. Jap.* **1990**, 63(4), 988-992

⁷¹ Beck, J. S.; Vartuli, J. C.; Roth, W. J.; Leonowicz, M. E.; Kresge, C. T.; Schmitt K.D.; Chu, T. W.; Olson, D. H.; Sheppard, E. W.; McCullen, S. B.; Higgins, J. B.; Schlenker, J. L., *J. Am. Chem. Soc.* **1992**, 114, 10834-10843.

⁷² Monnier, A.; Schuth, F.; Huo, Q.; Kumar, D.; Margolese, D.; Maxwell, R. S.; Stucky, G. D.; Krishnamurty, M.; Petroff, P.; Firouzi, A.; Janicke, M.; Chmelka, B.F., *Science* **1993**, 261, 1299-1303.

⁷³ Tang, J.; Zhou, X.; Zhao, D.; Lu, G. Q.; Zou, J.; Yu, C., *J. Am. Chem. Soc.* **2007**, 129, 9044-9048.

In the case of the HSP mechanism the assembly occurs after condensation with the packing of robust composite micelles with condensed walls.

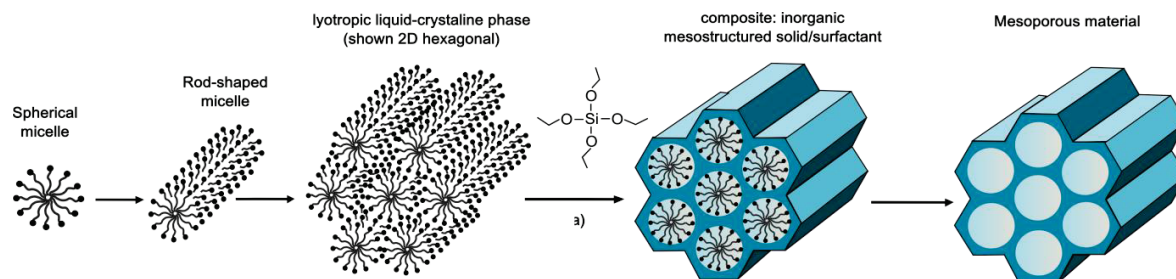


Figure 9. Formation of Mesoporous materials by structure-directing agents true liquid-crystal template mechanism

3.5. Strategies of preparation hybrid organic-inorganic materials

3.5.1. Grafting

In order to efficiently immobilize homogeneous complexes onto supports, several methods can be used. The most general and easy method is called “the post grafting” and it relies on the modification of the inner and the outer surfaces of an oxide with silane reagents containing the complex of interest or a precursor of the complex (a ligand or an organometallic fragment). Of the silanes, the most widely used are organotrialkoxysilanes $(R'O)_3SiR$, chlorosilanes $ClSiR_3$ or disilazanes $HN(SiR_3)_2$ which readily react with surface hydroxyl groups generating alcohol, HCl or NH_3 respectively as the side products (Figure10 Method B). Using this process a wide range of functional groups were efficiently introduced. This post- grafting approach is widely used as it is quite simple, straightforward and in some cases do not have efficient alternatives. However it also has some drawbacks. One of them is the non-homogeneous repartition of the organic fragments throughout the oxide surface. Such non-homogeneity occurs when organosilanes react preferentially in the entrance to the pore and the further diffusion of reagent inside the pore become limited. In extreme cases it can lead to a pore blocking.⁷⁴ The second drawback is the non-control of the structure of the grafted silicon species: the surface silane species can be attached to the surface *via* one, two or three (less likely) Si-O-Si bonds. This lack of control leads

⁷⁴ Hoffmann, F.; Cornelius, M.; Morell, J.; Froba, M., *Angew. Chem. Int. Ed.* **2006**, 45 (20), 3216-3251.

to several surface species and to an ill-defined environment around the metal center that can influence the catalytic activity of the final solid.⁷⁵

3.5.2. Direct synthesis

The alternative method to grafting consists on the introduction of the targeted organic or organometallic fragment directly during the synthesis of the material (here silica) by sol-gel process. This method therefore relies on the simultaneous hydrolysis and co-condensation of a tetraalkoxysilane compound $(\text{RO})_4\text{Si}$ (usually TEOS or TMOS) with a trialkoxyorganosilane $(\text{R}'\text{O})_3\text{SiR}$ precursor in the presence of a structure directing agent, that leads to formation of a well-structured functionalized silica in which the organic functionalities are covalently attached to the pore walls through three Si-O linkage. This synthesis can be performed without any SDA, however the control of the organic fragment-distribution is not secured. As organic functionalities are directly incorporated into the silica matrix the pore blocking is impossible, while the functionalities are homogeneously distributed along the silica pore channels (Figure10, method A).⁶⁶ However, this method also has its drawbacks. The loading of organic cannot normally overpass a certain level otherwise the formation of a non structured silica matrix is observed. Moreover, the increase of $(\text{R}'\text{O})_3\text{SiR}$ content can lead a partial embedding of organic functionalities inside the pore wall due to $(\text{R}'\text{O})_3\text{SiR}$ homocondensation processes.⁶⁶ Another drawback of this method is that mainly hydrophobic functionalities can be easily introduced. In the case of polar groups like amines, their interactions with the apolar micelle core are not favored and this leads to the formation of an unstructured material. In the specific case of amine groups, R.J.P. Corriu et al. proposed to protect polar amines with Boc groups to decrease their polar character.⁷⁶ The main way to overcome the problem of unsuccessful introduction of hydrophilic organic group is the preparation of platform materials containing easy transformable groups such as halogenoalkanes^{77,78} or azido groups.⁷⁹

⁷⁵ Conley, M. P.; Copéret, C.; Thieuleux, C., *ACS Catal.* **2014**, 4 (5), 1458-1469.

⁷⁶ Mehdi, A.; Reye, C.; Brandes, S.; Guillard, R.; Corriu, R.J.P., *New J. Chem.* **2005**, 29, 965-968.

⁷⁷ Corriu, R.J.P. ; Mehdi, A. ; Reye, C. ; Thieuleux, C., *Chem.Mater.* **2004**, 16, 159-166.

⁷⁸ Alauzun, J.; Mehdi, A.; Reye, C.; Corriu, R., *New J. Chem.* **2007**, 31, 911-915.

⁷⁹ Nakazawa, J.; Stack, T.D.P., *J. Am. Chem. Soc.* **2008**, 130 (44), pp 14360–14361.

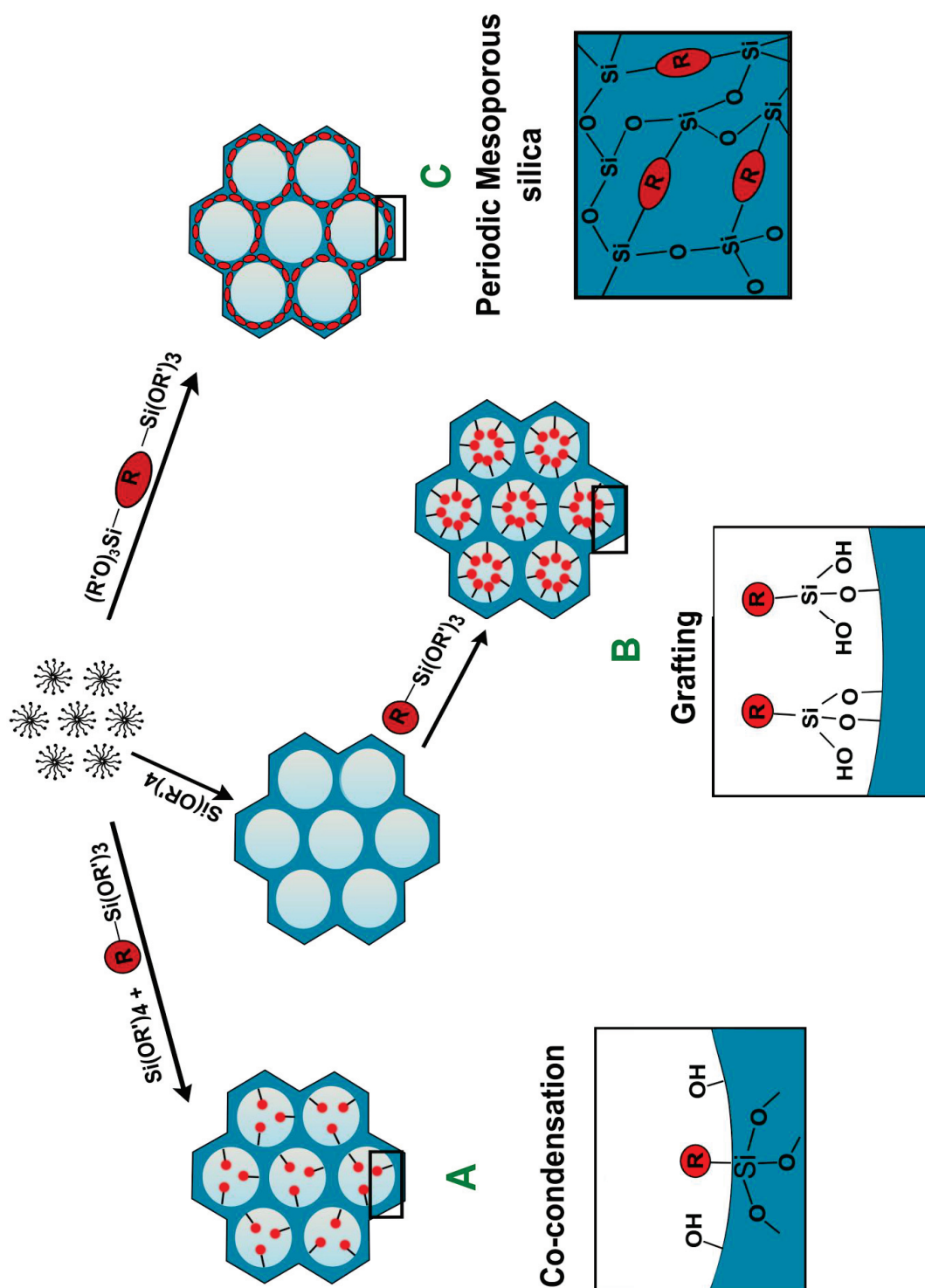


Figure 10. Strategies of preparation hybrid organic-inorganic materials

Chapter 1

Despite these aforementioned drawbacks, this method was successfully used for catalysts design and allowed to prepare well-defined supported species even with sensitive organometallic complexes.^{80, 67}

3.5.3. Periodic Mesoporous Organosilica

The particular case of direct synthesis approach is hydrolysis and polycondensation of bridged organosilanes $[(R'O)_3Si]_m-R$ ($m \geq 2$) with or without TEOS precursor in the presence of SDA that results in formation of Periodic Mesoporous Organosilicas (PMOs). The organic fragment in PMOs is located in the framework of mesoporous silica through covalent Si-C bonds and density of the organic groups is very high. The PMOs have high density of the organic groups, surface area (up to $1800\text{m}^2/\text{g}$) and thermal stability. However PMOs often have less ordered porous system with larger pore size distribution. The discovery of PMOs opened up an extraordinary field of investigation, as the properties of framework (optical, electronic and magnetic) can be tailored by changing the nature of the bridging organic group R.⁶⁷

3.5. Ir supported catalysts

The first iridium supported catalyst was immobilized in montmorillonite clay via an ion-exchange procedure. While the initial activity of this supported catalyst for the cyclohexene hydrogenation was 50-80% of its homogeneous analogue, it remained active for a longer period. This increase of catalyst life time may be related to the decrease of decomposition through cluster formation.⁸¹

The grafting method was also applied for immobilization of organometallic complexes onto mesoporous silica matrix. The synthesis can be carried out in two steps: synthesis of mesoporous silica and subsequent anchoring of a silylated organometallic complex through the reaction with surface silanols but in some case, the grafting of the ligand on the support is preferred and the further metal precursor coordination is achieved. As an example, F. Sanchez and coworkers proposed three different ways of chiral triaza Rh(I) and Ir(I) complexes immobilization onto

⁸⁰ D. Margolese, J. A. Melero, S. C. Christiansen, B. F. Chmelka, and G. D. Stucky, *Chem. Mater.* **2000**, *12*, 2448-2459.

⁸¹ Crocker, M.; Herold, R. H., *Catal. Lett.* **1993**, *18*, 243-251.

Chapter 1

MCM-41 and SBA-15 supports (Figure).⁸² Usually the multiple-step processes (Scheme B and C, Figure 11) are more widely used as they allow a more homogeneously distributed species. Such homogeneous distribution arises from the easier diffusion of small molecules inside the pores. The one step process (Scheme A, Figure 11) is preferred if the silane precursor containing the complex is easy to make and if the complex size is small enough to diffuse into the silica matrix. However the side process leading to homocondensation of organometallic complex is still possible if the synthesis is not carried out in very dry conditions.

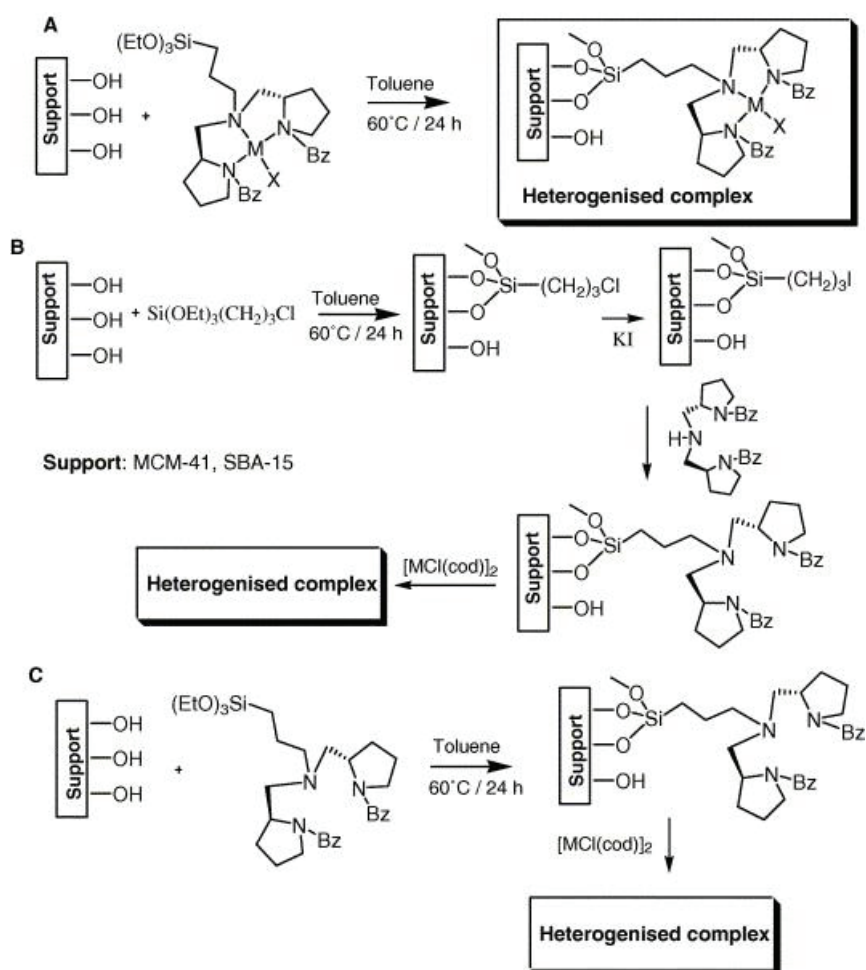


Figure 11. Hydrogenation strategies realized by grafting approach.

⁸² González-Arellano, C.; Corma, A.; Iglesias, M.; Sánchez, F., *Inorg. Chim. Acta.* **2004**, 357 (10), 3071-3078.

Chapter 1

The activities of Rh(I) and Ir(I) immobilized species were compared with their homogeneous analogues in the catalytic hydrogenation of 1,2-benzylidene succinate. In these specific cases, the turnover numbers increased after heterogenization of the complexes.⁴⁸

The similar improvement of the catalytic activity was also observed by X.-F. Hou and co-workers in case of SBA-15 heterogenized NHC–iridium (III) based catalysts for the N-alkylation of amines and β -alkylation of secondary alcohols with primary alcohols. The reason of this enhancement is not described.⁸³

The aforementioned examples are quite rare because many literature precedents reported poorer “heterogeneized” catalysts (prepared by grafting or intercalation approaches) in comparison with their homogeneous equivalents. We hypothesized that this decrease of activity was due to a lack of control of the metal surface species and the metal distribution.

Another example of significant enhancement of catalytic activity in ketones asymmetric hydrogenation by Imidazolium-based organoiridium-functionalized periodic Mesoporous silica was reported by G. Liu. In this case, a three fold increase of catalytic rate was explained by combination of imidazolium-functionality with high hydrophobicity of ethylene-bridged organosilicate.⁸⁴

The last example reporting the superior activity of an iridium supported complex over homogeneous analogue was developed by R. Menendez in 2013. The Ir(COD)Cl complex was covalently anchored to the imidazolium-functionalized carbon nanotubes. The heterogeneous catalyst was tested in hydrogen-transfer reduction of cyclohexanone to cyclohexanol with iPrOH as a hydrogen source and was found to be more efficient than the related homogeneous catalysts, but no explanation was given.⁸⁵

⁸³ Wang, D.; Guo, X.-Q.; Wang, C.-X.; Wang, Y.-N.; Zhong, R.; Zhu, X.-H.; Cai, L.-H.; Gao, Z.-W.; Hou, X.-F., *An Adv. Synth. Catal.* **2013**, 355 (6), 1117-1125

⁸⁴ Deng, B.; Xiao, W.; Li, C.; Zhou, F.; Xia, X.; Cheng, T.; Liu, G., *J. Catal.* **2014**, 320, 70-76.

⁸⁵ Blanco, M.; Álvarez, P.; Blanco, C.; Jiménez, M. V.; Fernández-Tornos, J.; Pérez-Torrente, J. J.; Oro, L. A.; Menéndez, R., *ACS Catal.* **2013**, 3 (6), 1307-1317.

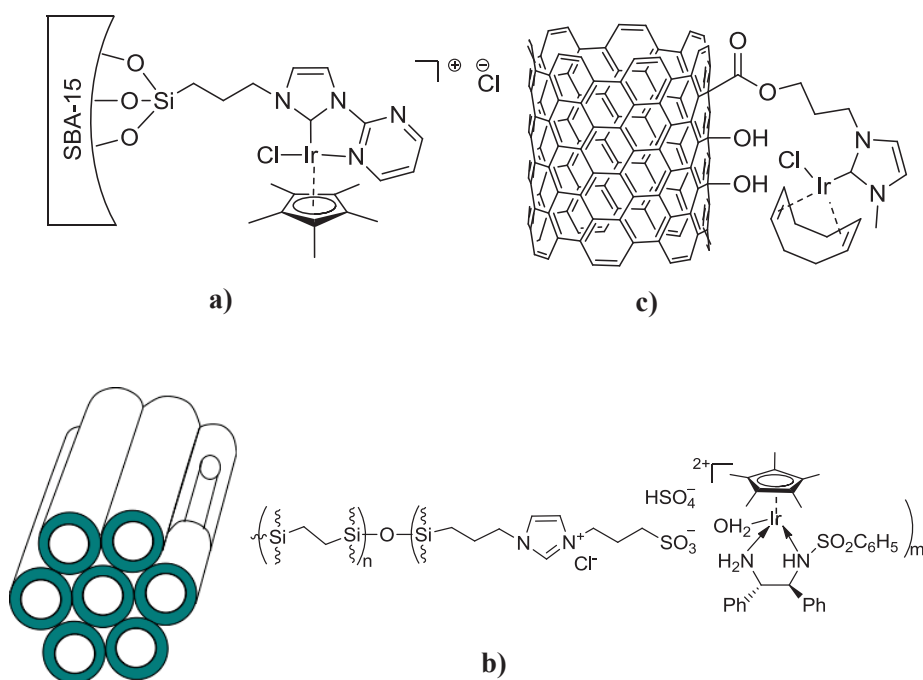


Figure 12. Examples of iridium supported complexes that shows higher catalytic activity in comparison to homogeneous analogues

However there are much more examples of Iridium supported catalyst where no increase or even decrease of catalytic activity were shown^{86, 87, 88, 89} Of these results, one may mention the work of H.-U. Blaser et al. which compared the catalytic activity of an immobilized Ir-diphosphine catalyst onto porous silica and polystyrene with homogeneous analogues in enantioselective imine hydrogenation. As a result, the immobilized catalyst gave the same enantioselectivities but lower activities and higher deactivation rates than homogeneous analogues. These negative effects were explained by high local catalyst concentration on the support leading to the increased tendency to deactivation. The activity of polystyrene immobilized catalyst was even lower than for the porous analogue.⁹⁰

⁸⁶ Liu, G.; Yao, M.; Wang, J.; Lu, X.; Liu, M.; Zhang, F.; Li, H., *Adv. Synth. Catal.* **2008**, 350 (10), 1464-1468.

⁸⁷ Sahoo, S.; Kumar, P.; Lefebvre, F.; Halligudi, S., *J. Catal.* **2008**, 254 (1), 91-100

⁸⁸ Shen, Y.; Chen, Q.; Lou, L.-L.; Yu, K.; Ding, F.; Liu, S., *Catal. Lett.* **2010**, 137 (1-2), 104-109.

⁸⁹ Lou, L.-L.; Du, H.; Shen, Y.; Yu, K.; Yu, W.; Chen, Q.; Liu, S., *Microporous Mesoporous Mater.* **2014**, 187, 94-99.

⁹⁰ Pugin, B.; Landert, H.; Spindler, F.; Blaser, H.-U., *Adv.Synth.Catal.* **2002**, 344, 974-979

Chapter 1

In order to secure the homogeneous distribution of organic groups onto surfaces, sol-gel strategies using SDA were implemented for hybrid materials preparation. In this area, our group developed the preparation of hybrid organic-inorganic mesostructured material containing 0,4mmol/g of functionalities i.e. one organic group per nm². This methodology implies the preparation of a mesostructured platform material with reactive functionalities such as halogenopropyl-fragments or halogenobenzyl-groups or azidopropyl-chain that were in-situ transformed into imidazolium salts and then into silver carbene. The AgOC(CF₃)₃ was found to be the best silver reagent to yield quantitatively the supported silver carbene due to its high solubility in organic solvents.

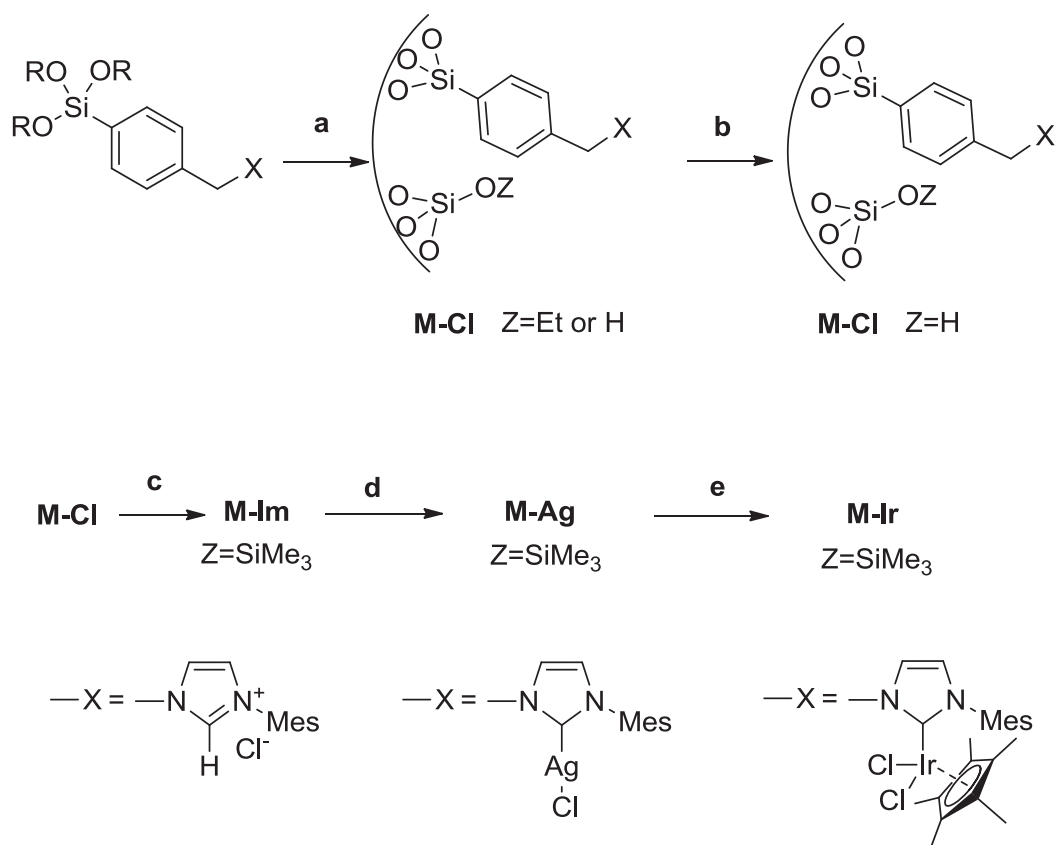


Figure 13. Preparation of Ir(III)-NHC based well-defined material (**M-Ir**): a) TEOS, HCl, Pluronic P123, room temperature; b) 2M HCl/H₂O, 45°C; c) mesitylimidazole, toluene, reflux, 2 days, then TMSBr, Et₃N, toluene, room temperature, 48h; d) AgOC(CF₃)₃, CH₃CN, 14h, room temperature; e) [Cp*IrCl₂]₂, 24h, 60°C.

Chapter 1

Using this silver route, the quantitative immobilization of Ir(III)-Cp*Cl₂ complex was achieved. The catalyst was tested in H/D exchange reaction of acetone with methanol[d₄] and showed comparable activities with homogeneous analogues.^{91,92}

Two years later, Li and co-workers synthesized a chiral Ir supported complex by a direct synthesis approach. However the N-sulfonylated diamine-based η^5 -Cp*-Ir supported complex didn't show superior activity over homogeneous counterparts in asymmetric ketone hydrogenation.⁹³ The immobilization of organoiridium(I) species onto metal organic framework UiO-66-NH₂ was also carried out. The catalyst preparation used to the tree-step approach : i) the UiO-NH₂ thermal synthesis, ii) the anchoring of imino-ligands trough condensation between the amine group of UiO and the aldehyde group of the ligand and iii) the coordination of Ir using [Ir(COD)Cl]₂ as precursor. The as-obtained catalyst which combines Lewis acid sites (Zirconium) and Iridium sites was able to hydrogenate aromatics under mild conditions (6 bars of H₂, T=60°C). Noteworthy, the hydrogenation of aromatics in mild conditions was already reported with Ir nanoparticles but not with organometallic complexes. In this literature presented the influence of substituent's electronic properties onto hydrogenation rate was also studied: substrates with electron donating groups were hydrogenated faster than those with electron withdrawing groups.⁹⁴

I-4 Strategy

4.1. Objectives

As described above, NHC-analogues of Crabtree's catalyst are among the most active and selective alkene hydrogenation catalysts. However these catalysts have the tendency to deactivate via bimolecular processes. The immobilization of such complexes was therefore undertaken to

⁹¹ Maishal, T. K.; Alauzun, J.; Basset, J. M.; Coperet, C.; Corriu, R. J.; Jeanneau, E.; Mehdi, A.; Reye, C.; Veyre, L.; Thieuleux, C., *Angew. Chem. Int. Ed.* **2008**, 47 (45), 8654-8656.

⁹² Maishal, T. K.; Boualleg, M.; Bouhrara, M.; Copéret, C.; Jeanneau, E.; Veyre, L.; Thieuleux, C., *Eur. J. Inorg. Chem.* **2010**, (31), 5005-5010.

⁹³ Liu, G.; Wang, J.; Huang, T.; Liang, X.; Zhang, Y.; Li, H., *J. Mater. Chem.* **2010**, 20 (10), 1970.

⁹⁴ Rasero-Almansa, A. M.; Corma, A.; Iglesias, M.; Sánchez, F., *Green Chem.* **2014**, 16 (7), 3522-3527.

Chapter 1

provide more robust catalysts however only a little number of publications reported an increase of the catalytic performances for the supported systems.

In this context, we decided to study the isolation of Ir-NHC complexes onto tailored hybrid silica surfaces as a way to generate highly active heterogeneous hydrogenation catalysts.

4.2. Formation of the Ir-NHC catalytic material

The design of the supported system for hydrogenation took into account several parameters (fig. 14) :

- i) the nature of the metal : Ir was chosen because literature precedents showed the high activity of Ir complexes (iridium based Crabtree's catalyst)
- ii) the tuning of the coordination sphere : NHC ligand was chosen as a promising alternative to phosphine (more stable and versatile architecture).
- iii) the anchoring of the Ir complex : Ir was coordinated to covalently immobilized NHC ligands because Ir-NHC bond should be strong enough to avoid Ir leaching during catalysis..
- iv) the choice of the support : in order to secure the regular distribution and the isolation of Ir-NHC supported sites on oxide support, an hybrid organic-inorganic support was prepared by sol-gel process using a templating route. The loading of organic groups (here iodopropyl fragments) was set at 0,4 mmol/g in order to avoid a close vicinity between the organic groups. The sol-gel experimental conditions were chosen to yield a SBA-15 type material (2D hexagonal arrangement of the pore channels) with big pores (ca 7 nm) in order to avoid at maximum mass transfer limitations.. This strategy was elaborated in our lab and was already successively applied to Pd(II)⁹⁵, Ru(IV)^{96, 97, 98}, Ir(III)^{63, 64}.

⁹⁵ Conley, M. P.; Drost, R. M.; Baffert, M.; Gajan, D.; Elsevier, C.; Franks, W. T.; Oschkinat, H.; Veyre, L.; Zagdoun, A.; Rossini, A.; Lelli, M.; Lesage, A.; Casano, G.; Ouari, O.; Tordo, P.; Emsley, L.; Coperet, C.; Thieuleux, C., *Chem. Eur. J.* **2013**, 19 (37), 12234-8.

⁹⁶ Karame, I.; Boualleg, M.; Camus, J. M.; Maishal, T. K.; Alauzun, J.; Basset, J. M.; Coperet, C.; Corriu, R. J.; Jeanneau, E.; Mehdi, A.; Reye, C.; Veyre, L.; Thieuleux, C., *Chem. Eur. J.* **2009**, 15 (44), 11820-3.

⁹⁷ Baffert, M.; Maishal, T. K.; Mathey, L.; Coperet, C.; Thieuleux, C., *ChemSusChem* **2011**, 4 (12), 1762-5.

⁹⁸ Kavitate, S.; Samantaray, M. K.; Dehn, R.; Deuerlein, S.; Limbach, M.; Schachner, J. A.; Jeanneau, E.; Coperet, C.; Thieuleux, C., *Dalton Trans.* **2011**, 40 (46), 12443-6.

Chapter 1

v) a flexible propyl tether was chosen in order to allow silica-metal interactions. Indeed, we recently found that surface-metal interactions were key for catalyst lifetime and rate in the case of Ru-NHC supported systems.⁹⁹

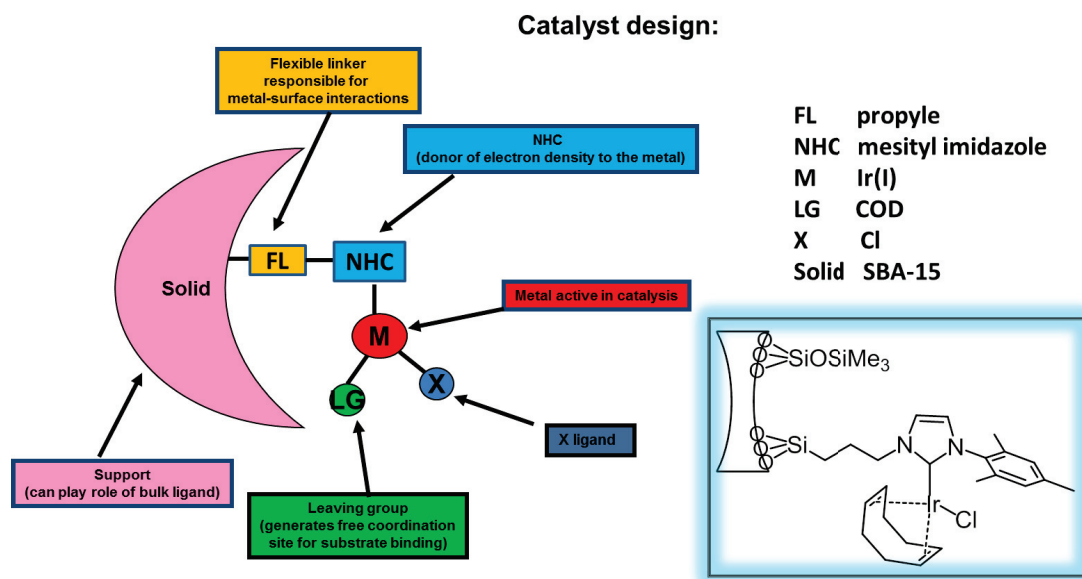


Figure 14. Strategy of hydrogenation catalyst design

In term of methodology, the coordination of Ir on the solid will be achieved through transmetallation with Ag-NHC supported complexes because this route was found more effective than a classical deprotonation of imidazolium units.¹⁰⁰ The supported systems will be tested in the hydrogenation of different substrates and their catalytic performances will be compared to those of homogeneous complexes with the same molecular structure.

⁹⁹ Samantaray, M. K.; Alauzun, J.; Gajan, D.; Kavitate, S.; Mehdi, A.; Veyre, L.; Lelli, M.; Lesage, A.; Emsley, L.; Coperet, C.; Thieuleux, C., *J. Am. Chem.Soc.* **2013**, 135 (8), 3193-3199.

¹⁰⁰ Maishal, T. K.; Alauzun, J.; Basset, J. M.; Coperet, C.; Corriu, R. J.; Jeanneau, E.; Mehdi, A.; Reye, C.; Veyre, L.; Thieuleux, C., *Angew. Chem. Int. Ed.* **2008**, 47 (45), 8654-6.

Chapter 2

Synthesis and characterization Ir(I)-NHC based hybrid material

Table of content

II-1. Introduction.....	49
II-2. Formation of Ir(I)-NHC model molecular complex	51
II-3. Formation of Ir(I)-NHC hybrid material.....	56
3.1. Grafting of $[\text{Ir}(\text{cod})\text{Cl}]_2$ on a 1-propyl-3-mesityl-imidazolium functionalized hybrid material.....	56
3.2. Formation of the Ir-NHC material from a ^{13}C enriched imidazolium in carbenic position	61
3.3. Advance technics in material characterization.....	63
3.3.1. Introduction	63
3.3.2. 2D NMR of ^{13}C enriched material	63
3.3.3. DNP NMR.....	69
3.3.4. In situ liquid NMR under hydrogen pressure	77
II-4. Conclusions.....	78
II-5. Experimental section	79
5.1. General procedures.....	79
5.2. Synthesis of molecular complexes	80
5.3. Synthesis of materials.....	82
II-5. Appendix.....	84

List of Figures

Figure 1. Selective formation of tantalum-silica monopodal species	49
Figure 2. ^1H NMR of $[\text{AgI}(\text{MesImPr})]$ and $[\text{IrCl}(\text{MesImPr})(\text{COD})]$	52
Figure 3. ^1H - ^{13}C HMQC NMR spectrum of $[\text{IrCl}(\text{COD})(\text{MesImPr})]$ 1 in C_6D_6	53

Chapter 2

Figure 4. Crystal structure of [IrCl(MesImPr)(COD)] defined by X-Ray diffraction	54
Figure 5. XRD pattern of M-Ir.	58
Figure 6. TEM micrograph of M-Ir.	58
Figure 7. ^1H and ^{29}Si CPMAS NMR of M-Ir.	60
Figure 8. ^{13}C CPMAS NMR of M-Ir.	61
Figure 9. ^{13}C CPMAS NMR of labelled silver M*-Ag and iridium M*-Ir materials.	62
Figure 10. ^1H - ^{13}C HETCOR NMR spectrum of M*-Im with short and long distance correlations	65
Figure 11. ^1H - ^{13}C HETCOR NMR spectra of M*-Ag and M*-Ir.	67
Figure 12. Block-scheme of solid state DNP spectrometer.....	69
Figure 13. Pulse sequence for ^{13}C DNP NMR	70
Figure 14. Comparison ^{13}C (a) and ^{29}Si DNP NMR with the routine CP MAS technique. ..	70
Figure 15. DNP ^{13}C CPMAS NMR of M-Ir.....	71
Figure 16. 2D ^1H - ^{13}C HETCOR spectrum of M-Ir acquired with long contact time (0.5 ms) under DNP conditions.	72
Figure 17. 2D ^1H - ^{29}Si HETCOR DNP NMR of M-Ir acquired with short and long contact time	73
Figure 18. Determination quantity of COD by <i>in situ</i> liquid NMR under hydrogen pressure	75
Figure 19. STEM micrographs and EDX of the recovered solid after 94 hours under H_2 in C_6D_6 and toluene as internal standard.	77

List of Schemes

Scheme 1 Formation of $[\text{Ir}(\text{cod})\text{Cl}]_2$ by transmetallation	51
Scheme 2. Formation of Ir(I)-NHC hybrid material.....	57

List of Figures in Appendix

Figure A1. ^{13}C NMR of $[\text{IrCl}(\text{MesImPr})(\text{COD})]$	84
Figure A2. ^{13}C dept135 NMR of $[\text{IrCl}(\text{MesImPr})(\text{COD})]$	84
Figure A3. ^1H - ^1H COSY NMR of $[\text{IrCl}(\text{MesImPr})(\text{COD})]$	85
Figure A4. ^1H NMR of $[\text{AgI}(\text{MesImPr})]$ and $[\text{IrCl}(\text{MesImPr})(\text{COD})]$	85
Figure A5. ^1H NMR of M-Im	86
Figure A6. ^{13}C NMR of M-Im	86
Figure A7. ^{29}Si NMR of M-Im	87
Figure A8. ^{13}C NMR of M*-Im	87

Chapter 2

II-1 Introduction

Easy separation, recovery and recycling make heterogeneous catalysts attractive for industrialization. Despite these previously mentioned advantages, heterogeneous catalysts are often inferior to their homogeneous counterparts in term of catalytic activity and especially selectivity.¹⁰¹ Such decrease in catalytic activity and selectivity is associated with a broad spectrum of active sites, independently existing on the catalyst surface, each with their own energetics, activity and selectivity.

On the contrary, homogeneous molecular catalysts (when they operate under ideal conditions) have molecularly defined and their activity/selectivity can be controlled by the control the coordination sphere. In order to combine the high selectivity and activity of homogeneous catalyst with the simple separation and recycling of heterogeneous catalysts, single-site heterogeneous catalysts (SSHC) approach was introduced.¹⁰² Single-site heterogeneous catalysts possess the advantages of classical solid catalysts, in terms of separation and recycling, together with a defined tailored chemical and steric environment around the catalytically active metal site. Thus, such type of catalyst is easy to separate and they have exhibit well-defined active sites. The pioneer in the field of SSHC development was J.M. Basset, who first started the development of catalytic systems based on the grafting of early transition metal complexes or metalloids (Ti, Se, Fe, Ge, Sn, Rh, etc) on flame silica nanoparticles (Aerosil silica). This methodology is called surface-organometallic chemistry (SOMC) and relies on producing SSHC by reaction of a metal complex with residual surface silanol groups ($\equiv\text{SiOH}$). As an example, the monopodal tantalum species were generated by grafting of the $\text{Ta(=CHtBu)(CH}_2\text{tBu)}_3$ onto dehydroxylated at 700°C silica. (Fig1.).¹⁰³

Later, the same approach was applied for grafting organometallic precursors onto mesoporous silica.¹⁰⁴ Significant advances were obtained by Matchmeyer et al. who synthesized highly stable

¹⁰¹ Ertl, G.; Knözinger, H.; Schüth, F.; Weitkamp, J. Wiley-VCH Verlag GmbH & Co. KGaA, Weinheim, Germany, 2008, p.3865

¹⁰² Thomas, J. M.; Raja, R.; Lewis, D. W., *Angewandte Chemie* **2005**, 44 (40), 6456-6482.

¹⁰³ Lefort, L.; Chabanas, M.; Maury, O.; Meunier, D.; Coperet, C.; Thivolle-Cazat, J.; Basset, J.M.J. *Organomet. Chem.* **2000**, 593-594, 96-100.

¹⁰⁴ a) Corma, A.; Navarro, M. T.; Pariente, J. P., *J. Chem. Soc., Chem. Commun.* **1994**, 147; b) Sankar, G.; Rey, F.; Thomas, J.M.; Greaves, G. N.; Corma, A.; Dobson, B. R.; Dent, A. J., *J. Chem. Soc., Chem. Commun.* **1994**,

Chapter 2

epoxidation catalyst based on Ti(IV) species. This methodology was extended for grafting other transition metals as for examples Mo(VI), Cr(VI), VO(IV).¹⁰⁵ The same Ti(IV) SSHC was prepared by D. Tilley, Bell and co-workers using a different precursor route.¹⁰⁶

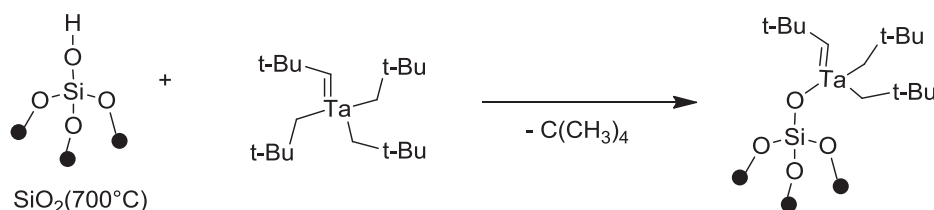


Figure 1. Selective formation of tantalum-silica monopodal species

Even if various complexes can be immobilized onto oxide supports *via* SOMC approach, this method is mainly limited to early transition metals for which the Metal-O-Si bond is strong. When shifting from early transition metal to late transition metals, such surface bonding is not strong enough to prevent metal agglomeration or leaching. As an example, the grafting of Ru complexes (Grubbs-Hoveyda II) onto silica led to unstable supported species due to the Si-O-Ru bond cleavage in presence of water traces.¹⁰⁷ In this context, we decided to perform the selective grafting of late transition metal complexes onto ligands that were introduced at the surface of silica frameworks. This methodology led to the development of Ru(IV)-, Pd(II)- and Ir(III)-NHC supported catalysts for metathesis reactions, semi-hydrogenation of alkynes and H/D exchange reactions respectively.

We decided to implement this methodology to the preparation of [IrCl(MesImPr)(COD)] single-site heterogeneous catalyst for hydrogenation reactions. The synthesis of an homogeneous [IrCl(MesImPr)(COD)] analogue was also performed for sake of comparison.

2279; c) Thomas, J. M., *Nature* **1994**, 368, 289-290; d) Tanev, P. T.; Chibwe, M.; Pinnavaia, T. J., *Nature* **1994**, 368, 321-323.

¹⁰⁵ T. Maschmeyer, F. Rey, G. Sankar, J.M. Thomas, *Nature* **1995**, 378, 159; b) P. E. Sinclair, G. Sankar, C. R.A. Catlow, J. M. Thomas, T. Maschmeyer, *J. Phys. Chem.B* **1997**, 101, 4232.

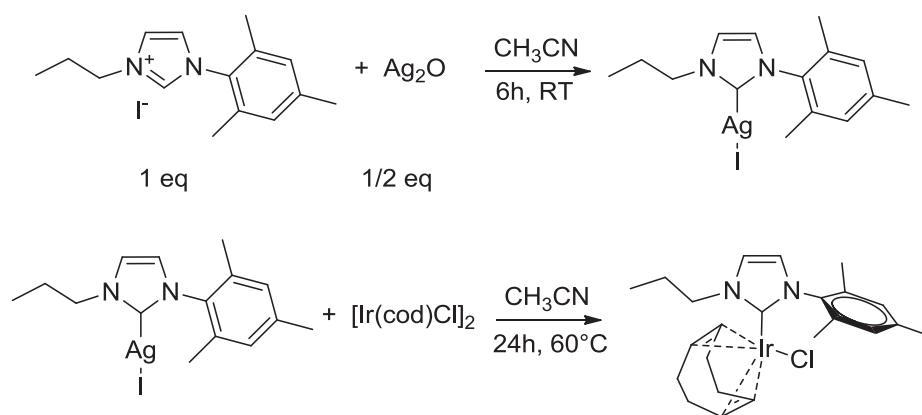
¹⁰⁶ a) Jarupatrakorn, J. D. Tilley, *J. Am. Chem. Soc.* **2002**, 124, 8380-8388; b) Fajdala, K. L.; Tilley, T.D., *J. Catal.* **2003**, 216, 265-275.

¹⁰⁷ Marciniak, B.; Rogalski, S. ; Potrzebowski, M. J.; Pietraszuk, C., *ChemCatChem* **2011**, 3, 904 – 910

II-2 Formation of Ir(I)-NHC model molecular complex

The synthesis of $[\text{IrCl}(\text{MesImPr})(\text{COD})]$ was performed in a two-step process using transmetallation for Ir introduction (Scheme1). The first step is the formation of the silver carbene using silver oxide (Ag_2O). Silver oxide was found to be a perfect reagent (basic and silver source) as well as commercially available and cheap. Moreover, the end of reaction can be visually detected: The reaction is complete when the solubilisation of the black silver oxide powder is complete. The as-obtained product was characterized by ^1H and ^{13}C NMR.

The next step is the transmetallation of silver carbene by $[\text{Ir}(\text{COD})\text{Cl}]_2$ followed by column purification and recrystallization with dichloromethane. It yields a yellow to orange crystals that were characterized NMR spectroscopy, ESI-MS and X-Ray diffraction (Fig. 4).



Scheme1. Formation of $[\text{Ir}(\text{cod})\text{Cl}]_2$ by transmetallation

The attribution of the ^1H NMR signals of $[\text{IrCl}(\text{MesImPr})(\text{COD})]$ was possible due to the combination of different NMR techniques (COSY, dept135 and ^1H - ^{13}C HSQC) and comparison with silver carbene ^1H NMR spectrum (Fig. 2). As shown in the spectra, new signals appear for $[\text{IrCl}(\text{MesImPr})(\text{COD})]$ compared to those of $[\text{AgI}(\text{MesImPr})]$: the wide splitted peaks in the region of 1.2-2.4 ppm, one intense signal (corresponding to 3 protons) at 2.57 ppm, two wide multiplets at 2.93 and 3.15 ppm, a new multiplet at 5.0 ppm and two singlets at 6.70 and 6.79 ppm. Comparison with ^1H NMR spectrum of the silver carbene allows to unambiguously attribute the terminal methyl group of the propyle chain **1'** at 0.79 ppm, one of the methyl groups from mesityl **8'** at 2.12 ppm and the imidazolydene protons **5'** and **4'** at 6.19 and 5.90 ppm. Based on signal integration, the methyl groups of mesityl in ortho and para positions were attributed.

Chapter 2

They give 3 different signals at 1.73, 2.11 and 2.56 ppm: the CH₃ in para position (**8'**) was attributed to the peak at 2.11 ppm and the two CH₃ in ortho position (**7'**) were attributed to the signals at 1.73 and 2.56 ppm. A signal splitting was also found for two aromatic protons, that give two separate signal at 6.68 and 6.77 ppm instead of one peak at 6.66 ppm as it was found for [AgI(MesImPr)]. The two signals at 3.98 and 4.83 ppm were attributed to methylene protons in alpha position of the imidazole ring (**3'**) and they integrate each as one proton where s only one signal (**3**) was present at 3.69 ppm for the Ag-NHC complex with an integration of two protons..

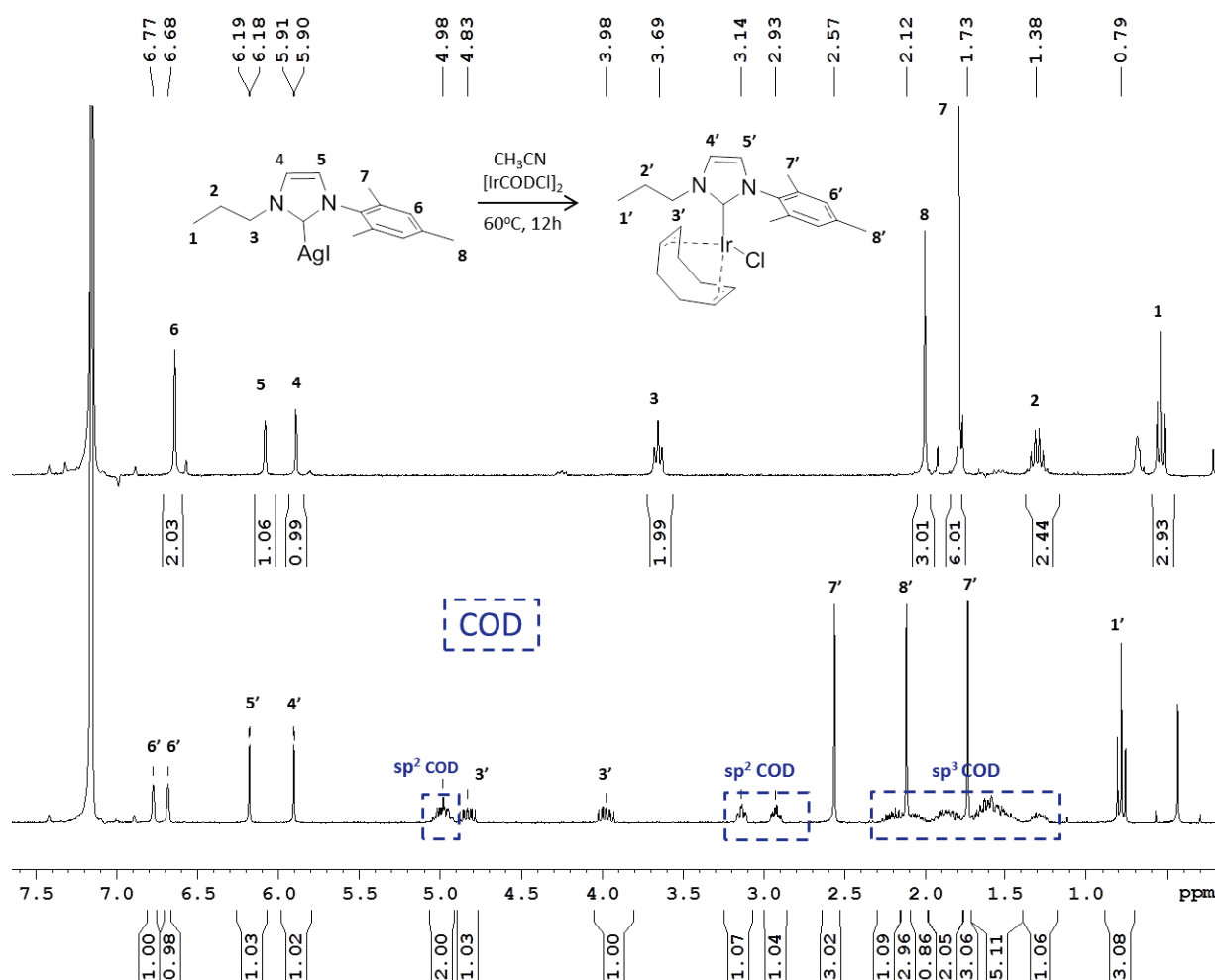


Figure 2. ¹H NMR of [AgI(MesImPr)] and [IrCl(MesImPr)(COD)]

The signals around 5 ppm usually corresponds to -CH- protons of COD (sp² COD) in trans position to the Chloride ligand , while the signals of -CH- protons of COD (sp² COD) that are in

Chapter 2

cis position usually appear at higher field around 3 ppm. The highest field shifted signals at 1.2-2.4 ppm correspond to CH₂ of COD (sp³ COD). The integration of all the signals gives 32 protons that is consistent with the formula of the expected [IrCl(MesImPr)(COD)] complex.

To shed light on the structure and define precisely methylene protons chemical shifts, ¹H-¹H COSY and ¹H-¹³C HSQC spectra were acquired. The results show that the methylene signals split into two multiplets at 3.98 ppm and 4.83 ppm.

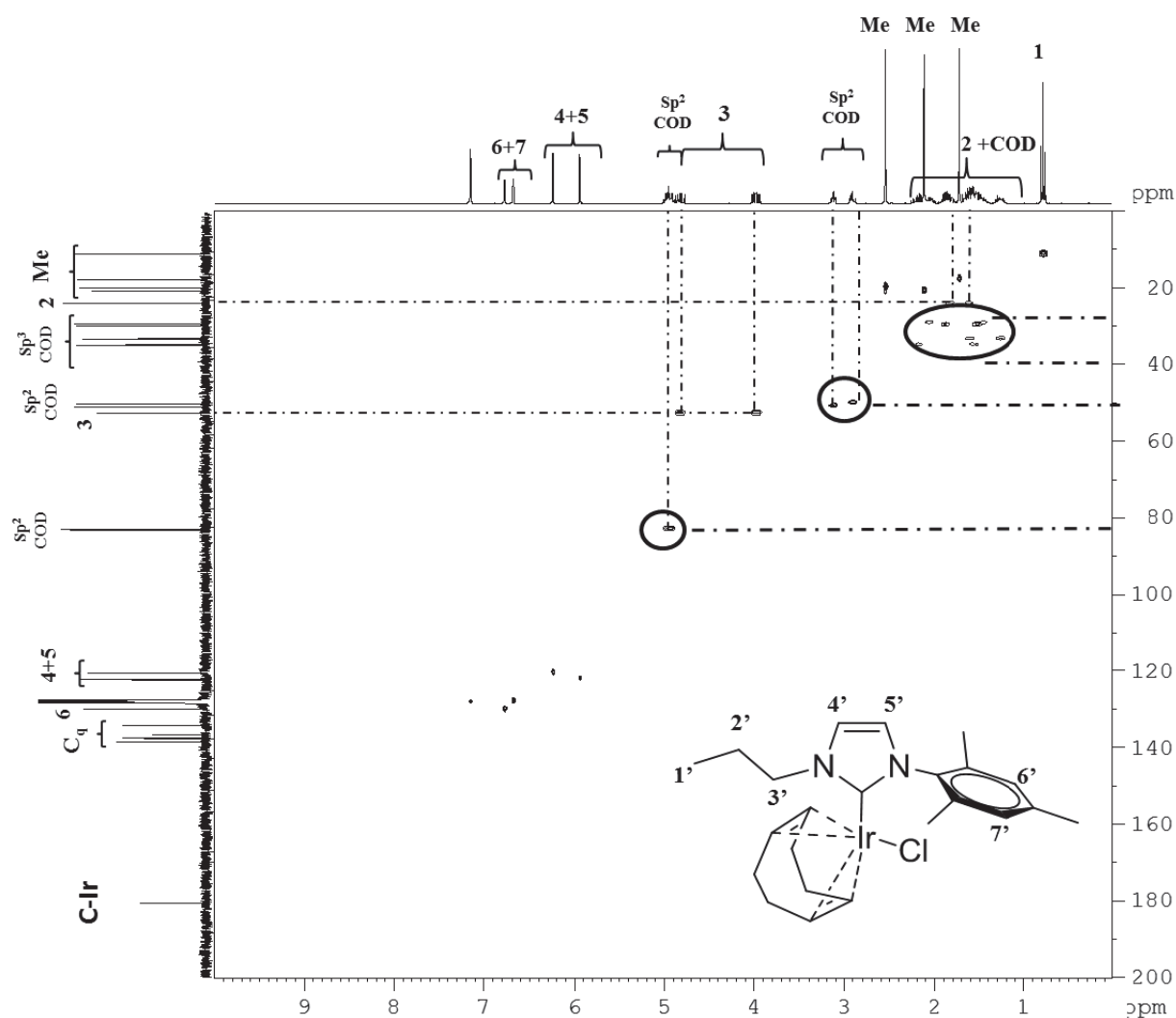


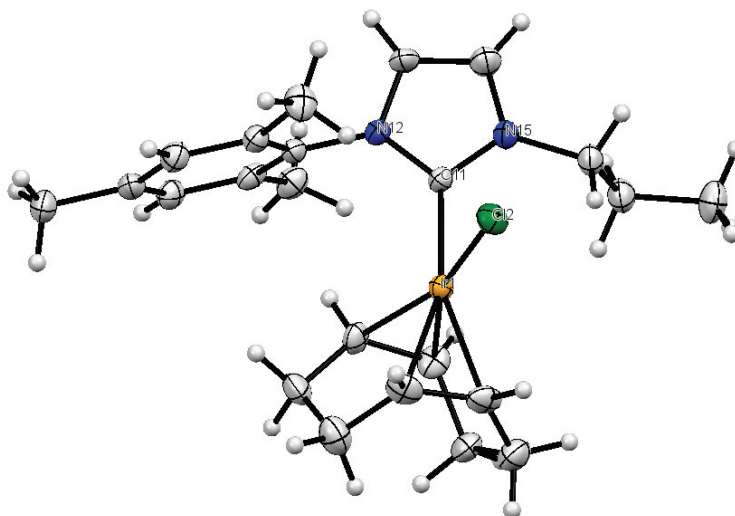
Figure 3. ¹H - ¹³C HSNMR spectrum of [IrCl(COD)(MesImPr)] 1 in C₆D₆. Correlations corresponding to COD are encircled.

Chapter 2

This kind of signal splitting after complexation was already noticed for Iridium complexes with bulky ligands and was explained by hindered rotation of the NHC ligand due to steric pressure brought by the ligand.

From ^1H - ^{13}C HSQC, the chemical shift of methylene group in beta position to N o (**2'**) was defined and fully confirmed the splitting of methylene protons in alpha position (**3'**) (Fig. 3). As expected, the CH_2 of COD appears at 29-35 ppm and the CH of COD at 50 ppm (cis to Cl) and around 80 ppm (trans to Cl). In comparison with ^{13}C NMR spectrum of $[\text{AgI}(\text{MesImPr})]$ in which the Carbene (C-Ag) signal is at 186.47ppm, the Carbene signal (C-Ir) is shifted and appears at 180.60ppm.

There are also 4 signals at 134.37; 136.53; 137.51 and 138.30 ppm related to quaternary carbons of mesityl ring, as expected.



Chapter 2

complexes having a COD ligand.¹⁰⁸ The bond angle observed at the carbene center (N12-C11-N15 103.4°) is in a good agreement with that reported for mono-N-heterocyclic carbene.¹⁰⁹

¹⁰⁸ Nanchen, S.; Pfaltz, A., *Chem. Eur. J.* **2006**, 12, 4550 – 4558.

¹⁰⁹ Bourissou, D.; Guerret, O.; Gabbaie, F. P.; Bertrand, G., *Chem. Rev.* **2000**, 100, 39 – 91.

II-3 Formation of Ir(I)-NHC hybrid material

3.1 Grafting of [Ir(cod)Cl]₂ on a 1-propyl-3-mesityl-imidazolium functionalized hybrid material

The synthesis of the targeted catalytic material containing Ir(I)-NHC sites was performed in accordance with known procedures from our group, starting from a material containing iodopropyl-fragments, namely **M-I**.¹¹⁰ **M-I** was prepared by co-hydrolysis and co-condensation of 1 equivalent of iodopropyltriethoxysilane and 30 equivalents of tetraethoxysilane (also named tetrathylorthosilicate, TEOS) in the presence of a triblock copolymer, Pluronic P123, as the structure-directing agent in aqueous acidic conditions (Scheme2, step a). The surfactant removal from the material was performed by soxhlet extraction using hot ethanol. The imidazolium groups were further introduced by subsequent treatment of the iodopropyl-containing material with an excess of mesitylimidazole (Scheme2, step b). To prevent side reactions between surface silanols or alcoxysilane and the basic silver precursor, the quantitative transformation of silanols into trimethylsilyl-groups (TMS groups) was carried out using a two-step process (Scheme 2, step c and d) leading to **M-Im** material. **M-Im** was prepared by hydrolysis of surface alcoxysilanes groups into silanols using hydroiodic acid and subsequent transformation of silanols into TMS groups using Me₃SiBr/NEt₃ in toluene at room temperature (Scheme2, step c and d).

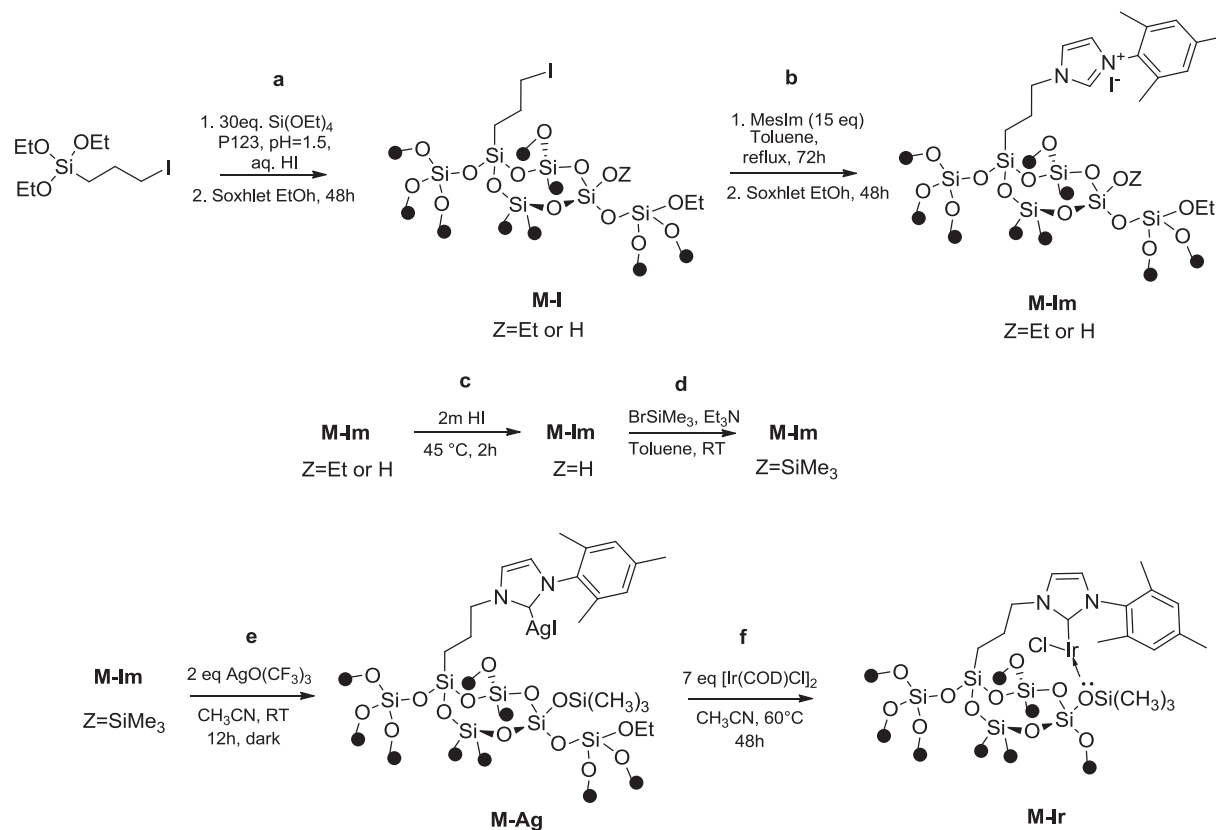
The as-obtained **M-Im** material was fully characterized by elemental analyses, N₂ adsorption/desorption analysis (Appendix A4), ¹H, ¹³C, ²⁹Si solid-state NMR spectroscopy (Appendix A5-7).

M-Im was then converted into **M-Ag** by treatment with 1.5 equivalent of AgOC(CF₃)₃ at 25°C for 15h in the absence of light. Through transmetallation with [Ir(COD)Cl]₂ (7 equiv) at 60°C during 48h, **M-Ag** was converted into **M-Ir**. A brown powder was obtained and characterized by elemental analyses, X-Ray powder diffraction, HR-TEM and ¹H, ¹³C, ²⁹Si NMR. Elemental analyses of the resulting solid gave iridium, silicon, nitrogen and silver contents of 2.57%, 33.7%, 0.79% and 3.91% respectively. These data correspond to 0.013mmol of Ir, 0.056 mmol of N or 0.027 mmol of NHC par gram of solid and to a transmetallation yield of 49%. The quantity

¹¹⁰ Alauzun, J.; Mehdi, A.; Reye, C.; Corriu, R., New J. Chem. 2007, 31, 911-915.

Chapter 2

of silver (0.036mmol) that is twice bigger than the imidazolium loading suggests the formation of silver or silver halides aggregates at the surface of the materials.



Scheme 2. Formation of Ir(I)-NHC hybrid material

The well-defined 2D-hexagonal porous structure of **M-Ir** was proved by small angle XRD and TEM. As seen from Fig. 5, the XRD pattern exhibits an intense peak at $2\theta = 0.82^\circ$ that correspond to the (100) plane. According to the Bragg's law, the calculated interplane distance is 98 Å. There is also small reflection coming from (110) plane at $2\theta = 1.6^\circ$.

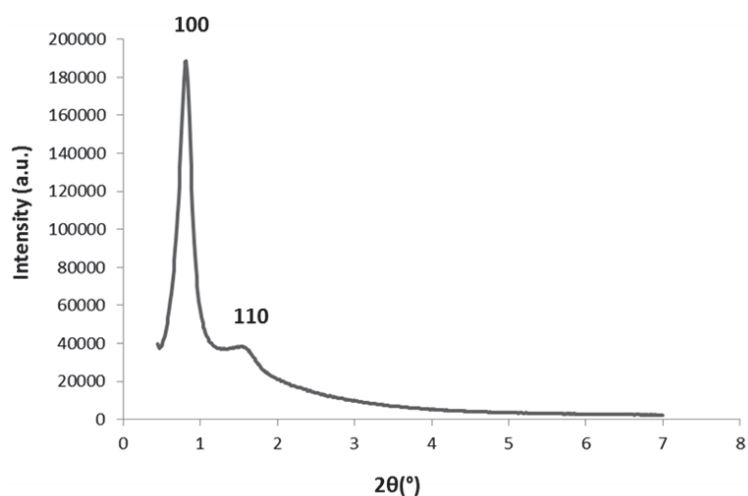


Figure 5. XRD pattern of M-Ir.

Noteworthy, the presence of Iridium nanoparticles was not detected by HR-TEM.

The ^1H NMR of the obtained material (Fig. 7a) is not very informative. It however shows intense peaks at 0 ppm corresponding to SiMe_3 groups and low intense peaks at 2, 3 and 7 ppm. The peak at 3 ppm can correspond to physically absorbed water that usually diffuse inside the rotor during the analysis and/or sample preparation or to residual $-\text{OMe}$ surface groups. The peaks at 2 and 7 ppm were attributed respectively to the alkyl-chains and aromatics.

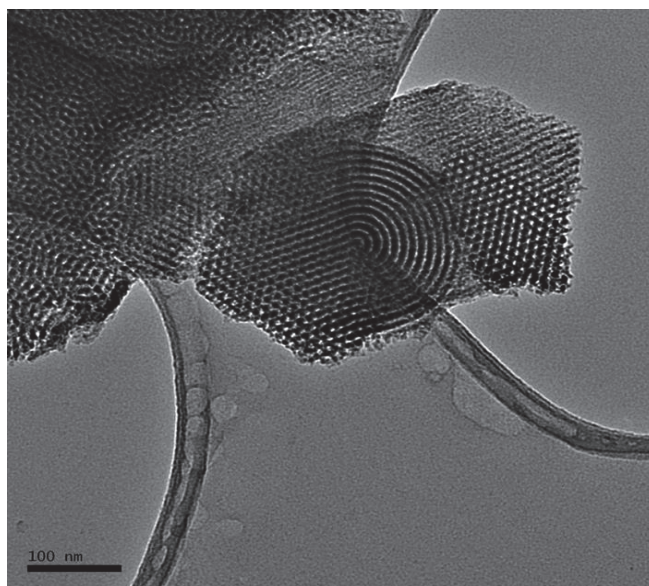


Figure 6. TEM micrograph of M-Ir

Chapter 2

The ^{29}Si CPMAS NMR of **M-Ir** shows the presence of the expected four main peaks: 13 (M), –65 (T_3), –100 (Q_3), –109 ppm (Q_4) (Fig. 7). The first peak corresponds to the SiMe_3 surface groups and shows that passivation occurred successfully, while the presence of a T_3 peak shows that the organosilane residue is completely fused within the silica network leading to a fully condensed tetrahedral Si surface site. Q_4 sites correspond to the bridged siloxanes (O_4Si) of the silica framework while the Q_3 sites can be attributed to residual silanols or alkoxysilane ($-\text{O}_3\text{Si}-\text{OR}$, $\text{R} = \text{Me}$ or H) that are inaccessible (blocked in the silica micropores). One should mention that Cross polarization technique (CP) allows the transfer of polarization from an abundant nucleus (usually ^1H) to a dilute species which is under observation (^{29}Si in this case). The benefits are primarily an intensity enhancement of the silicon signal and a reduction of the recycle delay between experiments, since the rate-determining relaxation time is now that of the protons. Based on this, the intensities of the different silicon atoms depend on the number of protons around them. Thus the method enhances favorably Q_3 sites with respect to Q_4 as the former has directly bonded hydroxyl or alkoxy-groups. This therefore overestimates the quantity of Q_3 substructures with respect to Q_4 .¹¹¹

The most informative spectrum is that of ^{13}C CP MAS (Fig.8) the peaks associated to the imidazolidene fragments are observed: aromatic carbons (122-143 ppm), the CH_2 in α -position to silicon (9 ppm), CH_2 in α -position to nitrogen of imidazolidene ring (50 ppm) along with some residual Si-OMe surface groups, the methyl groups of mesityl and the CH_2 in β -position to silicon (17-27 ppm). Noteworthy, spectrum of **M-Ir** and that of **M-Im** are very similar (Appendix A6) at the exception of a new signal around 30 ppm that might be attributed to CH_2 groups of COD. There is also a hardly visible signal at 80 ppm attributed to the CH signal of COD. Such low signal intensity can be explained by two reasons: 1) the relaxation time (T_1) of CH group of COD is small that results in significant peak broadening; 2) the quantity of COD is low due to its decoordination and stabilization of Ir low coordinated species by surface siloxane groups, as it was already noticed for ruthenium metathesis catalyst.¹⁰⁰ From this spectrum, it is difficult to define the real reason, however elemental analyses along with the absence of Ir particles (HR-TEM micrographs) and the homogeneous loading of Ir throughout the material given by EDX suggest the formation of Ir-NHC units.

¹¹¹ Zhao, X. S.; Lu, G. Q.; Whittaker, A. K.; Millar, G. J.; Zhu, H. Y., *J. Phys. Chem. B* **1997**, 101(33), 6525-6531

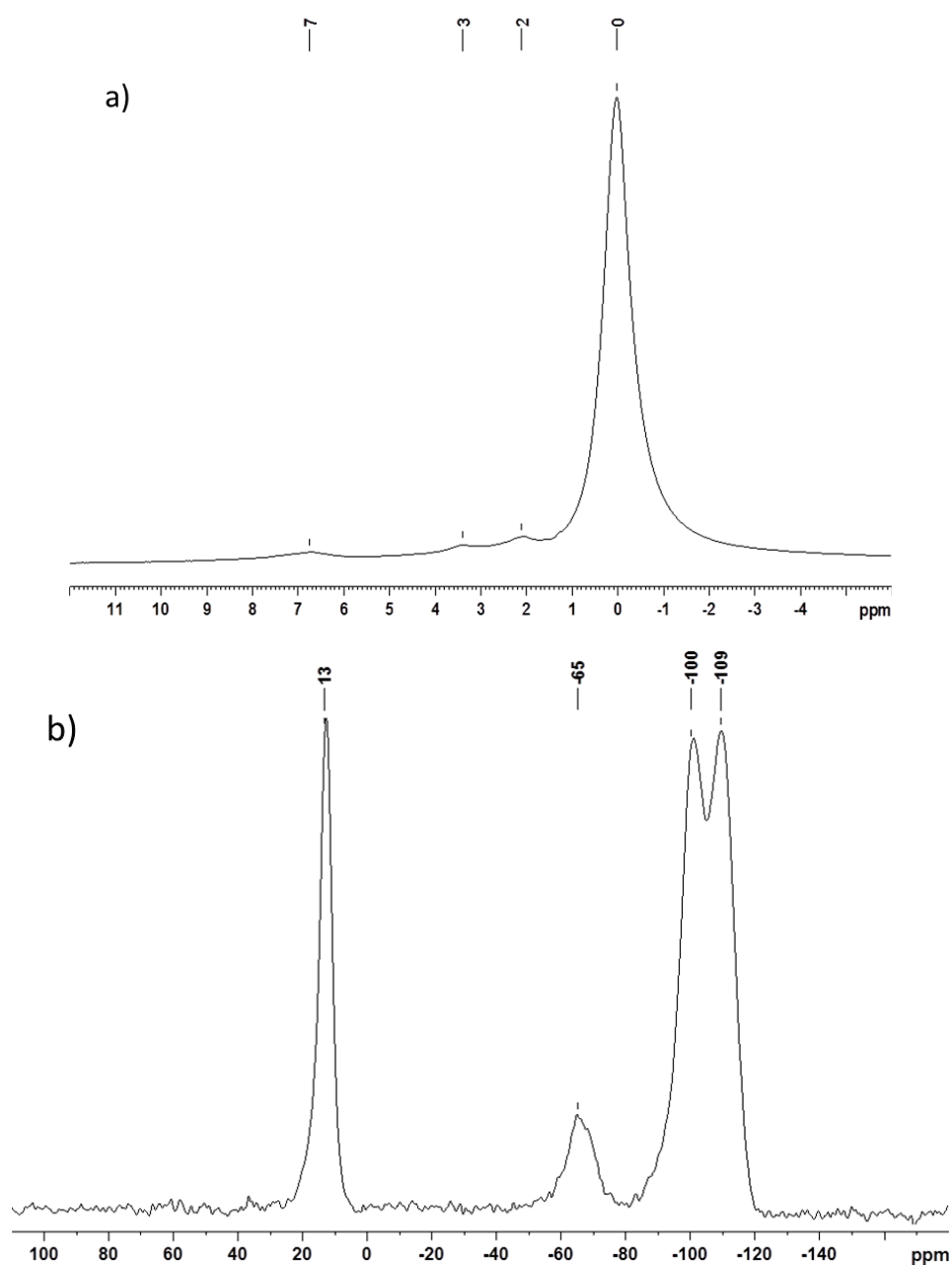


Figure 7. a) ^1H NMR of M-Ir (obtained with 8 scans); b) ^{29}Si CPMAS NMR of M-Ir (30000 scans with recycle delay 2 seconds).

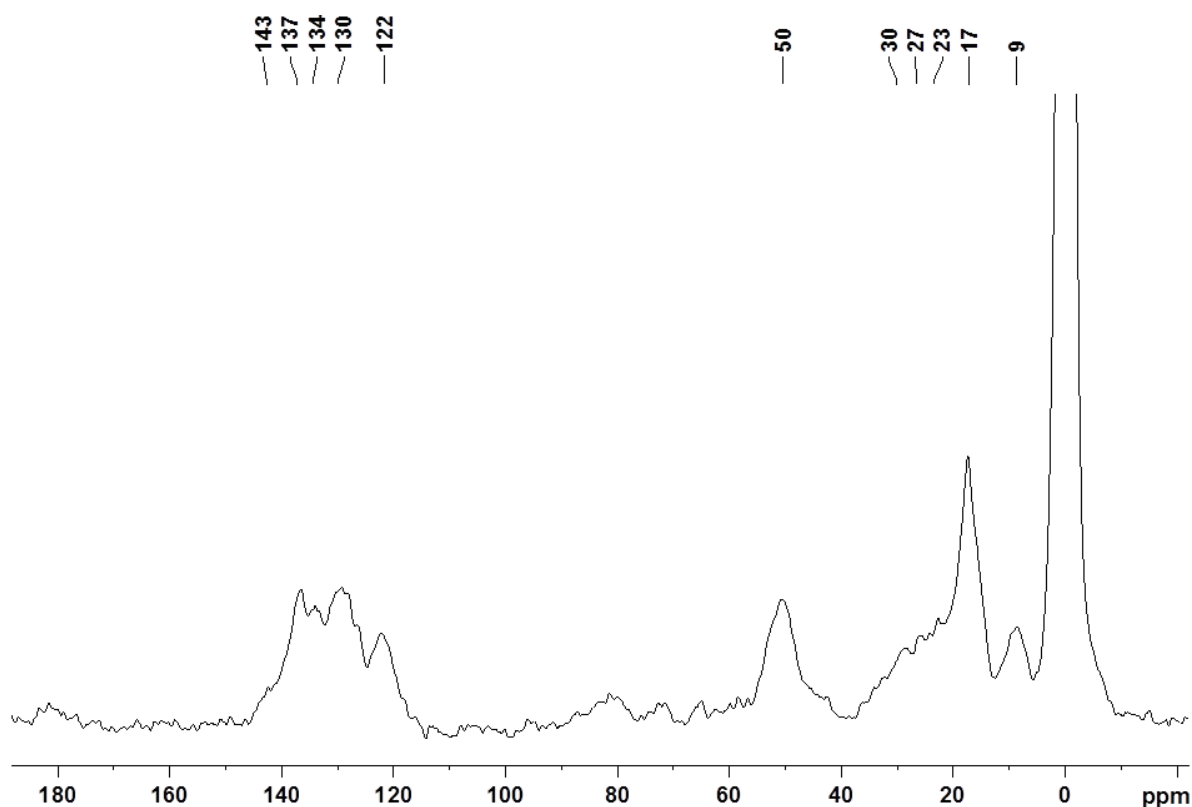


Figure 8. ^{13}C CPMAS NMR of M-Ir (recorded with 30000 number of scans and 2 ms of recycling delay)

3.2 Formation of the Ir-NHC material from a ^{13}C enriched imidazolium in carbenic position

The best way to prove the Ir coordination to NHC units in the materials is to detect the chemical shift of the carbene Carbon. As such carbene does not have any hydrogen atom around, it is impossible to detect it by routine ^{13}C CPMAS NMR experiment. We therefore prepared **M-Ir** materials with ^{13}C isotopic labeling of the carbene carbon atom, namely material **M-Ir***. **M-Im***, **M-Ag*** and **M-Ir*** were synthesized by the previously detailed methodology starting from C2 labelled mesitylimidazole. Taking into account that the width of the peaks in NMR spectrum is in direct dependence of the magnetic field applied and that the difference between silver and iridium carbenes is just 5 ppm, NMR spectra were recorded at high NMR field (800 MHz) in the european centre of high field NMR in Lyon (CRMN Lyon).

Chapter 2

The ^{13}C NMR spectra of **M-Im*** and **M-Ag*** were the same as for non-labelled materials, except for the appearance of an intense peak for the C2 Carbon at 135ppm for **M-Im*** and at 180 ppm for **M-Ag***.

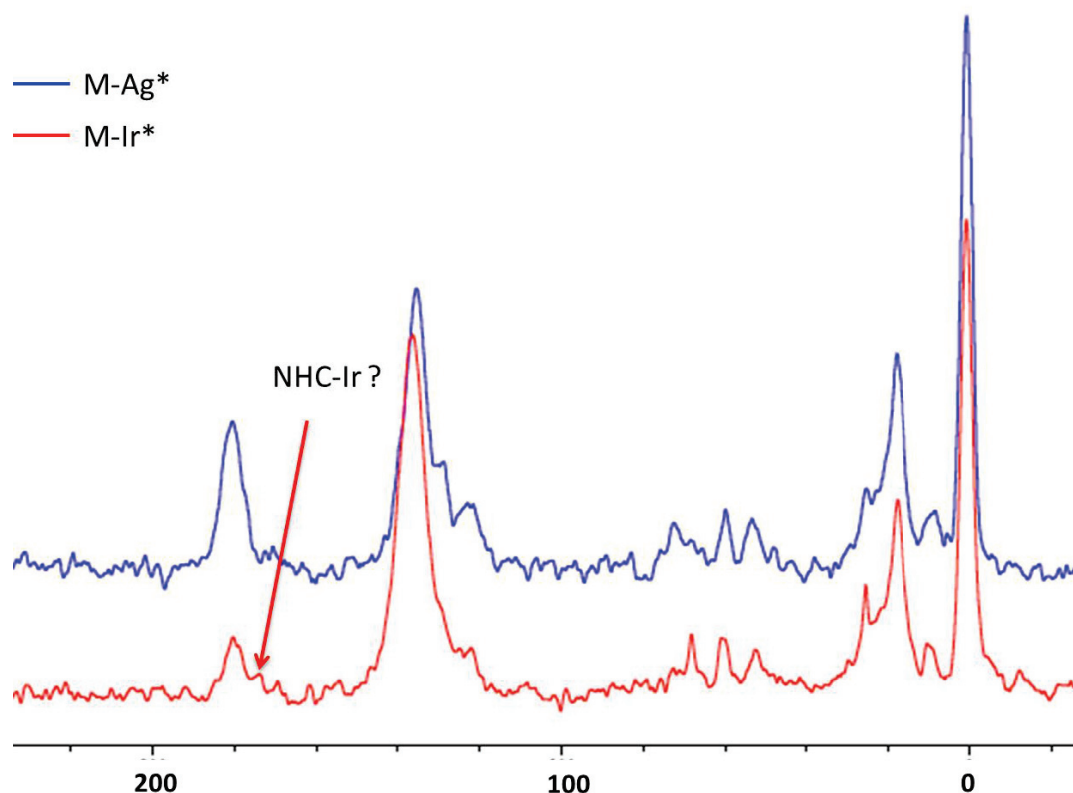


Figure 9. ^{13}C CPMAS NMR spectrum of labelled silver (up) and iridium (down) materials

Some differences in the ^{13}C spectra were detected after transmetallation. As shown in from Fig. 9, the intensity of the silver-carbene peak decreased together with an increase of peak width. The change of peak width is probably coming from overlapping of silver and iridium carbene peaks due to transmetallation.

Noteworthy, no COD was detected in the ^{13}C labelled material. However, the absence of COD needs confirmation by others experiments (*vide infra*).

3.3 Use the advanced techniques for the characterization of materials

3.3.1 Introduction

The detailed study concerning the determination of active species, catalytic intermediates or catalyst resting states on solid materials is difficult and requires a large set of complex techniques.¹¹² The characterization of the surface species at the atomic level can not be achieved just by classical solid state ^{13}C CPMAS NMR technique because of its low sensitivity due to the low natural abundance of ^{13}C nuclei and the small concentration of surface functionalities compared to the bulk sample. Even with isotopically labeled NHC surface units, it was difficult to gain insight into the chemical structure of surface sites (vide infra for 2D experiments). We therefore use a high field SS NMR techniques (800MHz) and a new advanced SS NMR technique based on dynamic nuclear polarization (DNP) of nuclei spin states. DNP allows the hyper-polarization of nuclei i.e. the nuclear spin polarization of nuclei far beyond thermal equilibrium conditions which allows strong NMR enhancements up to two orders of magnitude and reduced acquisition times.¹¹³

3.3.2 2D NMR of ^{13}C enriched material

From classical 1D ^{13}C CPMAS NMR spectrum of labelled **M-Ir***, discrimination of iridium carbene signal from silver carbene was difficult. We therefore performed 2D ^1H - ^{13}C NMR experiments. It should be mentioned that correlation spectroscopy can give important information about chemical structures and interactions of organic units with the surface and thus can help to build hypotheses about the existence of iridium complex on the silica surface. In order to discriminate species directly bonded to each other from those interacting through space, the 2D ^1H - ^{13}C spectra were recorded with different correlation times.

Fig. 10 (up) represent the ^1H - ^{13}C NMR spectrum of **M-Im*** recorded with a short correlation time (500 μs). The diagonal spots in the spectrum represent directly bonded species. As one can see there are 3 intense diagonal correlation spots: i) at 0 ppm in ^{13}C and ^1H dimension that corresponds to the surface trimethylsilyl-groups (OSiMe_3), ii) at 18 ppm in ^{13}C dimension and 2

¹¹² he M., Védrine J.C., Characterization of Solid Materials and Heterogeneous Catalysts, Wiley-VCH, Weinheim XXVII – LXV (2012).

¹¹³ Nikolaou, P.; Goodson, B. M.; Chekmenev, E. Y., *Chem. Eur. J.* **2015**, 21(8), 3156-3166.

Chapter 2

ppm in ^1H dimension that corresponds to the methyl groups of mesityl and iii) at 120-145 ppm in ^{13}C dimension and 7-12 ppm in ^1H dimension, an intense correlation refers to aromatic groups. The weak diagonal peak at 60 ppm in ^{13}C dimension and 4 ppm in ^1H dimension was attributed to residual alkoxysilane groups. Beside the diagonal peaks, one crosspeak was detected. This crosspeak at 140 ppm in ^{13}C dimension and 2 ppm in ^1H dimension indicates spatial proximities between methyl substituents of mesityl and aromatics. Dashed line underlines these spatial interactions.

Fig. 10 (bottom) represents the same spectrum recorded with a long correlation time (2ms) in order to detect ^1H nuclei spatially close to ^{13}C nuclei. The diagonal peaks represent directly bonded ^1H to ^{13}C as seen in the short correlation time spectrum. However a series of new crosspeaks appear in the region of the surface TMS groups and aromatics. Crosspeaks between protons of the CH_3 of mesityl groups (2 ppm), the NCH_2 moities (4.2 ppm), residual alcoxy (4 ppm) and aromatics (7 ppm) with the carbons of TMS at 0 ppm are observed. The absence of symmetrical crosspeaks between carbons from NCH_2 , CH_3 groups of mesityl and residual alcoxy with TMS protons can be explained by the low sensitivity of ^{13}C NMR in comparison with the ^1H NMR. The interactions of the surface TMS groups with the organic functionalities show that the organic moieties are folded towards the surface. This folding is allowed by the use of a flexible propyl-tether.

As in the case of **M*-Ir**, the main interest is to detect the presence/absence of COD and/or discriminate the iridium carbene from silver carbene, it was therefore decided to perform ^1H - ^{13}C HETCOR spectra with long correlation time (2 ms) for both **M*-Ag** (Fig.11 top) and **M*-Ir** (Fig.11 bottom). First, when comparing the spectrum of **M*-Ag** with the parent solid, **M*-Im**, a new crosspeak (180 ppm in ^{13}C ; 2 ppm in ^1H) assigned to the silver carbene Carbene spatially close to methyl groups of mesityl appears. This cross-peak is further split upon transmetallation with Ir, as shown in the spectrum recorded for **M*-Ir**; the new peaks being

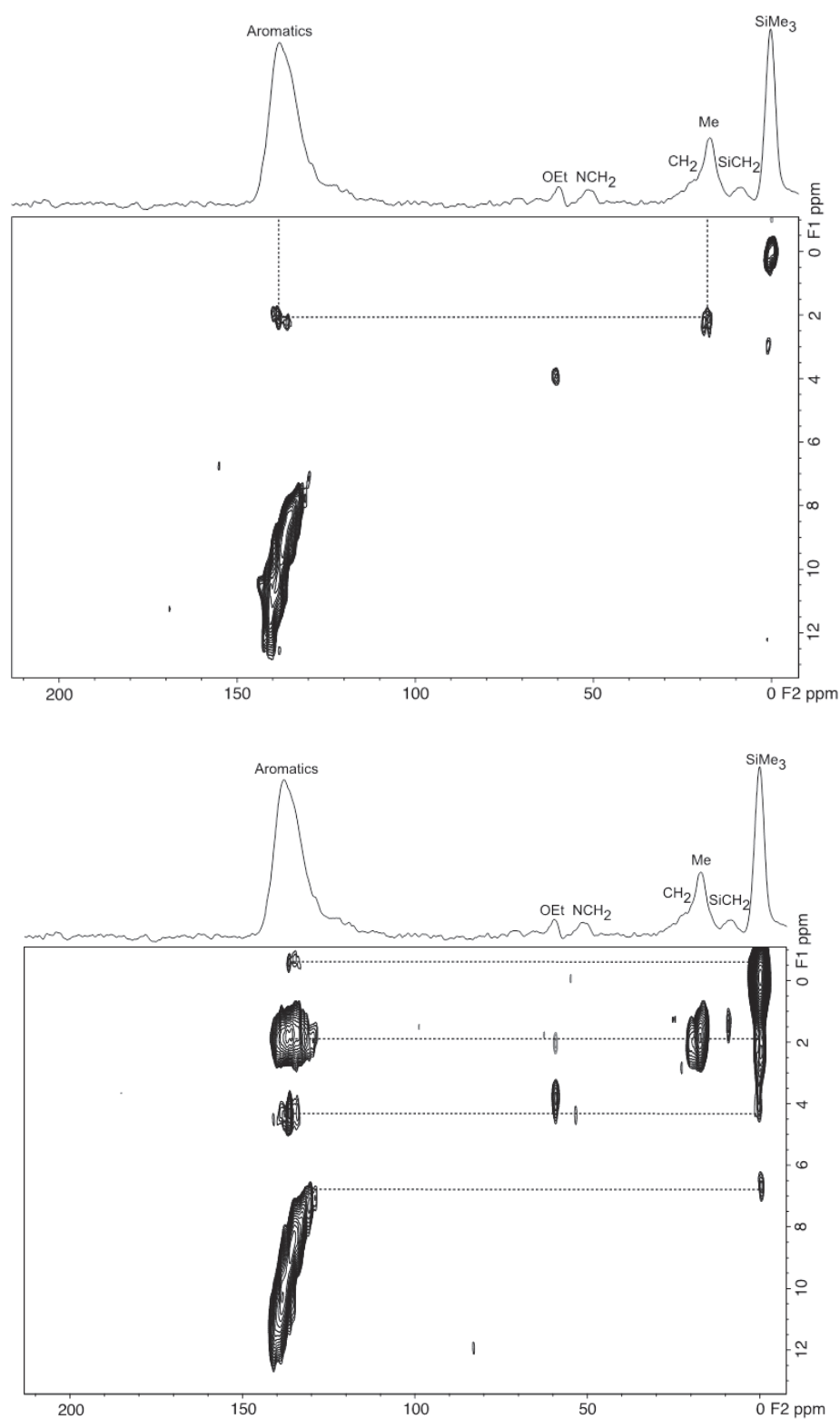


Figure10. ^1H - ^{13}C HETCOR NMR spectrum of $\text{M}^*\text{-Im}$ with short (up) and long (down) distance correlation (contact time: $500\mu\text{s}$ and 2ms).

Chapter 2

at 2.0 and 2.6 ppm in ^1H dimension. This new correlation at 2.6 ppm, can be attributed to a new metallo-carbene surface species: the Ir-NHC. Noteworthy, no COD signal was detected by NMR for **M-Ir***, we have therefore no evidence that COD is coordinated to the surface Ir-NHC sites and we therefore hypothesized that silica surface could stabilize the Ir-NHC sites *via* coordination of surface Si–O–Si groups, acting as a “bulk ligand”. This stabilization of Ir(I)-NHC sites by silica was never observed but our group recently showed that this interaction does exist when Ru-NHC species are supported onto silica *via* a flexible tether (propyl chain).

This kind of surface stabilization is consistent with the observed interactions between the aromatic carbons and the surface TMS groups in **M-Ir** (Fig.11 encircled crosspeaks).

As classical solid state NMR has low sensitivity it is however difficult to draw a definitive conclusion about COD absence. Thus we used the more sensitive technique: SS NMR using DNP (also names SENS DNP for Surface Enhanced Spectroscopy using Dynamic Nuclear Polarization) technique for detection of COD in **M-Ir**.

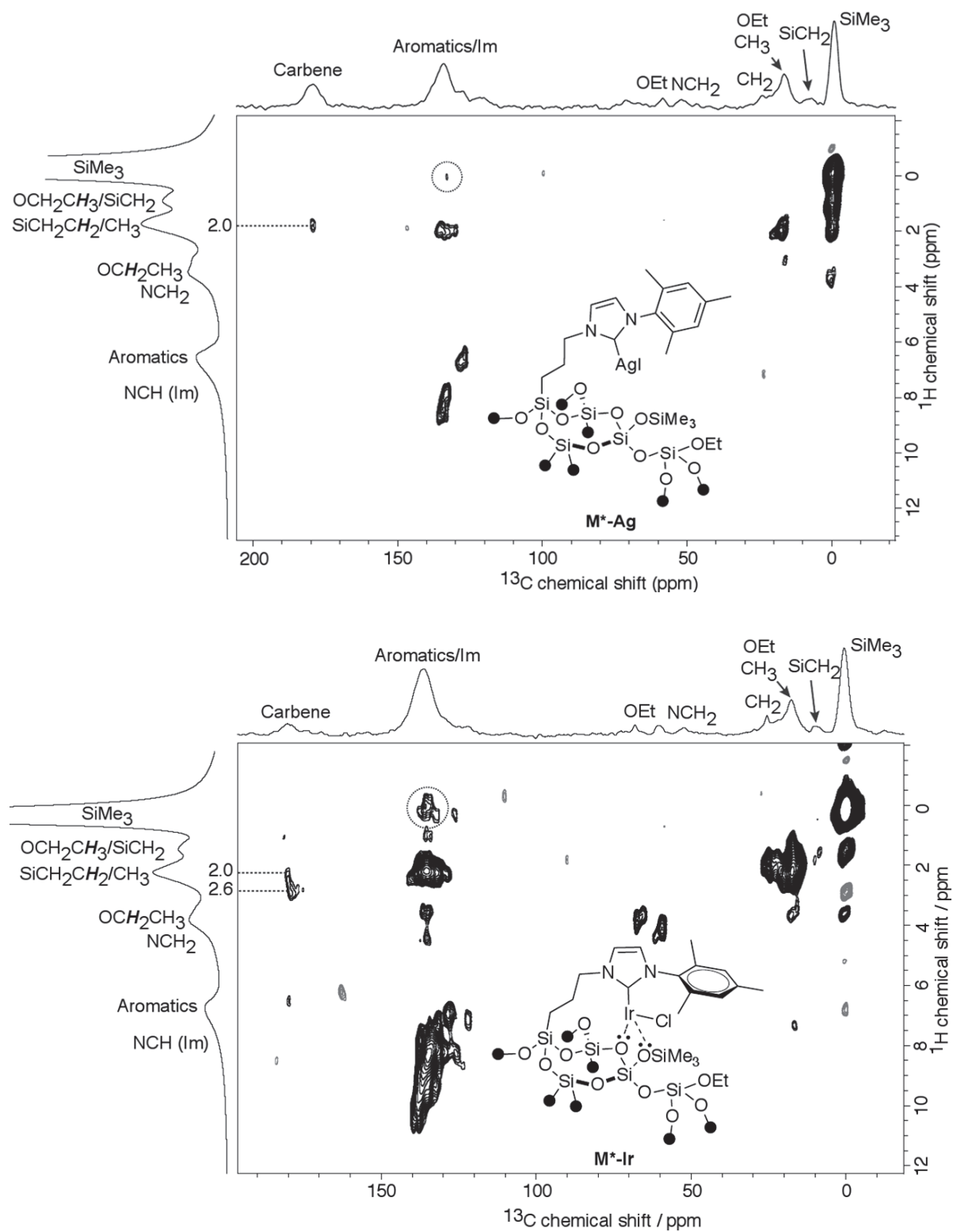


Figure 11. ^1H - ^{13}C HETCOR NMR spectra of $\text{M}^*\text{-Ag}$ and $\text{M}^*\text{-Ir}$ recorded on a 800 MHz with a long contact time (2 ms)

3.3.3 SS NMR using DNP

The SS NMR using DNP is a very recent technique for the material characterization, allowing the drastic enhancement of surface NMR signals of molecules and therefore reducing SS-NMR acquisition times.

The basic principle of DNP relies on a substantial transfer of polarization from unpaired electrons to a nucleus. In order to ensure an effective polarization transfer, four main components should be introduced in standard NMR Spectrometer: 1) a microwave irradiation source, called gyrotron, that induce the polarization of unpaired electrons; 2) the presence of a source of unpaired electron (persistent radicals such as nitroxides), also called polarizing agent, in vicinity to the surface organics to be analyzed by NMR; 3) an NMR probe that allows MW irradiation and NMR detection at multiple resonance frequencies- ^1H , ^{13}C , ^{15}N (often at cryogenic temperatures) ; 4) effective transmission waveguides, responsible for transfer of MW from the source to the probe. (Fig. 12).¹¹⁴

Performing the experiments at low temperatures allows to lengthen the spin-lattice relaxation (T_1) that enables efficient polarization transfer from the electron spin reservoir to the desired nuclei. Low temperature also affects the Boltzmann equilibrium resulting in bigger differences in populations between spin states, thus enhancing the NMR signal. The nature of the polarizing agent in combination with solvent is essential for signal amplification. The glass-forming matrices that provide uniform distribution of polarizing agent were found to give better enhancements.¹¹⁵ The DNP NMR can be utilized for liquid as for solid samples. It is especially useful to study functionalized porous materials in which the concentration of surface species is very low. From this point of view, the study of porous materials by classical SS NMR requires many hours or days of accumulation to acquire a simple 1D spectrum with reasonable signal to noise ratio. The signal enhancement obtained with DNP helps to significantly decrease the acquisition time.^{116,117} The DNP SENS is therefore crucial to give insights into the surface

¹¹⁴ Griffin, R.G.; Prisner, T.F. *Phys.Chem.Chem.Phys.* **2010**, 12, 5737-5740.

¹¹⁵ Barnes, A. B.; De Paepe, G.; van der Wel, P. C. A.; Hu, K.-N.; Joo, C.-G.; Bajaj, V. S.; Mak-Jurkauskas, M. L.; Sirigiri, J. R.; Herzfeld, J.; Temkin, R. J.; Griffin, R.G. *Appl.Magn.Reson.* 2008, 34, 237-263.

¹¹⁶ By Rossini, Aaron J.; Zagdoun, Alexandre; Lelli, Moreno; Lesage, Anne; Coperet, Christophe; Emsley, Lyndon *From Accounts of Chemical Research* (2013), 46(9), 1942-1951.

Chapter 2

species structure at the molecular level, particularly their conformations and modes of binding/interaction to/with the oxide surface.¹¹⁸

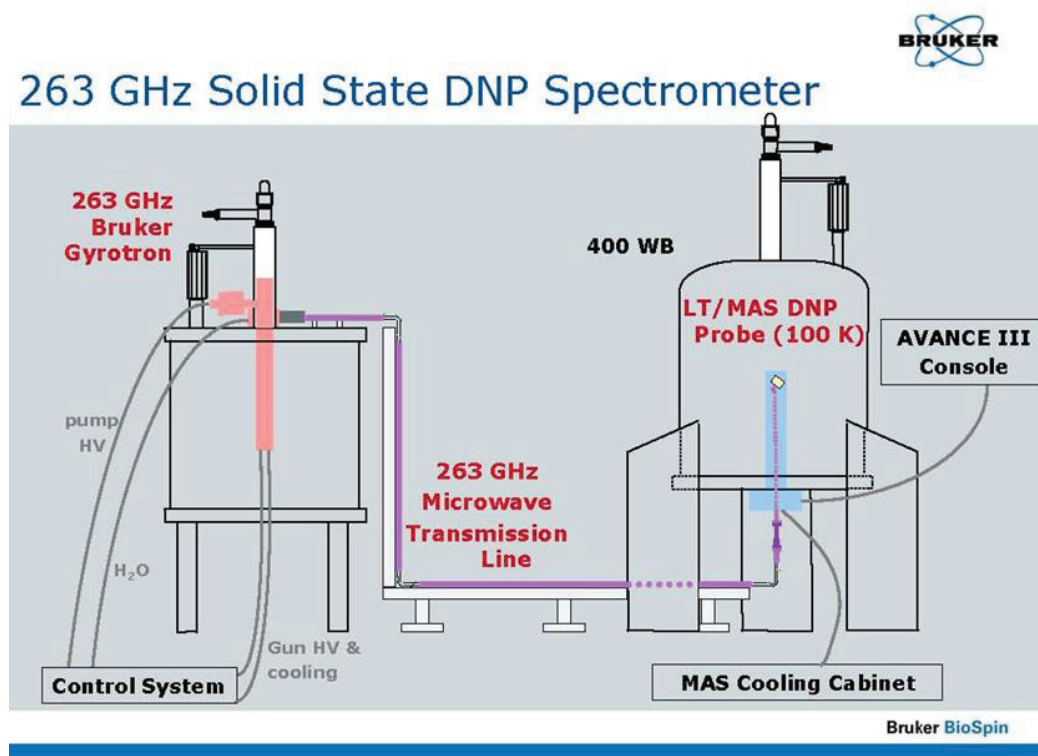


Figure12. Block-scheme of solid state DNP spectrometer

In our project, the **M-Ir** solid was filled by wetness impregnation with 20 mL of 16 mM solution of bCTbK (a specific nitroxide radical) in 1,1,2,2-tetracholorethane. To get the maximum enhancement in ^{13}C NMR, we combined DNP (transfer polarization from electrons to protons) with the known cross polarization (CP) technique. By utilizing the pulse sequence presented in Fig. 13, the saturation of EPR transition of radicals led to polarization enhancements of the nearby protons with subsequent transfer polarization to other nuclei (here carbon).

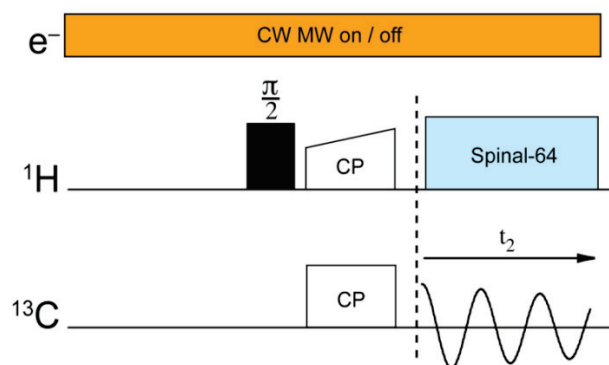
¹¹⁷ Lesage, A.; Lelli, M.; Gajan, D.; Caporini, M. A.; Vitzthum, V.; Mieville, P.; Alauzun, J.; Rossey, A.; Thieuleux, C.; Mehdi, A.; Bodenhausen, G.; Coperet, C.; Emsley, L. *J. Am. Chem. Soc.* **2011**, *133*, 15459–15461

¹¹⁸ Lelli, M.; Gajan, D.; Lesage, A.; Caporini, M. A.; Vitzthum, V.; Mieville, P.; Heroguel, F.; Rascon, F.; Roussey, A.; Thieuleux, C.; Boualleg, M.; Veyre, L.; Bodenhausen, G.; Coperet, C.; Emsley, L., *J. Am. Chem. Soc.* **2011**, *133*, 2104–2107

Chapter 2

We also combined DNP and CP to polarize efficiently ^{29}Si atoms instead of ^{13}C atoms (vide infra). The effective ^{13}C and ^{29}Si enhancements due to DNP and CP were calculated by subtraction between the spectra recorded with MW ON and OFF.

The spectra collected under MW are presented in Fig.14, the ^{13}C enhancement of signal was at



least 4.8 times. This proved enough to get well resolved ^{29}Si NMR spectra with only 32 scans. In similar conditions, well-resolved ^{29}Si CPMAS spectra were also acquired using 3000 scans. This means that DNP method allowed to decrease the number of scans by two orders of magnitude that finally results in substantial gain in NMR acquisition time.

Figure13. Pulse sequence for ^{13}C DNP NMR ⁹³

The ^{13}C CP MAS solid echo SENS DNP NMR spectrum of **M-Ir** was recorded on a 400MHz DNP system with an echo time of 40 rotor periods (Fig. 15). Noteworthy, Solid echo is a pulse sequence usually used in DNP SS NMR to remove intense solvent signal.¹¹⁹ As we can see the intense signal of tetrachloroethane at 80 ppm (Fig.13(a)) decreased a lot with solid echo (Fig.15). The obtained DNP spectra shows the presence of all the expected signals (aromatic carbons, residual alkoxy groups, CH_3 from mesityl, CH_2 from the propyl-chain and CH_3 from TMS) and also that of the metallo-carbene at 180 ppm (invisible when using usual ^{13}C CP MAS NMR). However, no signal of COD was detected.

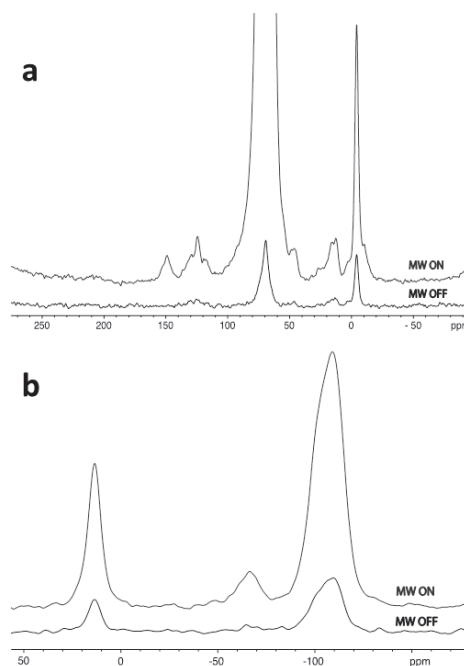


Figure14. Comparison ^{13}C (a) and ^{29}Si DNP NMR with the routine CP MAS technique.

¹¹⁹ B. Blümich, NMR Imaging of Materials, Clarendon Press, Oxford 2000, p.560

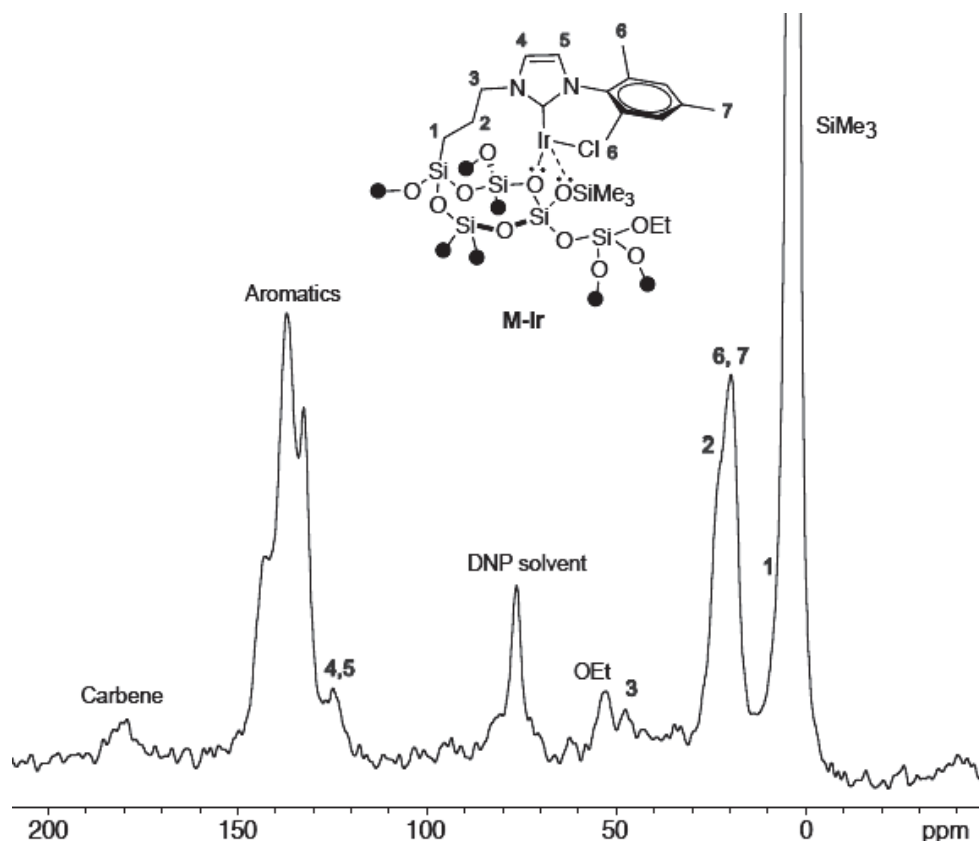


Figure 15. DNP ^{13}C CPMAS NMR of **M-Ir**

To further detect COD signal, a 2D ^1H - ^{13}C HETCOR spectrum of **M-Ir** (Fig. 16) was acquired with 0.5 ms contact time under DNP conditions. Even with such a technique, expected correlations at 50 ppm in ^{13}C dimension and 3 ppm in ^1H dimension as well as correlations at 25-35 ppm in ^{13}C dimension and 5 ppm in ^1H dimension corresponding to the sp^2 and sp^3 hybridized carbons of COD were not be observed. At the reverse, correlations between the aromatic carbons at 140 ppm in ^{13}C dimension and 0 ppm in the ^1H dimension (TMS protons) as well as correlations at 0 ppm in ^{13}C dimension with 7-10 ppm in ^1H dimension were detected and suggest that the organometallic complex folded towards the surface, as already observed with conventional solid-state NMR spectroscopy.

The folding of organic functionalities onto the surface of silica was also proved by 2D ^1H - ^{29}Si HETCOR DNP NMR spectrum of **M-Ir** (Fig. 17) acquired with short (0.2 ms) and long (2.0 ms) contact times. The top spectrum collected with short contact time ensures the presence of

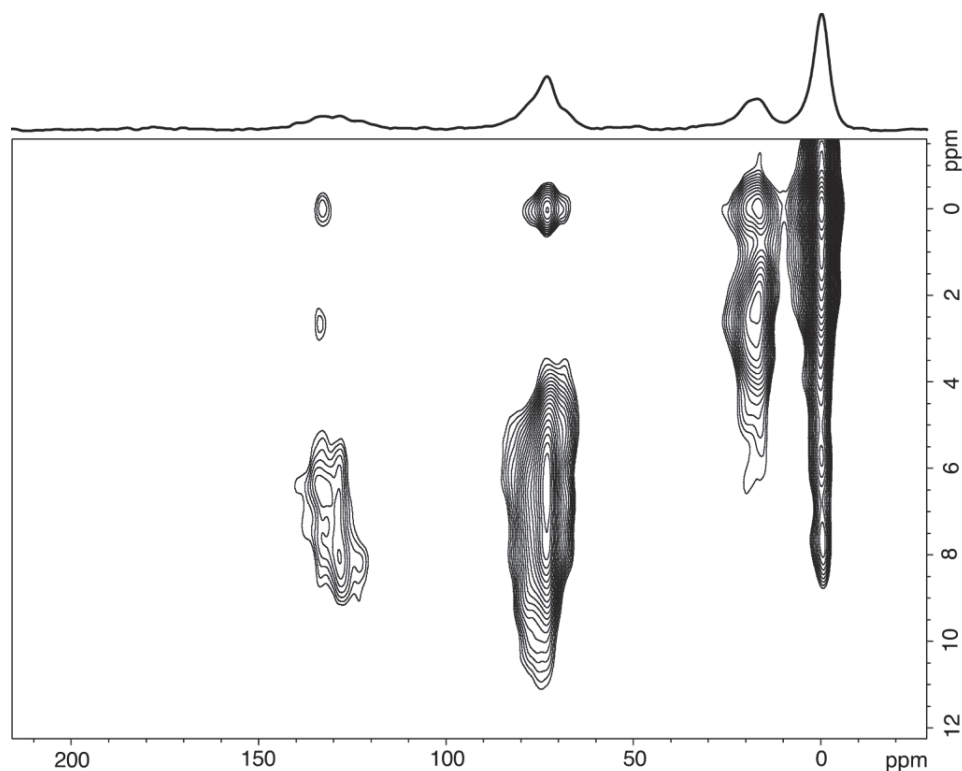


Figure16. 2D ^1H - ^{13}C HETCOR spectrum of M-Ir acquired with long contact time (0.5 ms) under DNP conditions.

correlations between spins that are in close spatial proximity. As expected, we see correlations between the silicon T_3 -sites and the nearest protons of SiCH_2 group (-65 ppm in ^{29}Si dimension and 2 ppm in ^1H dimension) and auto correlation of TMS groups (at 0 ppm in both dimensions). There are also intense correlations between the Q_n sites with all the surface organic functionalities (at -110 ppm in ^{29}Si direction and 0-11 ppm in ^1H dimension). This last correlation proves that the organic groups are very close to the Q_n sites. By applying a longer contact time (2.0ms) all interactions becomes more intense and new additional crosspeaks at 20 ppm in ^{29}Si dimension and 2-7 ppm in ^1H dimension appear. These correlations are assigned to spatial proximities between the TMS groups and the organic functionalities (CH_3 of mesityl at 2 ppm, NCH_2 at 4 ppm, aromatic protons at 7 ppm), illustrating again the folding of the organic functionalities onto the surface. These interactions between the organic functionalities and the support together with the incapacity to detect the presence of COD strongly suggests the COD decoordination during Ir transmetallation and stabilization of low-coordinated iridium species by surface siloxanes.

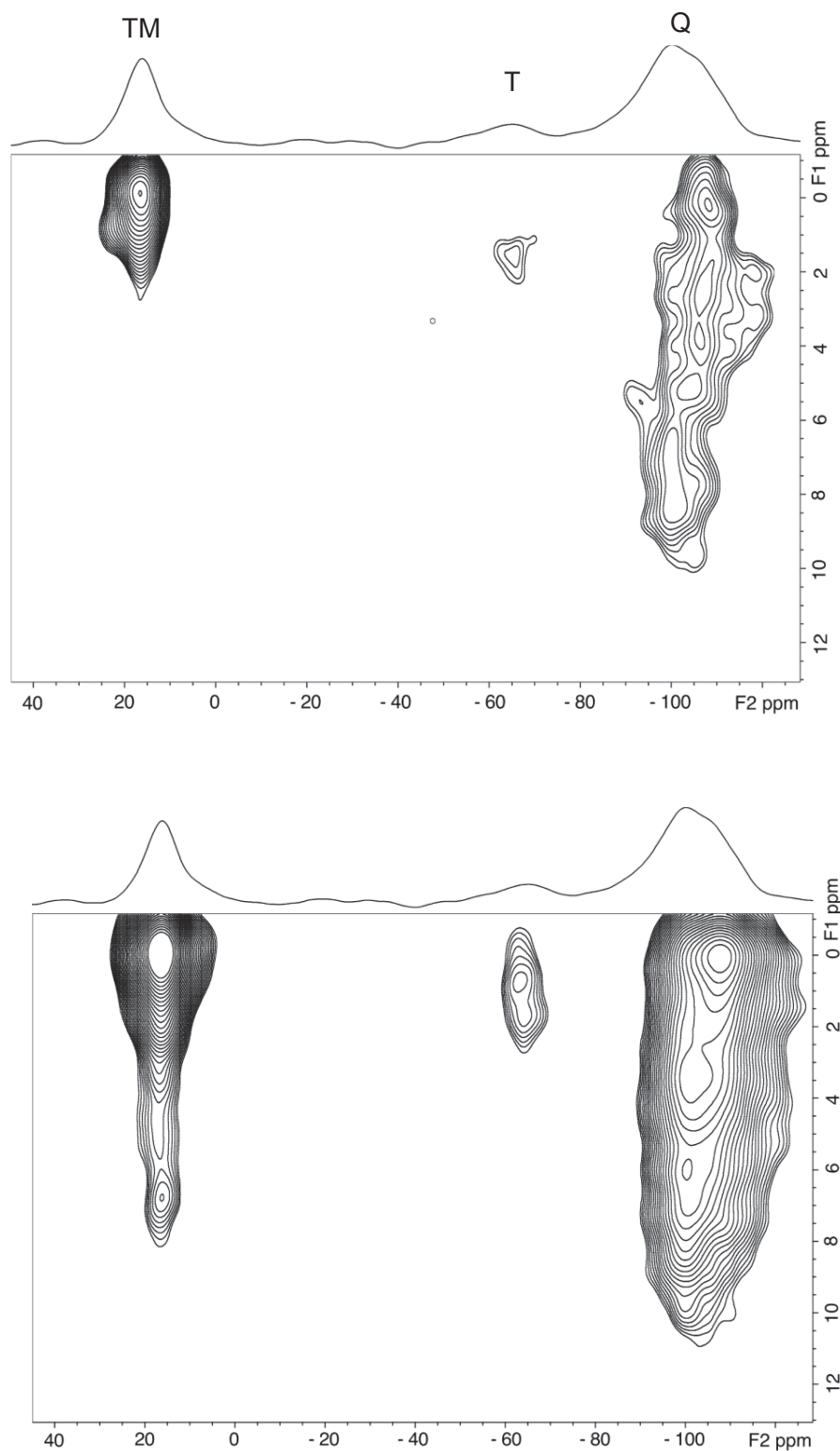


Figure 17. 2D ^1H - ^{29}Si HETCOR spectrum of M-Ir acquired with short (0.2 ms, top) and long (2.0 ms, bottom) contact time under DNP conditions.

3.3.4 In-situ liquid NMR under hydrogen pressure

To further assess the absence of COD coordinated to Ir surface sites. Chemical tests were carried out and monitored by liquid state NMR. As reported in the literature, the first step in olefin hydrogenation with Crabtree catalyst is the hydrogenation of the COD ligand which delivers cyclooctane or cyclooctene.^{120,121} Thus the detection of these hydrogenated byproducts could provide an indirect proof that COD was present. We therefore introduced the **M-Ir** material in C₆D₆ with toluene as internal standard under H₂ in a high pressure stable QVP NMR tube. The NMR tube was prepared under inert atmosphere, with 36 mg of material **M-Ir** (with 47% Silver to Iridium conversion), 2.8 ml of dry degassed C₆D₆ and 10 µL (0.094 mmol) of dry degassed toluene as a standard. The tube was then pressurized under 3 bars of H₂ and the release of products in C₆D₆ was monitored by ¹H NMR at 25 °C. A small signal at 1.5 ppm, corresponding to cyclooctane, was detected (Fig.18). No more release of cyclooctane was detected after 27 h reaction. To confirm the cyclooctane formation, 0.5 µL of pure cyclooctane was added to the NMR tube (Fig.18 inset).

The calculation of COD concentration was done by measuring the relative integration of cyclooctane peak in respect to methyl group of toluene (internal standard) after 94h of reaction.

If all Iridium sites contains a COD ligand, the expected quantity of COD should be equal to the quantity of Iridium:

$$v_{cod} = v_{Ir} = \frac{m}{M} \times conversion = \frac{36 \text{ mg}}{2963 \text{ mg/mmol}} \times 0.47 = 5.9 \times 10^{-3} \text{ mmol}$$

The quantity of internal standard (toluene) can be defined as follows:

$$m_{toluene} = \rho \times V = 10 \times 10^{-3} \text{ ml} \times 0.87 \frac{\text{g}}{\text{ml}} = 8.7 \text{ mg}$$

$$v_{toluene} = \frac{8.7 \text{ mg}}{92.14 \text{ mg/mmol}} = 9.4 \times 10^{-2} \text{ mmol}$$

¹²⁰ Zhu, Y.; Burgess, K., Acc. Chem. Res. 2012, 45 (10), 1623-1636.

¹²¹ Sparta, M.; Riplinger, C.; Neese, F., J. Chem. Theory Comput. 2014, 10 (3), 1099-1108.

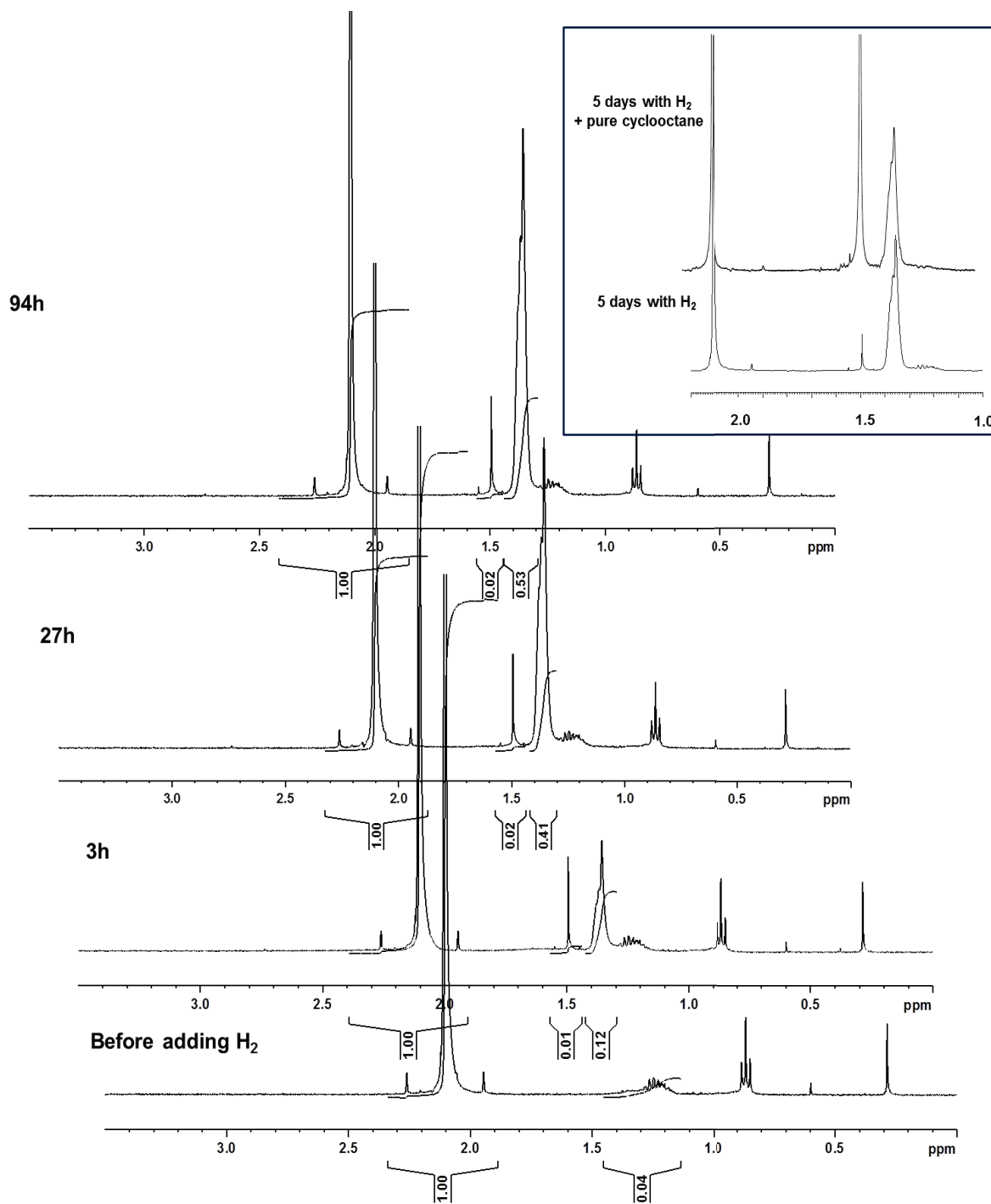


Figure18. Determination quantity of COD by *in situ* liquid NMR under hydrogen pressure

Taking into account that methyl group of toluene has 3 protons and cyclooctane has 16, the real quantity of COD can be calculated by:

Chapter 2

$$v_{cod} = \frac{I_{coa} \times v_{toluene}}{I_{toluene}} \times \frac{3}{16} = \frac{0.025 \times 9.4 \times 10^{-2} mmol}{1} \times \frac{3}{16} = 4.5 \times 10^{-4} mmol,$$

where I_{coa} is integral of cyclooctane peak and $I_{toluene}$ of methyl from toluene.

By dividing the real quantity of COD onto the expected one, we are able to get the percent of COD coordinated to Iridium species:

$$\%(COD) = \frac{4.5 \times 10^{-4}}{5.9 \times 10^{-3}} = 7.6\% \approx 8\%$$

The quantity of COD in the material was only 8% with respect to Iridium, meaning that 92% of Iridium species do not contain COD. That can explain why it was so difficult to detect COD by ^{13}C SS NMR even by applying such advanced techniques as DNP NMR.

Interesting, beside the appearance of cyclooctane signal, another signal at 1.37 ppm appeared and increased all over the reaction. The intensity of this signal showed that it could not be associated with cyclooctane or other product of COD hydrogenation. The chemical shift suggests the hydrogenation of deuterated benzene, which was used as a solvent. It is known that organometallic iridium species are not able to hydrogenate benzene at room temperature whereas Ir NPs can.¹²² This results suggest that Ir-NHC supported species readily decompose under H_2 (when not olefinic substrate is present) into Ir NPs. The spent material was therefore analyzed by HR-TEM: The micrograph clearly shows the presence of small Ir NPs along the silica channels (fig 19).

At the reverse, fresh catalysts, i.e. after Ir introduction *via* transmetallation, do not exhibit Ir NPs as shown by HR-TEM experiments.

To conclude, the absence of COD and Ir NPs in “fresh” **M-Ir** solids together with the presence of interactions between the organic moieties with surface siloxanes suggest that iridium sites are Ir(NHC)Cl complexes stabilized by surface siloxanes.

¹²² Ercan, B.; Mehmet, Z.; Ozkar, S.; Finke, R.G., *Langmuir* **2010**, 26, 12455-12464

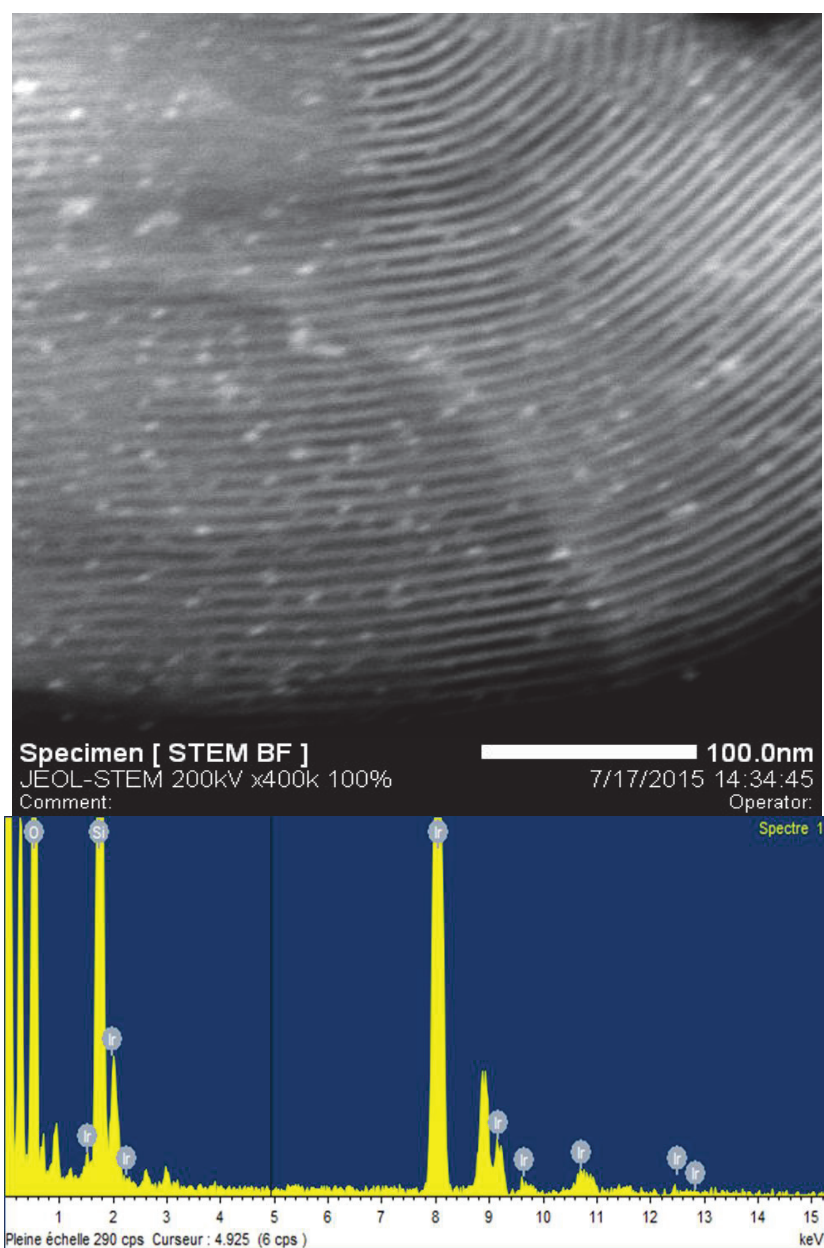


Figure19. STEM micrographs and EDX of the recovered solid after 94 hours under H_2 in C_6D_6 and toluene as internal standard.

II-4 Conclusions

The $[\text{IrCl}(\text{MesImPr})(\text{COD})]$ complex was successfully synthesized and characterized. The transmetallation strategy was then used to generate a supported analogue of the molecular Ir(I)-NHC complex. The as-obtained materials were further analyzed by several techniques (TEM, EA, N_2 adsorption/desorption, SS NMR...) of which advanced SS-NMR technique using DNP. From the study, the presence of Ir-NHC surface sites and the absence of Iridium nanoparticles was shown. NMR techniques along with chemical tests indicated that only 8% of Iridium supported complexes were coordinated with a COD ligand. These results are in line with 2D ^{29}Si DNP NMR spectra that show the presence of interactions between the Ir-NHC sites and the silica surface allowed by the use of a short flexible tether (propyl-chain). These interactions can probably explain the decoordination of COD during the catalysts preparation, leading to low-coordinated iridium complex stabilized by surface siloxanes. This has to our knowledge never been observed before in Ir-chemistry. A similar phenomenon between supported Ru complexes and the surface was already strongly suggested by our group in 2013, but not directly observed on the final catalyst.

II-5 Experimental section

5.1 General procedures

All experiments were carried out using Schlenck techniques, vacuum lines and glove box. Toluene, dichloromethane and diethyl ether were purified with an SPS800 Braun solvent purification system and degassed by freeze-pump technique prior to use. Acetonitrile and Methanol were distilled over magnesium.¹²³ Iodopropyltriethoxysilane,¹²⁴ 1-mesythylimidazole¹²⁵ and nanofluorotetrabutanal silver¹²⁶ were synthesized according to literature procedures.

A Suitable crystal was selected and mounted on a Gemini kappa-geometry diffractometer (Agilent Technologies UK Ltd) equipped with an Atlas CCD detector and using Mo radiation ($\lambda = 0.71073 \text{ \AA}$).

Intensities were collected at 100 K by means of the CrysAlisPro software. Reflection indexing, unit-cell parameters refinement, Lorentz-polarization correction, peak integration and background determination were carried out with the CrysAlisPro software.¹²⁷ An analytical absorption correction was applied using the modeled faces of the crystal.¹²⁸ The resulting set of hkl was used for structure solution and refinement.

The structures were solved by direct methods with SIR97¹²⁹ and the least-square refinement on F2 was achieved with the CRYSTALS software.^{130 [5]}

All non-hydrogen atoms were refined anisotropically. The hydrogen atoms were all located in a difference map, and then were repositioned geometrically. The H atoms were initially refined with soft restraints on the bond lengths and angles to regularize their geometry (C---H in the range 0.93--0.98 Å) and Uiso(H) (in the range 1.2-1.5 times Ueq of the parent atom), after which the positions were refined with riding constraints.

¹²³ Wilfred L.F. ; Li Lin Chai A.; Li Lin Chai, C., Purification of Laboratory Chemicals(6th edition) Elsevier Butterworth Heinemann May 2009, 743p.

¹²⁴ Lombardo, M.; Easwar, S.; de Marco, A.; Pasi, P.; Trombini, C., *Org. Biomol. Chem.* **2008**, 6(22), 4224-4229.

¹²⁵ Occhipinti, G.; Jensen, V.R.J.; Tornroos, K.W.; Froeystein, N. A.; Bjoersvik, H.-R., *Tetrahedron* **2009**, 65(34), 7186-7194

¹²⁶ Reisinger, A.; Himmel, D.; Krossing, I., *Angew. Chem. Int. Ed.* **2006**, 45(42), 6997-7000

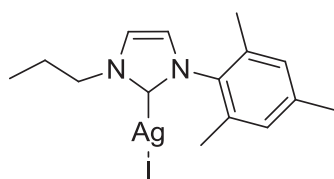
¹²⁷ CrysAlisPro, Agilent Technologies, Version 1.171.34.49 (release 20-01-2011 CrysAlis171 .NET) (compiled Jan 20 2011,15:58:25)

¹²⁸ R. C. Clark & J. S. Reid, *Acta Cryst. A* **1995**, 51, 887-897.

¹²⁹ A. Altomare, M.C. Burla, M. Camalli, G.L. Cascarano, C. Giacovazzo, A. Guagliardi, A. Grazia, G. Moliterni, G. Polidori, R. Spagna, *J. App. Cryst.* **1999**, 32, 115-119.

¹³⁰ P.W. Betteridge, J.R. Carruthers, R.I. Cooper, K. Prout, D.J. Watkin, *J. Appl. Cryst.* **2003**, 36, 1487-1487.

5.2 Synthesis of molecular complexes



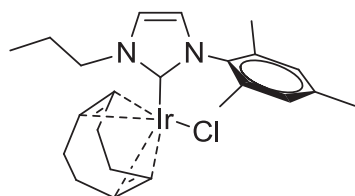
1-mesityl-3-propylimidazol-2-ylidene silver(I) iodide (1)

200mg (0,6mmol) of well dried MesImPrI were mixed with 67mg (0,3mmol) of Ag₂O in argon atmosphere in the absence of light.

The mixture was dissolved in 20ml of dried CH₃CN and left stirring at room temperature for 4h. Than the rest of Ag₂O was filtered under inert conditions and transparent filtrate was evaporated under vacuum. The silver carbene was characterized by ¹H, ¹³C NMR

¹H NMR (C₆D₆, 300K): δ (ppm)= 0.62 (t, J=7.4 Hz, 3H, CH₃ of Pr); 1.36 (sext., J=7.1 Hz, 2H, NCH₂CH₂ of Pr); 1.83 (s, 6H, CH₃ of Mes); 2.06 (s, 3H, CH₃ of Mes); 3.69 (t, J=6.9 Hz, 2H, NCH₂ of Pr); 5.90 (s, 1H, CH of Im); 6.09 (s, 1H, CH of Im); 6.65 (s, 2H, CH of Mes).

¹³C NMR (C₆D₆, 300K): δ (ppm)=10.87 (CH₃ of Pr); 17.82 (2CH₃ of Mes); 20.99 (CH₃ of Mes); 24.59 (NCH₂CH₂ of Pr); 52.84 (NCH₂ of Pr); 121.27(CH of Im); 120.31 (CH of Im); 129.34 (2CH of Mes); 134.92 (2C quat. of Mes); 136.17(C quat. of Mes), 138.67 (C quat. of Mes); 186.47 (C-Ag, Im).



1-mesityl-3-propylimidazole-2-ylideneiridium (I) 1,5-cyclooctadiene chloride (2)

195mg (0,30 mmol) of [IrCODCl]₂ were dissolved in 20ml of dry CH₃CN and transferred by cannula to the 260 mg (0.6 mmol) previously prepared silver carbene . The reaction was heated at 60°C during 12h. After the solvent was evaporated and obtained solid was purified by column using CH₂Cl₂ as an eluent. The pure complex was characterized by ¹H, ¹³C , ¹³C dept 135 and 2D ¹H-¹H, ¹H-¹³C NMR, MASS ESI, IR.

¹H NMR (C₆D₆, 300K): δ (ppm)=0.78 (t, J=7.4 Hz, 3H, CH₃ of Pr); 1.25-1.45(m, 1H, CH₂ of COD), 1.50-1.65 (m, 5H, CH₂ of COD); 1.73 (s, 3H, CH₃ of Mes); 1,75-1.98 (m, 3H, CH₂ of COD); 1,98-2.09 (m, 1H, CH₂ of COD); 2.11 (s, 3H, CH₃ of Mes); 2.56 (s, 3H, CH₃ of Mes); 2.91 (ddd, J=13.0 Hz, J=8.1 Hz, J=7.1 Hz, 1H, =CH of COD); 3.14 (ddd, J=13.0 Hz, J=8.1 Hz,

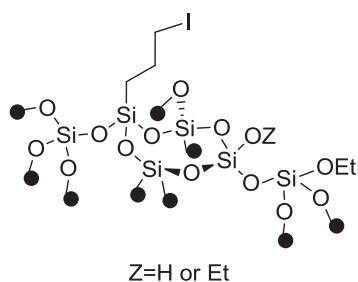
Chapter 2

$J=7.1$ Hz, 1H, =CH of COD); 3.99 (td, $J=7.1$ Hz, $J=2.5$ Hz, 1H, NCH₂ of Pr); 4.80 (td, $J=7.1$ Hz, $J=2.5$ Hz, 1H, NCH₂ of Pr); 4.90-5.10 (m, 2H, =CH of COD); 5.91 (d, $J=2.0$ Hz, 1H, CH of Im); 6.18 (d, 1H, CH of Im); 6.68 (s, 1H, CH of Mes); 6.77 (s, 1H, CH of Mes).

¹³C NMR (C₆D₆, 300K): δ (ppm)=11.21 (CH₃ of Pr); 17.51 (CH₃ of Mes), 19.96 (CH₃ of Mes); 20.85 (CH₃ of Mes); 23.80 (NCH₂CH₂, Pr); 29.33 (CH₂ of COD); 29.90 (CH₂ of COD); 33.44 (CH₂ of COD); 35.02 (CH₂ of COD); 50.95 (=CH of COD); 50.17 (=CH of COD); 53.12 (NCH₂ of Pr); 83.22 (2CH of COD); 122.37 (CH of Im), 120.60 (CH of Im); 129.84 (CH of Mes); 134.37 (C quat. of Mes); 136.53 (C quat. of Mes); 137.51 (C quat. of Mes); 138.30 (C quat. of Mes); 180.60 (C-Ir, Im).

HRMS (ESI⁺): calculated for [(MesImPr)Ir(COD)(CH₃CN)]⁺ ([M-Cl + CH₃CN]) 570.2; found 570.2 .

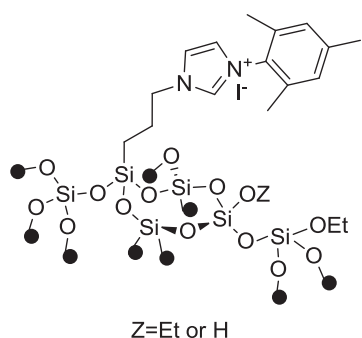
5.3 Synthesis of materials



Iodopropyl material (M-PrI)

8.04 g of Pluronic 123 were placed in the flask and 320 ml of HI solution (pH=1.5) were added, the mixture was left stirring for 24h. Then into the new flask 18.24 g (0.0087 mol, 30 eq) of TEOS and 0.97 g (0.0029 mol, 1eq) of iodopropyltriethoxysilane were placed and filled with the solution of Pluronic123. The mixture was left to stirring for 3h. After the mixture was heated to 45°C. When temperature reached 40°C 0.152 g (0.0036 mol) of NaF were added. Suspension was left for stirring during 2 days. After iodopropyle material was isolated by filtration, washed 3 times with H₂O, EtOH, Et₂O. Obtained material was washed with hot ethanol for 48 h using a Soxhlet apparatus and then dried during the night under the vacuum (10⁻³ bars) at 120°C.

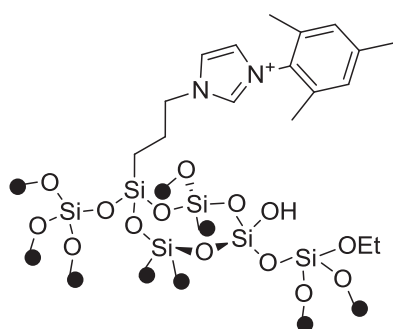
The powder was characterized by N₂ absorption and ¹H, ¹³C, ²⁹Si NMR. Spectral data corresponded to what is already described^{ref}



Mesitylimidazolepropyl material (M-Im)

A solution of mesitylimidazole (7.5g, 0.039 mol) in toluene (110 mL) was added into 5.4 g (0.0027mol) of the **M-PrI**, and the reaction mixture was heated to reflux for 72 h. After filtration, the solid was washed successively with toluene, acetone and diethyl ether. The solid was then washed with hot ethanol for 48 h using a Soxhlet apparatus, and then washed at room temperature with acetone and diethylether before drying under vacuum (10^{-3} bars) overnight at 120°C.

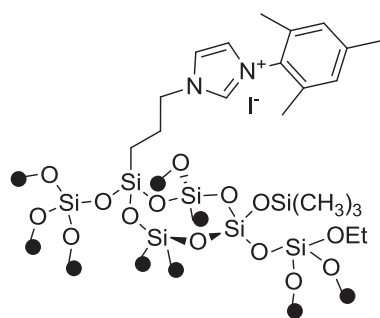
The powder was characterized by N₂ absorption and ¹H, ¹³C, ²⁹Si NMR. Spectral data corresponded to what is already described ^{ref}



Mesitylimidazolepropyl hydrolyzed material

4.7 g of the mesitylimidazolium functionalized material was dissolved in 440ml of HI (2M) solution and was left for 3h at 45°C. Then powder was filtered and washed 3 times with H₂O, Acetone, Et₂O and dried under vacuum (10^{-3} bars) at 120°C during the night.

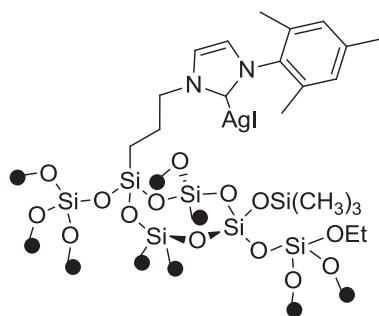
The powder was characterized by N₂ absorption and ¹H, ¹³C, ²⁹Si NMR. Spectral data corresponded to what is already described ^{ref}



Mesitylimidazoliumpropyl protected material

3.7g (0.0016 mol) of solid was suspended in 110ml of Toluene and 50ml of Et₃N and 22.87 ml (0.17mol) of Me₃SiBr were added. The mixture was left stirring for 24h at 25°C. After filtration, the solid was washed by Toluene, MeOH, CH₂Cl₂ and dried under vacuum (10^{-3} bars) at 120°C overnight.

The powder was characterized by N₂ absorption and ¹H, ¹³C, ²⁹Si NMR. Spectral data corresponded to what is already described ^{ref}

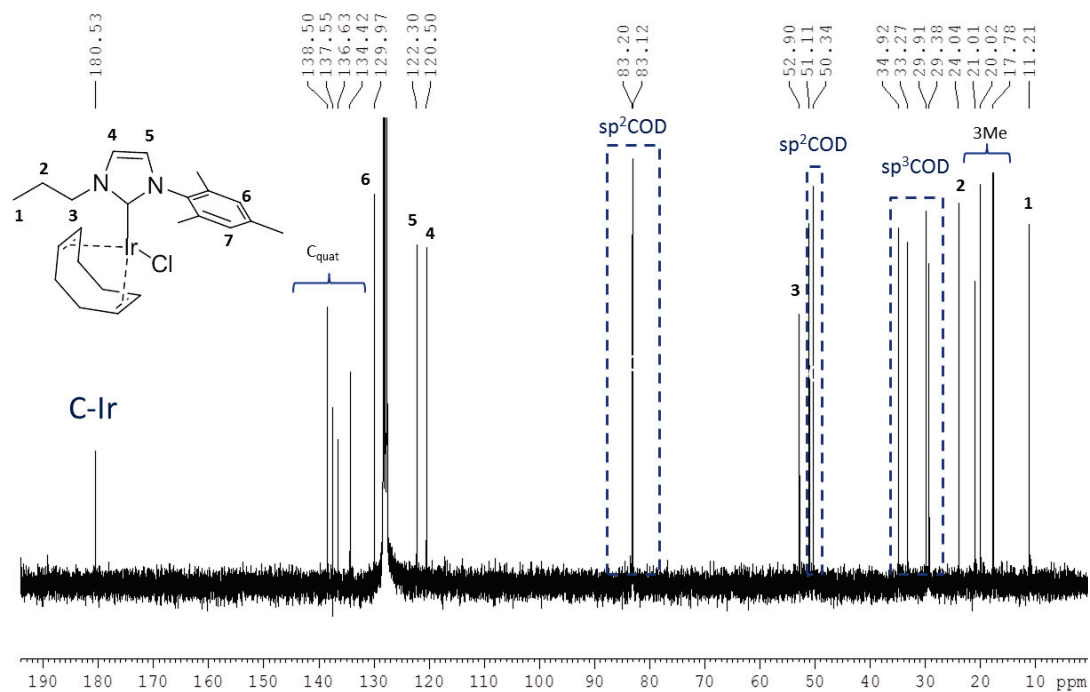
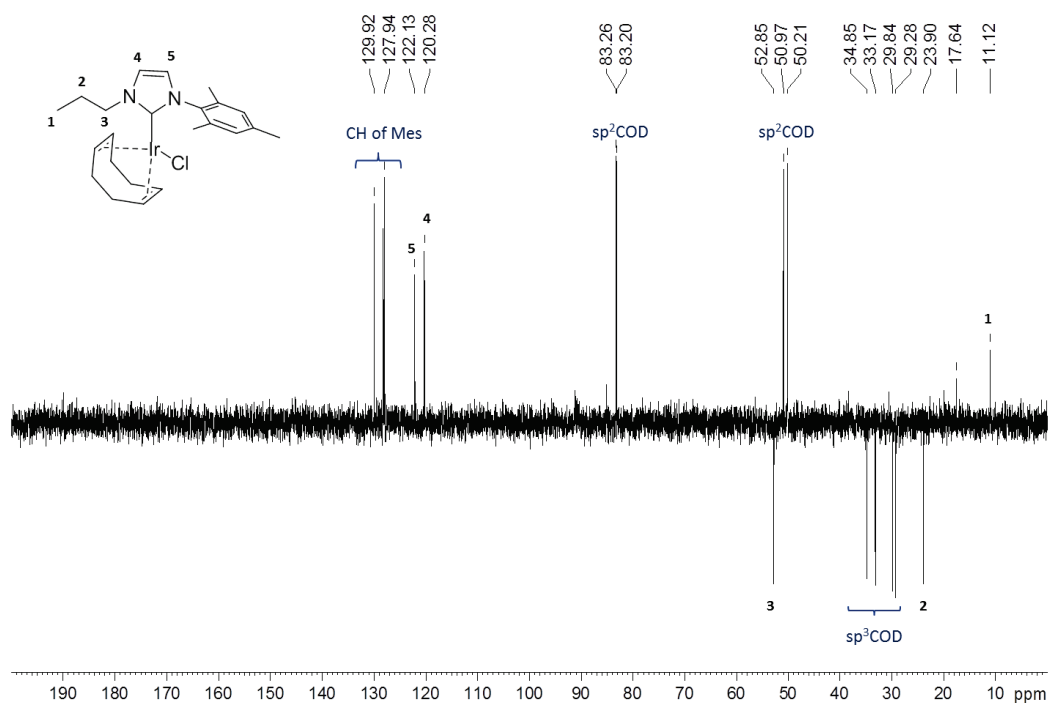


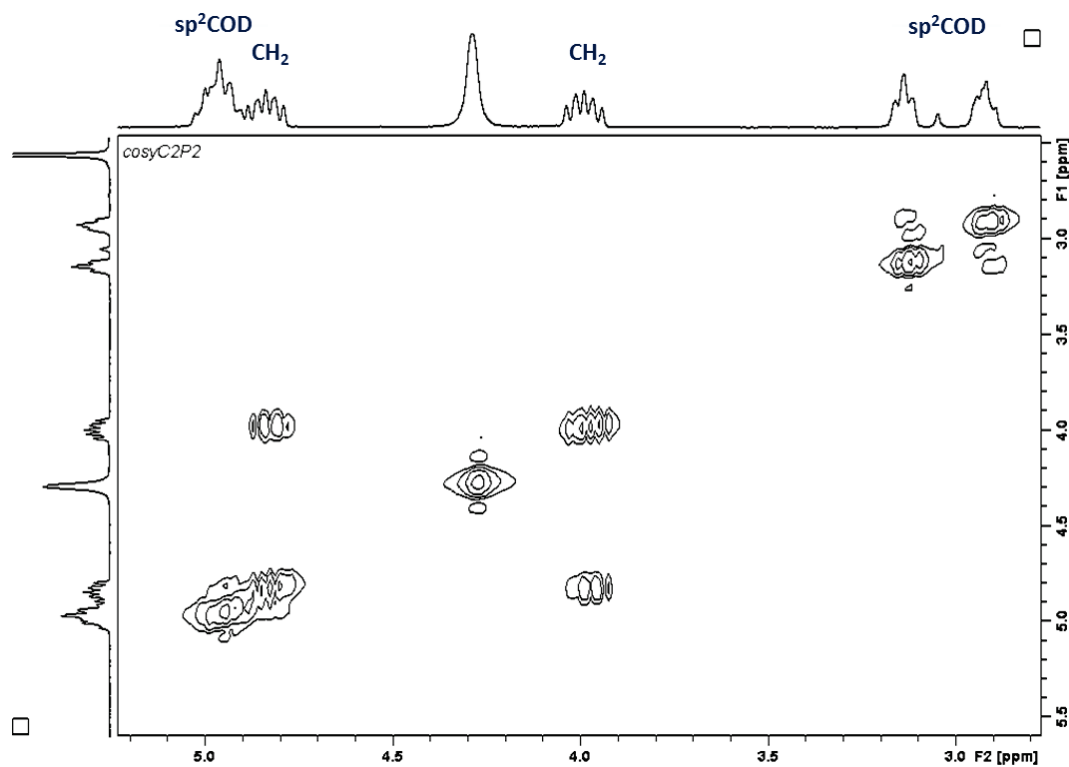
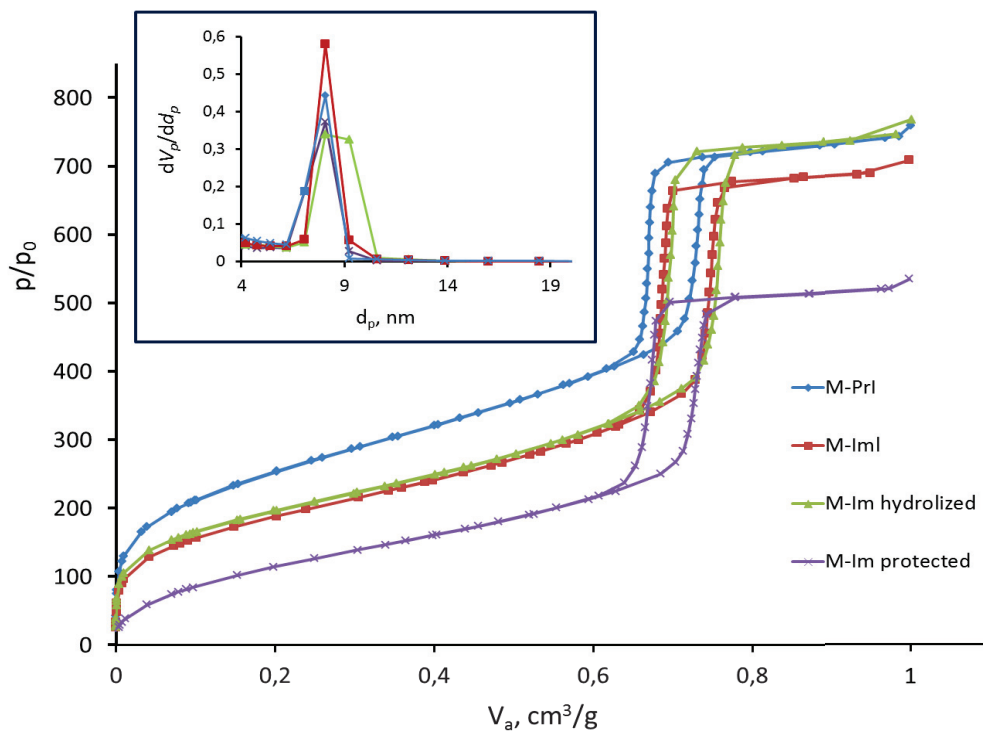
Mesitylimidazolepropyl silver carbene material (M-Ag)

2,6g of material (0,001mol) was mixed with 0,782 g of $\text{AgOC}(\text{CF}_3)_3$ (0,002 mol) and dissolved in 45ml of dried CH_3CN . The mixture was left for stirring overnight at RT. Next day solid was filtered under the Ar and washed 3 times by degased and dried CH_3CN and CH_2Cl_2 . The material was dried under the vacuum overnight.

The material was characterized by ^1H , ^{13}C , ^{29}Si NMR, TEM. Spectral data corresponded to what is already described^{ref}

II-6 Appendix

Figure A1. ¹³C NMR of [IrCl(MesImPr)(COD)]Figure A2. ¹³C dept135 NMR of [IrCl(MesImPr)(COD)]

Figure A3. ^1H - ^1H COSY NMR of $[\text{IrCl}(\text{MesImPr})(\text{COD})]$ Figure A4. N_2 adsorption data

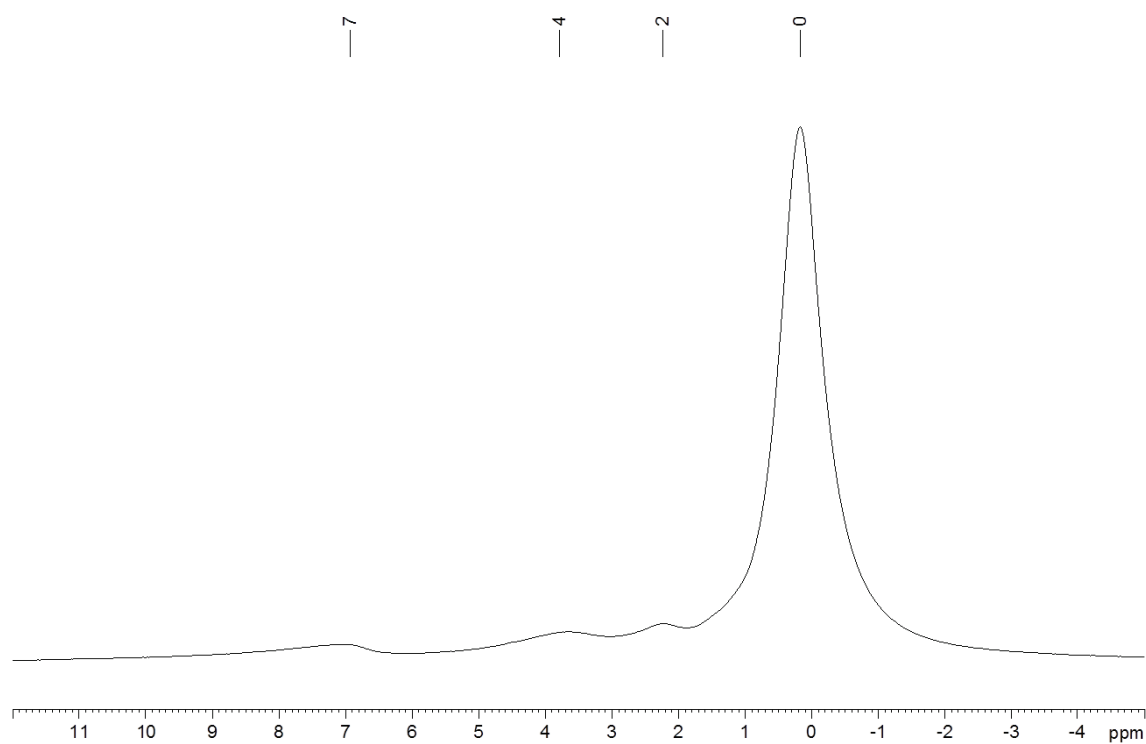


Figure A5. ^1H NMR of M-Im

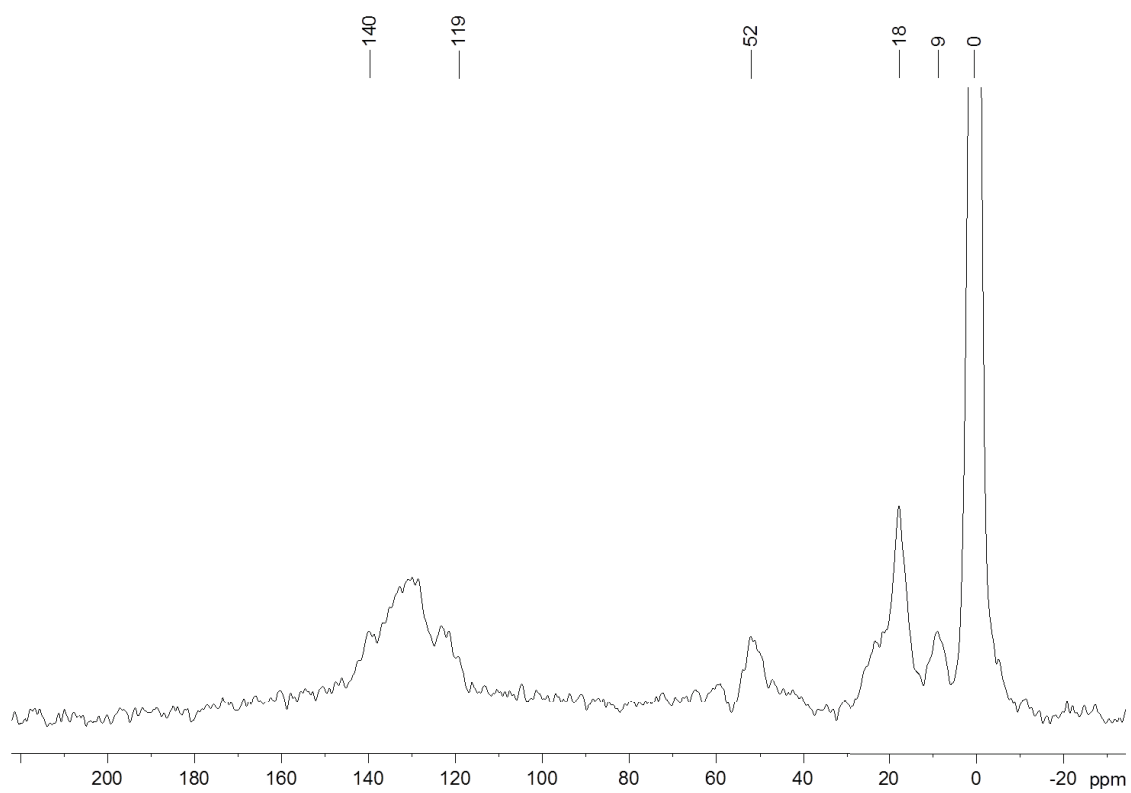


Figure A6. ^{13}C NMR of M-Im

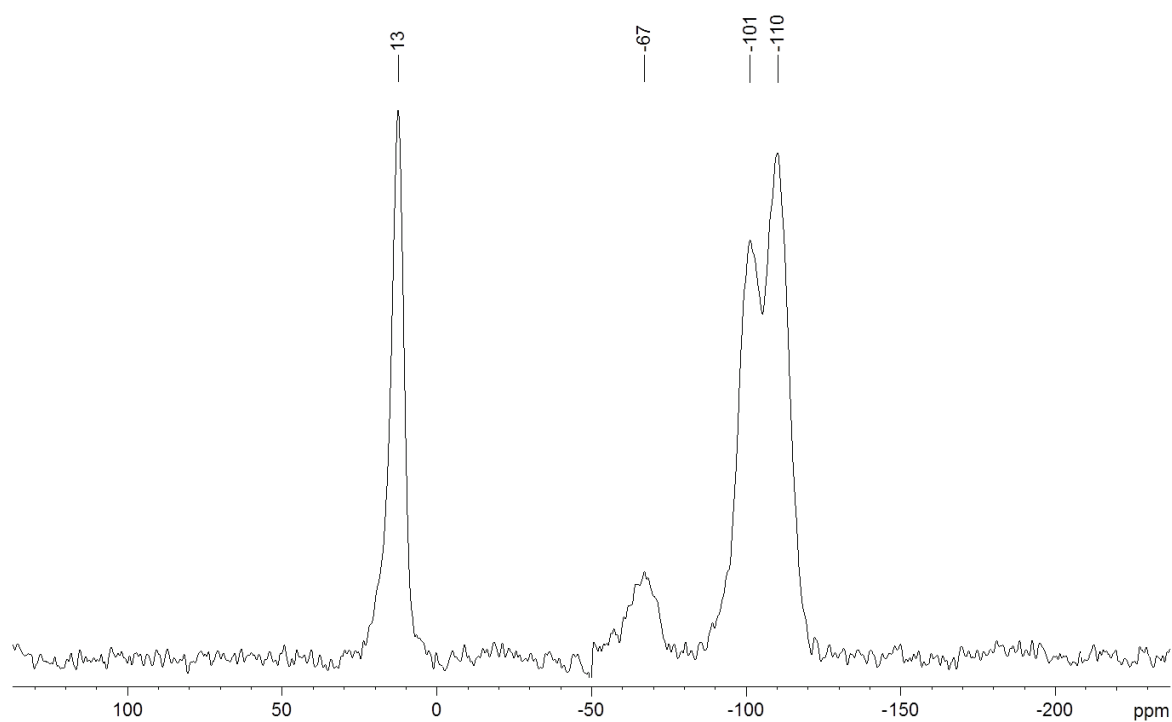


Figure A7. ^{29}Si NMR of M-Im

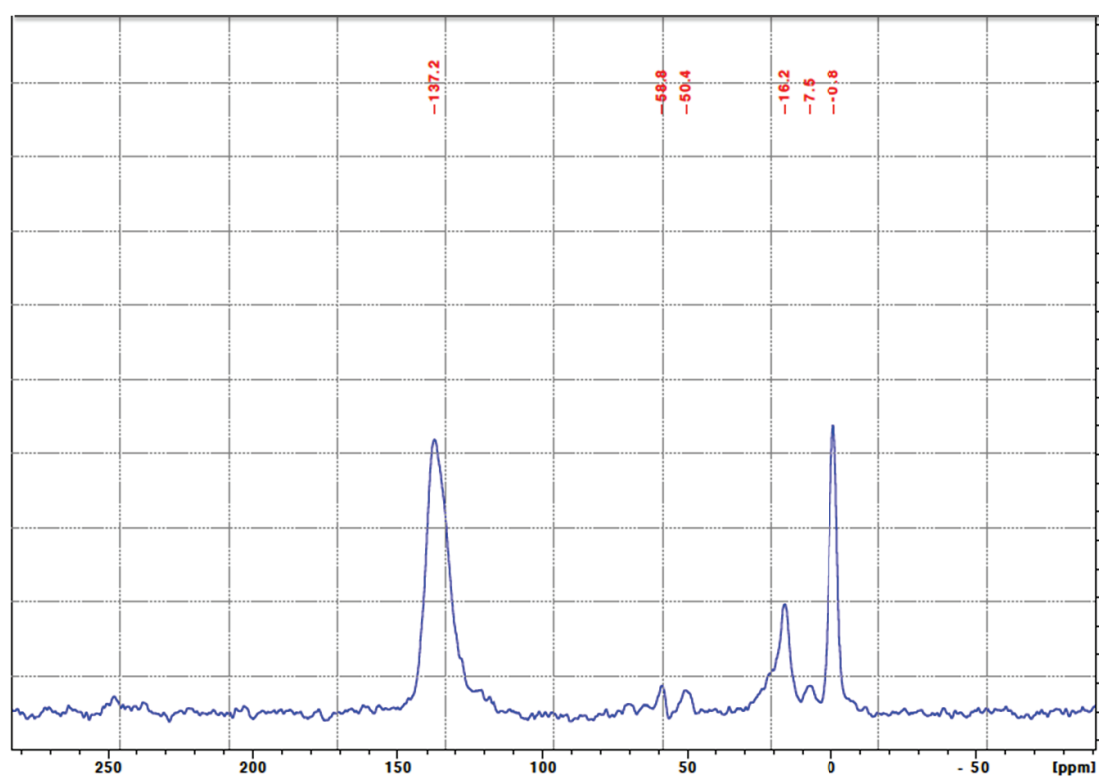


Figure A8. ^{13}C NMR of M*-Im

Chapter 2

Table A1. Crystal data structure refinement for [IrCl(MesImPr)(COD)]

$C_{23}H_{32}ClIrN_2$	$Z = 2$
$M_r = 564.19$	$F(000) = 556$
Triclinic, $P\bar{1}$	$D_x = 1.731 \text{ Mg m}^{-3}$
Hall symbol: $-P\ 1$	Mo $K\alpha$ radiation, $\lambda = 0.7107 \text{ \AA}$
$a = 9.9815 (3) \text{ \AA}$	Cell parameters from 10034 reflections
$b = 10.2821 (3) \text{ \AA}$	$\theta = 3.7\text{--}29.0^\circ$
$c = 11.5971 (4) \text{ \AA}$	$\mu = 6.30 \text{ mm}^{-1}$
$\alpha = 97.793 (3)^\circ$	$T = 150 \text{ K}$
$\beta = 95.183 (3)^\circ$	Needle, yellow
$\gamma = 111.720 (3)^\circ$	$0.82 \times 0.45 \times 0.30 \text{ mm}$
$V = 1082.66 (7) \text{ \AA}^3$	

Data collection

Xcalibur, Eos, Nova diffractometer	5218 independent reflections
Radiation source: Mova (Mo) X-ray Source	4820 reflections with $I > 2.0\sigma(I)$
mirror	$R_{\text{int}} = 0.093$
Detector resolution: $15.9897 \text{ pixels mm}^{-1}$	$\theta_{\text{max}} = 29.2^\circ$, $\theta_{\text{min}} = 3.1^\circ$
ω scans	$h = -12 \rightarrow 13$
Absorption correction: analytical <i>CrysAlis PRO</i> , Agilent Technologies, Version 1.171.36.28 (release 01-02-2013 CrysAlis171.NET) (compiled Feb 1 2013, 16:14:44) Analytical numeric absorption correction using a multifaceted crystal model based on expressions derived by R.C. Clark & J.S. Reid. (Clark, R. C. & Reid, J. S. (1995). <i>Acta Cryst. A</i> 51, 887-897)	$k = -14 \rightarrow 14$
$T_{\text{min}} = 0.087$, $T_{\text{max}} = 0.292$	$l = -15 \rightarrow 15$
18778 measured reflections	

Refinement

Refinement on F^2	Primary atom site location: structure-invariant direct methods
Least-squares matrix: full	Hydrogen site location: difference Fourier map
$R[F^2 > 2\sigma(F^2)] = 0.042$	H-atom parameters constrained
$wR(F^2) = 0.104$	Method = Modified Sheldrick $w = 1/[\sigma^2(F^2) + (0.07P)^2 + 0.0P]$, where $P = (\max(F_o^2, 0) + 2F_c^2)/3$

Chapter 2

$S = 0.97$	$(\Delta/\sigma)_{\max} = 0.001$
5210 reflections	$\Delta_{\max} = 2.79 \text{ e } \text{\AA}^{-3}$
244 parameters	$\Delta_{\min} = -3.66 \text{ e } \text{\AA}^{-3}$
0 restraints	

Chapter 3

**Catalytic performance of the Ir(I)-NHC based material and its
homogeneous analogues**

Application to alkene hydrogenation reactions

Table of content

III-1 Introduction	97
III-2 Catalytic activity of heterogeneous Ir(I)-NHC material	100
2.1 Catalytic activity for heterogeneous catalyst Ir(I)-NHC material versus homogeneous analogues in trans-stilbene hydrogenation reaction	100
2.2 Ir(I)-NHC material life-time evaluation	102
2.3 Investigation the scope of substrates	103
2.3.1. Scope of substrates for Ir(I)-NHC material	103
2.3.2. Scope of substrates for Ir(I)-NHC model molecular complex	105
2.3.3. Selectivity	107
2.3.4. Conclusions	109
2.4 Following homogeneous hydrogenation by NMR	110
2.5 Temperature influence on trans-stilbene hydrogenation rate	112
2.6 Directing effects	113
2.7 Deactivation	116
2.8 Recycling.....	119
III-3 Conclusions	120
III-4 Experimental section.....	121
4.1 General information	121
4.2 Hydrogenation conditions	121
4.2.1. Heterogeneous catalysis	121

4.2.2. Homogeneous catalysis	122
4.2.3. Scope of substrates	122
4.2.4. Diastereoselective hydrogenation	123
4.2.5. Split tests	123
III-5 Appendix	124

List of Figures

Figure 1. Conversion of trans-stilbene hydrogenation as a function of reaction time using: neutral $[\text{IrCl}(\text{COD})\text{MesImPr}]$, cationic $[\text{Ir}(\text{COD})(\text{MesImPr})]\text{BF}_4$ and heterogeneous M-Ir catalyst	101
Figure 2. Turnover number (TON) of trans-stilbene hydrogenation as a function of reaction time using: neutral organometallic $[\text{IrCl}(\text{COD})\text{MesImPr}]$, cationic $[\text{Ir}(\text{COD})(\text{MesImPr})]\text{BF}_4$ and M-Ir material	102
Figure 3. Catalytic profiles of trans-stilbene hydrogenation with different mol% of M-Ir...	103
Figure 4. Selected substrate for evaluation of catalytic activity of $[\text{IrCl}(\text{COD})(\text{MesImPr})]$ and M-Ir.	104
Figure 5. Substrate scope for M-Ir.	104
Figure 6 . Substrate scope for $[\text{IrCl}(\text{COD})\text{MesImPr}]$	105
Figure 7. Conversion as a function of time in acetoxystyrene hydrogenation by $[\text{IrCl}(\text{COD})\text{MesImPr}]$ and $[\text{IrCl}(\text{COD})]_2$	106
Figure 8. Conversion of limonene hydrogenation as a function of reaction time using: $[\text{IrCl}(\text{COD})\text{MesImPr}]$ and M-Ir material	107
Figure 9. Change the composition during limonene hydrogenation as a function of time.	

Catalysis was carried out in Toluene at 40°C with 0.05mol% of M-Ir	108
Figure 10. Selectivity towards p-Mentene and p-Mentane as a function of limonene conversion. Catalysis was carried out in Toluene at 40°C with 0.05mol% of M-Ir	108
Figure 11. In situ monitoring acetoxystyrene hydrogenation with [IrCl(COD)MesImPr]. .	111
Figure 12. Temperature impact in trans-stilbene hydrogenation with M-Ir material.	113
Figure 13. Conversion of terpinen-4-ol hydrogenation as a function of reaction time using [IrCl(COD)MesImPr] and M-Ir material .Temperature impact into hydrogenation rate.....	114
Figure 14. Selectivity towards directed product formation as a function of terpinen-4-ol conversion measured using M-Ir and [IrCl(COD)MesImPr] catalysts at 40°C	115
Figure 15. Selectivity towards directed product formation as a function of terpinen-4-ol conversion measured using M-Ir and [IrCl(COD)MesImPr] catalysts at 80°C.	116
Figure 16. Photos of substrate and [IrCl(COD)MesImPr] catalyst solution before (a) and after (b) catalytic reduction of Terpinen-4-ol at 80°C with 0.1mol% of catalyst.....	116
Figure 17. STEM micrographs and EDX of the recovered solid after full trans-stilbene reduction (2.5 hours) at 80°C with 0.1mol% of M-Ir in toluene	117
Figure 18. Recycling of M-Ir in trans-stilbene hydrogenation	119

List of Tables

Table 1. Comparison of TOF (h^{-1}) for homogeneous and heterogeneous catalysts	109
Table 2. Investigation of spent M-Ir catalyst for the Iridium nanoparticles formation by TEM and EDX technics	118

List of Figures in Appendix

Figure A1. Study the solvent effect in trans-stilbene hydrogenation with $[\text{Ir}(\text{COD})(\text{MesImPr})]$	124
Figure A2. . ^1H NMR spectra of limonene hydrogenation by recovered supernatant from acetoxystyrene hydrogenation	125

List of Tables in Appendix

Table A1. Investigation of $[\text{IrCl}(\text{COD})\text{MesImPr}]$ decomposition related to Iridium nanoparticles formation by TEM and EDX techniques	126
Table A2. Study the presence of Ir NPs on spent catalyst (recovered after trans-stilbene hydrogenation at 40°C with 0.33mol% of cat) by TEM and EDX	127

III-1 Introduction

In this chapter, the catalytic performances of the as-obtained Ir(I)-NHC based material will be studied and compared to those of homogeneous homologues in solution. As previously mentioned, low coordinated Iridium species are putatively formed during the transmetallation process due to COD decoordination assisted by surface stabilization. The absence of COD in Ir coordination sphere may influences positively its reactivity in alkene hydrogenation as far as COD decoordination is considered as the initial step for the generation of Ir-catalytically active species. Consequently, the absence of COD modifies the catalyst' initial rate (no initiation period required to convert the pre-catalyst into the active site).

Usually, catalytic performances are characterized by several parameters: turnover number, turnover frequency, selectivity, stability and functional group tolerance. In general the rate of any solid-liquid reaction can be expressed as the product of the rate coefficient k and a pressure (or concentration) dependent term:

$$rate = kf(p_i), \quad (1)$$

where p_i is the partial pressure of reagent i . For catalytic reactions involving a large number of elementary steps, the overall reaction rate is limited by the rate of the slower elementary step also called the limiting step. The rate coefficient k is influenced by the reaction conditions (temperature, pressure, surface concentrations...) as it can be described by the Arrhenius equation:

$$k = A\exp\left(-\frac{E_a}{RT}\right), \quad (2)$$

where A is a temperature-dependent pre-exponential factor and E_a is the apparent activation energy of the catalytic reaction. This datum is of interest to compare catalysts but also to gain insight into the catalytic mechanisms.

In general, for sake of convenience, catalysts performances are defined by two major figures: turnover numbers (TON) and turnover frequencies (TOF).

The turnover number is the molar ratio between the quantity of product formed during the reaction (in mol.) and the quantity of spent catalyst (in mol.). It can also be represented as a product of substrate to catalyst ratio (R) by the conversion (X_A):

$$TON = \frac{v(\text{product})}{v(\text{catalyst})} = R \times X_A \quad (3)$$

Conversion is defined as a number of moles of substrate converted during the course of the reaction per initial number of moles of substrate.

The TOF is defined as the number of times n that the overall catalytic reaction takes place per catalytic site within a unit of time. TOF expressed in s^{-1} is actually a TON referred to particular period in time:

$$TOF = \frac{v(\text{product})}{v(\text{catalyst}) \times \text{time}} = \frac{TON}{\text{time}} = \frac{X_A \times R}{\text{time}} \quad (4)$$

or:

$$TOF = \frac{1}{S} \frac{dn}{dt} \quad (5)$$

Where S is the number of active sites and dn/dt characterizes the change of the quantity of product with time. Thus, TOF characterizes catalyst activity and rate where the maximum TON (TON_{max}) represents the catalyst productivity. Noteworthy, during the catalytic reaction, catalytic performances have a tendency to deteriorate with time. This phenomenon is called catalyst deactivation. Generally, deactivation phenomena occur on a much longer time scale than that of the desired reaction. However, large variations in time scales for deactivation are reported. The shortest are in the order of seconds or even shorter, while the longest are of the order of a few years. Catalyst deactivation is generally due to three major phenomena: solid state transformations, poisoning and coking. Solid state transformations cover a wide variety of phenomena that induce modifications of the catalysts features (formation of nanoparticles, phase transformations...). Catalyst poisoning refers to the chemisorption of impurities from the feed at the surface of the catalyst which inhibits the catalytically active sites and catalyst poisoning is generally considered as irreversible. Coking consists of the irreversible deposition of carbonaceous residues from reactants, products or intermediates and is to be considered as a side reaction.

It should be mentioned that TON and TOF make sense in defined reaction conditions (temperatures, pressures or concentrations, reactant ratio).¹³¹

¹³¹ J.M. Thomas and W.J. Thomas in *Principles and Practice of Heterogeneous Catalysis*, Wiley-VCH Verlag GmbH & Co, KGaA, Boschstr. 12, 69469 Weinheim, Germany, **2014**, p.

Chapter 3

The catalytic performance of a catalyst is characterized not only by its rate and productivity but also by its selectivity (S_p). Selectivity reflects the ability of a catalyst to convert the substrate into specific products. In general, the selectivity is the production rate of a targeted product (r_d) per production rate of undesired one (r_u):

$$S_p = \frac{r_d}{r_u} = \frac{N_d}{N_u} \quad , \quad (6)$$

where N_d is the number of moles of the desired product and N_u of number of moles of the undesirable one.

However, more illustrative and thus usually used is the selectivity expression as the number of moles transformed into a desired product compared to the total number of moles converted:

$$S_p = \frac{N_p}{N_{A0} - N_A} \times 100\% \quad , \quad (7)$$

where N_p is number moles of product, N_{A0} the starting number of moles of the substrate and N_A the number of moles of substrate after a defined amount of time during the catalytic reaction .

In contrast to the definition of the selectivity, the definition of a yield is not related to the number of moles converted but to the starting number of moles of substrate:

$$Y = \frac{N_p}{N_{A0}} \quad (8)$$

selectivity, conversion and yield are connected by equation 9:

$$Y_p = S_p \times X_A \quad (9)$$

Finally, the last (but not less important) catalyst characteristic is functional group tolerance i.e. the scope of possible substrates that can be transformed successfully. The substrate scope represents the versatility of the catalyst.¹³²

¹³² a)Industrial Catalysis: A Practical Approach, Second Edition. Jens Hagen2006 WILEY-VCH Verlag GmbH & Co. KGaA, Weinheim, 1-14.

b)Vol. 5 (Eds.: J. L. Atwood, J. E. D. Davies, D. D. MacNicol, F. Vögtle, K. S. Suslick), Pergamon, Oxford, 1996, pp. 317–343.

III-2 Catalytic performances of heterogeneous Ir(I)-NHC based materials

2.1 Comparison between the catalytic performances of Ir(I)-NHC based materials and those of homogeneous analogues in trans-stilbene hydrogenation

The goal of this project is to prepare a highly active and productive alkene hydrogenation catalyst that can be used under mild hydrogenation conditions associated with low hydrogen pressures and low reaction temperatures. In such mild conditions, the hydrogenation can be carried out even in a glass reactor.

The catalytic performances of our material, namely M-Ir, and those of two Ir-NHC complexes, neutral $[\text{IrCl}(\text{MesImPr})(\text{COD})]$ and cationic $[\text{Ir}(\text{MesImPr})(\text{COD})]\text{BF}_4$, were evaluated in trans-stilbene hydrogenation under mild conditions: typically, a solution of trans-stilbene in toluene was heated at 40°C in a Fisher-Porter reactor under 3 bar of dihydrogen in the presence of 0.1 mol% of catalysts (based on iridium). As the Crabtree's catalyst is known to be poisoned by coordination solvents, hydrogenation usually proceeds in non-coordinative solvents like CH_2Cl_2 . For M-Ir material, which contains hydrophobic surface TMS groups, apolar solvents like toluene are preferred. The activity of $[\text{IrCl}(\text{MesImPr})(\text{COD})]$ in trans-stilbene hydrogenation in both toluene and CH_2Cl_2 was found to be similar (Fig A1). However the activity of M-Ir was decreased dramatically when switching from toluene to CH_2Cl_2 (such results being explained by diffusion transfer limitation related to the bad dispersion of the solid in DCM). As a result, all the experiments depicted below were carried out into toluene for sake of comparison.

The cationic iridium complex, $[\text{Ir}(\text{COD})(\text{MesImPr})]\text{BF}_4$, was generated in-situ from $[\text{IrCl}(\text{COD})(\text{MesImPr})]$ by addition of AgBF_4 (1eq) in solution. The reaction was monitored by liquid state NMR to build conversion vs. time profiles (Fig.1).

Surprisingly, M-Ir showed a 50 times superior activity in terms of TON in comparison with the neutral $[\text{IrCl}(\text{MesImPr})(\text{COD})]$ complex and 15-20 times superior activity with respect to that of the cationic complex $[\text{Ir}(\text{MesImPr})(\text{COD})]\text{BF}_4$. For M-Ir, full conversion was reached within 18h whereas $[\text{IrCl}(\text{MesImPr})(\text{COD})]$ failed to reach full conversion after more than 80 days! The cationic iridium complex, $[\text{Ir}(\text{COD})(\text{MesImPr})]\text{BF}_4$, was found to be faster than its neutral derivative but the reaction was not complete after 60 days. Calculated TOF after 5h of

reaction are 38h^{-1} for M-Ir, 1.8h^{-1} for $[\text{IrCl}(\text{MesImPr})(\text{COD})]$ and 0.75h^{-1} for $[\text{Ir}(\text{MesImPr})(\text{COD})]\text{BF}_4$ respectively.

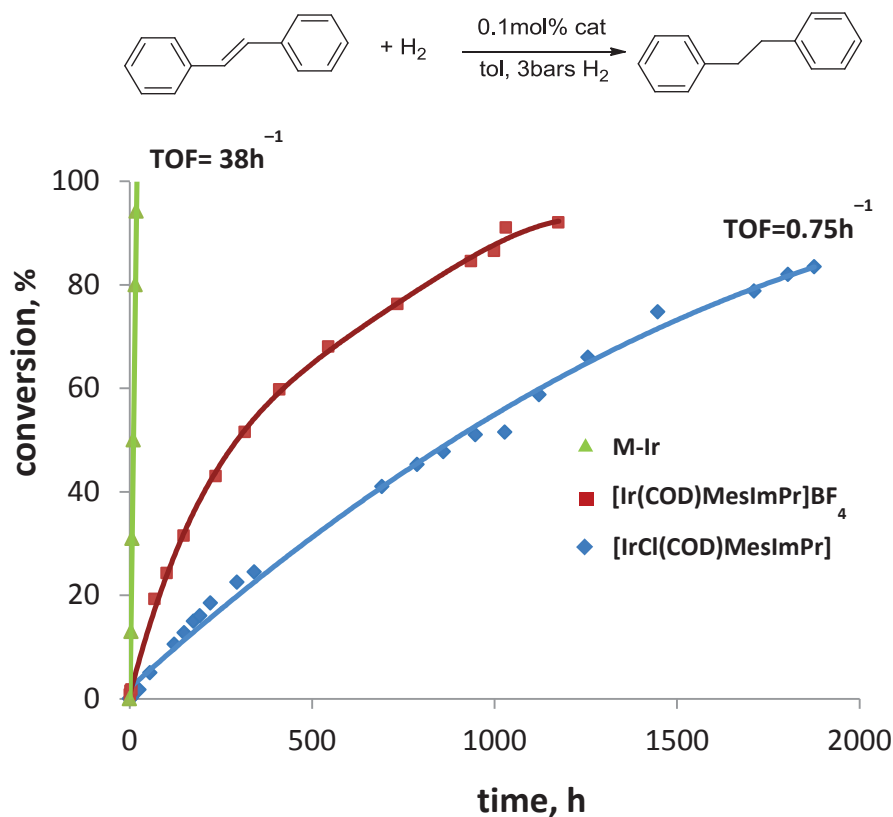


Figure 1. Conversion of trans-stilbene as a function of reaction time using: neutral $[\text{IrCl}(\text{COD})\text{MesImPr}]$, cationic $[\text{Ir}(\text{COD})\text{MesImPr}]\text{BF}_4$ and M-Ir material. The hydrogenation experiments were carried out in toluene at 40°C under 3 bar of H₂ (0.1 mol% of Ir).

Furthermore, the hydrogenation profile of M-Ir in Fig.1 is linear thus suggesting no catalyst deactivation of the catalysts during the catalytic test and a kinetic law with a zero order with respect to trans-stilbene.

A blank test using the parent material M-Ag left the substrate unchanged, showing that catalysis was only due to the supported Ir sites.

Moreover, a standard split test was therefore performed with M-Ir and showed no activity, thus suggesting the absence of any active Ir-species in solution (Fig.A2). Finally, no leaching of Ir was detected in the reaction supernatants by ICP measurements.

2.2 Ir(I)-NHC material life-time evaluation

As observed in Fig.1, a small deactivation of both homogeneous catalysts was observed before reaching full conversion of trans-stilbene. In contrast to homogeneous complexes, M-Ir was found highly stable in the same conditions (40 °C, 3 bars of H₂, 0.1 mol% of Ir) and full conversion of trans-stilbene was rapidly reached. In order to estimate the productivity of M-Ir (the maximum turnover numbers accessible before catalyst death), the reaction was performed with lower catalyst loading (0.01mol% of Ir). As shown in Fig.2, the two complexes deactivated rapidly and only reached a $\text{TON}_{\text{max}} \leq 1000$ after 700 h (observation of the catalyst death at 89% conversion using 0.1 mol% of [IrCl(COD)(MesImPr)]), while M-Ir exhibited a much higher productivity, reaching 80% conversion (TON = 8000). Unfortunately, we could not determine the TON_{max} because trace impurities remaining after purification of the large amounts of solvent and substrate necessary for the tests at lower catalysts loadings induced side poisoning of the catalyst.

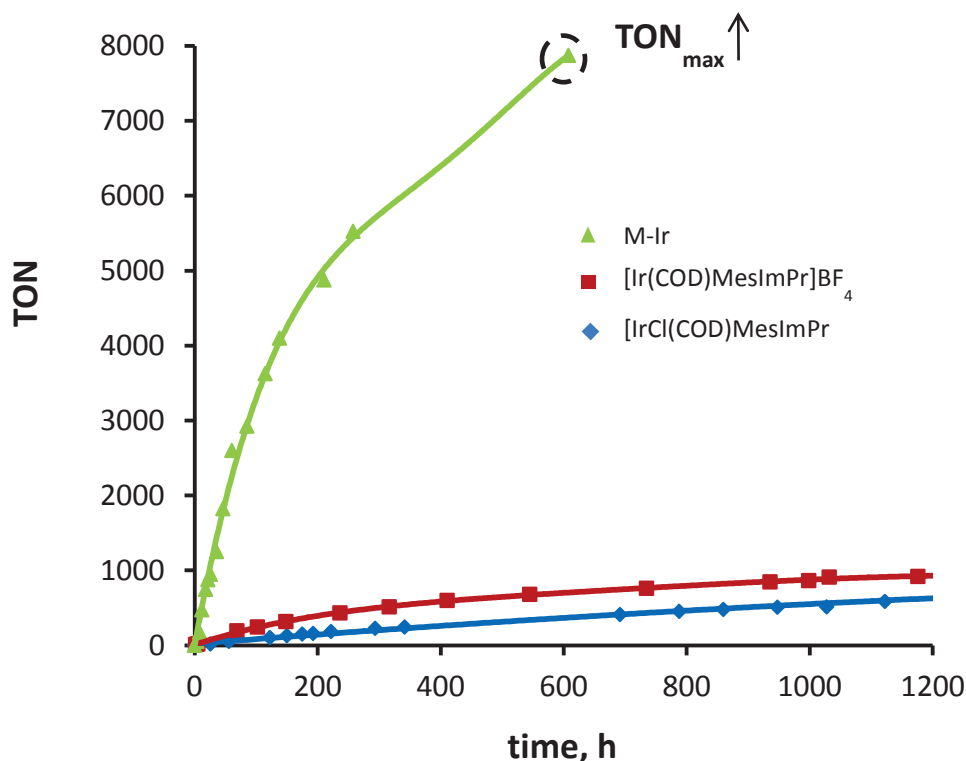


Figure2. Turnover number (TON) as a function of reaction time using: neutral organometallic complex 1 (♦diamonds); cationic [Ir(COD)(MesImPr)]BF₄ (■ squares); M-Ir material (▲triangles). The trans-stilbene hydrogenation experiments were carried out in toluene at 40 °C under 3 bar of H₂.

Interestingly, the trans-stilbene hydrogenation with different substrate/catalyst ratio of M-Ir showed a linear profile (related to a kinetic law with a zero order with respect to the olefinic substrate) without any activation period. (Fig. 3)

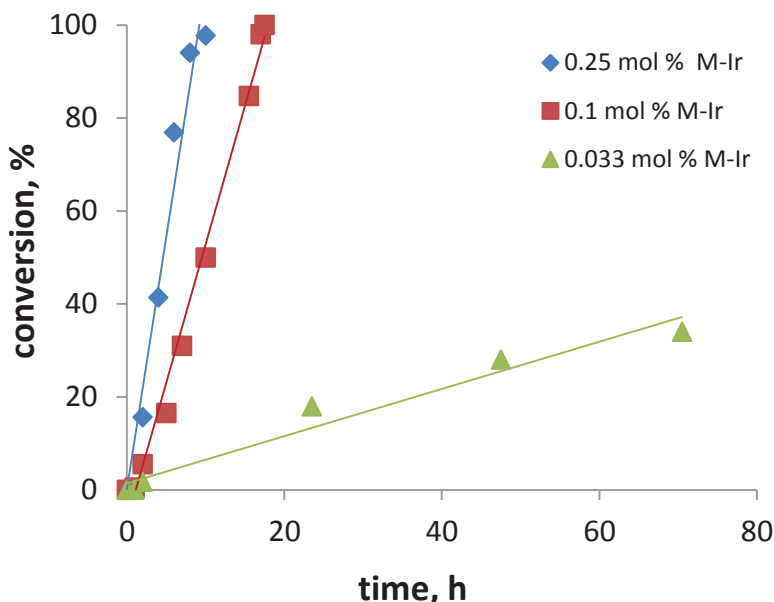


Figure 3. trans-stilbene conversion as a function of time with different M-Ir loadings (mol% of Ir)

2.3. Scope of substrates

2.3. 1. Ir(I)-NHC material

The next logical step for the evaluation of the catalytic performances was to study the scope of possible substrates to be efficiently hydrogenated. It was interesting to study the influence of electron donating and electron-withdrawing groups onto the hydrogenation rate. Thus a series of functionalized styrenes with electron withdrawing groups (p-fluorostyrene) and with electron donating substituents (p-vinylanisole and p-acetoxystyrene) were used as standard substrates (Fig4, a-d). As styrenes are less sterically hindered than trans-stilbene (Fig4, f), their catalytic hydrogenation was found faster as expected. The next point to be studied is the selectivity of C=C bonds hydrogenation in the presence of other reactive functional groups. Nilsson and co-workers reported that in contrast to industrial Pd/C catalyst, Ir-NHC complexes are able to hydrogenate alkenes selectively leaving organic functionalities (Bromide, amide and ketone) unchanged.¹³³

¹³³ Bennie, L. S.; Fraser, C. J.; Irvine, S.; Kerr, W. J.; Andersson, S.; Nilsson, G. N., *Chem. Commun.* **2011**, 47 (42), 11653-11655.

Chapter 3

The typical hydrogenation experiment was performed in toluene with 0.033mol % of catalyst loading at 40°C under 3 bars of H₂. The initial TOFs for styrene, fluorostyrene and vinylanisole seemed to be similar. However, acetoxystyrene was hydrogenated much more slowly than other functional styrenes; the bulkiest substrate (trans-stilbene) being the most difficult to hydrogenate.

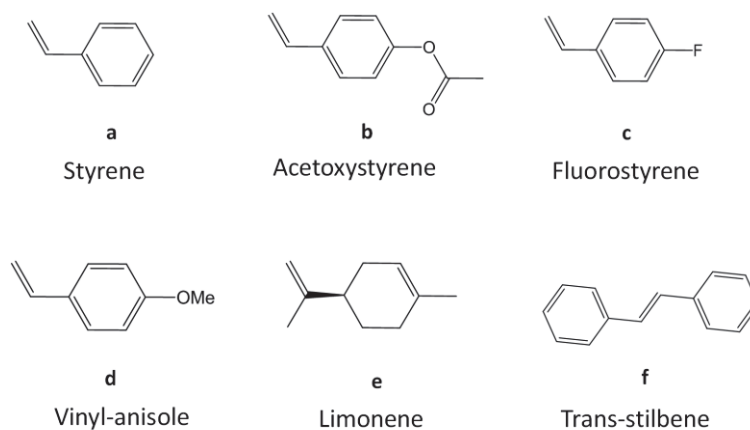


Figure 4. Selected substrate for evaluation of catalytic activity of [IrCl(COD)(MesImPr)] and M-Ir

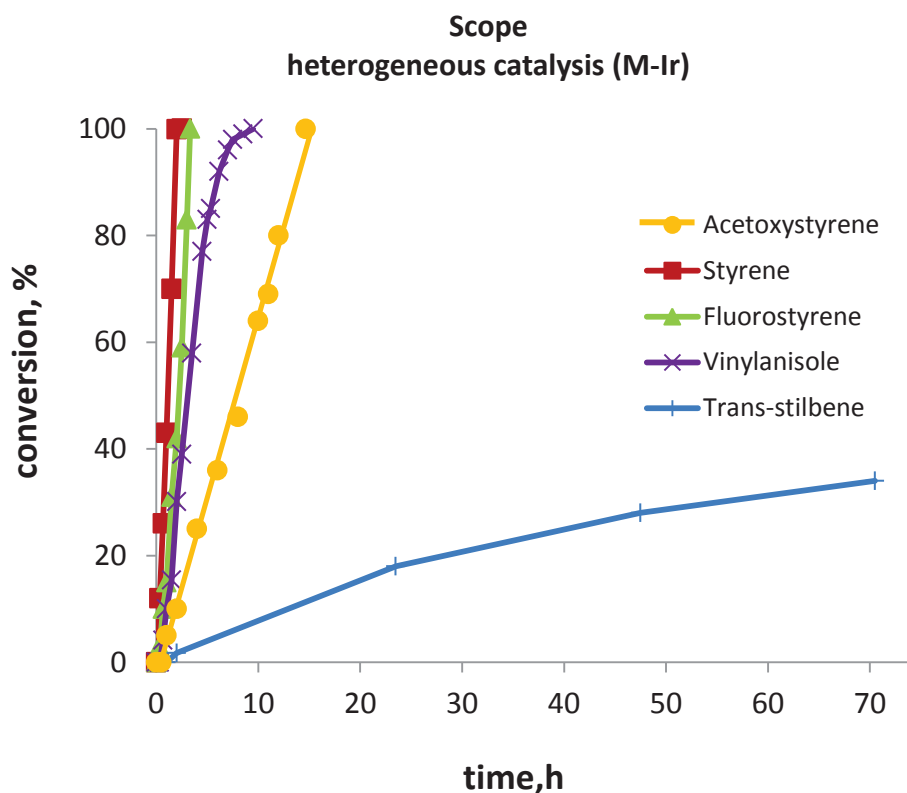


Figure 5. Substrate scope for M-Ir. Catalysis performed in Toluene at 40°C under 3 bars of H₂ with 0.033mol % of catalyst

Overall, our results do not show any obvious dependence between hydrogenation rate and electronic properties of the functional group whereas a dependence between the steric bulkiness of substrate and hydrogenation rate could be observed.

2.3.2. Ir(I)-NHC model molecular complex

The neutral $[\text{IrCl}(\text{COD})(\text{MesImPr})]$ was also tested for the hydrogenation of the same array of substrates and in the same conditions as for M-Ir. The hydrogenation profiles are presented on the Fig.6. One can see that for the homogeneous catalysts the ranking for substrate hydrogenation remains the same as for M-Ir. Styrene, fluorostyrene and vinylanisole are transformed into their hydrogenated products with similar rates. However, we can observe that $[\text{IrCl}(\text{COD})(\text{MesImPr})]$ is almost inactive in trans-stilbene hydrogenation reaching less than 5% conversion in 70 h.

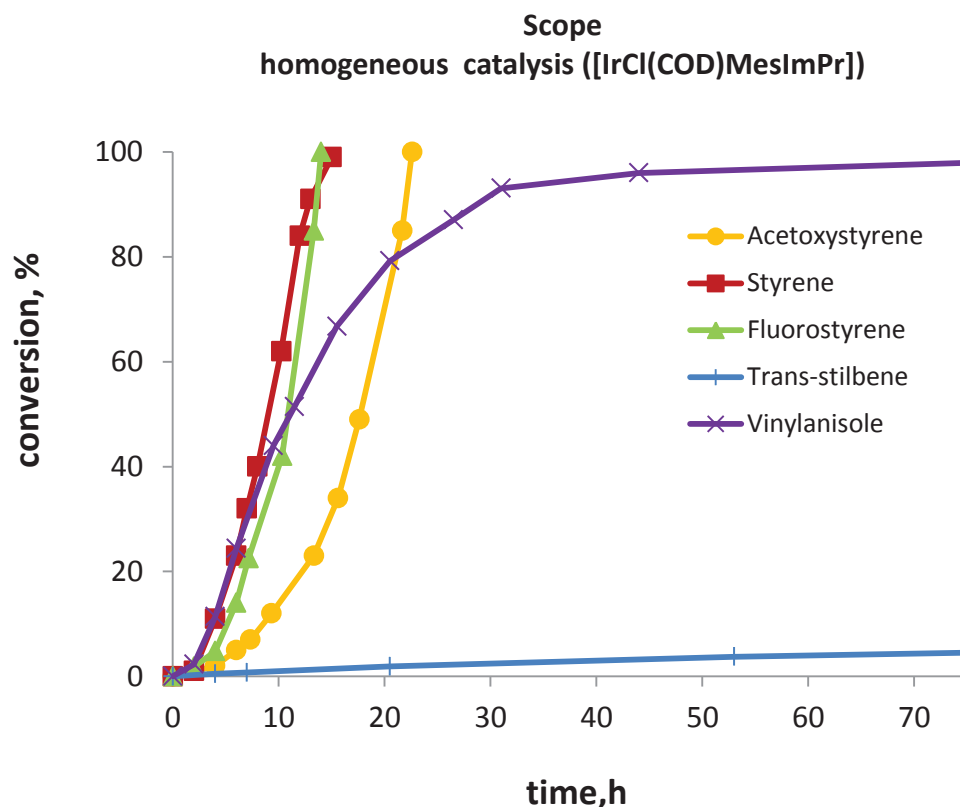


Figure 6. Substrate scope for $[\text{IrCl}(\text{COD})\text{MesImPr}]$. Catalysis performed in Toluene at 40°C under 3 bars of H_2 with 0.033mol % of catalyst

The most impressive difference between the homogeneous and heterogeneous systems is related to the catalytic profiles (conversion vs time). In homogeneous conditions, for all substrates, except trans-stilbene, an increase of the hydrogenation rate with time was observed, showing a so called initiation period. At the reverse, no initiation period was

detected for M-Ir. The absence of initiation period for M-Ir is probably connected to the absence of COD.

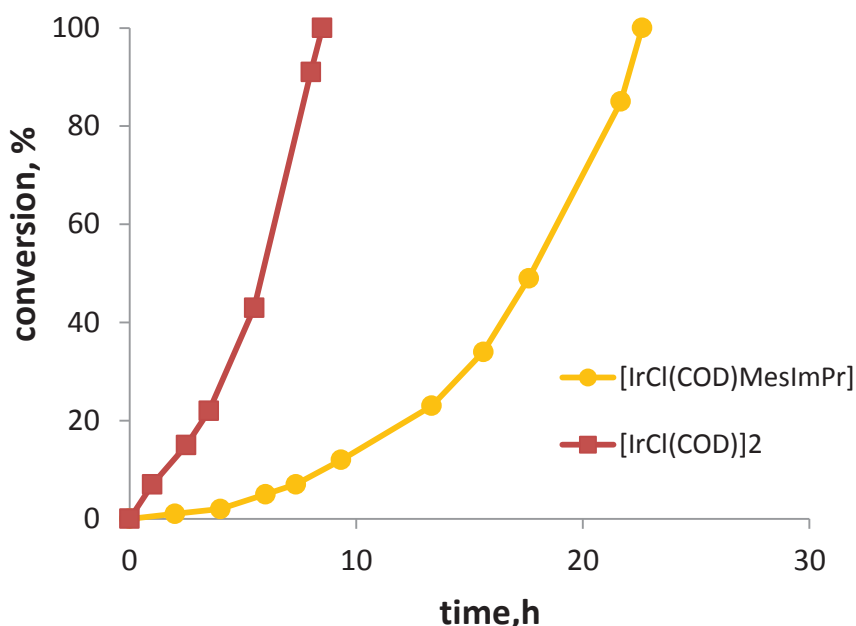


Figure 7. Conversion as a function of time in acetoxystyrene hydrogenation by $[\text{IrCl}(\text{COD})\text{MesImPr}]$ and $[\text{IrCl}(\text{COD})]_2$

In order to understand if homogeneous $[\text{IrCl}(\text{COD})(\text{MesImPr})]$ and the precursor used for its synthesis $[\text{IrCODCl}]_2$ have a similar hydrogenation pathway, we performed the acetoxystyrene hydrogenation with $[\text{IrCODCl}]_2$. The catalytic conditions were kept the same as those used for $[\text{IrCl}(\text{COD})(\text{MesImPr})]$. $[\text{IrCl}(\text{COD})(\text{MesImPr})]$ was found to be less active for acetoxystyrene hydrogenation in comparison with $[\text{IrCODCl}]_2$ which was used as a precursor for its synthesis. As shown in Fig.7, the initial TOF measured in 30 % conversion for precursor is equal to 200 h^{-1} versus only 100 h^{-1} for $[\text{IrCl}(\text{COD})(\text{MesImPr})]$. Despite the different hydrogenation rates, the kinetic profiles were found similar, meaning that the hydrogenation pathway remains the same. Taking into account that both catalysts contained the COD ligand and showed an initiation period while M-Ir, which contains only 8% of COD, exhibited a linear hydrogenation profile, we can conclude that this initiation period is likely related to COD hydrogenation/dissociation. Previously Burgess and co-workers reported that the dissociation of COD is required to convert pre-catalyst into a real catalyst.¹³⁴

¹³⁴ Perry, M. C.; Cui, X.; Powell, M. T.; Hou, D. R.; Reibenspies, J. H.; Burgess, K., *J. Am. Chem. Soc.* **2003**, 125 (1), 113-123.

2.3.3. Selectivity

The selective hydrogenation the one type of double bond in the presence of others is highly important for industrial purposes therefore limonene (Fig4,e) which contains one terminal and one internal double bond was selected as an appropriate standard to study hydrogenation selectivity. The catalytic experiments with M-Ir and $[\text{IrCl}(\text{MesImPr})(\text{COD})]$ were performed in the same conditions, i.e. in toluene under 3 bars of H_2 with 0.033 mol% of catalyst (based on Ir loading) at 40 °C.

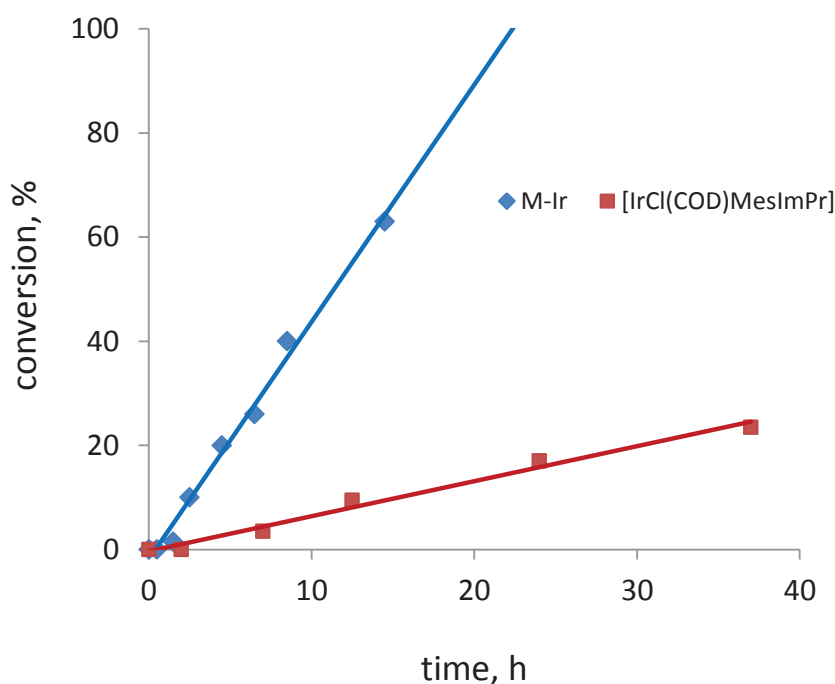


Figure 8. Conversion of limonene hydrogenation as a function of reaction time using: $[\text{IrCl}(\text{COD})\text{MesImPr}]$ and M-Ir material

The terminal double bond of limonene was hydrogenated first, in perfect agreement with the steric control of the reactivity. Again M-Ir was found to be more active than the homogeneous catalyst (Fig.8). The experiment however was initially stopped before the total hydrogenation of the terminal bond due a mass balance problem. This problem was solved by freezing the substrate solution before removing the H_2 .

Another experiment was performed with 0.05mol% of M-Ir loading in toluene at 40 °C under 3 bars of H_2 . Fig.9 shows the change of composition mixture during the hydrogenation of limonene with M-Ir. One can see that M-Ir selectively reduces the terminal double bond as shown in Fig.10 which shows the selectivity versus conversion. The formation of p-menthane is only observed when more than 95% of limonene is already converted into p-menthene.

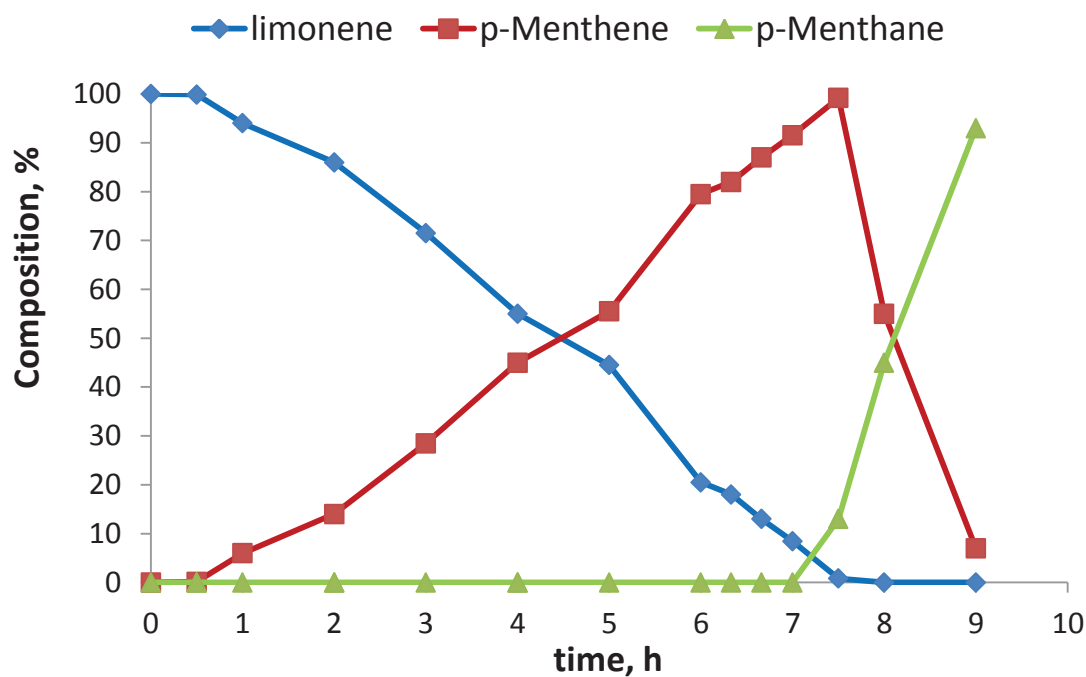


Figure 9. Change the composition during limonene hydrogenation as a function of time. Catalysis was carried out in Toluene at 40 °C with 0.05mol% of M-Ir

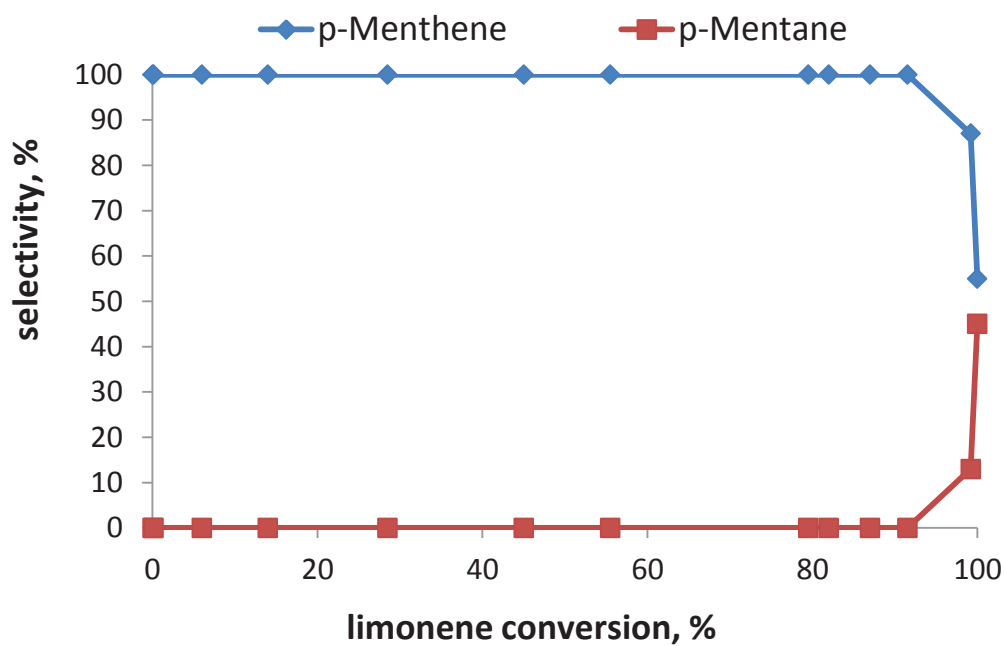


Figure 10. Selectivity towards p-Menthene (blue dimonds) and p-Mentane (red squeres) as a function of limonene conversion. Catalysis was carried out in Toluene at 40 °C with 0.05mol% of M-Ir

2.3.4. Conclusions

In summary, we tested the catalytic activity of the M-Ir material in hydrogenation of functional styrenes, limonene and trans-stilbene. Its catalytic performances (in term of TON and TOF) were compared to those of homogeneous homologues in solution. In all cases, a significant increase in activity was observed for the heterogeneous catalyst with respect to homogeneous analogues (Table1). An even larger difference in hydrogenation rate was noticed at higher catalysts loading (0.1mol % cat). In this case, M-Ir is 50 times more active for the trans-stilbene hydrogenation than $[\text{IrCl}(\text{MesImPr})(\text{COD})]$ and 20 times than the molecular cationic $[\text{Ir}(\text{MesImPr})(\text{COD})]\text{BF}_4$ analogue. The decrease of hydrogenation rate with increase of catalyst loading is well known for Crabtree's catalyst and is explained by increasing the input of bimolecular deactivation processes which are probably prevented when site isolating the Ir centers onto a solid support.

We didn't find a significant influence of the electron donating character of the substituents on reaction rate. However it was shown that steric bulkiness influenced the hydrogenation rate in the same way as for Wilkinson catalyst: less steric hindered substrates are hydrogenated faster. Both homogeneous and heterogeneous catalysts were able to hydrogenate selectively C=C bonds without damaging other functional groups. Moreover, M-Ir demonstrated a high degree of selectivity (>95%) for limonene hydrogenation onto p-Menthene.

Table1. Comparison of TOF (h^{-1}) for homogeneous and heterogeneous catalysts

Substrate	TOF, h^{-1*}		Improvement
	M-Ir	$[\text{IrCl}(\text{COD})(\text{MesImPr})]$	
styrene	1400	177	8 times faster
4-fluorostyrene	750	170	4.5 times faster
4-vinylanisole	190	120	4 times faster
4-acetoxystyrene	490	125	1.5 times faster
<i>trans</i> -stilbene [#]	44	4	10 times faster
Limonene [*]	125	20	6 times

TOF was calculated for the substrate at Sub:cat ratio 3000 at 70% conversion. *-at 25% conversion and #-at 4% conversion.

Differences between homogeneous and heterogeneous catalysis were also observed in the hydrogenation profile obtained for styrenes. In homogeneous conditions, the hydrogenation of

styrenes proceeds after an initiation period. The same initiation period was also detected with $[\text{Ir}(\text{COD})\text{Cl}]_2$, suggesting common hydrogenation pathways with both catalysts. In contrast, the hydrogenation profile obtained with M-Ir did not exhibit any initiation period for all the substrates. Taking into account that M-Ir contains only 8% of Ir sites with coordinated COD, this strongly suggests that the lack of initiation period for M-Ir is related to the absence of COD.

2.4. Following homogeneous hydrogenation by NMR

The *in situ* monitoring of the homogeneous catalytic hydrogenation is a very practical and useful method as it can give insights into the mechanistic pathway. Generally this method is known for metal-phosphine complexes used in hydrogenation reactions. The NMR coupling arising between the phosphorus and the proton in ^1H NMR gives the possibility to discriminate the cis and trans-hydride metal intermediates that possess different activities. Another purpose of *in situ* monitoring is to study the decomposition processes through the polyhydride complex formation. Indeed polyhydride complexes exhibit different types of hydrides that could be determined by combination of different 1D and 2D NMR techniques together with DFT calculations.

From these points of view it was interesting to follow *in situ* the homogeneous hydrogenation of acetoxystyrene with $[\text{IrCl}(\text{MesImPr})(\text{COD})]$. The experiment was performed in a Young tube with 50mol% of catalyst loading. Such a high catalyst loading is required as it gives the possibility to track the changes in the catalyst structure during hydrogenation. H_2 was introduced by bubbling through the mixture, dissolved in toluene. Acetoxystyrene was chosen as a substrate because it is hydrogenated more slowly than other substrates and an initiation period was observed. The goal of the experiment was to detect the decoordination/hydrogenation of COD ligand.

Surprisingly, we detected just small quantities of COD hydrogenated to cyclooctane (COA). As it can be seen from Fig.11, at 63% of acetoxystyrene conversion into p-ethylacetoxystyrene the peak corresponding to COA is very small. At the same time no COD decoordination was detected. After full substrate reduction the quantity of COA dramatically increases, suggesting a competition between substrate and hydrogen for Iridium coordination sites. As reduction of the substrate is impossible without COD decoordination/hydrogenation it seems that hydrogenation of the substrate proceeds with very small quantity of catalyst and that a big amount of complex exists as a pre-catalyst, forming a reservoir of active catalyst.

Thus the initiation period, previously reported for styrenes hydrogenation by $[\text{IrCl}(\text{MesImPr})(\text{COD})]$ and $[\text{Ir}(\text{COD})\text{Cl}]_2$ is probably due to the slow conversion of the pre-catalyst into the real catalyst due to COD hydrogenation. The conversion of all $[\text{IrCl}(\text{MesImPr})(\text{COD})]$ into an active catalyst could be possible by addition of hydrogen before introducing of substrate. Unfortunately, in this case, deactivation processes become dominant. For M-Ir the situation seems different, deactivation processes are precluded due to isolation of active sides on silica surface and the absence of COD led to formation of enough binding sites for both substrate and hydrogen.

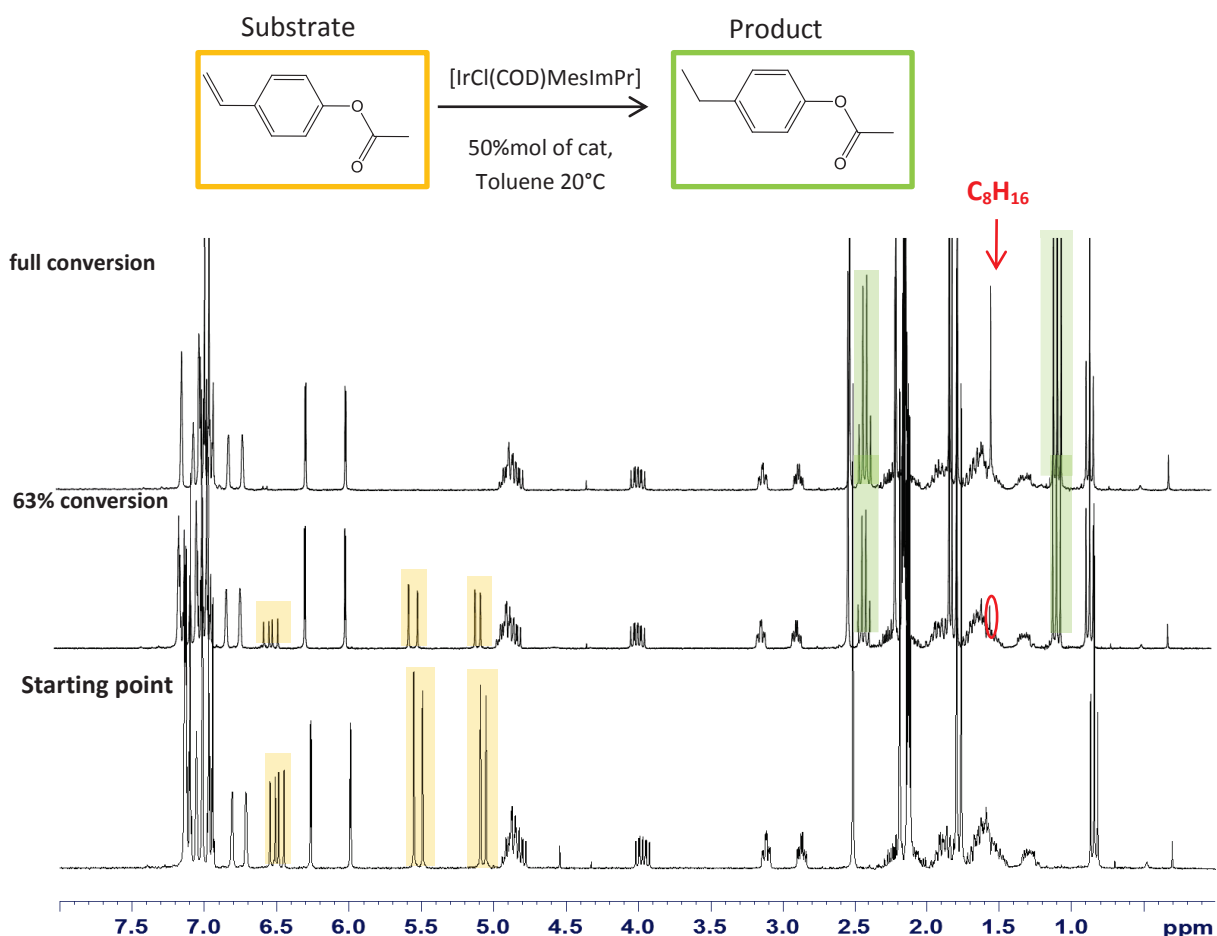


Figure 11. *In situ* monitoring of acetoxystyrene hydrogenation with $[\text{IrCl}(\text{COD})\text{MesImPr}]$. Hydrogenation was performed in a Young tube with 1 bar of H_2 at 40 °C and 50 mol % of catalyst.

2.5 Temperature influence on hydrogenation rate

The relation between reaction rate and activation temperature can be described by Arrhenius equation (2). By taking the natural logarithm of reaction rate (calculated through Arrhenius equation) at T_1 and T_2 it is possible to express the difference in rate as:

$$\ln \frac{k_2}{k_1} = \frac{E_a}{R} \left(\frac{1}{T_1} - \frac{1}{T_2} \right) \quad (10)$$

$$\ln \frac{k_2}{k_1} = \frac{E_a}{R} \left(\frac{\Delta T}{T_1 T_2} \right), \quad (11)$$

where k_1 is the rate constant at temperature T_1 , and k_2 is the rate constant at temperature T_2 ($T_2 > T_1$). Taking into account that for many chemical reactions the activation energy has a magnitude about $E_a = 5 \times 10^4$ J/mole, a general rule of temperature influence onto reaction rate can be postulated: 10 °C of temperature increase results in a double increase of reaction rate.¹³⁵

The catalytic hydrogenation with Crabtree's catalyst is never performed at temperatures higher than 40 °C due to the high increase of deactivation process rate. Thus it was interesting to study the hydrogenation with M-Ir where the deactivation through polyhydride formation seems precluded. However, the deactivation through Ir-NHC bond cleavage is still possible. The temperature influence onto the M-Ir catalytic performance was studied at 40 °C and 80 °C in toluene with 0.1 mol% of catalyst using trans-stilbene as a substrate. As seen in Fig.12, the catalytic activity of M-Ir increased 8.4 times with increase of temperature from 40 °C to 80 °C. The complete hydrogenation of substrate at 80 °C therefore takes place in no more than 2.5h, while at 40°C the reaction is complete only after 18 h.

The calculated TOF for M-Ir at 40 °C is 63 h⁻¹ while the 40 °C increase of temperature results in a TOF of 530 h⁻¹.

The rough estimation of trans-stilbene hydrogenation activation energy calculated from equation (11) is around 60 kJ/mole (14,6 kcal). This is in agreement with the calculation reported by K. Hopmann and A. Bayer¹³⁶ for alkene hydrogenation with PHOX-Ir(I) complexes that was found to be in the range of 12-16 kcal. However, for a more accurate E_a

¹³⁵ Petrucci, Harwood, Madura, Herring. General Chemistry: Principles & Modern Applications, 9th edition., Sec.14-9: The Effect of Temperature on Reaction Rates, p. 594.

¹³⁶ Hoppman, K.H.; Bayer, A., *Organometallics* **2011**, 30, 2483-2497.

determination, we should carry out the hydrogenation reaction with M-Ir at other temperatures (20 °C and 60°C)

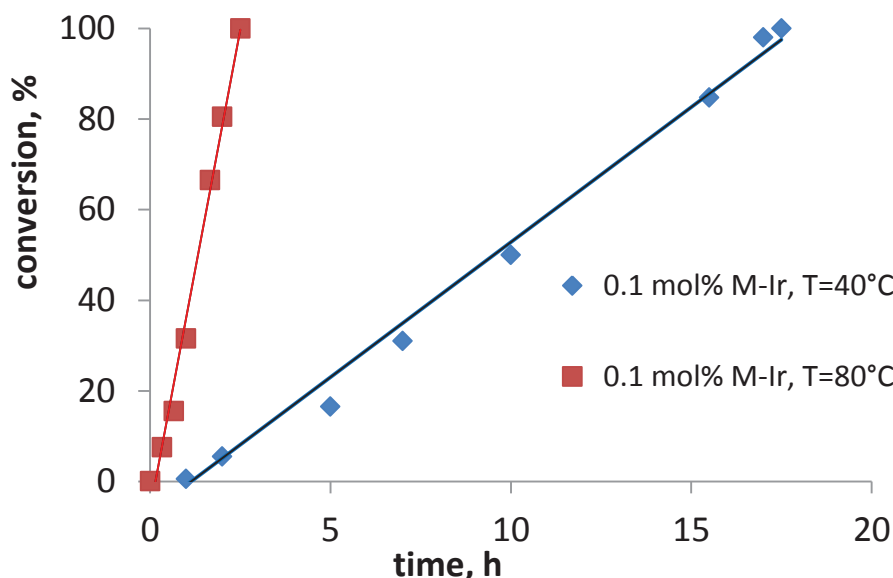


Figure 12. Conversion of trans-stilbene hydrogenation as a function of reaction time using M-Ir material. The hydrogenation experiments were carried out in toluene at 40 °C and 80 °C under 3 bar of H₂

2.6 Directing effects

As mentioned in Chapter 1, the Crabtree catalyst can also lead to directed hydrogenation through binding of coordinating groups to the Iridium center. Inspired by Crabtree's¹³⁷ results, we therefore test our M-Ir and [IrCl(COD)(MesImPr)] in diastereoselective hydrogenation of terpinen-4-ol. The hydrogenation with M-Ir and [IrCl(COD)(MesImPr)] was performed in toluene with 0.1 mol% of catalyst at 40 °C under 3 bars of H₂. In these conditions, the [IrCl(COD)(MesImPr)] catalyst deactivates rapidly reaching a maximum conversion of 10%. The heterogeneous M-Ir catalyst was found to be twice faster, but was also deactivated albeit reaching a higher maximum conversion of 35% in 500h (Fig. 13).

Interestingly, M-Ir showed high level of diastereoselectivity (95%). In contrast to M-Ir, the diastereoselectivity of terpinen-4-ol with [IrCl(COD)(MesImPr)] decreased during the

¹³⁷ a) Crabtree, R. H.; Davis, M. W., *Organometallics* **1983**, 2, 681-682; b) Crabtree, R. H.; Davis, M. W., *J. Org. Chem.* **1986**, 51 (14), 2655-2661.

hydrogenation, starting from 100% selectivity at 4 % conversion and finishing with 92% selectivity at 10% conversion (Fig14). The decrease of selectivity with homogeneous catalyst can be a sign for catalyst deactivation through formation of Ir NPs that are known to be unselective. We noticed that a black deposit was formed after leaving catalyst solution in NMR tube under hydrogen pressure for a long time. It supports our hypothesis that $[\text{IrCl}(\text{COD})(\text{MesImPr})]$ complex decomposes through formation of Ir NPs.

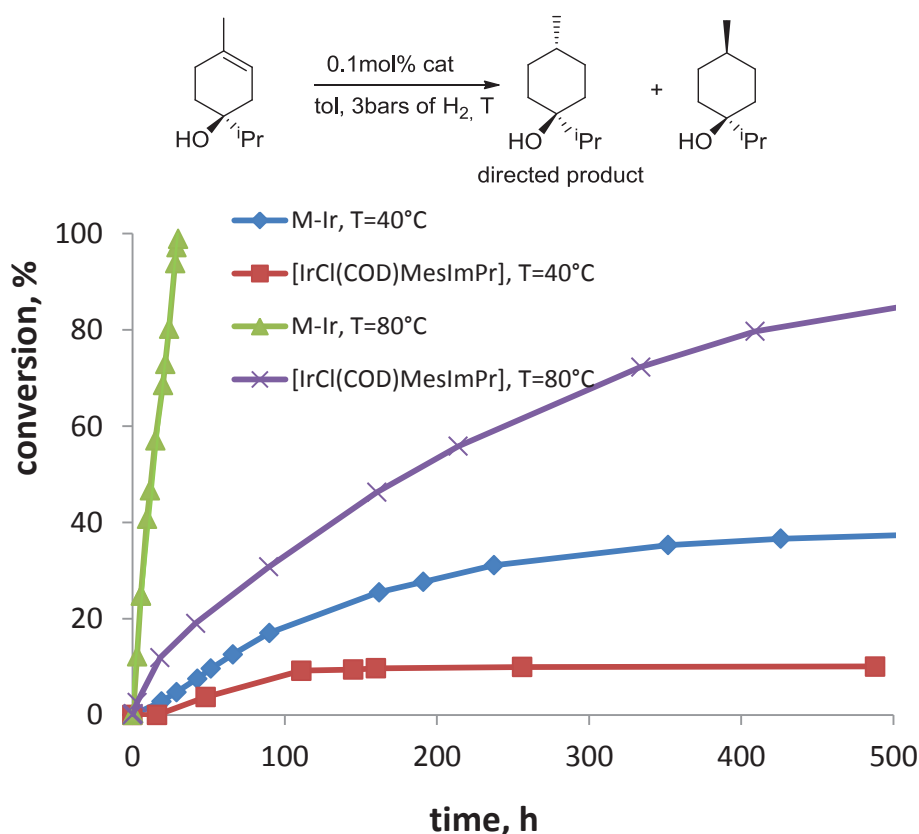


Figure13. Conversion of terpinen-4-ol hydrogenation as a function of reaction time using $[\text{IrCl}(\text{COD})\text{MesImPr}]$ and M-Ir material. The hydrogenation experiments were carried out in toluene at 40°C and 80°C under 3 bar of H_2

We therefore performed an hydrogenation test at 80°C with both M-Ir and $[\text{IrCl}(\text{COD})(\text{MesImPr})]$ catalysts. The reaction was carried out in toluene with 0.1mol % of catalyst loading under 3 bars of H_2 . As shown in Fig. 13, the two fold increase of temperature resulted in a significant increase in hydrogenation rate for both catalysts. Thus initial TOFs (calculated at 25% conversion) for M-Ir were 1.4h^{-1} at 40°C and 45h^{-1} at 80°C , resulting in a 32 fold enhancement of reaction rate. For the homogeneous catalyst, the enhancement was smaller (11 times) and TOFs at 40°C and 80°C were equal to 0.6h^{-1} and 6.6h^{-1} respectively.

The most important fact is that, with M-Ir, the reaction proceeded till 98% conversion in 30h, whereas the homogeneous catalyst was not able to reach this number in 520 h (plateau at 80% conversion).

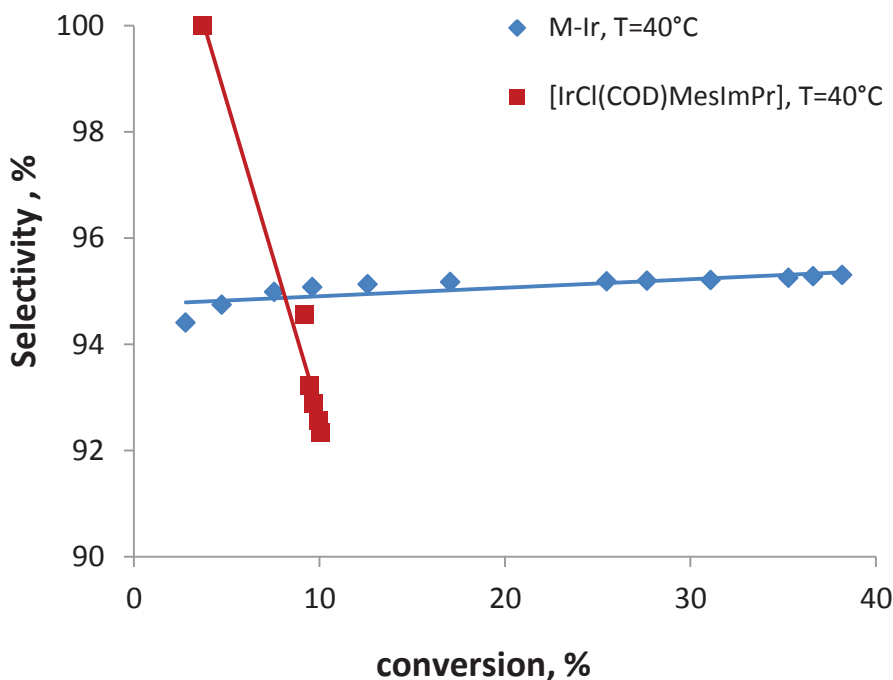


Figure 14. Selectivity towards directed product formation as a function of terpinen-4-ol conversion measured using M-Ir and [IrCl(COD)MesImPr] catalysts at 40 °C

Moreover, the temperature increase resulted in some selectivity decrease. At 40 °C the hydrogenation with M-Ir led to 95% (Fig.14, blue diamonds), of selectivity toward the directed product whereas at 80 °C a slightly lower selectivity (90%) was observed (Fig.15, green triangles). For [IrCl(COD)(MesImPr)] the selectivity toward the directed product decreased both at 40°C (Fig.14, red squares) and 80°C (Fig.15, violet crosses). However at 80°C, the selectivity dropped more dramatically: from 100% at 0.2% conversion to 60% at 80% conversion. Here also, this drastic decrease strongly suggests the formation of Ir particles that do not possess high directing effects.

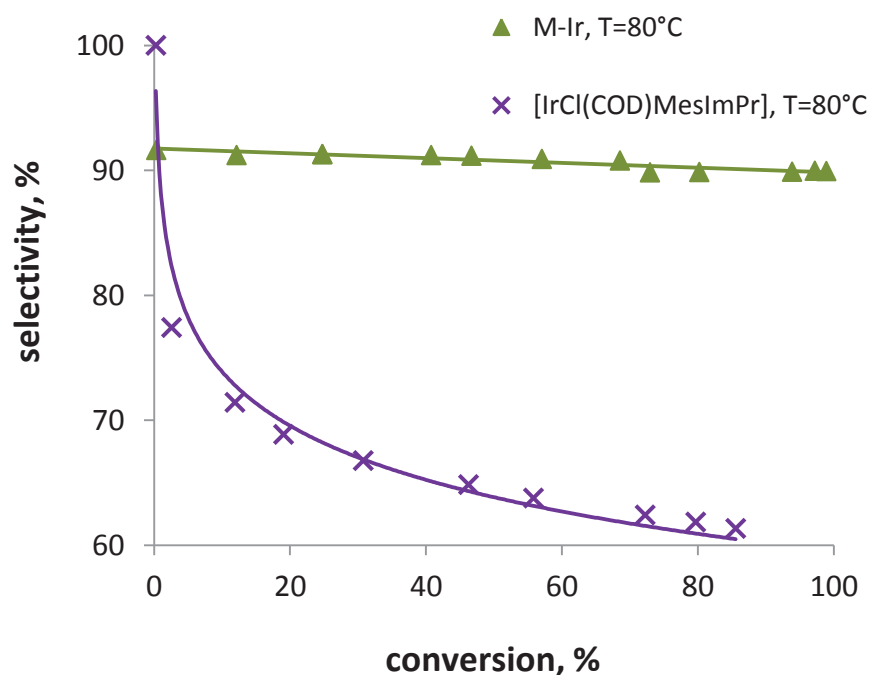


Figure 15. Selectivity towards directed product formation as a function of terpinen-4-ol conversion measured using M-Ir and [IrCl(COD)MesImPr] catalysts at 80 °C

2.7 Deactivation

During the terpinen-4-ol hydrogenation under elevated temperatures (80°C) with [IrCl(COD)(MesImPr)], we noticed the modification of Ir complex color and formation of a black deposit (Fig16). The solution was observed by TEM and EDX analysis (Table A1) and we could clearly see Ir particles.

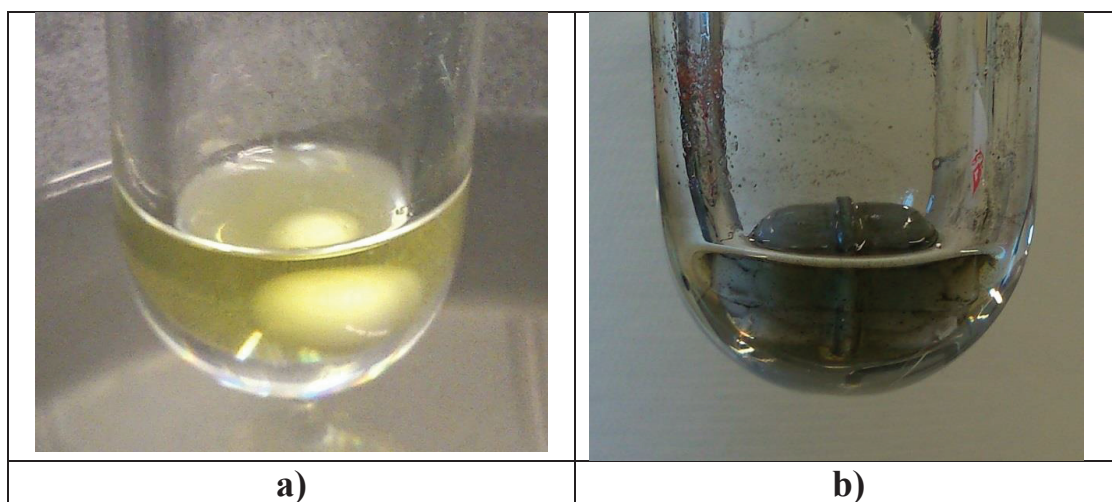


Figure 16. Photos of substrate and [IrCl(COD)MesImPr] catalyst solution before (a) and after (b) catalytic reduction of Terpinen-4-ol at 80°C with 0.1mol% of catalyst

Such decomposition of homogeneous catalyst may also be possible in case of heterogeneous M-Ir but to a lower extent. First, at low temperature (40°C), after trans-stilbene hydrogenation (toluene, 0.033mol% of cat) the spent catalyst was thus analyzed by TEM and EDX (Table 2 and Table A2). Besides, the observation of silver agglomerates by TEM, no Ir NP could be detected by TEM. The absence of substrate dearomatization (for aromatic substrates) also strongly suggests that no Ir NPs were formed during the hydrogenation tests. However, Ir NPs were formed under H₂ when the olefinic substrate is completely hydrogenated (see chapter 2).

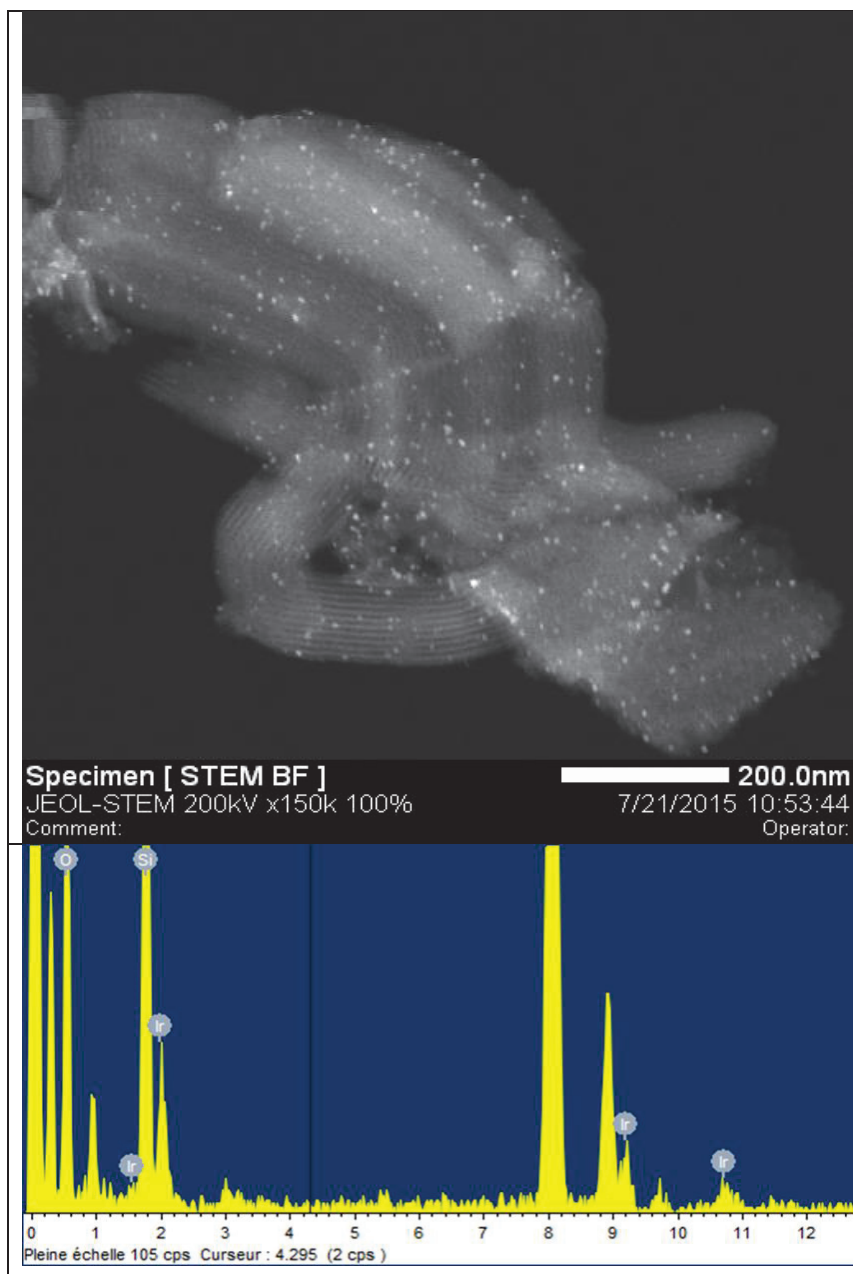
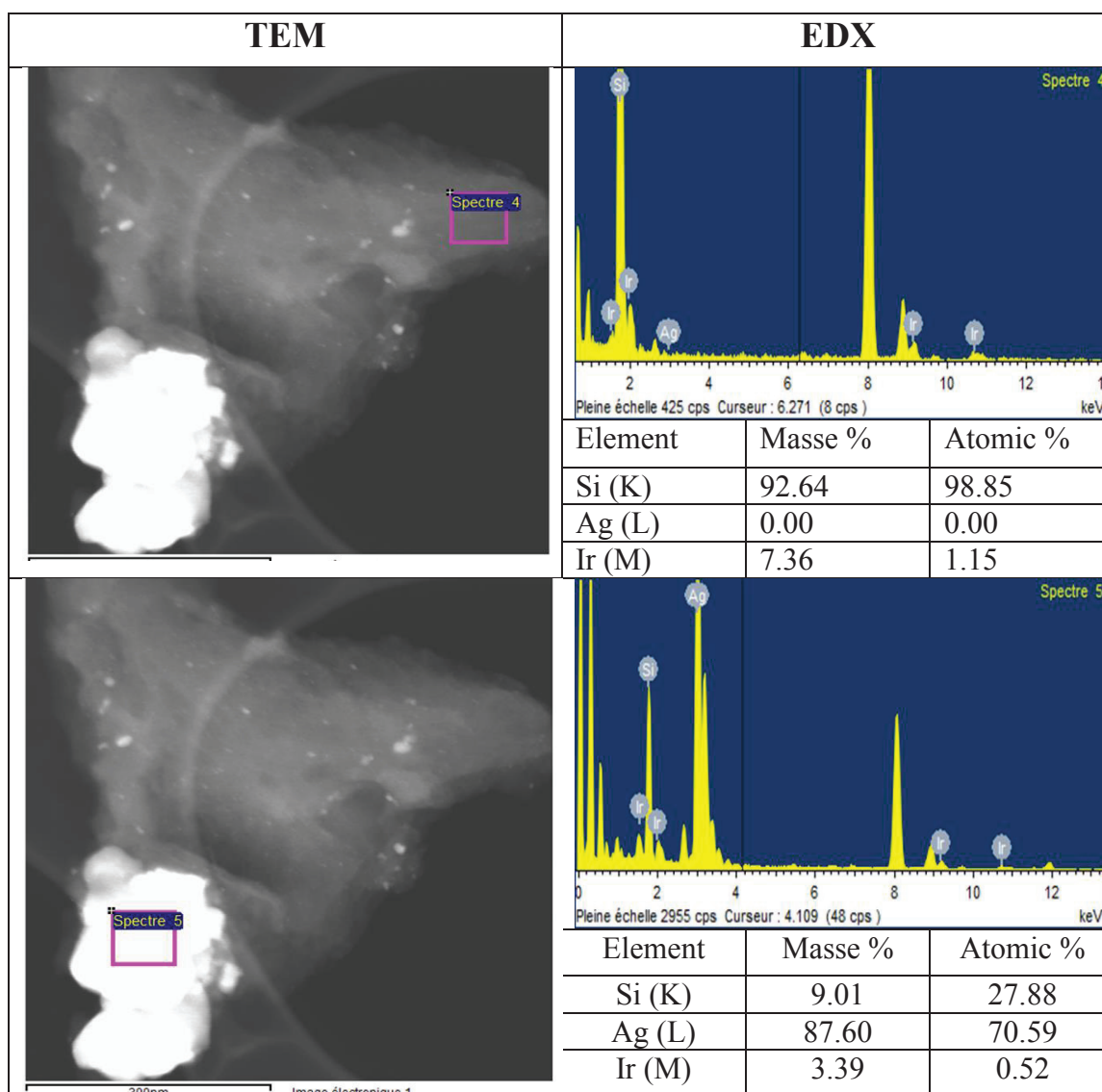


Figure 17. STEM micrographs and EDX of the recovered solid after full trans-stilbene reduction (2.5 hours) at 80°C with 0.1mol% of M-Ir in toluene

Second, at elevated temperatures (80°C) using M-Ir, TEM images showed the presence of small Ir NPs in the spent catalyst (Fig.17). This latter result may however be explained by the fact that, for terpinen-4-ol, 32h were required to reach 98% conversion and the accurate determination of the end of terpinen-4-ol hydrogenation was therefore difficult. The Ir NPs may therefore be formed at the final stage of the catalytic test when the catalyst is still in contact with H₂ while all the terpinen-4-ol is consumed. This point would need to be clarified in a near future.

Table2.Investigation of spent M-Ir catalyst for the Iridium nanoparticles formation by TEM and EDX technics



2.8 Recycling

The recyclability of a catalyst is also an advantage for heterogeneous catalyst. Recycling tests for M-Ir were performed after trans-stilbene hydrogenation with 0.25mol % of catalyst under standard conditions (toluene, 40 °C, 3 bars of H₂). The recycling was performed by exchanging the supernatant with a new portion of dry degassed solvent. Unfortunately after recycling the material lost some of its reactivity (Fig18.). The loss in reactivity after 1st and 2nd cycle is equal to 36%. Taking into account that no leaching of Ir was detected by ICP-MS together with the absence of Ir NPs in spent catalyst (see TableA2), we suppose that the material deactivation is in consequence of catalyst poisoning by impurities present in the solvent or by strong adsorption of reactants on the catalyst surface. Extra experiments need to be performed to clarify this point.

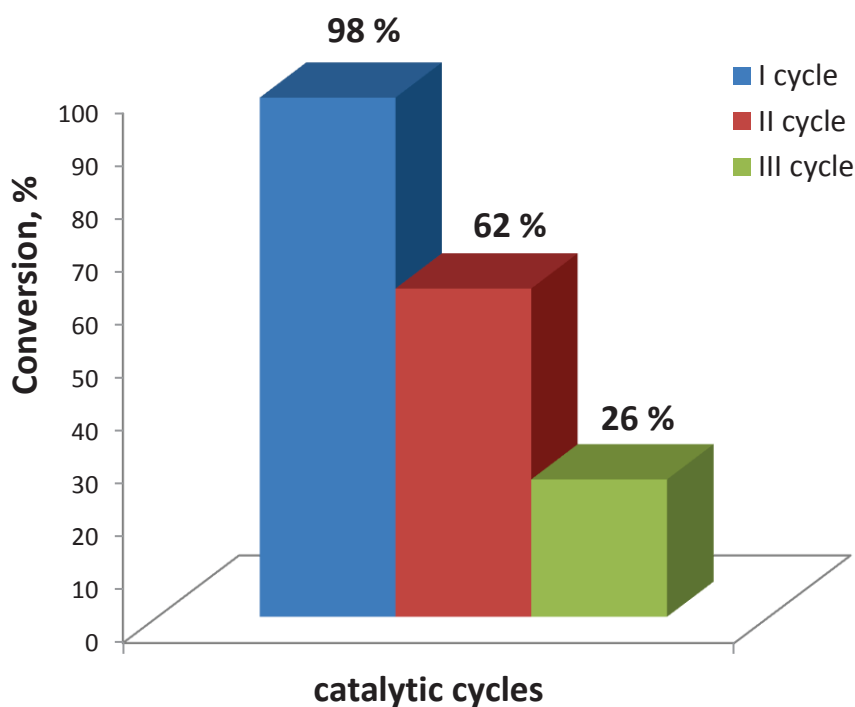


Figure18. Recycling of M-Ir in trans-stilbene hydrogenation

III-3 Conclusions

The catalytic activities of heterogeneous M-Ir and its homogeneous counterpart, [IrCl(COD)(MesImPr)], were evaluated in different olefin hydrogenation reactions. The heterogeneous catalyst was found to be one to two orders of magnitudes faster than its homogeneous analogue in trans-stilbene hydrogenation, and also faster than the corresponding molecular cationic complex. The reason of such an enhancement is related to: 1) the isolation of Ir species on support that could suppress bimolecular deactivation processes; 2) the absence of initiation period as a result of the lack of COD ligand in the heterogeneous catalyst.

M-Ir was found to be highly selective in limonene hydrogenation (the terminal C-C bond was selectively hydrogenated), yielding only p-menthene till limonene conversion reached 95%.

M-Ir also demonstrated a high and stable diastereoselectivity in the terpinen-4-ol hydrogenation even at 80 °C. This high degree of diastereoselectivity is quite rare for heterogeneous catalyst. This diastereoselectivity slightly decreases with temperature, reaching 95% of the directed product at 40 °C and 92% at 80 °C. At the reverse, the hydrogenation rate dramatically increases (32times) with temperature. For the homogeneous analogue, a sharp drop of diastereoselectivity within time was noticed. The drop of diastereoselectivity was sharper when the reaction was conducted at 80°C due to the complex decomposition into Ir aggregates.

Finally, the stability of M-Ir and [IrCl(COD)(MesImPr)] were tested at 40°C in the presence and the absence of substrate and at 80°C in the presence of substrate. The unsupported catalyst was found to be unstable in all conditions, decomposing into Ir NPs whereas the stability of M-Ir was found far higher. At the reverse, the heterogeneous catalyst was found stable in the presence of substrate, but seemed to decompose in the absence of substrate to form Ir NPs. However at 80°C, this latter point needs to be more accurately addressed in a very near future.

III-4 Experimental section

4.1. General information

All the tests were performed in Fisher-Porter glass reactor with connection to vacuum, argon and hydrogen lines. The catalyst, substrates and internal standard were introduced into the reactor under argon using standard Schlenk techniques. Trans-stilbene was received from Sigma-Aldrich and was recrystallized from methanol prior to use. Before each catalytic test, reactor was purged with Argon. The substituted styrenes and terpinen-4-ol (sum of enantiomers) were received from Sigma-Aldrich and dried with 5 Å molecular sieves prior to use.

4.2. Hydrogenation conditions

4.2.1. Heterogeneous catalysis

10 mg of **M-Ir** (0.0017 mmol of Ir) were mixed in a glove box with 300 mg of trans-stilbene (1.67 mmol). The mixture was dissolved in 3.5 ml of dry degassed toluene. 0.1ml of internal standard was added and all mixture was transferred to glass reactor (reactor volume=30 mL) with the help of cannula. The reaction performed under 3 bars of H₂ at two different temperatures: 40 °C and 80 °C Reaction was monitored by ¹H NMR. The conversion was measured by relative disappearance of peak at 3.78 ppm which corresponds to =CH of double bond and appearance of peak at 2.98 ppm which corresponds to -CH₂ of hydrogenated product. 1, 2-tetrachloroethane was used as internal standard.

For the determination of maximum TON was used more diluted system (0.01mol% of catalyst). 60mg of M-Ir (0.005 mmol of Ir, batch with 25% silver to iridium conversion) were mixed in glove box with 8.460g of trans-stilbene (47 mmol). The mixture was dissolved in 85mL of dry degassed toluene. 0.5ml of internal standard was added and all mixture was transferred to glass reactor (reactor volume=400mL) with the help of cannula. The reaction performed under 3 bars of H₂ at 40°C. Reaction was monitored by ¹H NMR. The conversion was measured by relative disappearance of peak at 3.78 ppm which corresponds to =CH of double bond and appearance of peak at 2.98 ppm which corresponds to -CH₂ of hydrogenated product. 1, 2-tetrachloroethane was used as internal standard.

4.2.2. Homogeneous catalysis

752 μL of 0.022 M solution of $[\text{IrCl}(\text{COD})(\text{MesImPr})]$ (0.017 mmol) was introduced in a Schlenk already containing 3 g of trans-stilbene (16.7 mmol) dissolved in 35 mL of dry degassed toluene. After 0.2 ml of internal standard were added. The mixture was transferred to glass reactor (reactor volume=300ml) with the help of cannula. The reaction performed under 3 bars of H_2 at 40°C . Reaction was monitored by ^1H NMR. The conversion was measured by relative disappearance of peak at 3.78 ppm which corresponds to $=\text{CH}$ of double bond and appearance of peak at 2.98 ppm which corresponds to $-\text{CH}_2$ of hydrogenated product. 1, 2-tetrachloroethane was used as internal standard.

The cationic species $[\text{Ir}(\text{COD})(\text{MesImPr})]\text{BF}_4$ was generated *in situ* with addition of 0.0017 mmol of AgBF_4 (300 μL of dry degassed 0.056 M solution in toluene) inside the glass reactor (reactor volume=300ml) before pressurizing with H_2 . It was seen the precipitation of white solid of AgI .

4.2.3. Scope of substrates

Styrene and its derivatives with electron donating (4-vinylanisole, 4-acetoxystyrene) and electron withdrawing (4-fluorostyrene) substituents were chosen as substrates for hydrogenation. Trans-stilbene was used as a bench mark and was purified as previously described. The catalysis performed in toluene with 0.03 mol% of catalyst loading (corresponding to Ir) at 40°C under 3 bars of H_2 .

10 mg of M-Ir (0.0017 mmol) were suspended at 10ml of dry degassed toluene. Solution was transferred in the reactor under Argon. 5.1mmol of Substrate was then introduced followed by addition of 0.1 mL of the internal standard. Reaction was monitored by ^1H NMR. The conversion was measured by relative disappearance of peak corresponds to $=\text{CH}$ of double bond and appearance of peak which corresponds to $-\text{CH}_2$ of hydrogenated product. 1, 2-tetrachloroethane was used as internal standard.

Homogeneous and heterogeneous catalytic experiments were performed with similar conditions $[\text{IrCl}(\text{COD})(\text{MesImPr})]$ was introduced as 1.4 mL of 0.001M stock solution and 8.5 mL of solvent was added.

4.2.4. Diastereoselective hydrogenation

10 mg of M-Ir (0.0017 mmol) were suspended at 10ml of dry degassed toluene. Solution was transferred in the reactor under Argon (reactor volume=30 mL). 1.65 mmol of Substrate was then introduced followed by addition of 0.1 mL of the internal standard (dodecane). The reaction performed under 3 bars of H₂ at two different temperatures: 40 °C and 80 °C. Reaction was monitored by GC using HP-INNOWAX column (L=30m, d=0.320mm, f=0.25μm

4.2.5. Split tests

Leaching of active species:

After full conversion of substrate (acetoxystyrene), the supernatant was collected and filtered under Ar and portion of substrate (limonene) was added. No conversion of limonene was detected during 30h.

Leaching of inactive species:

After full conversion of substrate, the supernatant was collected and separate from **M-Ir** by filtration and send to elemental analysis. According to the results, the detected Ir leaching is less than 1ppm.

II-6 Appendix

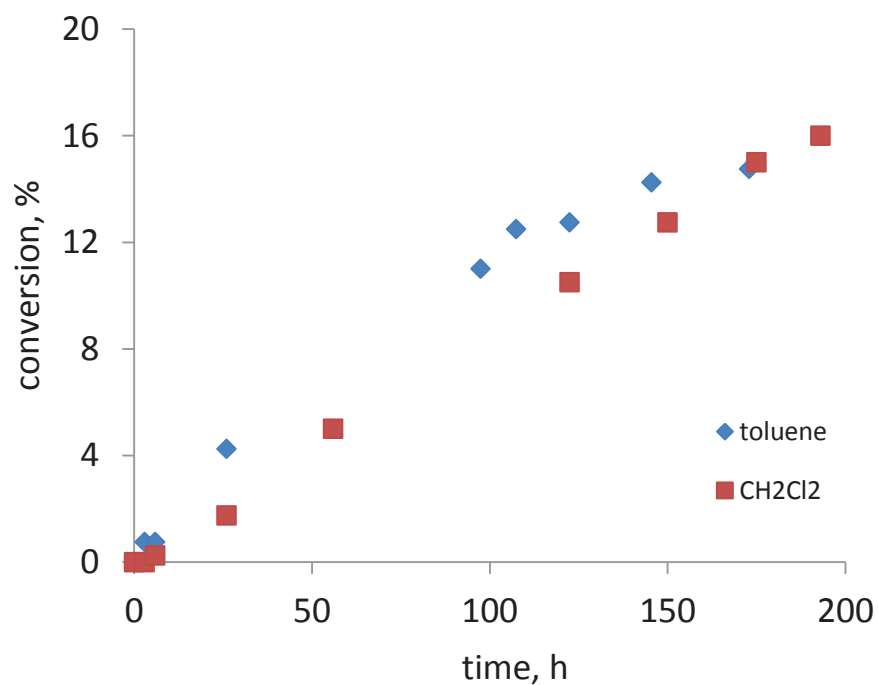


Figure A1. Study of the solvent effect in trans-stilbene hydrogenation with [Ir(COD)(MesImPr)]
Conditions: Sub/cat ratio is 1000 (16.67mmol of Substrate and 0,017mmol of cat). Volume of reactor is 300ml, the catalysis performed in 35ml of Toluene (32mmol of H₂).

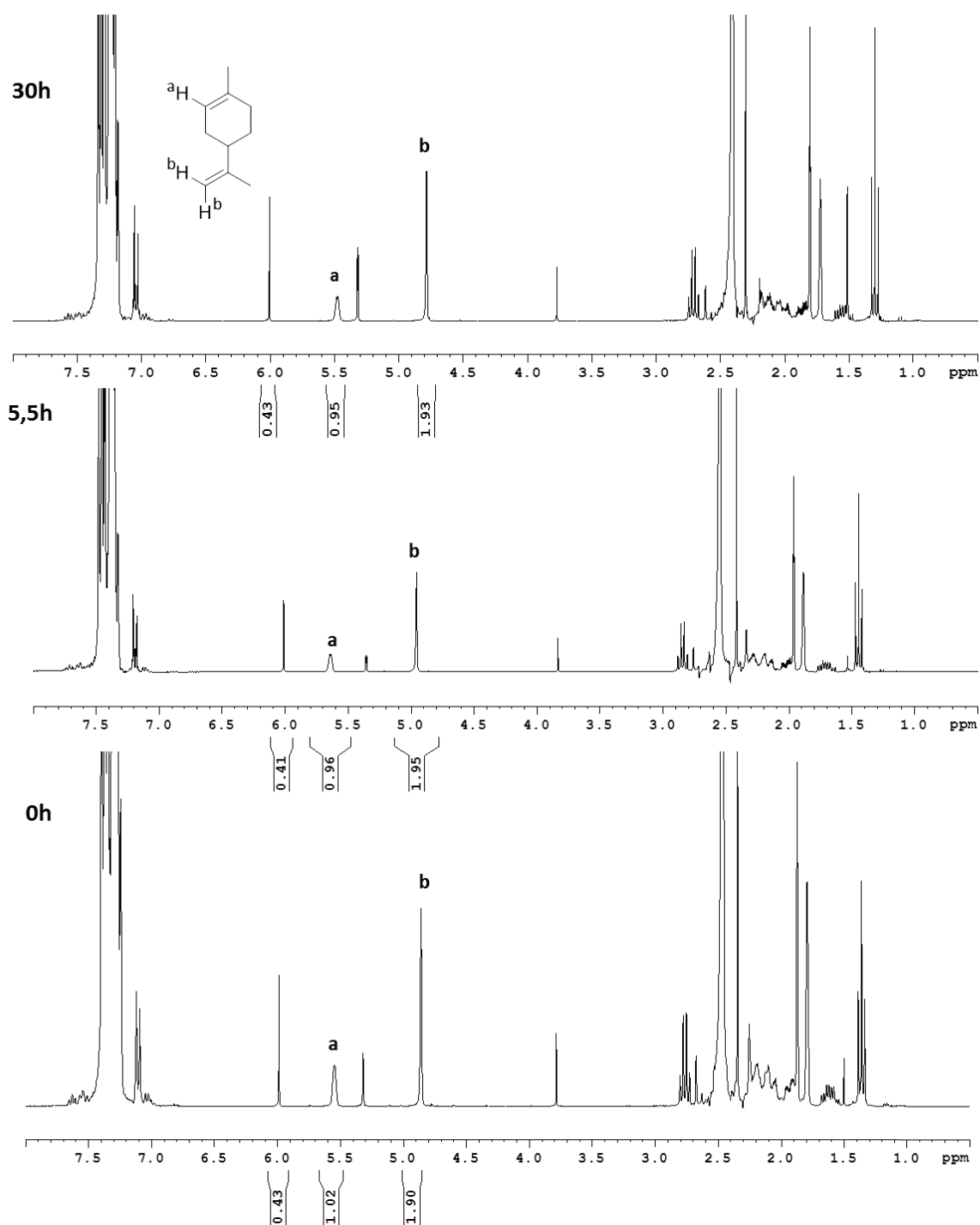


Figure A2. ^1H NMR spectra of limonene hydrogenation by recovered supernatant from acetoxystyrene hydrogenation

TableA1. Investigation of [IrCl(COD)MesImPr] decomposition related to Iridium nanoparticles formation by TEM and EDX technics

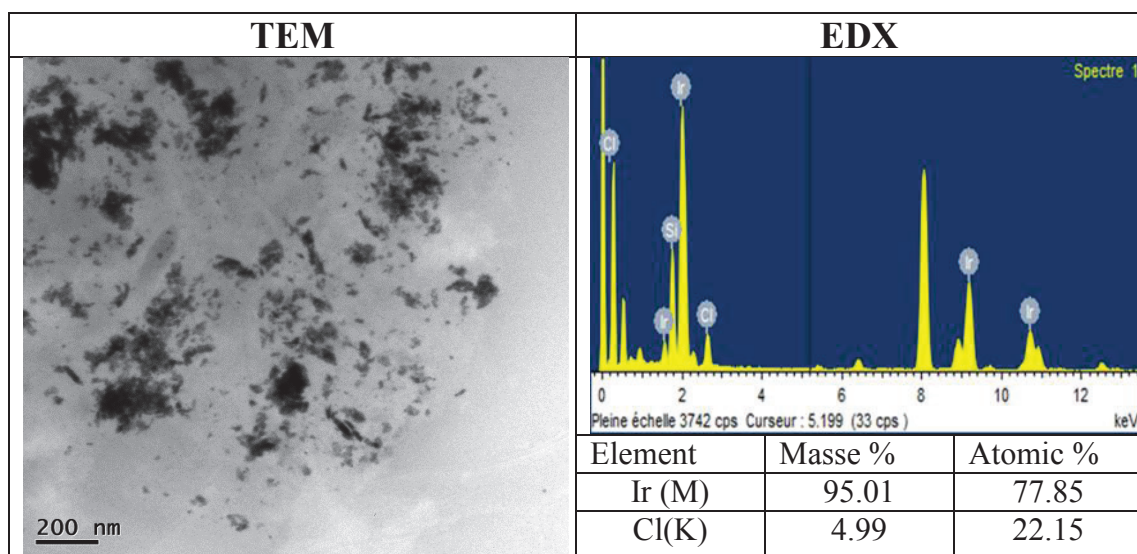
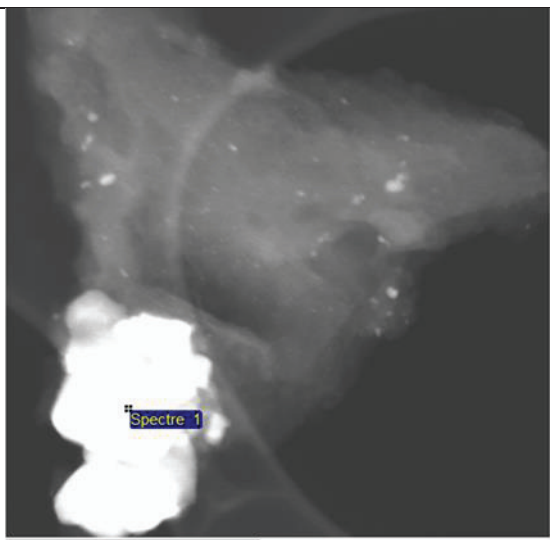
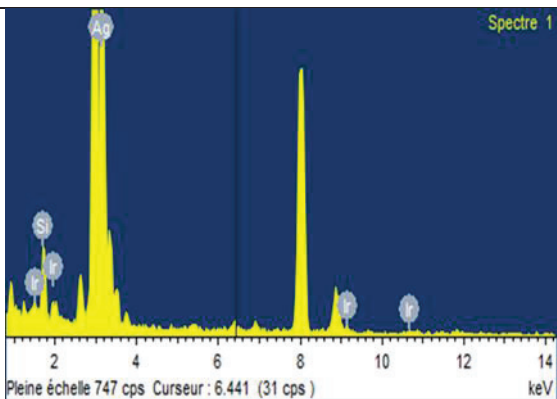

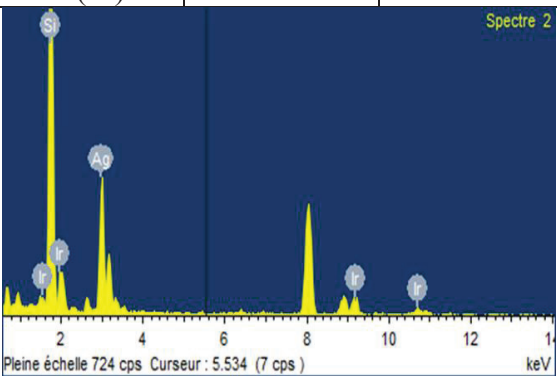
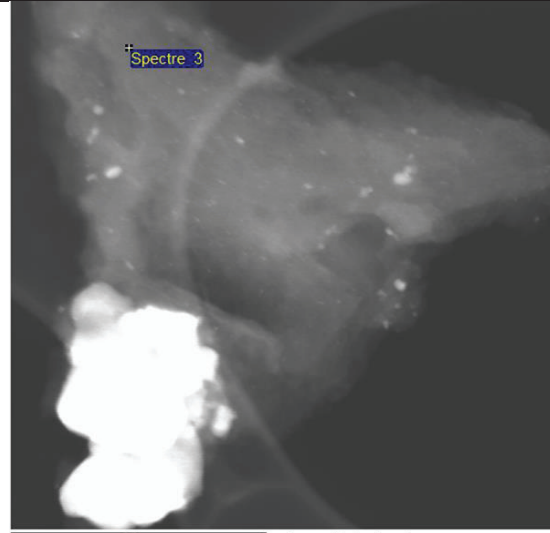
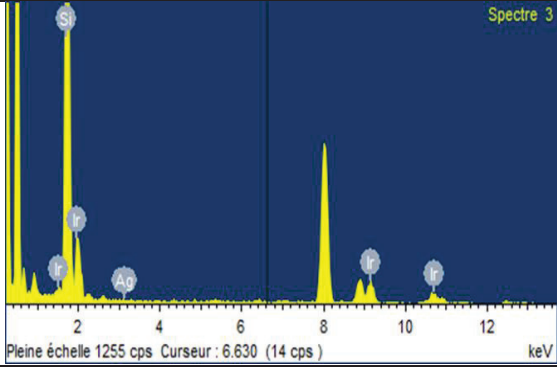


Table A2. Study the presence of IrNPs on spent catalyst (recovered after trans-stilbene hydrogenation at 40 °C with 0.33mol% of cat) by TEM and EDX

TEM	EDX												
 <p>300nm Image électronique 1</p>	 <table><tr><th>Element</th><th>Masse %</th><th>Atomic %</th></tr><tr><td>Si (K)</td><td>1.79</td><td>6.57</td></tr><tr><td>Ag (L)</td><td>96.94</td><td>92.74</td></tr><tr><td>Ir (M)</td><td>1.28</td><td>0.68</td></tr></table>	Element	Masse %	Atomic %	Si (K)	1.79	6.57	Ag (L)	96.94	92.74	Ir (M)	1.28	0.68
Element	Masse %	Atomic %											
Si (K)	1.79	6.57											
Ag (L)	96.94	92.74											
Ir (M)	1.28	0.68											
 <p>300nm Image électronique 1</p>	 <table><tr><th>Element</th><th>Masse %</th><th>Atomic %</th></tr><tr><td>Si (K)</td><td>52.39</td><td>82.29</td></tr><tr><td>Ag (L)</td><td>37.81</td><td>15.46</td></tr><tr><td>Ir (M)</td><td>9.80</td><td>2.25</td></tr></table>	Element	Masse %	Atomic %	Si (K)	52.39	82.29	Ag (L)	37.81	15.46	Ir (M)	9.80	2.25
Element	Masse %	Atomic %											
Si (K)	52.39	82.29											
Ag (L)	37.81	15.46											
Ir (M)	9.80	2.25											
 <p>300nm Image électronique 1</p>	 <table><tr><th>Element</th><th>Masse %</th><th>Atomic %</th></tr><tr><td>Si (K)</td><td>85.37</td><td>97.56</td></tr><tr><td>Ag (L)</td><td>0.00</td><td>0.00</td></tr><tr><td>Ir (M)</td><td>14.63</td><td>2.44</td></tr></table>	Element	Masse %	Atomic %	Si (K)	85.37	97.56	Ag (L)	0.00	0.00	Ir (M)	14.63	2.44
Element	Masse %	Atomic %											
Si (K)	85.37	97.56											
Ag (L)	0.00	0.00											
Ir (M)	14.63	2.44											

Chapter 4

Functionalized polyethylene as a new support for organometallic complexes

Table of content

IV-1. Introduction	135
IV-2. Polyethylene	136
2.1. New approach in synthesis of telechelic polyethylene.....	136
2.2. Application of low density telechelic polyethylene	139
IV-3. Introducing organometallic complexes	143
IV-4. Catalytic performance of Ir modified PE	150
4.1. Alkene hydrogenation with Ir(cod)-PE	150
4.1.1. Performance	150
4.1.2. Comparison with Silica supported analogue	151
4.2. H/D exchange with IrCp*-PE	152
IV-5. Introducing boron functionalities	155
IV-6. Conclusions	157
IV-7. Experimental section.....	158
7.1. General information	158
7.2. Synthesis and characteristic of polymers	158
7.3. Synthesis and characteristic of organometallic complexes	162
7.4. Catalysis	164
7.4.1. Hydrogenation with PE-IrCODCl.....	164
7.4.2. H/D exchange with PE-IrCP*Cl	164

IV-8. Appendix 166

List of Figures

Figure 1. ^1H NMR of PE-I	137
Figure 2. ^{13}C NMR of PE-I	138
Figure 3. ^1H NMR of PE-MesIm	143
Figure 4. ^{13}C NMR of PE-MesIm	144
Figure 5. ^1H NMR of PE-AgI	146
Figure 6. ^{13}C NMR of PE-AgI	146
Figure 7. ^1H NMR of PE-IrClCOD	147
Figure 8. ^1H NMR of PE-IrCp*Cl ₂	148
Figure 9. MALDI-TOF spectra of PE-IrCp*Cl ₂	149
Figure 10 Catalytic activity of PE-IrClCOD in trans-stilbene hydrogenation. The hydrogenation experiments were carried out in toluene at 40 °C and 80°C under 3 bar of H ₂ with 0.1 mol% and 1mol% of Ir	150
Figure 11. Comparison of catalytic activity of PE-IrClCOD, neutral [IrCl(COD)MesImPr], cationic [Ir(COD)(MesImPr)]BF ₄ and M-Ir material in trans-stilbene hydrogenation.	151
Figure 12. Comparison of catalytic activity of [PE-IrCp*Cl]OTf (red circles) and [IrCp*(MesImPr)Cl]OTf (blue diamonds) in acetophenone deuteration.....	153
Figure 13. ^{11}B NMR of PE-BBN (a) and PE-BH ₃ (b).....	156

List of Schemes

Scheme 1. Preparation of telephelic polyethylene	136
Scheme 2. Different pathway for preparation of Ru polyethylene supported catalyst	140
Scheme 3. Synthesis of Cr(III)-Salen catalyst	141
Scheme 4. Preparation of PE-supported porphyrin-Cobalt complex	142
Scheme 5. Modification of polyethylene	145
Scheme 6. Catalytic acetophenone deuteration	152
Scheme 7. Formation of normal(C2) and abnormal(C5, C4) carbenes	155

List of Tables

Table T1. Catalytic performance of [PE-IrCp*Cl]OTf and [IrCp*(MesImPr)Cl]OTf in acetophenone deuteration	154
Table T2. Experimental conditions for H/D exchange catalysis	165

List of Figures in Appendix

Figure A1. ^{13}C NMR of PE-IrCp*	166
Figure A2. ^{13}C NMR of PE-IrCODCl	167
Figure A3. ^{13}C NMR of PE-BBN	167
Figure A4. MALDI-TOF mass spectrum of PE-IrCODCl	168
Figure A5. MALDI-TOF mass spectrum of PE-IrCODCl (major population).....	169

Figure A6. MALDI-TOF mass spectrum of PE-IrCODCl (minor population)	170
Figure A7. ESI-MS spectrum of [IrCp*(MesImPr)Cl ₂]	171
Figure A8. Catalytic activity of [PE-IrCp*Cl]OTf and [IrCp*(MesImPr)Cl]OTf in acetophenone deuteration carried out in toluene at 100 oC with 0.02 mol% cat (R=5000) ..	172

List of Tables in Appendix

Table A1. Crystal data structure refinement for [IrCp*(MesImPr)Cl ₂]	173
Table A2. Crystal data structure refinement for [MesImPr*BBN]	175

IV-1. Introduction

The high catalytic activity of M-Ir in comparison with that of its homogeneous counterpart can be explained by two main reasons: 1) isolation of active iridium species on the support that physically precludes the polyhydride cluster formation; 2) surface-metal interaction that stabilizes the low valent iridium species allowing their fast activation.

Here, we therefore tried to implement our synthetic procedure to generate an other supported catalytic system: a polymer supported Ir-NHC material where interactions between the support atoms and iridium centers are precluded but at the same time the polymer chains could help to isolate the iridium centers from each other

Among the large variety of polymeric supports, low density polyethylene was chosen as support for immobilization of Iridium complexes because of its thermomorphic properties. Thermomorphic compounds exhibit extreme differences in solubility over a comparably low range of temperatures. As an example, polyethylene is fully soluble in hot nonpolar solvents but completely insoluble at room temperature. Therefore, transition metal complexes bonded to such polymers could catalyse homogeneous reactions at elevated temperatures and be easily isolated as a solid at low temperature. In addition, polyethylene enters in the composition of a wide range of materials and would potentially enable the preparation of catalytic systems at an industrial scale. “Classical” polyethylene materials are known for their high inertness, mainly limiting their use as support for catalysis. Therefore, we decided here to investigate the potentials of recently developed polyethylenes containing terminal iodo groups.

In addition to the synthesis of PE supported [PrMesImIrCODCl] complex, the preparation of a PE supported Ir(III) complex, namely PE-MesImPrIrCp*Cl₂, was also examined here in order to compare its catalytic performances in H/D exchange reactions to those of a silica supported system, namely Si-MesImBzIrCp*Cl₂ that was reported by our group a few years ago.¹³⁸ In the case of the silica supported complex, its catalytic performances were found equivalent to those of the homogeneous counterpart and no surface stabilization was found.

¹³⁸ Maishal, T. K.; Alauzun, J.; Basset, J. M.; Coperet, C.; Corriu, R. J.; Jeanneau, E.; Mehdi, A.; Reye, C.; Veyre, L.; Thieuleux, C. *Angew. Chem. Int. Ed.* **2008**, 47 (45), 8654-8656.

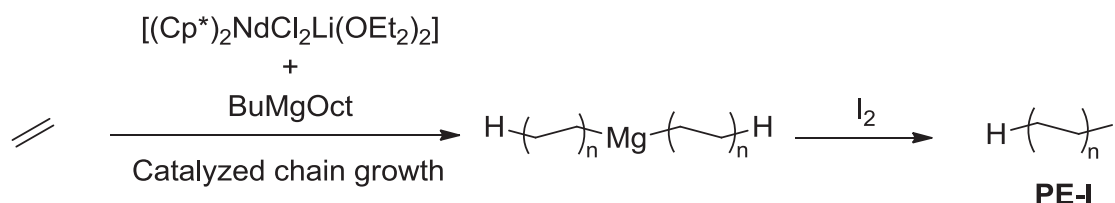
IV-2. Functionalized Polyethylene

2.1. New approach for the synthesis of telechelic polyethylene

Despite the great breakthrough achieved in the field of polyolefin synthesis, the introduction of reactive functional groups in these nonpolar materials is still a challenge. Indeed, the introduction of functional groups is a way to widen the field of polyolefin applications. The preparation of telechelic polyethylene, in which both chain ends contain the same functional group (X-PE-X) or chemically distinct group (X-PE-Z), is thus highly desirable.¹³⁹

Several methods have been used to obtain functionalized polyolefins. However, they are often non-catalytic (use of a stoichiometric amount of high-cost initiators). They require multistep processes or employ expensive monomers, like butadiene or cyclic olefins. Thus these methods are not straightforward for industrial production.

A new effective method for the preparation of end-functionalized polyethylene was elaborated in our laboratory, using a catalyzed chain grows polymerization (CCG).¹⁴⁰ The catalytic system is based on the $[(\text{Cp}^*)_2\text{NdCl}_2\text{Li}(\text{OEt}_2)_2]$ complex ($\text{Cp}^*=\text{C}_5\text{Me}_5$) associated to the chain transfer agent (CTA) (*n*-butyl)(*n*-octyl)magnesium (Scheme 1). The control of polymerization relies on a reversible PE chain transfer between the Neodymium-based catalyst and the CTA, which is much faster than propagation. CCG is actually a unique controlled coordination catalysis polymerization technique that proceeds according to a degenerative transfer mechanism similar to the well-known controlled RAFT radical polymerization.^[11] Dipolyethylenylmagnesium (MgPE_2) is thus produced. The PE chains number-average molar mass is adjusted by following the consumption of ethylene ($M_n = m_{\text{ethylene}}/2 \cdot n_{\text{Mg}}$ where m_{ethylene} is the mass of ethylene consumed and n_{Mg} is the number of moles of CTA employed).



Scheme 1. Preparation of telechelic polyethylene

¹³⁹ German, I.; Kelhifi, W.; Norsic, S.; Boisson, C.; D'agosto, F. *Angew. Chem. Int. Ed.* **2013**, 52, 3438–3441;

¹⁴⁰ a) Briquel, R.; Mazzolini, J.; Le Bris, T.; Boyron, O.; Boisson, F.; Delome, F.; D'Agosto, F.; Boisson, C.; Spitz, R. *Angew. Chem. Int. Ed.* **2008**, 47, 9311–9313; b) Mazzolini, J.; Espinosa, E.; D'Agosto, F.; Boisson, C. *Polym. Chem.* **2010**, 1, 793–800; c) Norsic, S.; Thomas, C.; D'Agosto, F.; Boisson, C. *Angew. Chem. Int. Ed.* **2015**, 54, 4631–4635.

The introduction of the desired functionalities becomes possible due to high nucleophilicity of the methylene group bonded to Mg in MgPE_2 which reacts easily with electrophiles. Thus, the *in situ* addition of iodine to MgPE_2 leads to highly functionalized crystalline iodo end-capped polyethylene (**PE-I**).⁴ The as-obtained polymer was characterized by ^1H and ^{13}C liquid state NMR (Figures 1-2) and size exclusion chromatography (SEC).

^1H NMR spectrum clearly exhibits an intense broad signal at 1.24 ppm related to polyethylene units, and the signals attributed to the chain ends: at 0.84 ppm for methyl (CH_3 -) and 2.94 ppm for methylene iodide ($-\text{CH}_2\text{-I}$). The signal at 1.66 is attributed to $-\text{CH}_2\text{-CH}_2\text{-I}$. At lower field, small signals attributed to vinyl ends could be detected at 4.9 ppm and 5.7 ppm. The formation of vinyl ends is related to a side reaction of β -H elimination from dipolyethylenylmagnesium.

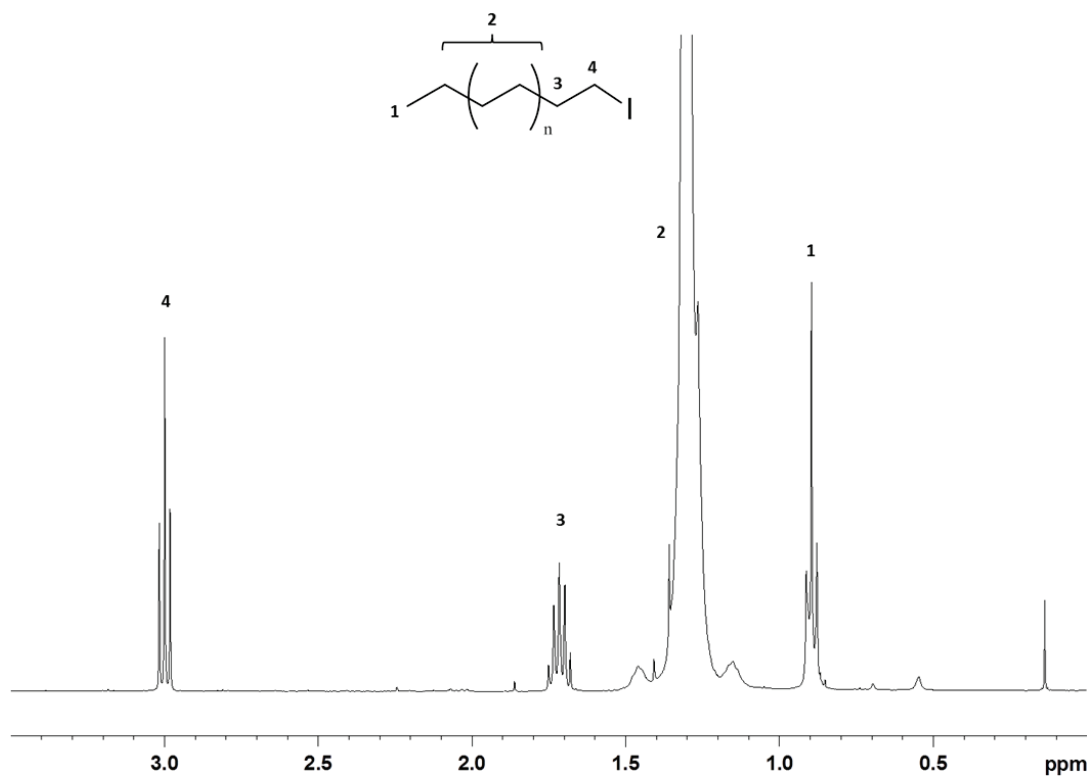


Figure 1: ^1H liquid state NMR of PE-I

The degree of functionalization was calculated using the ratio between the vinyl ends quantity ($N_{\text{-CH}_2\text{-I}}$) and the quantity of all chain ends (N_c) and by taking into account that polymer chain has two ends, as follows:

$$F = \frac{N_{-CH_2-I}}{N_c} = \frac{I_{-CH_2-I}/2}{\left(\frac{I_{-CH_2-I}}{2} + \frac{I_{-CH=CH_2}}{3} + \frac{I_{-CH_3}}{3}\right)/2},$$

where I is the integral intensity of appropriate functional end.

A degree of functionalization of 92% was found from ^1H NMR. The calculated molecular weight of **PE-I** is 1221 g. This is in agreement with the SEC results where the calculated molecular weight was found equal to 1260 g mol $^{-1}$. This datum corresponds to a degree of polymerization equal to 39. As found by SEC, PE-I possesses a low degree of polydispersity ($D=1.17$).

The ^{13}C NMR spectrum of **PE-I** is more complicated. However, it is still possible to attribute the signal of methylene iodide group at 4.93 ppm, the methyl group at 14.03 ppm and the second methylene group closest to iodine. The other methylene groups are situated in the region from 20 to 35 ppm and based on ChemDraw assumption it is possible to determine some of them.

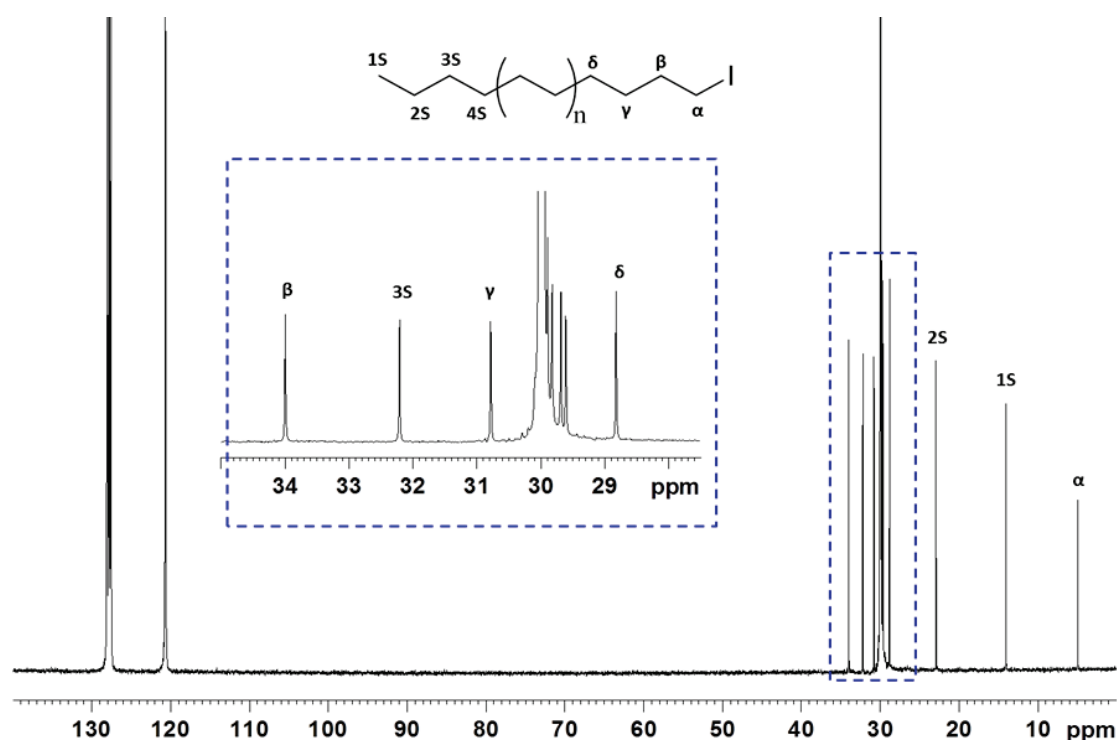


Figure 2. ^{13}C liquid state NMR of PE-I

2.2. Application of low density telechelic polyethylene in catalysis

Telechelic polyolefins have important commercial applications as cross-linkers, chain linkers or starting building blocks¹⁴¹. Recently attention was also directed towards the thermomorphic properties of such polyethylenes.

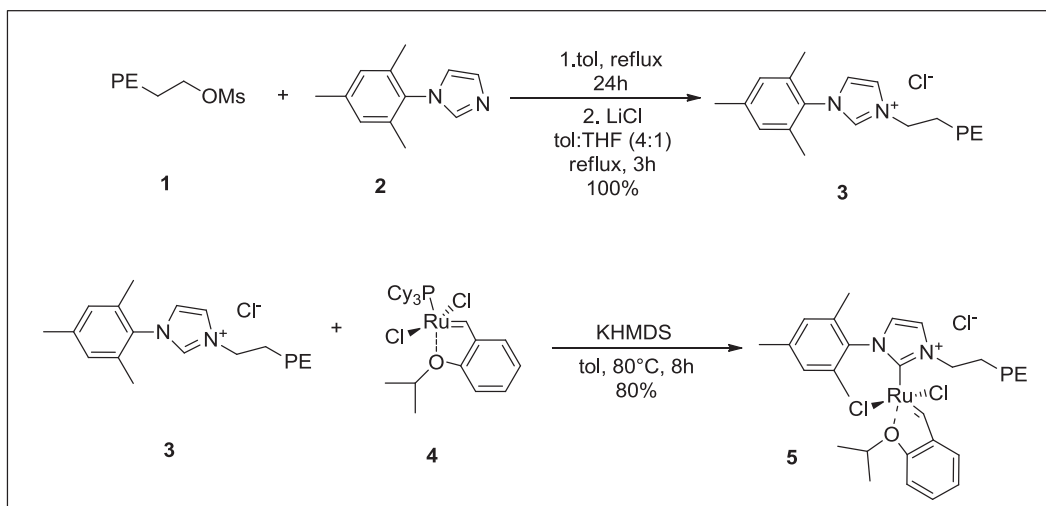
The elaboration of thermomorphic catalysts was first investigated by the group of Bergbreiter, who synthesized thermomorphic polyethylene supported complexes of Ru and Cr. The highly active ring-closing metathesis PE-NHC-Ru catalyst **5** was prepared from commercially available hydroxyl-polyethylene PE-OH (Scheme 2, pathway A). The mesylation of PE-OH followed by treatment with N-mesityl imidazole **2** resulted in formation of PE-imidazolium mesylate salt. The subsequent treatment with LiCl led to anion exchange and formation of **3**. The introduction of the Ru complex was performed classically after deprotonation of the imidazolium group by KHMDS and addition of the ruthenium precursor **4**. The PE-NHC-Ru solid **5** was obtained as a brownish /green powder. The as obtained catalyst was found to be an effective catalyst in RCM reactions (see Scheme2). The RCM reaction was fully completed in less than 5min when catalysis was performed with 5mol% of catalyst loading at 65°C in degassed toluene. It could be recycled up to 4 times without any loss of activity. However, after the 4th cycle its activity dramatically dropped. More stable catalysts were also obtained by introducing more hindered substituents on the NHC ligand. On this purpose, Bergbreiter and co-workers developed another synthetic strategy which requires numerous steps (Scheme 2, pathway B): i) Mitsunobu¹⁴² reaction between Boc protected-4-amino-3,5-xyleneol **1** and PE-OH **2**, ii) a Boc-deprotection leading to the formation of polyethylene supported aniline **3**, iii) the coupling of **3** with glyoxal in a toluene/propanol solution (1/3) at 75°C to yield quantitatively the bisimine compound **4**, iv) conversion of **4** into the polyethylene functionalized with the imidazolium salt **6** after a reduction-cyclization sequence, v) yielding of the targeted Ru complex **7** by deprotonation of imidazolium and coordination of the Ru precursor.¹⁴³ The supported complex **7** was found even more active in RCM reactions than **5** reaching full conversion of substrate in less than 5 min using 2.5mol%

¹⁴¹ Tasdelen, M.A.; Kahveci, M.U.; Yagci, Y, *Prog.Polym.Sci.* **2011**, 36, 455-567.

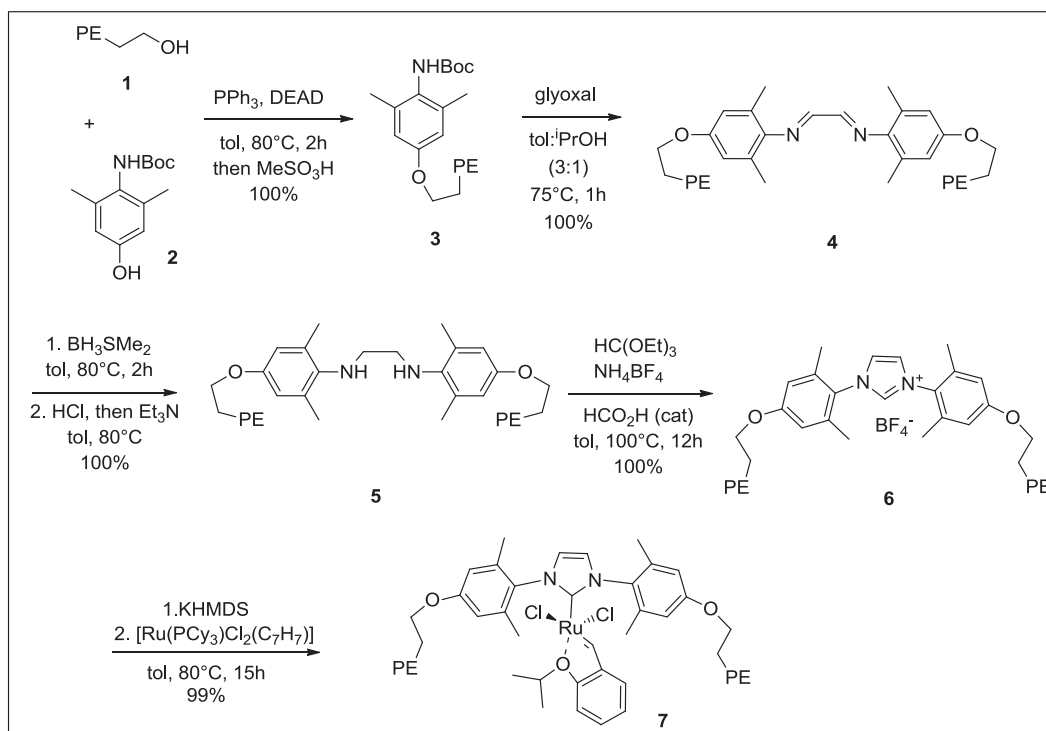
¹⁴² a)Swamy, K. C. Kumara; Kumar, N. N. Bhuvan; Balaraman, E.; Kumar, K. V. P. Pavan. *Chem. Rev.* **2009**, 109(6), 2551-2651; b) d'Arcy, R.; Tirelli, N. *Macromol. Rapid Commun.* 2015 Ahead of print

¹⁴³ Hobbs, C.; Yang, Y.-C.; Ling, J. ; Nicola, S.; Su, H.-L.; Bazzi, H. S.; Bergbreiter, D. E., *Ogr.Lett.*, **2011**, 15(15), 3904-3907.

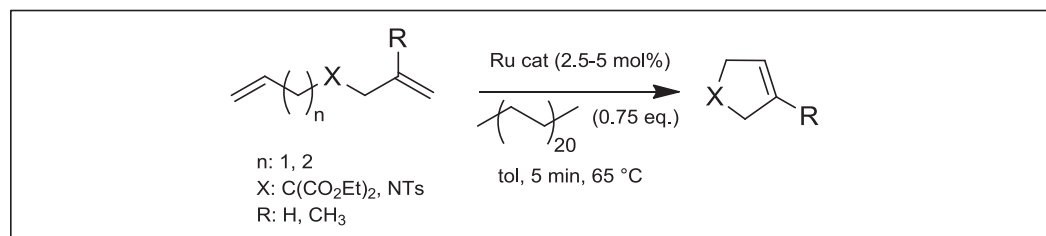
Pathway A



Pathway B



Catalysis



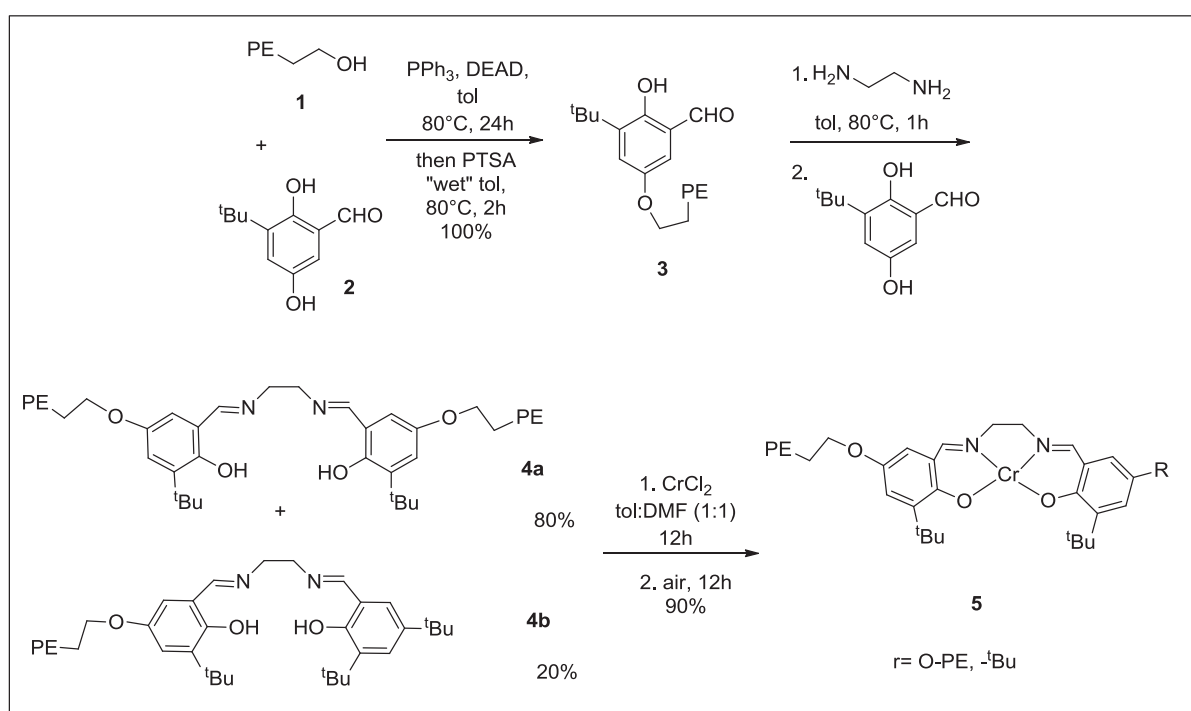
Scheme 2. Different pathway for preparation of Ru polyethylene supported catalyst and its catalytic performance

Chapter 4

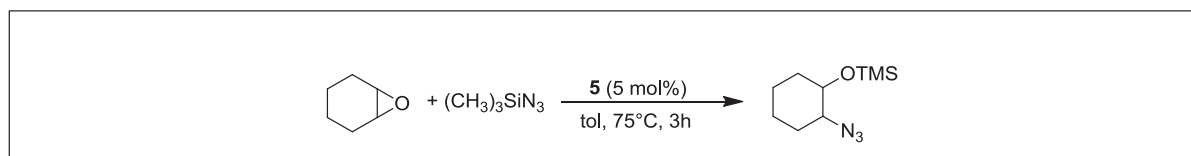
of catalyst loading under similar conditions (65°C, toluene). **7** was also found to be more stable and was recycled up to 10 times with little change in product yields.

A similar strategy was also used for the PE-immobilization of a Cr(III)-Salen complex (Scheme3). The catalytic performance of **5** was tested in reaction of cyclohexene oxide with azidotrimethylsilane. The full cyclohexane conversion was reached after 3h of reaction using 5 mol% of catalyst (reaction performed at 75°C in toluene with cyclohexane/azidotrimethylsilane=0.95) The solid could be recycled up to six times without significant activity loss.¹⁴⁴

Synthesis



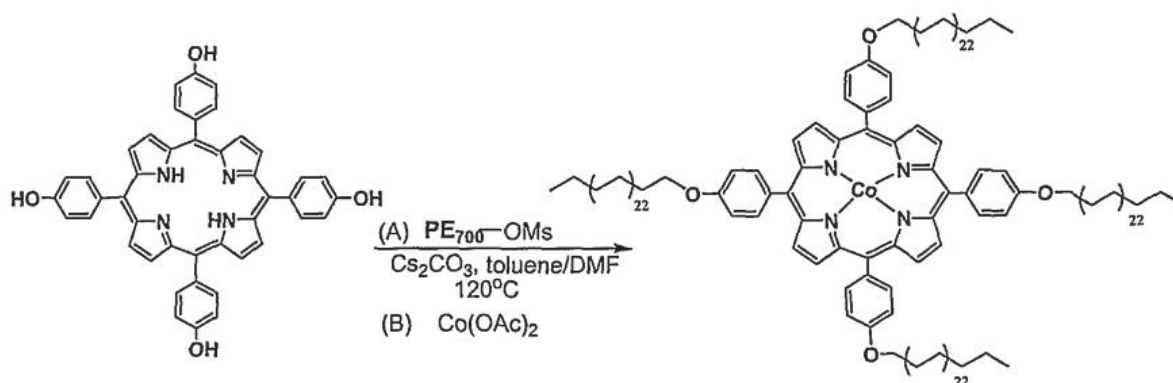
Catalysis



Scheme 3. Synthesis and catalytic performances of Cr(III)-Salen catalyst

¹⁴⁴ Bergbreiter, D.E.; Hobbs, C.; Hongfa, C. *J.Org.Chem.* **2011**, 76, 523-533.

The industrial production of thermomorphic polyethylene-based catalysts is also known. Thus in 2009, DuPont reported the preparation of radical polymerization catalysts based on PE-bound porphyrine and phthalocyanine metal complexes (Scheme 4).¹⁴⁵



Scheme 4. Preparation of PE-supported porphyrine-Cobalt complex.

¹⁴⁵ Older, C.M.; Kristjansdottir, S.; Ritter, J.C.; Tam, W.; Grady, M.C. *Chem.Ind.* **2009**, 123, 319–328.

IV-3. Introducing organometallic complexes

Having the PE-I in hands, we prepared the supported catalysts by nucleophilic substitution of iodide with mesitylimidazole by refluxing **PE-I** with 5 equiv. of mesitylimidazole in toluene for 96h at 100°C. The resulting mesitylimidazolium-polyethylene (**PE-MesIm**) was characterized by ^1H , ^{13}C liquid state NMR (Fig. 3-4). The success of the modification was shown by the disappearance of the signal at 3.00 ppm, corresponding to the methylene in alpha position of the iodo-group, and the appearance of a new signal at 4.75 ppm assigned to the $-\text{CH}_2\text{-N}-$ moiety. Besides, four new peaks were detected in the aromatic region at 6.81, 7.04, 8.15 and at 10.28 ppm and attributed as shown in figure 3. The resonance at 10.28 ppm is characteristic of the acidic proton of the imidazolium ring.

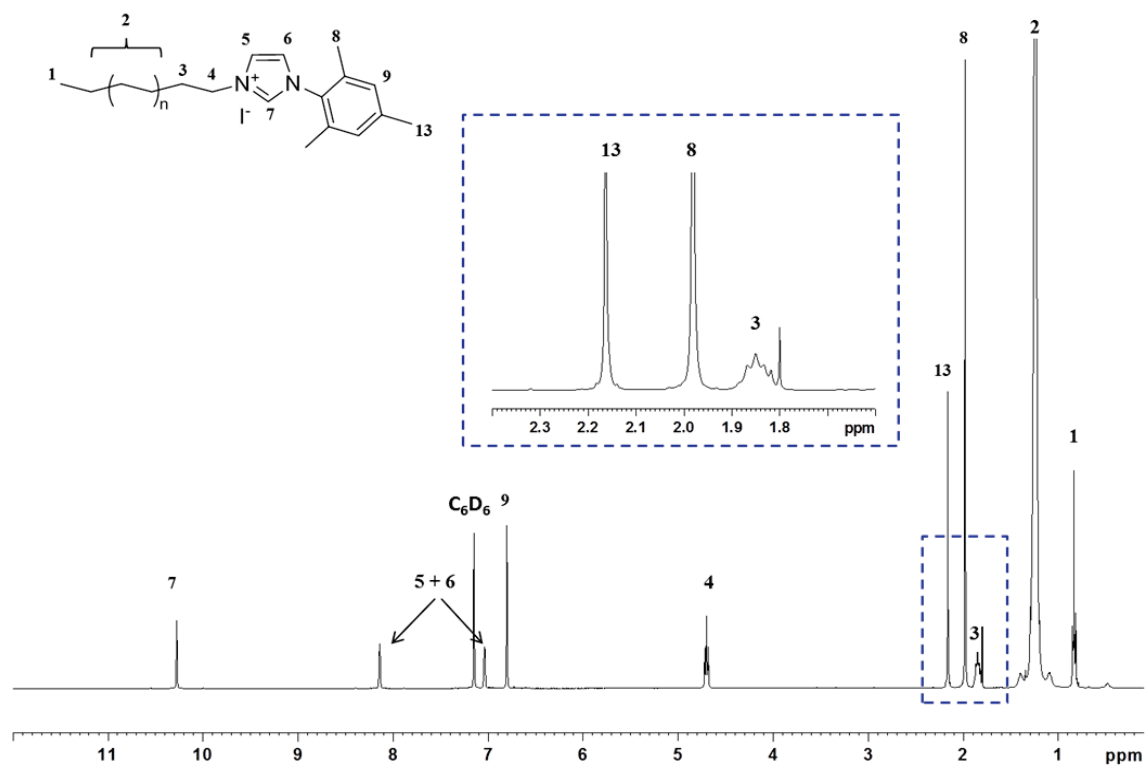


Figure 3: ^1H NMR of **PE-MesIm** (400 MHz, $\text{C}_6\text{D}_6/\text{TCE}$, 363 K)

The ^{13}C NMR spectrum also proved the attachment of the mesitylimidazolium ring to the polyethylene by the appearance of 7 new peaks in the aromatic region and by the disappearance of methylene iodide group signal at 4.93 ppm. A new signal at 50.62 ppm was attributed to the methylene group in α -position to imidazolium ($-\text{CH}_2\text{-N}$).

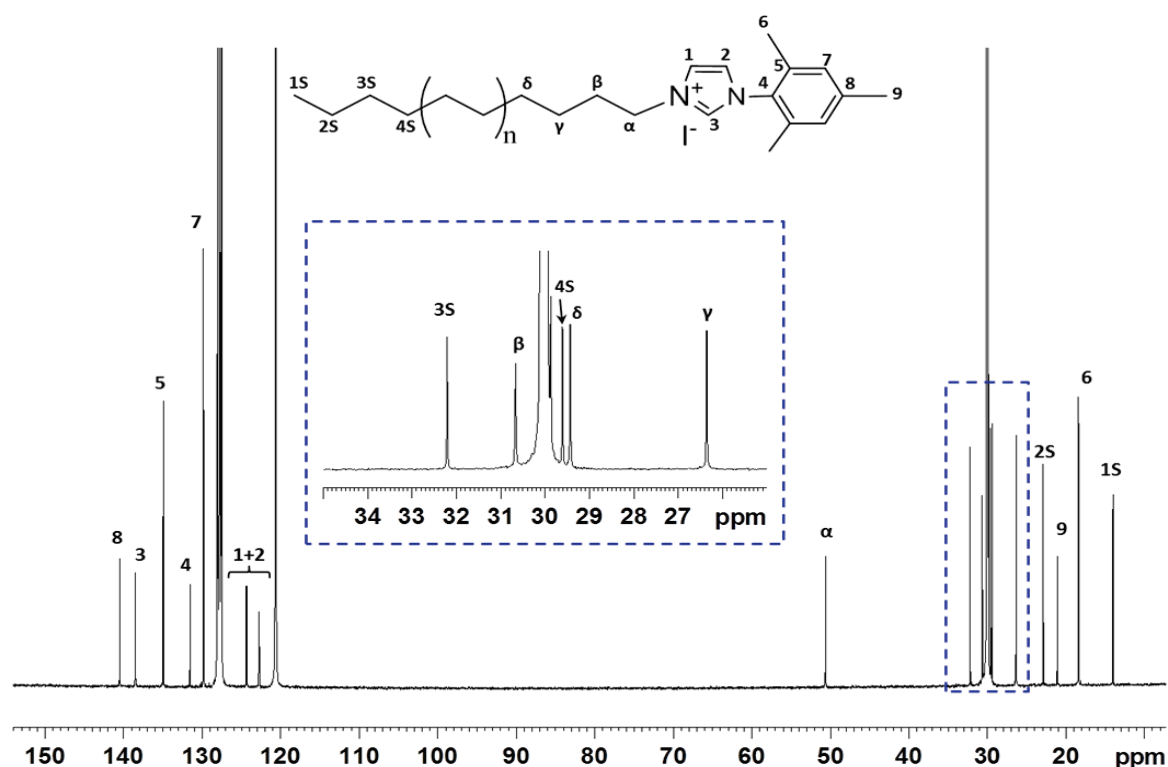
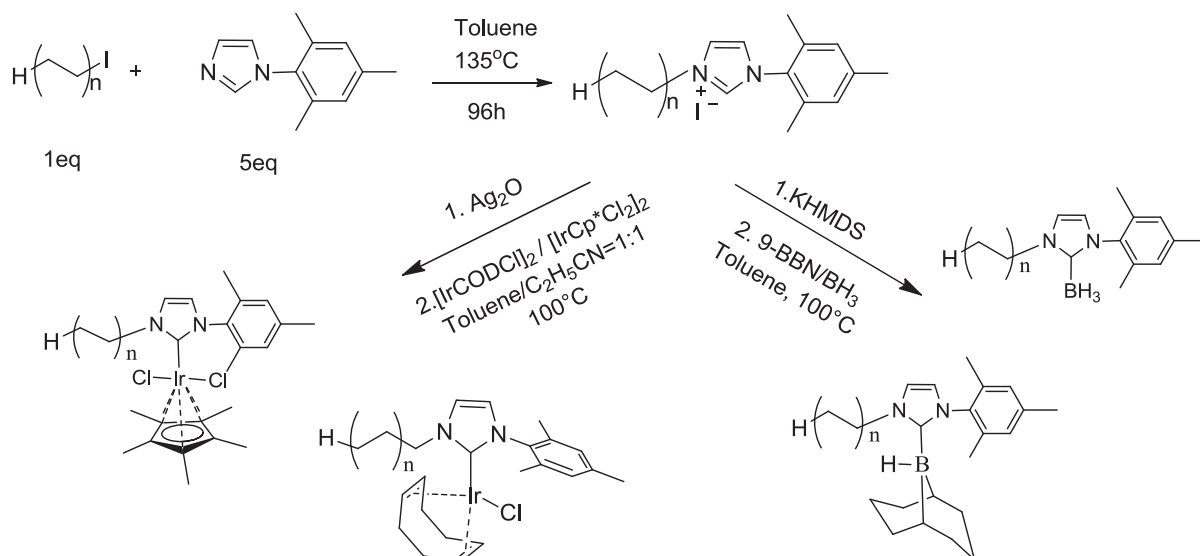


Figure 4. ^{13}C NMR of **PE-MesIm** (101MHz $\text{C}_6\text{D}_6/\text{TCE}$, 363K, ppm)

Kretschmer and co-workers reported another pathway to reach **PE-MesIm** via a four step methodology starting from yttrium catalyzed coordinative chain transfer polymerization of ethylene with aluminium alkyls. The resulting aluminium functionalized polyethylene was oxidized by dry oxygen, yielding 66% of the hydroxyl terminated PE (PE-OH). The subsequent treatment of PE-OH with bromoacetyl bromide in cumene at 110°C resulted in the formation of bromo-terminated PE. Finally the reaction of PE-OCOCH₂Br at 110°C in cumene with imidazole derivatives led to the quantitative formation of imidazolium bromides.¹⁴⁶ Our synthetic pathway is however more straightforward as it involves less steps and requires readily available reagents.

The synthesis of **PE-IrClCOD** and **PE-IrCl₂Cp*** was achieved by transmetallation through the formation of a silver carbene modified polyethylene (Scheme 5).

¹⁴⁶ Kretschmer, W.P.; Bauer, T.; Hessen, B.; Kempe, R. *Dalton Trans.* **2010**, 39, 6847-6852.



Scheme 5. Modification of polyethylene

PE-AgI was easily formed by treatment of **PE-MesIm** with $\frac{1}{2}$ equivalent of silver oxide during 30 minutes at 100°C in a mixture of toluene and propionitrile. The end of the reaction was visually detected by the complete solubilization of black Ag₂O powder leading to a transparent homogeneous grey solution. **PE-AgI** was precipitated at room temperature and recovered by filtration. The as-obtained polymer was characterized by liquid state ¹H, ¹³C NMR (Fig.5-6). Its formation was shown by the disappearance of the resonance of the acidic proton at 10.35 ppm on the ¹H NMR spectrum and the appearance of a characteristic carbene signal at 189.11 ppm in the ¹³C NMR spectrum. Noteworthy, dry **PE-AgI** was found stable at room temperature and can be stored under air and light.

Subsequent treatment of **PE-AgI** with $\frac{1}{2}$ equivalent of [IrCODCl]₂, during 24h at 100°C in toluene-acetonitrile mixture (1:1), resulted in the formation of a yellow solution of **PE-IrCp*** and a precipitate of AgI. The **PE-IrCICOD** was separated from the precipitate by hot filtration and it was crystallized as a deep orange powder. **PE-IrCICOD** was characterized by ¹H, ¹³C NMR, MALDI-TOF mass spectrometry and elemental analyses.

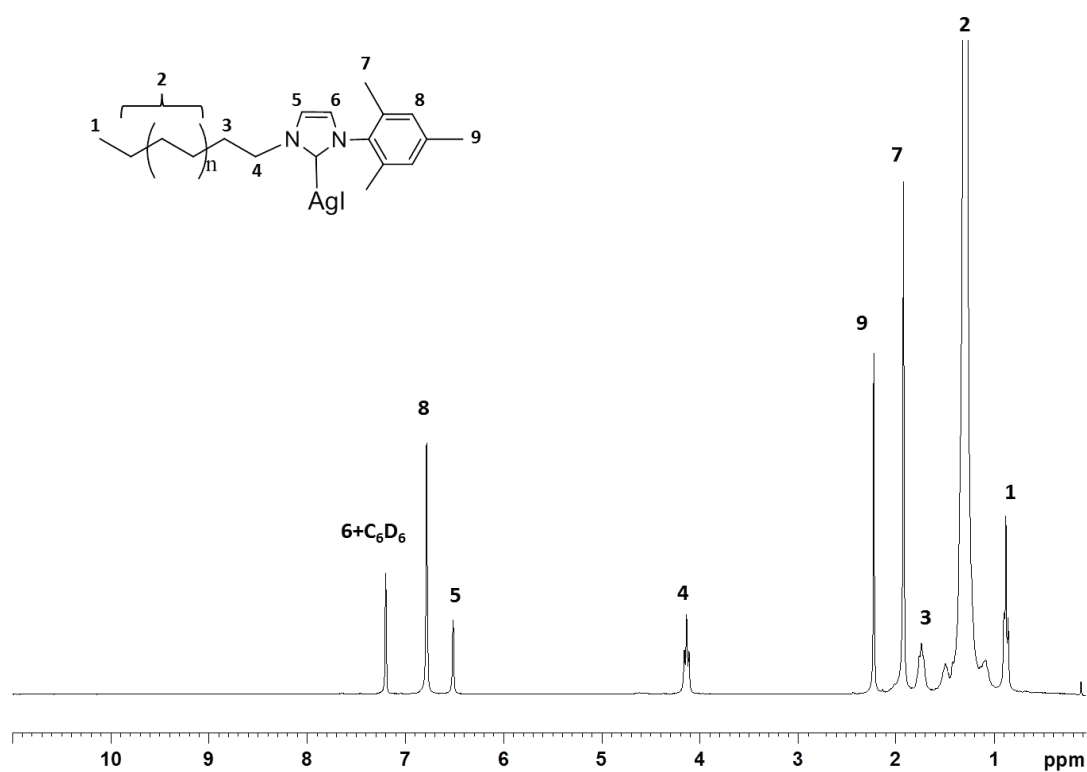


Figure 5. ^1H NMR of PE-AgI (300 MHz, $\text{C}_6\text{D}_6/\text{TCE}$, 363 K)

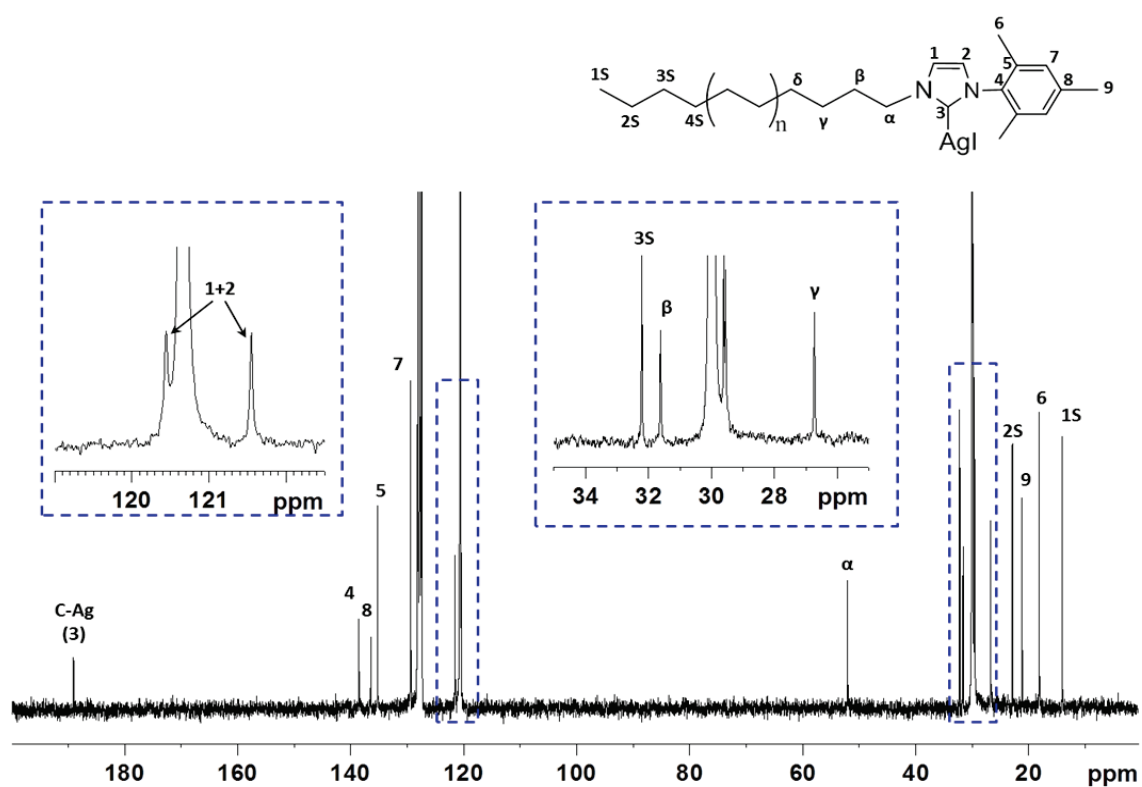


Figure 6. ^{13}C NMR of PE-AgI (75.43 MHz, $\text{C}_6\text{D}_6/\text{TCE}$, 363 K, ppm)

The success of the transmetallation process was evaluated by ^1H NMR (Fig.7), as shown by new signals in the region 2.6 - 3.0 ppm and 4.5 ppm attributed to the sp^2 -CH- protons of COD (sp^2 COD) in cis and trans positions to the NHC ligand, respectively. The split of the methylene signal into two multiplets at 4.17 ppm and 4.74 ppm and the split of the previously equivalent two methyl groups of mesityl into two singlets at 2.29 ppm and 1.77 ppm are consistent with the data recorded for the molecular $[\text{IrCl}(\text{MesImPr})(\text{COD})]$ complex for which the two methylenes and two methyls are not equivalent. The formation of the PE-IrClCOD was also confirmed by ^{13}C NMR where new signals at 29-35 ppm (CH_2 of COD), 50 ppm (CH of COD cis to Cl) and 80 ppm (CH of COD trans to Cl) appeared (Fig.A2). The ^1H and ^{13}C NMR spectra also indicated that the product was pure, suggesting a high degree of functionalization. Elemental analyses confirmed the NMR results and showed 10.6 wt.% of Ir (0.55mmol) i.e a transmetallation yield of 83%.

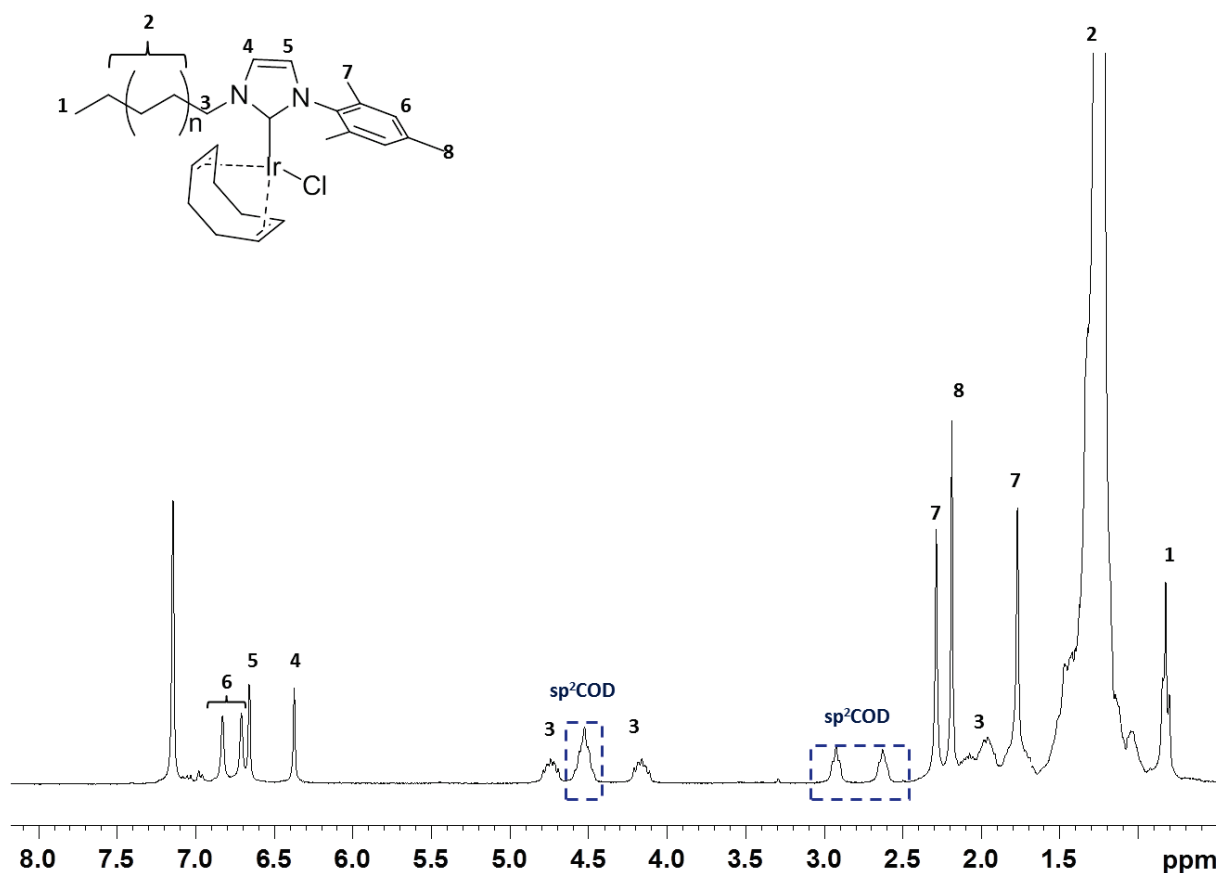


Figure 7. ^1H NMR of PE-IrClCOD (300 MHz, $\text{C}_6\text{D}_6/\text{TCE}$, 363 K)

MALDI-TOF mass spectrometry (Fig.A12-13) showed the presence of two different distributions. The difference between the various populations inside one distribution was 28g mol^{-1} , corresponding to one ethylene unit. Based on the isotopic distributions, the family with

the bigger molar mass and less intensities is related to $[M - Cl]^+$, where M is PE-IrClCOD. The most intense family corresponds to the $[M - IrCODCl]^+$ that we believe is generated under ionization conditions due to Ir-carbene bond cleavage. The absence of Iridium in the second family fits perfectly with what is expected from simulated data using the free software ISOPRO (Fig. A4-A6).

The same synthetic strategy was applied to the preparation of **PE-IrCp***. The as-obtained polymer was fully analyzed by 1H , ^{13}C NMR. As observed in the 1H NMR spectrum of **PE-IrCl₂Cp*** (Fig. 8), an intense resonance at 1.4 ppm was attributed to methyl groups of Cp*. ^{13}C NMR spectrum was also recorded for **PE-IrCl₂Cp***. Although its resolution was low, it clearly exhibited new intense peaks at 88 ppm and 9 ppm that were assigned to the sp^2 and sp^3 carbons of the Cp* ring respectively.

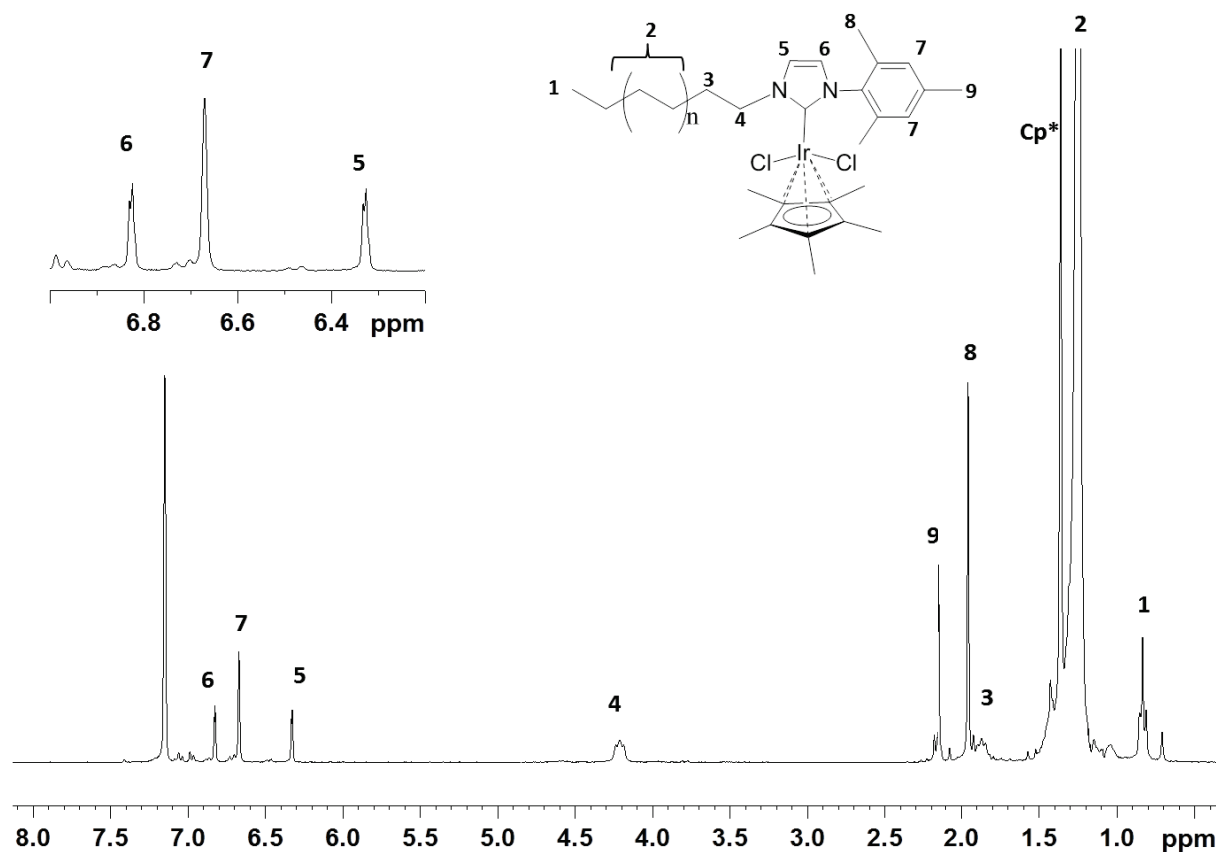


Figure 8. 1H NMR of **PE-IrClCp*** (300 MHz, C_6D_6/TCE , 363 K)

PE-IrCl₂Cp* was also analyzed by MALDI-TOF mass spectrometry (Fig. 9). A single isotopic distribution was observed and the various populations were separated by 28 g mol^{-1} which corresponds, as expected, to the molar mass of an ethylene unit. Based on the isotopic

distribution and the molecular weight, the cation observed in Mass spectra is $[M - Cl]^+$, where M is PE-IrCl₂Cp*. An additional molar mass distribution was also observed at -36g mol⁻¹ from the main one. It probably corresponds to the loss of one HCl molecule. The same behavior was also found for the analogue [IrCp*(MesImPr)Cl₂] (FigA7). We believe that a proton abstraction happens on a methyl group of the Cp* moieties, leading to a negatively charged methylene unit stabilized by the cationic Iridium center. The perfect match between the calculated molar mass of the expected structure for a fixed polymerization degree and the associated isotopic distribution with the obtained simulated data showed that the expected structure **PE-IrCl₂Cp*** was obtained. Finally, elemental analyses showed 7.38 wt.% of Ir (0.38mmol) resulting in a transmetallation yield of 57%.

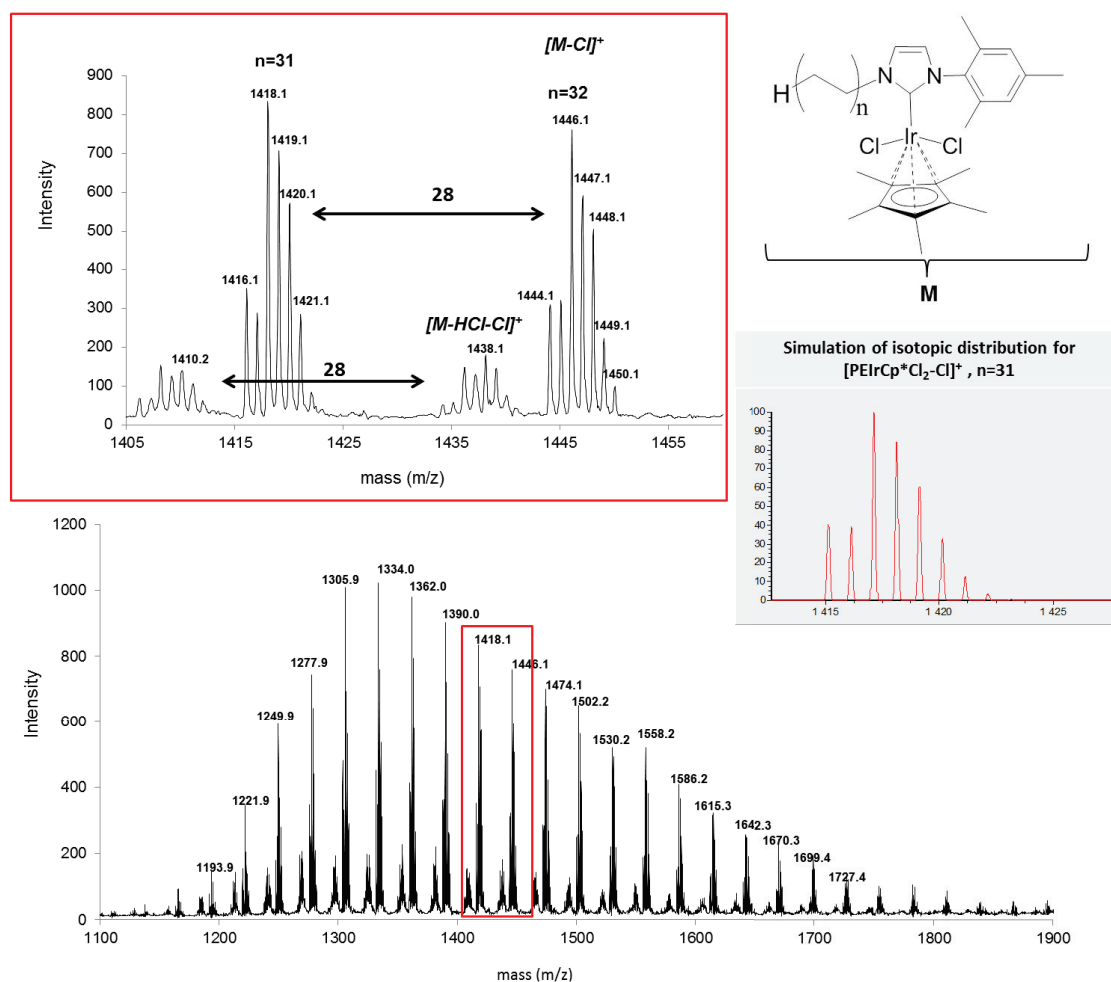


Figure 9. MALDI-TOF spectra of **PE-IrCP*Cl₂**

IV-4 Catalytic performance of Ir modified PE

4.1 Alkene hydrogenation with PE-Ir(COD)Cl

4.1.1 Performance

The Catalytic performance of PE-IrCODCl was tested in our standard trans-stilbene hydrogenation at two different temperatures (40°C and 80°C), with 0.1mol% and 1 mol% of catalyst loading. As shown in Fig.1, PE-IrCODCl is almost inactive in trans-stilbene hydrogenation at 40°C with 0.1mol% of catalyst loading. A maximum of 5% conversion could be obtained after 400h of reaction under these conditions. The increase of temperature till 80°C resulted in a 6 fold reaction rate increase, however catalyst was found to deactivate. A maximum of 26% conversion could be obtained by increasing the reaction time up to 800h. Even with an increased catalyst loading (1mol%) and temperature (80°C) the catalyst was found to deactivate, reaching a maximum of 64% conversion in 500h (reaction performed at 80°C). Interestingly, under elevated temperatures the color of the polymer changed from yellow to black, suggesting catalyst degradation through Ir particles formation.

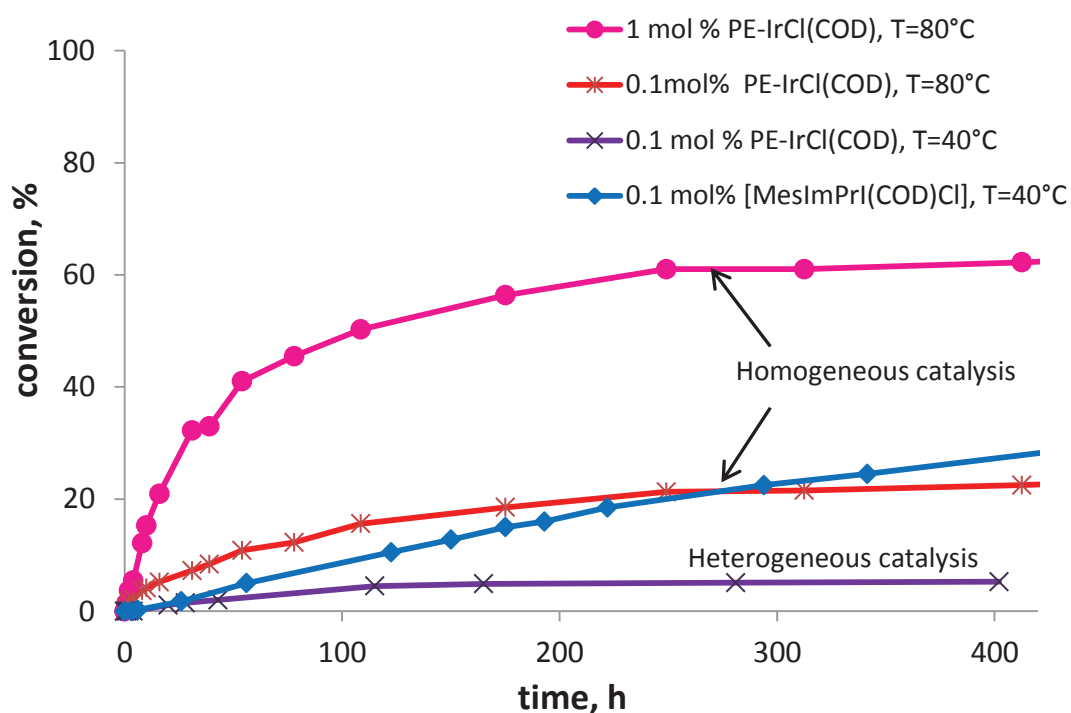


Figure 10. Conversion of trans-stilbene hydrogenation as a function of reaction time using PE-IrCODCl. The hydrogenation experiments were carried out in toluene at 40 °C and 80°C under 3 bar of H₂ with 0.1 mol% and 1mol% of Ir.

4.1.2. Comparison with neutral, cationic and silica supported analogues

The catalytic activity of PE-IrClCOD was further compared with those of neutral molecular complex $[\text{IrCl}(\text{COD})\text{MesImPr}]$, cationic derivative $[\text{Ir}(\text{COD})(\text{MesImPr})]\text{BF}_4$ and **M-Ir** material (Fig.2). It was expected that due to the bulkiness of PE units, Ir species would be protected from bimolecular deactivation processes (leading to formation of oligomeric hydrides). However, the polymer supported catalyst, operated under heterogeneous conditions (at 40°C), was found to have similar activity as the neutral $[\text{IrCl}(\text{COD})\text{MesImPr}]$ complex at the beginning of reaction. The initial TOF measured after 20h of reaction were 0.75 and 0.7 h^{-1} for $[\text{IrCl}(\text{COD})\text{MesImPr}]$ and PE-IrClCOD respectively. Noteworthy, the activity of PE-IrClCOD decreased with time; full deactivation of the catalyst happening after 100h of reaction. In contrast, the silica supported **M-Ir** catalyst demonstrated a straight hydrogenation profile without deactivation. These results therefore highlight the key role of the support on catalytic performances.

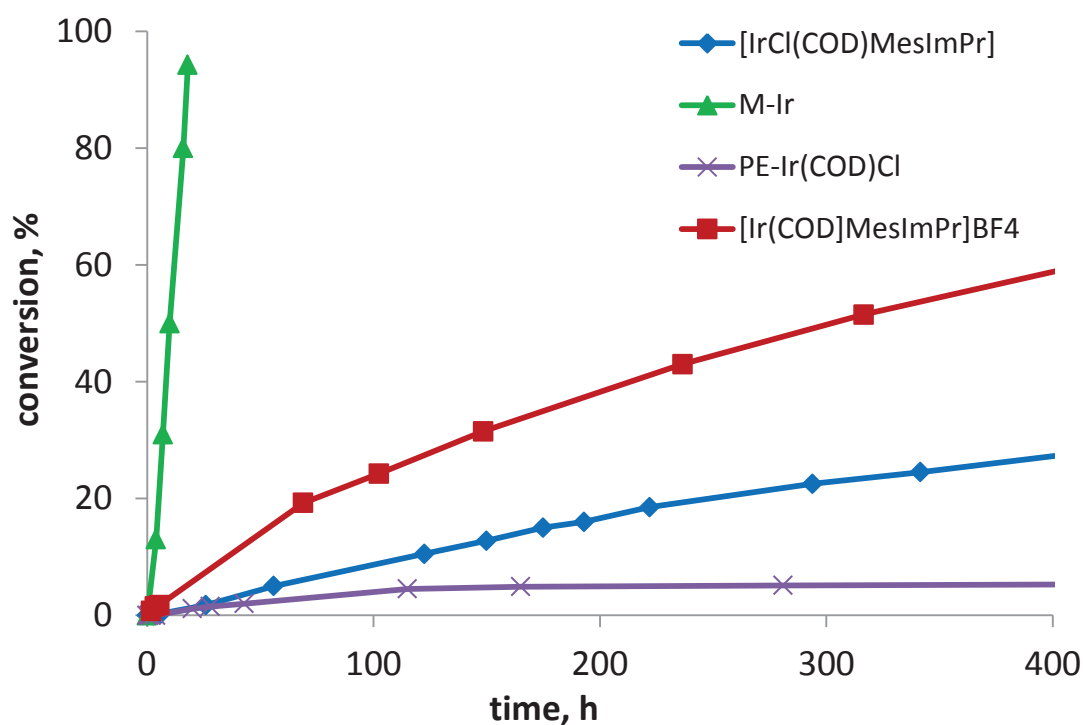
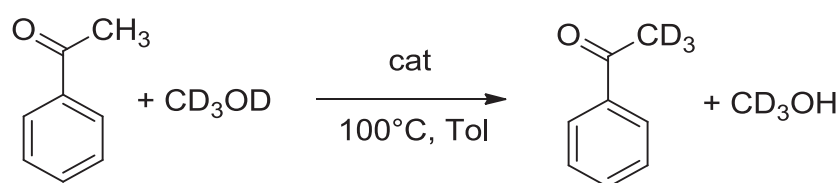


Figure 11. Conversion of trans-stilbene hydrogenation as a function of reaction time using: PE-IrClCOD, neutral $[\text{IrCl}(\text{COD})\text{MesImPr}]$, cationic $[\text{Ir}(\text{COD})(\text{MesImPr})]\text{BF}_4$ and **M-Ir** material. The hydrogenation experiments were carried out in toluene at 40 °C under 3 bar of H_2 (0.1 mol% of Ir).

4.2 H/D exchange with PE-IrCl₂Cp*

The H/D exchange reaction attracted considerable attention during the last 20 years¹⁴⁷ because it can be used to label chemical compounds. This can lead to applications in Mass-spectroscopy. MS has indeed a high demand of isotopically labeled internal standards for quantitative analysis of human, environmental or animal samples that are usually limited by strong matrix signals (matrix complicated substrates).¹⁴⁸ Moreover, if this type of reaction could be extended to H/T exchange, new horizons would be opened for metabolic studies and pharmacokinetics.¹⁴⁹

PE-IrCl₂Cp* and its analogue [IrCp*(MesImPr)Cl₂] were thus tested in the H/D exchange reaction using acetophenone as a standard substrate and methanol-d₄ as the deuterium source (molar ratio CD₃OD/acetophenone = 4.4). AgOTf was used as to generate the cationic Ir complex and toluene as solvent (Scheme7). The catalytic performance of the catalysts was tested with different substrate/catalyst ratios: 50, 500 and 5000 (Table1). It was found that [IrCp*(MesImPr)Cl₂] showed exactly the same catalytic profile and turnovers as **PE-IrCl₂Cp*** (Fig. 2). Similar catalytic behaviors were also observed when decreasing the amount of catalyst down to 0.02 mol% (R = 5000, see Fig.A8). Even with such a low catalyst loading, the reaction occurred till 81% of conversion. A final TON of 4100 was obtained. Blank tests performed without catalyst showed no conversion.



Scheme 6. Catalytic acetophenone deuteration

¹⁴⁷ a) Atzrodt, J.; Derdau, V.; Fey, T.; Zimmermann, J. *Angew. Chem. Int. Ed.* **2007**, *46*, 7744-7765; b) Feng, Y.; Jiang, B.; Boyle, P.A.; Ison, E. *Organometallics* **2010**, *29*, 2857-2867; c) Lehman, M.C.; Gary, J.B.; Boyle, P.D.; Sanford, M.S.; Ison, E.A. *ACS Catal.* **2013**, *3*, 2304-2310.

¹⁴⁸ a) Pirman, D.A.; Reich, R.F.; Kiss, A.; Heeren, R.M.A.; Yost, R.A. *Anal. Chem.* **2013**, *85*, 1081-1089; b) Tai, S.S.-C.; Bedner, M.; Phinney, K.W. *Anal. Chem.* **2010**, *82*, 1942-1948; c) Parise, R.A.; Ramanathan, R. K.; Hayes, M. J.; Egorin, M.J. *J. Chromatogr. B* **2003**, *791*, 39-44.

¹⁴⁹) Horiguchi, T.; Rithner, C.D.; Croteau, R.; Williams R.W. J. *Label. Compd. Radiopharm.* **2008**, *51*, 325-328; b) Ren, S.; Hesik, D.; McNamara, P.; Koharski, D.; Borges, S. J. *Label Compd. Radiophar.* **2014**, *57*, 632-636; c) Marathe, P. H.; Shyu, W. C.; Humphreys, W. G. *Curr. Pharm. Design* **2004**, *10*, 2991-3008.

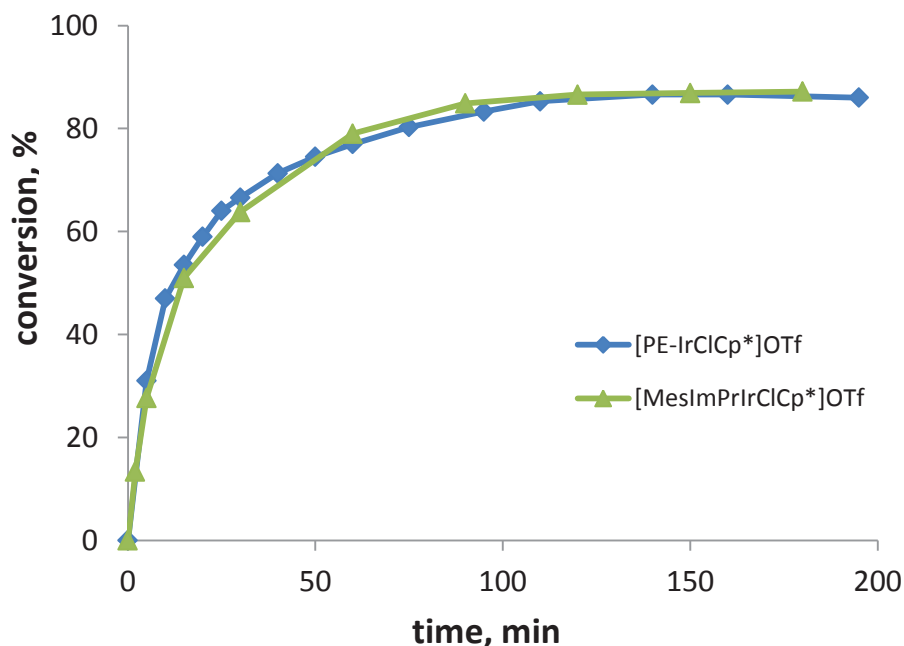


Figure 12. Comparison of catalytic activity of [PE-IrCp*Cl]OTf (red circles) and [IrCp*(MesImPr)Cl]OTf (blue diamonds) in acetophenone deuteration. The deuteration was carried out in toluene at 100 °C with 0.2 mol% cat (R=500)

Finally, **PE-IrCl₂Cp*** was also tested for recyclability (entries 2-4, Table1) and it was found that the polymer was able to be recycled at least two times without loss of activity. Moreover no leaching of active Iridium species could be detected in the supernatant after separation of the solid **PE-IrCl₂Cp*** (split tests). Besides, **PE-IrCl₂Cp*** was found to be faster in terms of TOF than our previously reported silica supported Ir-NHC catalyst.

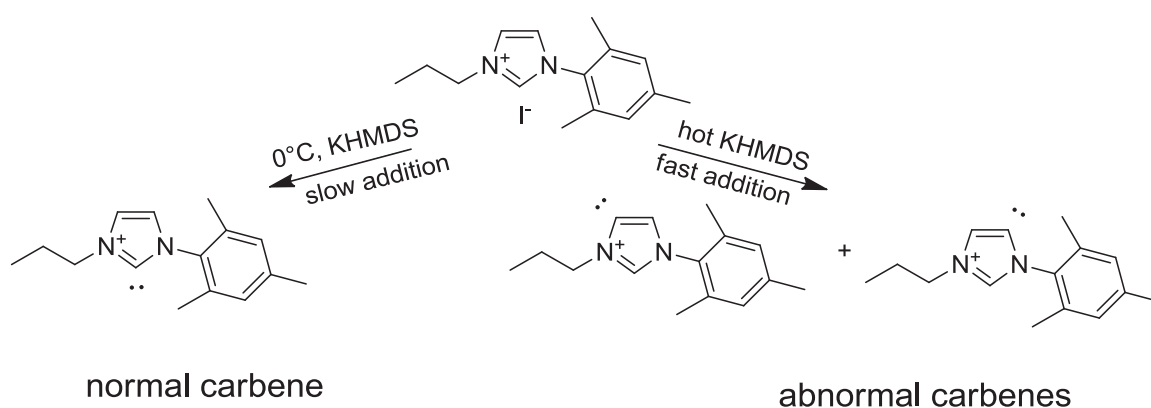
In conclusion, we elaborated a simple protocol to generate Ir-NHC-based polyethylene for H/D exchange reaction. Due to its thermomorphic properties, the as-obtained catalyst benefits from both an easy recovery and a recycling ability and showed the same catalytic activity than that of the homogeneous analogue. In this specific case, polyethylene supported catalyst was found slightly superior with respect to our previously reported silica supported catalyst.^{7b}

Table1. Catalytic performance of [PE-IrCp*Cl]OTf and [IrCp*(MesImPr)Cl]OTfin acetophenone deuteration

Entry	catalyst	Substrate/cat.	Conversion, %	t [min]	TOF, h ⁻¹
1	[IrCp*(MesImPr)Cl]OTf	50	81	5	-
2	[PE-IrCp*Cl]OTf	50	97	5	-
3	[PE-IrCp*Cl]OTf	50	99	5	-
4	[PE-IrCp*Cl]OTf	50	93	5	-
5	[IrCp*(MesImPr)Cl]OTf	500	86	120	1430 ^a
6	[PE-IrCp*Cl]OTf	500	86	120	1860 ^a
7	[IrCp*(MesImPr)Cl]OTf	5000	81	6600	692 ^b
8	[PE-IrCp*Cl]OTf	5000	83	6600	650 ^b

Termodinamically favored

Kinetically favored



The as-obtained products **PE-BBN** and **PE-BH₃** were analyzed by ¹¹B and ¹H NMR and **PE-BBN** also by ¹³C NMR. In both cases the formation of carbene boranes was observed. Both polymers gave just one boron signal in ¹¹B NMR, strongly suggesting the formation of only one carbene-borane product. As shown in Fig.3, the formation of **PE-BBN** that contains one proton on the boron atom was confirmed by the appearance of a doublet at -16 ppm in ¹¹B NMR and for **PE-BH₃**, the boron peak appeared as a quartet at -37 ppm. This is in agreement with the typical chemical shift for carbene boranes.¹⁵⁰

155

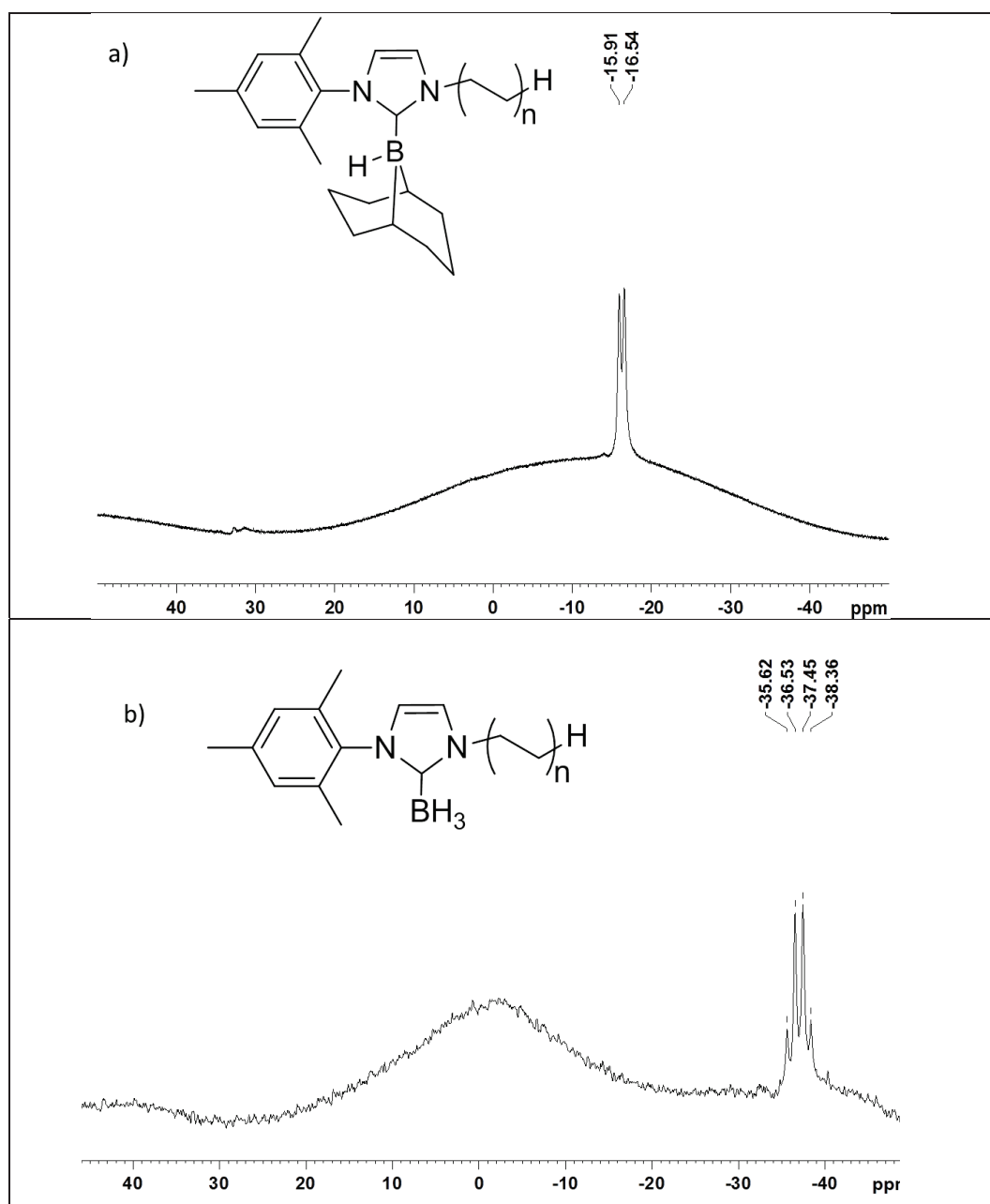


Figure 13. ^{11}B NMR of PE-BBN (a) and PE-BH₃ (b)

IV-6. Conclusions

The development of supported Ir-NHC complexes was implemented here to polymer-supported catalysts. The support of choice was a telechelic polyethylene iodide. It was transformed into the targeted catalytic system using a three step-process : i) transformation of the polyethylene iodide into imidazolium-containing PE, ii) in-situ formation of the supported silver carbene and iii) transmetallation of the PE-Ag-NHC with the Ir precursor, yielding the desired PE-Ir-NHC.

The quasi-quantitative (93% yield) formation of the silver-NHC polyethylene was unexpected as silver salts are known to be unstable upon heating suggesting a stabilizing role of the PE. After transmetallation, the loading of Iridium within the polymer was found much lower (yields in the range of 55-85%). All the modified polymers were characterized by ^1H and ^{13}C NMR and the Iridium polymeric catalysts were additionally characterized by elemental analysis and MALDI-TOF mass spectrometry.

The **PE-IrCODCl** was found to be a rather ineffective in alkene hydrogenation with respect to silica supported catalysts. Its initial catalytic activity at 40°C was similar to that of the molecular analogue [MesImPrIr(COD)Cl], however the catalyst decomposed with time, reaching a maximum of only 5% conversion in 400h. When hydrogenation was performed at 80°C, the catalyst decomposition rate increased. A maximum of 26% conversion could be obtained in 800h. The formation of a black deposit suggests the catalyst decomposition into Ir particles. The lability of the NHC-Ir(I) bond in the PE-catalyst was observed in MALDI-TOF spectra, where the major population is related to polyethylene derivatives without Iridium center.

On the contrary, **PE-Ir Cl₂Cp*** was found to be highly effective in H/D exchange reaction. It showed similar catalytic performances than its molecular analogue [MesImPrIrCp*Cl₂]. In addition, due to the polymer thermomorphic properties, the as-obtained catalyst was easily recovered and recycled. No population related to derivatives of PE-IrCp*Cl without Iridium were detected in MALDI-TOF spectra, suggesting that Ir(III) is more stable than its Ir(I) analogue. This new polyethylene supported catalyst was also found superior in term of TOF with respect to previously reported silica supported heterogeneous catalysts.

IV-7 Experimental section

6.7.1. General information

Ethylene (purity 99.95%) was purchased from Air Liquide. (n-butyl)(n-octyl)magnesium (BOMAG) in heptane (0.88 M) was provided by Chemtura. $((\text{Cp}^*)_2\text{NdCl}_2\text{Li}(\text{OEt}_2)_2)$ was prepared according to a literature procedure.^[1]

NMR. Solution-phase ^1H and ^{13}C NMR spectra were recorded on Bruker DRX300 and DRX400 spectrometers. For polymer analysis, high-resolution liquid NMR spectroscopy was carried out with a Bruker DRX 400 spectrometer operating at 400 MHz for the ^1H nucleus, and 101 MHz for ^{13}C . Spectra were recorded at 363 K using a 5 mm QNP probe for ^1H NMR, and a PSEX 10 mm probe for ^{13}C NMR. Polymer samples were examined as 5-15 % (w/v) solutions. A mixture of tetrachloroethylene (TCE) and deuterated benzene (C_6D_6) (2/1 v/v) was used as solvent. Chemical shift values are given in units of ppm, relative to an internal reference of tetramethylsilane for ^1H NMR and to the methylenes of the PE chain at 30 ppm for the ^{13}C NMR.

Size exclusion chromatography (SEC). High temperature Size Exclusion Chromatography (HT-SEC) analyses were performed using a Viscotek system (from Malvern Instruments) equipped with three columns (PLgel Olexis 300 mm x 7 mm I. D. from Agilent Technologies). 200 μL of sample solutions with concentration of 5 mg mL^{-1} were eluted in 1,2,4-trichlorobenzene using a flow rate of 1 mL min^{-1} at 150°C. The mobile phase was stabilized with 2,6-di(tert-butyl)-4-methylphenol (200 mg L^{-1}). The OmniSEC software was used for data acquisition and data analysis. The molar mass distributions were calculated with a calibration curve based on narrow poly(ethylene) standards (M_p : 170, 395, 750, 1110, 2155, 25000, 77500, 126000 g mol^{-1}) from Polymer Standard Service (Mainz).

6.7.2. Synthesis and characteristic of polymers

PE-I. Polymerization was carried out in a 500 mL glass reactor under anoxic, aprotic conditions, with ethylene supplied via a 2.13 L storage tank connected to the reactor via a regulator that maintains a constant pressure in the reactor. A solution of BOMAG was diluted in 400 mL of toluene. The resulting solution was transferred to a reactor under an argon

atmosphere. An antechamber was then charged with a solution of $(\text{Cp}^*)_2\text{NdCl}_2\text{Li}(\text{OEt})_2$ ($[\text{Mg}]/[\text{Nd}] = 150$) in toluene (10 mL). The reactor was heated to 75°C and then charged with ethylene at a pressure of 3 bars. The precatalyst solution was then injected in the reactor and the consumption of ethylene monitored. After the desired consumption of ethylene was reached, the reactor was degassed and purged with argon. The reaction medium was cooled to 10°C . A solution of iodine ($[\text{I}]/[\text{Mg}] = 4$) in tetrahydrofuran (50 mL) was added and the suspension was stirred for 3 hours. The reactor contents were poured in methanol (600 mL) and the suspension was filtered. The solid recovered was washed three times with methanol (3 x 100 mL) and dried under vacuum. The product was characterized by ^1H , ^{13}C NMR and SEC.

$M_n = 1260 \text{ g mol}^{-1}$, $\bar{D} = 1.17$ (obtained by SEC)

$M_n = 1221 \text{ g mol}^{-1}$; degree of polymerization: 39; functionalization: 92% calculated from ^1H NMR

^1H NMR 400 MHz (TCE/ C_6D_6 , 363K, ppm) δ 0.84 (t, $\underline{\text{CH}_3}$ -(CH_2CH_2) $_n$ -, $J = 7 \text{ Hz}$); 1.24 (br, CH_3 -($\underline{\text{CH}_2\text{CH}_2}$) $_n$ -); 1.66 (qt, $J = 7 \text{ Hz}$, $-\underline{\text{CH}_2}$ - CH_2 -I); 2.93 (t, $J = 7 \text{ Hz}$, $-\text{CH}_2$ -I);

^{13}C NMR 101MHz (TCE/ C_6D_6 , 363K, ppm) δ 4.93; 14.03 (CH_3); 22.89; 29.82; 29.89; 29.68; 29.61; 30.00 ($(\text{CH}_2\text{CH}_2)_n$); 30.78; 32.21; 33.99

PE-MesIm. PE-I (4 g, 3.0 mmol) was mixed with mesitylimidazole (2.55 g, 15 mmol) under argon. The mixture was suspended in 180 mL of toluene and left stirring for 96 h under reflux ($T = 135^\circ\text{C}$). The temperature of the solution was decreased to room temperature for precipitating PE-ImMes. The product was separated by filtration and characterized by ^1H , ^{13}C NMR. $M_n = 1392 \text{ g mol}^{-1}$ and full functionalization (100%) can be assigned by ^1H NMR.

^1H NMR 400 MHz (TCE/ C_6D_6 , 363 K, ppm) δ 0.84 (t, $J = 7 \text{ Hz}$, $\underline{\text{CH}_3}$ -(CH_2CH_2) $_n$ -); 1.24 (br, CH_3 -($\underline{\text{CH}_2\text{CH}_2}$) $_n$ -); 1.84 (m, $-\underline{\text{CH}_2}$ - CH_2 -N); 1.98. (s, 2CH_3 of Mes,); 2.17 (s, CH_3 of Mes); 4.70. (t, $J = 7 \text{ Hz}$, NCH_2); 6.81 (s, 2CH of Im); 7.04 (s, CH of Im); 8.15 (s, CH of Im); 10.28 (s, N-CH-N)

^{13}C NMR 101 MHz (TCE/ C_6D_6 , 363K, ppm) 14.04; 18.41; 21.11; 22.89; 26.36; 29.43; 29.61; 29.87; 30.00 ($(\text{CH}_2\text{CH}_2)_n$); 30.67; 32.21; 50.62; 122.78; 124.36; 129.82; 131.55; 134.95; 138.51; 140.49.

PE-AgI. PE-MesIm (0.2 g, 0.14 mmol) was mixed with Ag₂O (25 mg, 0.08 mmol) in glove box and suspended in 10 mL of toluene–propionitrile mixture (1:1). The reaction mixture was heated till 100 °C and left for stirring during 30 min. The suspension forms a transparent grey solution. The hot mixture was filtrated through a cannula in order to separate unreacted Ag₂O. PE-AgI was separated by filtration of the cold solution. The obtained product was characterized by ¹H, ¹³C NMR. Mn=1660g mol⁻¹; functionalization: 93 95 % (calculated from ¹H NMR).

¹H NMR 300 MHz (TCE/C₆D₆, 363 K, ppm) δ. 0.84 (t, J = 7 Hz, CH₃-(CH₂CH₂)_n-); 1.24 (br, CH₃-(CH₂CH₂)_n-); 1.68 (m, -CH₂-CH₂-N); 1.87 (s, 2CH₃ of Mes); 2.17 (s, CH₃ of Mes); 4.08 (t, J = 7 Hz, NCH₂); 6.46 (s, CH of Im); 6.73 (s, 2 CH of Mes); 7.15 (CH of Im mixed with C₆D₆).

¹³C NMR 101 MHz (TCE/ C₆D₆, 363 K, ppm) δ 14.04; 18.12; 21.14; 22.89; 26.72; 29.55; 29.61; 30.00 ((CH₂CH₂)_n); 31.61; 32.21; 52.07; 120.44; 121.55; 129.40; 135.26; 136.48; 138.57; 189.06 (C-Ag).

PE-IrCp*. PE-AgI (200mg, 0.16 mmol) was dissolved in 20 mL of a toluene/propionitrile mixture (1:1) at 100 °C. [IrCp*Cl₂]₂ (72 mg 0.09 mmol) was dissolved in 20 mL of toluene and was transferred by cannula to the PE-AgI mixture. After mixing solutions the precipitation of white AgI was noticed. The mixture was left for stirring for 24h under 100°C. The inorganic salt was separated from the polymer by hot filtration through cannula. After cooling, the PE-IrCp* precipitated as an orange powder. The product was separated by filtration. In order to avoid the presence of precursors in the final product, **PE-IrCp*** was recrystallized two times from toluene. The obtained product was characterized by ¹H, ¹³C NMR and MALDI-TOF mass spectroscopy and elemental analysis. Functionalization: 57% (calculated from elemental analysis)

¹H NMR 400 MHz (TCE/ C₆D₆, 363 K, ppm) δ. 0.84(t, J = 7 Hz, CH₃-(CH₂CH₂)_n-); 1.24 (br, CH₃-(CH₂CH₂)_n-); 1.36 (s, Cp*); 1.87(m, -CH₂-CH₂-N); 1.96(s, 2CH₃ of Mes); 2.15 (s, CH₃ of Mes); 4.21 (t, J = 7 Hz, NCH₂); 6.32 (d, J = 2.0Hz, CH of Im); 6.82 (d, J = 2.0Hz, CH of Im); 6.67(s, 2CH of Mes).

¹³C NMR 101 MHz (TCE/ C₆D₆, 363K, ppm) δ 9.1 (sp³, Cp*); 14.04; 19.05; 21.11; 22.890; 27.27; 29.61; 29.83; 29.87; 30.00((CH₂CH₂)_n); 32.21; 52.48; 88.54(sp², Cp*); 119.87; 125.18; 137.70; 137.88; 154.91; 169.7(C-Ir).

PE-IrClCOD. PE-AgI (1.0 g, 0.8 mmol) was dissolved in 20 mL of a toluene/propionitrile mixture (1:1) at 100 °C. [IrCODCl]₂ (292 mg 0.4 mmol) was dissolved in 20 mL of toluene and was transferred by cannula to the PE-AgI mixture. After mixing solutions the precipitation of white AgI was noticed. The mixture was left for stirring for 24h under 100°C. The inorganic salt was separated from the polymer by hot filtration through cannula. After cooling, the PE-IrCp* precipitated as an orange powder. The product was separated by filtration. In order to avoid the presence of precursors in the final product, **PE-IrCODCl** was recrystallized two times from toluene. The obtained product was characterized by ¹H, ¹³C NMR and MALDI-TOF mass spectroscopy and elemental analysis. Full functionalization was calculated from ¹H NMR.

¹H NMR 400 MHz (TCE/ C₆D₆, 363 K, ppm) δ. 0.83 (t, J = 7 Hz, CH₃-(CH₂CH₂)_n-); 1.24 (br, CH₃-(CH₂CH₂)_n-); 1.77 (m, -CH₂-CH₂-N); 1.96 (s, CH₃ of Mes); 2.19 (s, CH₃ of Mes); 2.29 (s, CH₃ of Mes); 2.63 (m, =CH of COD); 2.92 (m, =CH of COD); 4.16 (m, NCH₂); 4.53 (m, =CH of COD); 4.74 (m, NCH₂); 6.37 (d, J = 2.0 Hz, CH of Im₁); 6.66 (d, J = 2.0Hz, CH of Im₂); 6.70(s, CH of Mes); 6.8 (s, CH of Mes).

¹³C NMR 101 MHz (TCE/ C₆D₆, 363K, ppm) δ 14.04; 17.76; 19.91; 21.00; 22.9; 27.18; 29.21; 29.61; 30.00((CH₂CH₂)_n); 30.92; 32.21; 33.07 (sp³COD); 34.93 (sp³COD); 50.01 (sp²COD); 50.63 (sp²COD); 51.72; 120.14; 122.38; 129.88; 134.30; 136.67; 137.95; 138.36; 181.98 (C-Ir).

PE-BBN. 3.8ml of 1M toluene solution of KHMDS was added drop by drop to the solution of 1.36g (3.8mmol) MesIm in toluene .under dry conditions. After 5min stirring 7.6 mL of 0.5M solution of BBN in THF was added. The mixture was left for stirring for 15h under 100°C. After cooling down the PE-BBN precipitate as white powder. The product was separated by filtration and dried under vacuum (10⁻³) at 80°C during 12h. Obtained product was characterized by ¹¹B, ¹H, ¹³C NMR. The functionalization of 79% was calculated from NMR.

¹H NMR 300 MHz (TCE/ C₆D₆, 363 K, ppm) δ. 0.77 (br, BH); 0.83 (t, J = 7.Hz, CH₃-(CH₂CH₂)_n-); 1.24 (br, CH₃-(CH₂CH₂)_n-); 1.87 (m, -CH₂-CH₂-N); 1.95 (s, 2CH₃ of Mes); 2.14 (s, CH₃ of Mes); 4.12 (t, -CH₂-N, J = 7 Hz); 6.26 (d, CH of Im, J = 2 Hz); 6.57 (d, CH of Im, J = 2 Hz); 6.7(s, 2CH of Mes).

^{13}C NMR 75.43 MHz (TCE/ C_6D_6 , 363K, ppm) δ 14.04; 17.94; 20.98; 22.53÷24.08 (BBN, 2CH, br); 22.89; 25.84 (BBN, CH₂); 25.32 (BBN, CH₂); 26.85; 29.45; 29.61; 30.86; 32.21; 32.39 (BBN, 2CH₂); 48.92 (BBN, 2CH₂); 119.39; 120.86; 129.00; 135.55; 138.77.

PE-BH₃. 0.8ml of 1M solution of KHMDS was added drop by drop to the 1g (0.82mmol) of PE-MesIm. After 5min stirring 0.8mL of 1.0 M solution of BH₃ in THF was added. The mixture was left for stirring for 15h under 100°C. After cooling down the PE-BBN precipitate as white powder. The product was separated by filtration and dried under vacuum (10^{-3}) at 80°C during 12h. Obtained product was characterized by ^{11}B , ^1H , ^{13}C NMR. The functionalization of 81% was calculated from NMR.

^{11}B NMR 300 MHz (TCE/ C_6D_6 , 363 K, ppm) δ -36.5 (q, J=0.9Hz)

^1H NMR 300 MHz (TCE/ C_6D_6 , 363 K, ppm) δ 0.83 (t, $\text{CH}_3\text{-(CH}_2\text{CH}_2)_n$ -, J=7Hz); 1.24 (br, $\text{CH}_3\text{-(CH}_2\text{CH}_2)_n$ -); 1.7 (s, 2CH₃ of Mes); 1.86 (s, CH₃ of Mes); 4.00 (t, J=7Hz, NCH₂); 6.34 (d, J = 2.0Hz, CH of Im); 6.54 (d, J = 2.0Hz, CH of Im); 6.73(s, 2CH of Mes).

6.7.3. Synthesis and characteristic of organometallic complexes

[IrCp*(MesImPr)Cl₂]. MesImPrI 230 mg (1mmol) of dried was mixed with 115 mg (0.5 mmol) of Ag₂O in argon atmosphere in the absence of light. The mixture was dissolved in 20 ml of dried CH₃CN and left for stirring at 25 °C for 4 h. Then 400mg (0.5 mmol) of [IrCp*Cl₂]₂ were dissolved in 40ml of dried and degassed CH₃CN and transferred by cannula to the silver carbene. The reaction was carried out at 60 oC during 12 h. The product was purified by column chromatography, using Acetone/Heptane (1:1) mixture as an eluent. The orange crystals of 1 were obtained by crystallization at -28 °C from benzene and characterized by X-Ray. The crystals were dried under vacuum for 8h at 80°C and were characterized by ^1H , ^{13}C , dept 135 and 2D ^1H - ^1H COSY NMR spectroscopy, Mass ESI and X-Ray analysis.

^1H NMR (C_6D_6 , 300K; ppm): δ 0.97 (t, 3H, J=7Hz, $\text{CH}_3\text{-CH}_2$ -); 1.41 (s, 15H, Cp*); 1.90 (m, $\text{CH}_3\text{-CH}_2$ -); 1.94 (s, 6H, CH₃ of Mes); 2.19(s, 3H, CH₃ of Mes); 4.18 (br, 2H, NCH₂); 6.56 (s, 1H, CH of Im); 7.07 (d, J=2.0Hz, 1H, CH of Im); 6.72 (d, J=2.0Hz, 2H, CH of Mes).

^{13}C NMR (C_6D_6 , 300K, ppm): δ 9.34 (5CH₃, Cp*); 11.43 (CH₃, Pr) ; 19.27 (2CH₃, Mes); 21.42 (CH₃, Mes); 24.59 ($\text{CH}_3\text{-CH}_2$ -); 53.63 (NCH₂); 88.88 (sp² Cp*) 120.49(CH of Im); 125.47

(CH of Im); 128.47 (2CH, Mes); 137.22 (C quat., Mes); 138.52 (C quat., Mes); 154.01 (C quat., Mes). Carbene-Ir signal was not detected.

HRMS (ESI⁺): calculated for [IrCp*(MesImPr)Cl]⁺ ([M-Cl]) 591.2 and [IrCp*(MesImPr)] ([M-Cl-HCl]) 555.2; found 591.2 and 555.2).

[(MesImPr)BBN]. 0.32g of dry MesImPrI (0.9 mmol) was dissolved in 10mL of dry degassed THF. The mixture was cooled down till 0°C, than 2.8 ml of 1M KHMDS solution was added dropwise. After 30 min of stirring 5.4mL of 0.5M solution of 9-BBN in THF was added dropwise. The reaction mixture was left for stirring for 30min at 0°C. Than temperature was warmed up till 20°C and mixture was left for stirring for 2h more. After solvent evaporation the product was purified by column chromatography on dry alumina by using dry THF as a eluent. The transparent crystals of pure product were obtained by evaporation of solvent residuals under vacuum (10⁻⁵ mmHg). The crystals were analyzed by ¹H, ¹³C, dept 135 and X-Ray analysis.

¹H NMR (C₆D₆, 283K, ppm): δ 0,67(br, BH); 0.98 (t, J=7Hz, 3H, CH₃-CH₂-); 1.02-1.7 (m, 12H, CH₂ of BBN); 1.86 (sext., J=7.5Hz, 2H, CH₃-CH₂-); 4.2 (d.d;d., J=9Hz, J=7.5Hz, J=1.7Hz, 2H); 6.66 (d, J=2.0Hz, 1H, CH of Im); 6.9 (s, 2H, CH of Mes); 7.03 (d, J=2.0Hz, 1H, CH of Im).

¹³C NMR (CDCl₃, 283K, ppm) : δ 11.05(CH₃-CH₂-); 17.98 (2CH₃, Mes); 21.12 (CH₃, Mes); 21.7-21.8 (br, 2CH of BBN); 24.09(CH₃-CH₂-); 25.25 (2CH₂ of BBN); 25.54(2CH₂ of BBN); 31.71(CH₂ of BBN); 37.00(CH₂ of BBN); 50.09(NCH₂); 119.77 (CH, Im); 121.04 (CH, Im); 128.78 (CH, Mes); 135.40 (Cquat., Mes); 135.45 (Cquat., Mes); 138.89 (Cquat., Mes).

[(MesImPr)BH₃]. 200mg (0,6mmol) of well dried MesImPrI were mixed with 67mg (0,3mmol) of Ag₂O in argon atmosphere in the absence of light. The mixture was dissolved in 20ml of dried CH₃CN and left for stirring at room temperature for 4h. Than the rest of Ag₂O was filtered under inert conditions and transparent filtrate was evaporated under the vacuum. The complex was again dissolved in 20ml of distilled degased THF and 0,6 ml (0,6mmol) of 1M complex BH₃*THF were added. The reaction was left for stirring at room temperature. After 5 days of reaction the mixture was filtered under inert conditions. The solvent was evaporated under the vacuum. The product was separated by chromatography EtOAc/Hexane=1:1. The product was characterized by ¹H, ¹³C, ¹¹B NMR.

^1H NMR(CH_2Cl_2 , 300K, ppm): δ 0.21, 0.50, 0.80, 1.08 (q., $J=86\text{Hz}$, 3H, BH_3); 0.96 (t, $J=7\text{Hz}$, 3H, $\text{CH}_3\text{-CH}_2$); 1.87 (sext, $J=7.3\text{Hz}$, 2H, $\text{CH}_3\text{-CH}_2$); 1.94(s, 6H, CH_3 of Mes); 2.34 (s, 3H, CH_3 of Mes); 4.16 (dd, $J=8.5\text{ Hz}$, $J=6.5\text{ Hz}$, 2H, NCH_2); 6.79(d, $J=2.0\text{Hz}$, 1H, CH, Im); 6.97 (2H, CH of Mes); 7.02 (d, $J=2.0\text{Hz}$, 1H, CH of Im).

^{13}C NMR(CH_2Cl_2 , 300K, ppm): δ 11.03 ($\text{CH}_3\text{-CH}_2$); 17.66 (2 CH_3 , Mes); 21.23 (CH_3 , Mes); 23.77 ($\text{CH}_3\text{-CH}_2$); 50.69 (NCH_2); 120.09 (CH, Im); 119.95 (CH, Im); 129.09 (CH, Mes); 135.35 (Cquat., Mes); 135.49(Cquat., Mes); 139.23 (Cquat., Mes).

^{11}B NMR (C_6D_6 , 300K): quartet -35.84; -35.78; -36.72; -37.65 (1:2:2:1)

6.7.4. Catalysis

6.7.4.1. Hydrogenation with PE-IrCODCl

15mg of PE-IrClCOD (0. 009mmol) was placed in the reactor ($V=300\text{ml}$) together with 1620mg of trans-stilbene (9mmol). The reactor was left under vacuum for 15 min and after filled with Argon. Mixture was dissolved in 35mL of dry degassed toluene. 0.5ml of tetrachloroethane was used as an internal standard. Reaction was monitored by ^1H NMR. The mixture was heated until desired temperature (40 or 80°C) and reactor pressurized with 3 bars of H_2 .

For performing catalysis with 1 mol % of **PE-IrClCOD** catalyst loading the quantity of trans-stilbene was reduced till 162mg (0.9mmol). The hydrogenation performed in reactor with total volume of 25ml with 3.5ml of toluene. 0.1ml of 1,1,2,2, -tetrachloroethane was used as internal standard.

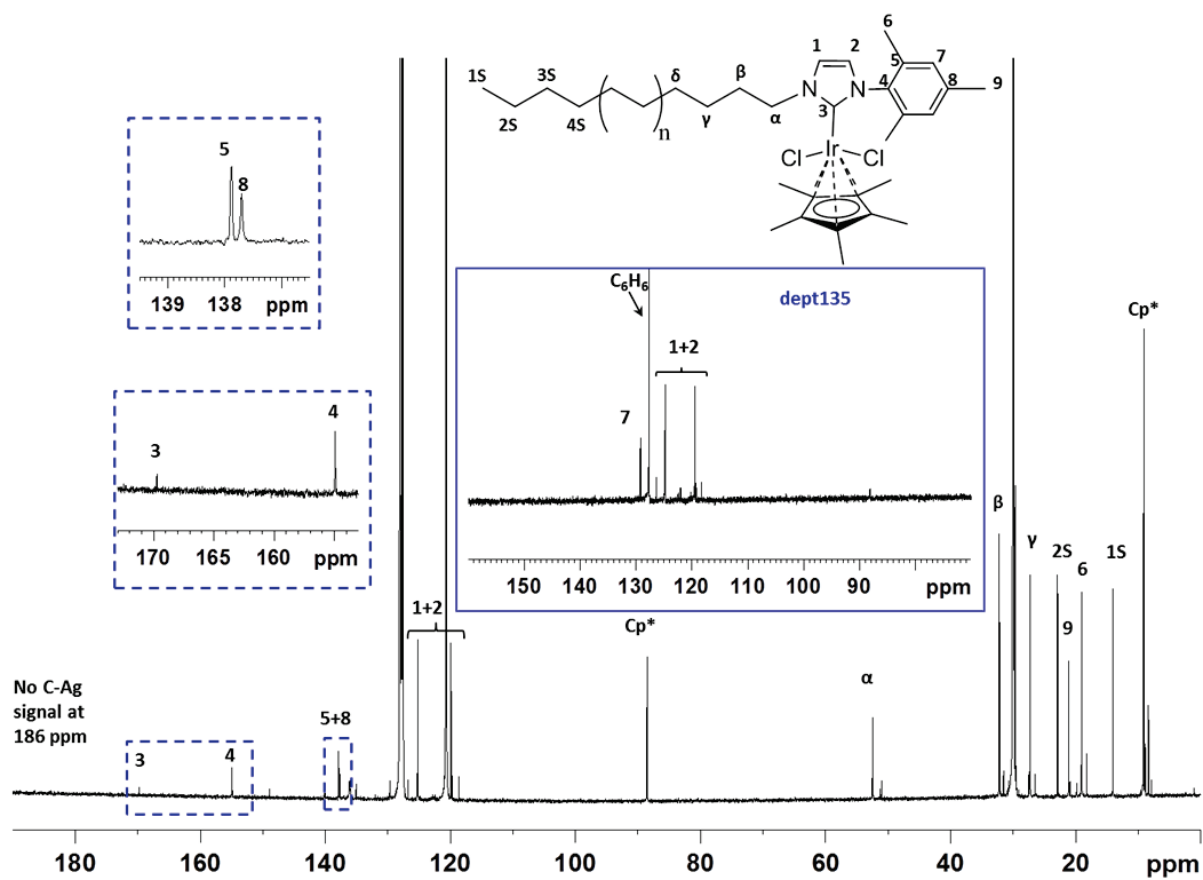
6.7.4.2. H/D exchange with PE-IrCP*Cl

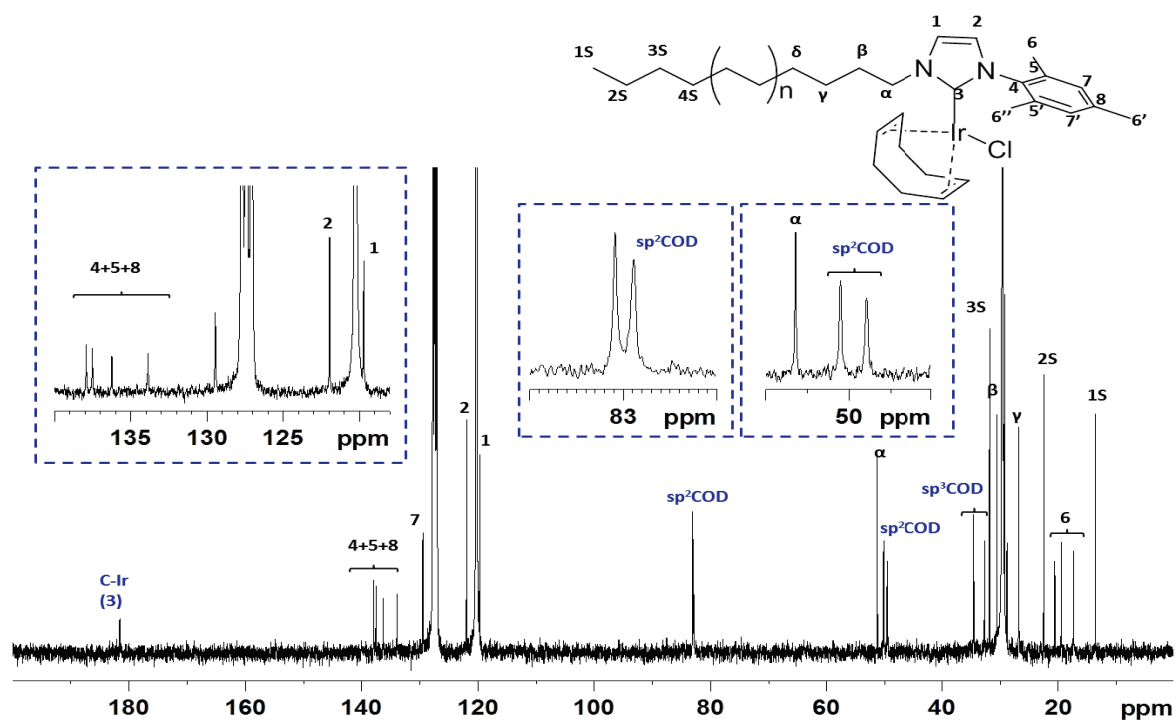
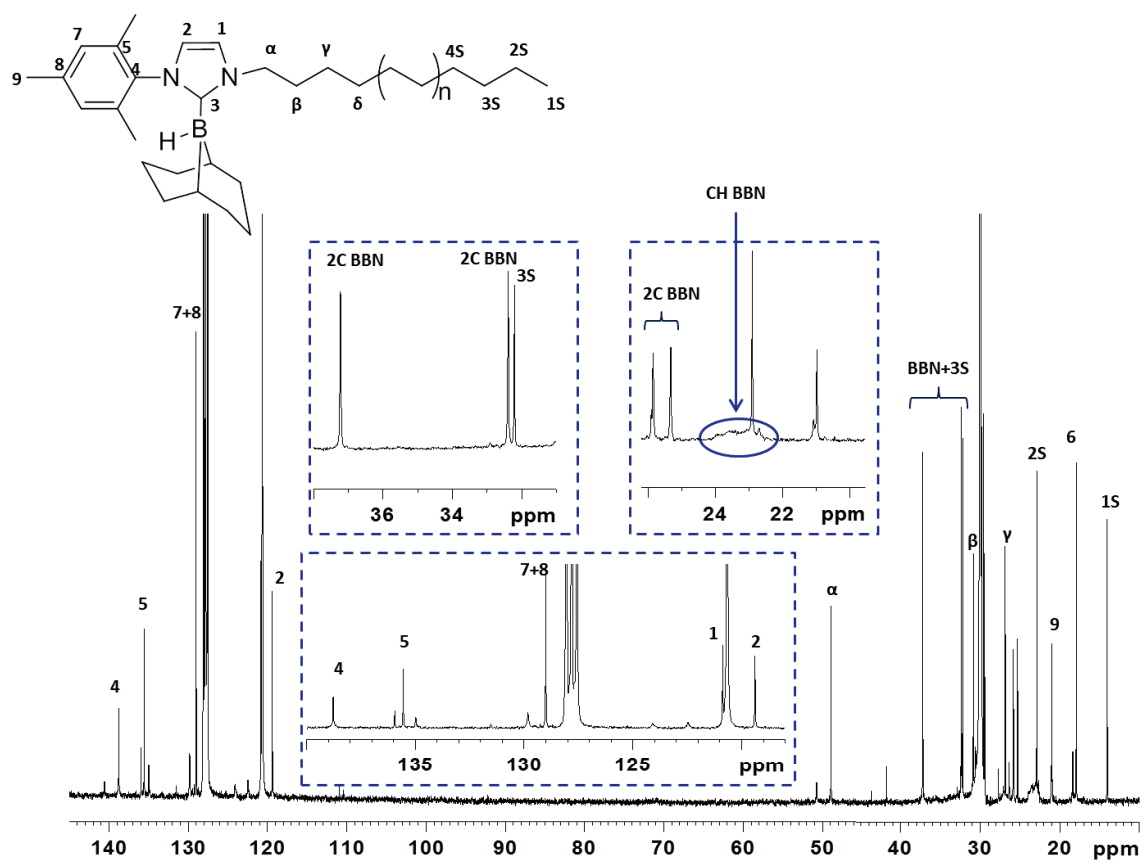
All catalytic tests were performed at 100°C in the toluene/methanol- d_4 mixture. Deuterated methanol (d_4 , 99.5%) and acetophenone were purchased from Sigma-Aldrich and used without further purification. Toluene was purified with an SPS800 Braun solvent purification system. Catalytic activity of $[\text{IrCp}^*(\text{MesImPr})\text{Cl}] \text{OTf}$ was compared with polymer analogue $[\text{PE-IrCp}^*\text{Cl}]\text{OTf}$ with tree different Sub/cat ratio (**R**): 50, 500, 5000. The turnover frequencies were determined by GS/MS. Detailed experimental conditions summarized in Table2

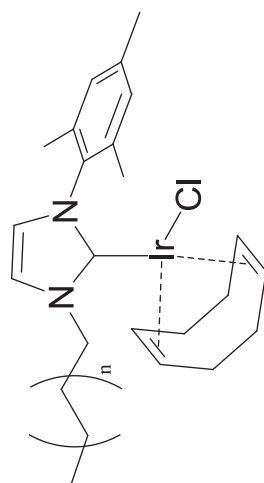
Table2. Experimental conditions for H/D exchange catalysis

R	Acetophenone, mmol	AgOTf mmol	Cat mmol	Toluene mL	CD₃OD mmol
Cat=[IrCp*(MesImPr)Cl]OTf					
50	0.8	3.4 *10⁻²	1.6*10⁻²	0.68	3.5
500	2.8	1.2*10⁻²	5.6 *10⁻³	2.4	12.5
5000	28	1.2*10⁻²	5.6 *10⁻³	24	125
Cat=[PE-IrCp*Cl]OTf					
50	0.28	1.2*10⁻²	5.6 *10⁻³	0.24	3.5
500	2.8	1.2*10⁻²	5.6 *10⁻³	2.4	12.5
5000	28	1.2*10⁻²	5.6 *10⁻³	24	125

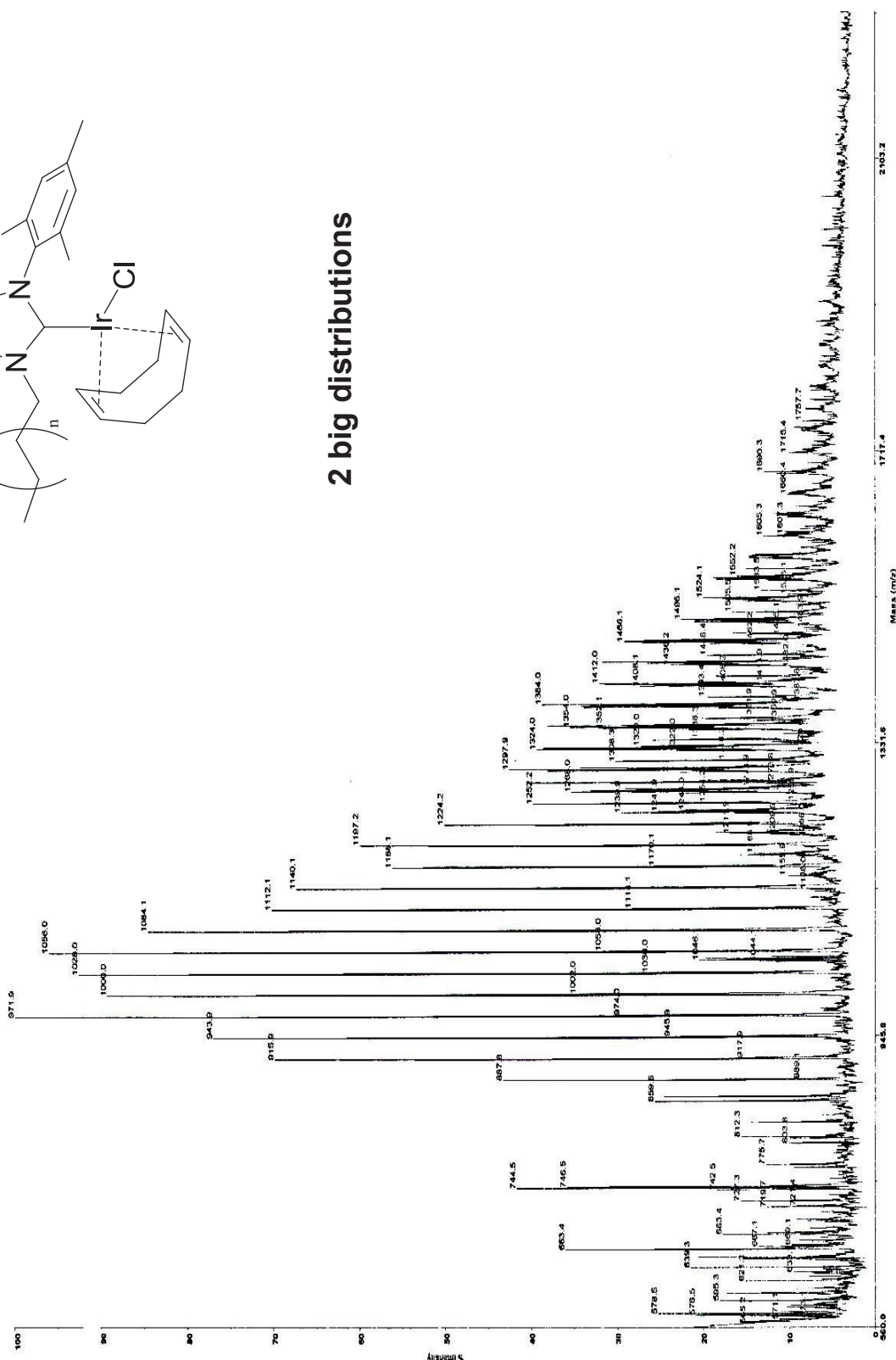
IV-8. Appendix

Figure A1: ^{13}C NMR of PE-IrCp*

Figure A2: ^{13}C NMR of PE-IrCODClFigure A3: ^{13}C NMR of PE-BBN



2 big distributions



Acquired: 12:39:00, April 29, 2014
 RI85 / THAP
 V:\MALDI_2014\CCMP_1404\140429\

Figure A4: MALDI-TOF mass spectrum of PE-IrCODCl

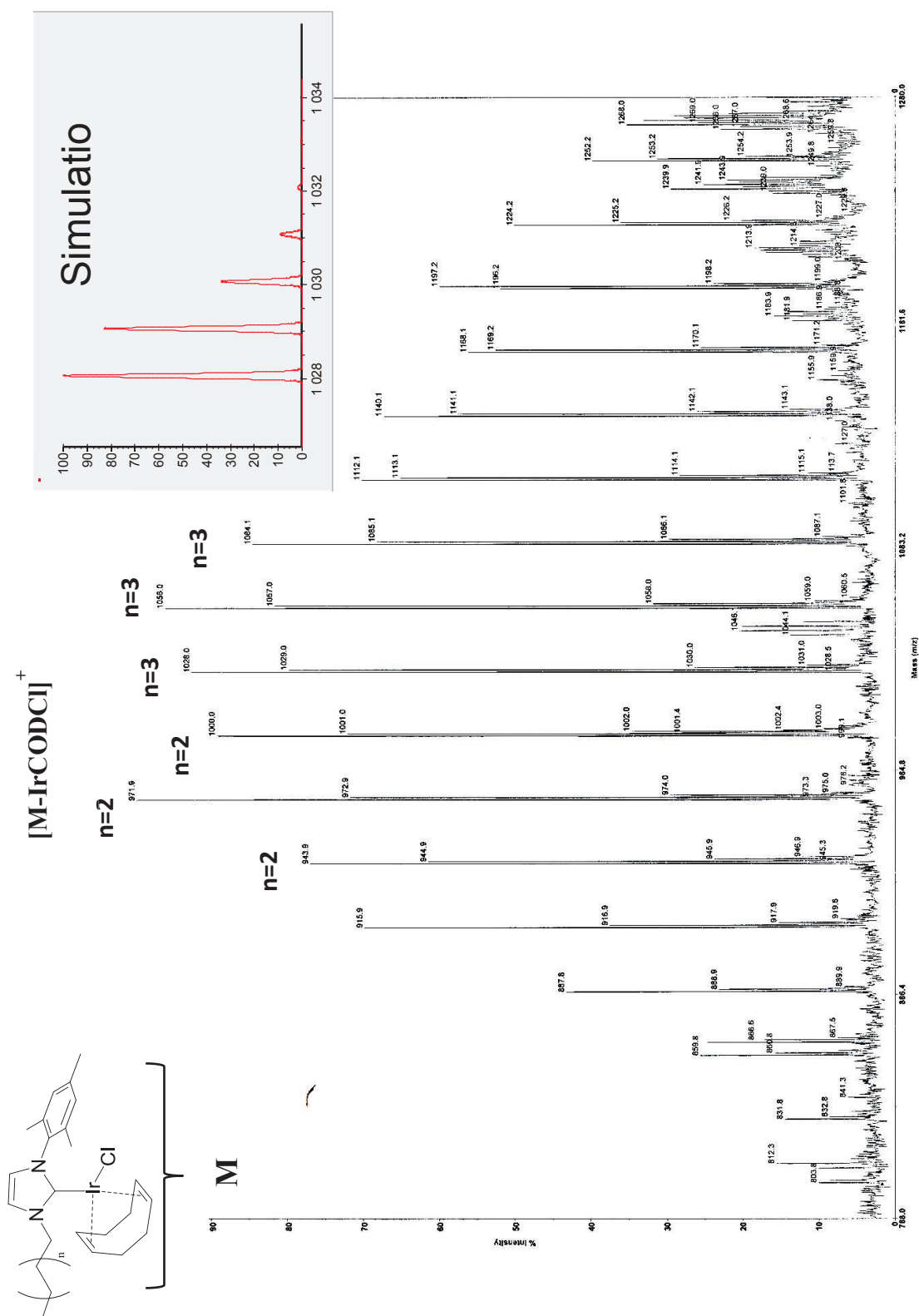


Figure A5: MALDI-TOF mass spectrum of PE-IrCODCl (major population)

RI85 / THAP
V:\10452_0003.dat
Acquired: 12:39:00, April 29,

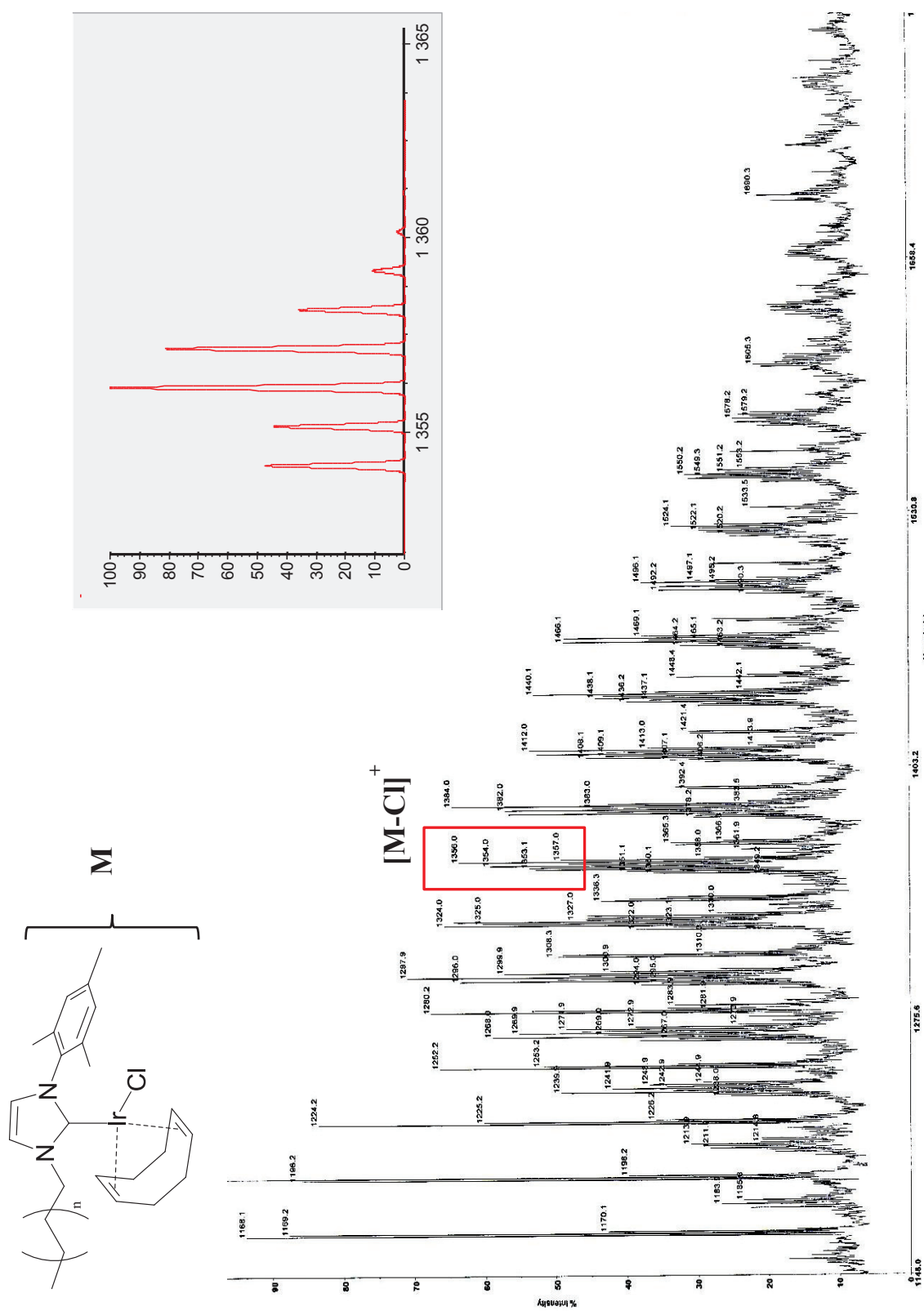
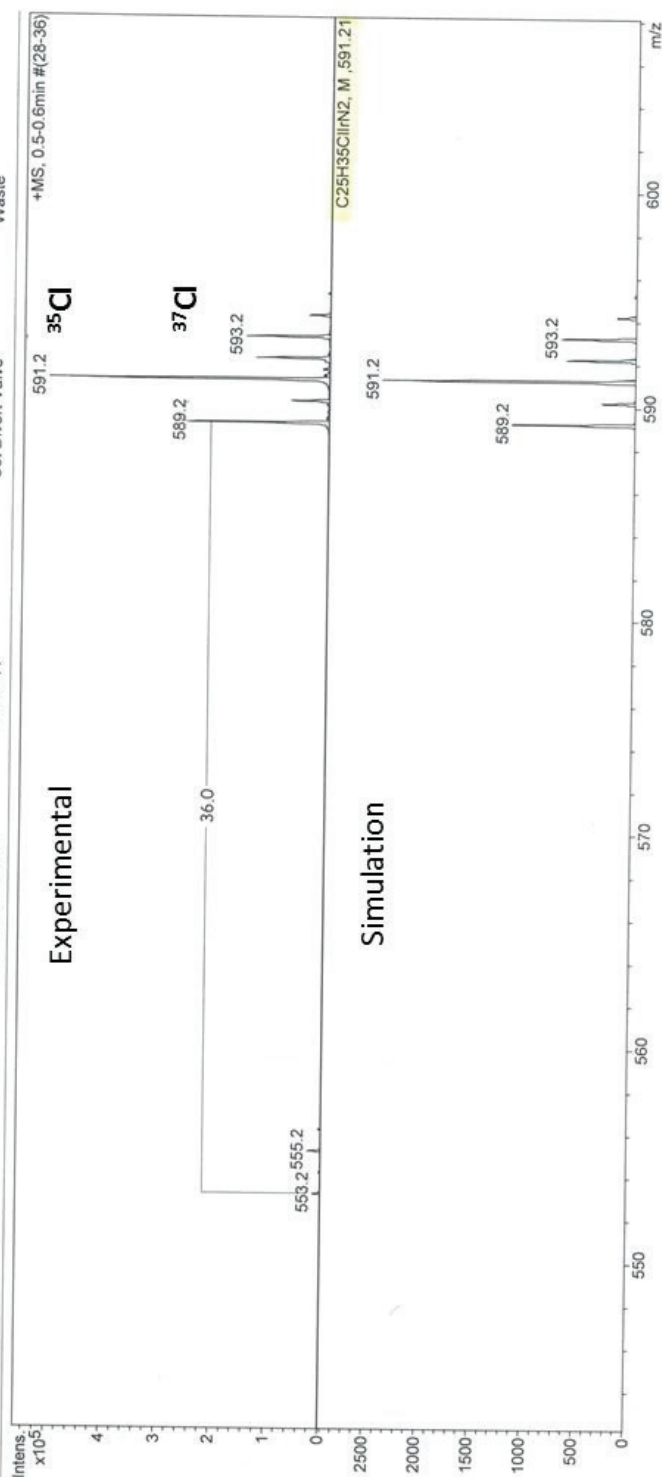


Figure A6: MALDI-TOF mass spectrum of PE-IrCODCl (minor population)

R185 / THAP
 V:\...0452_0003.dat
 Acquired: 12:39:00, April 29, 2014

Display Report

Analysis Info		1/27/2015 10:09:47 AM
Analysis Name	D:\Data\2015\2015_01\QTOF_150126_11_RI_157.d	Acquisition Date
Method	MS_inf_TL_50_1000_2014_wdCollSweep_Pos_CCSM.m	Operator
Sample Name		Instrument
Comment		10231
Acquisition Parameter		
Source Type	ESI	
Focus	Not active	
Scan Begin	50 m/z	
Scan End	2000 m/z	
Ion Polarity	Positive	
Set Capillary	1500 V	
Set End Plate Offset	-500 V	
Set Collision Cell RF	140.0 Vpp	
Set Nebulizer	0.4 Bar	
Set Dry Heater	200 °C	
Set Dry Gas	4.0 l/min	
Set Divert Valve	Waste	

Figure A7: ESI-MS spectrum of [IrCp*(MesImPr)Cl₂]

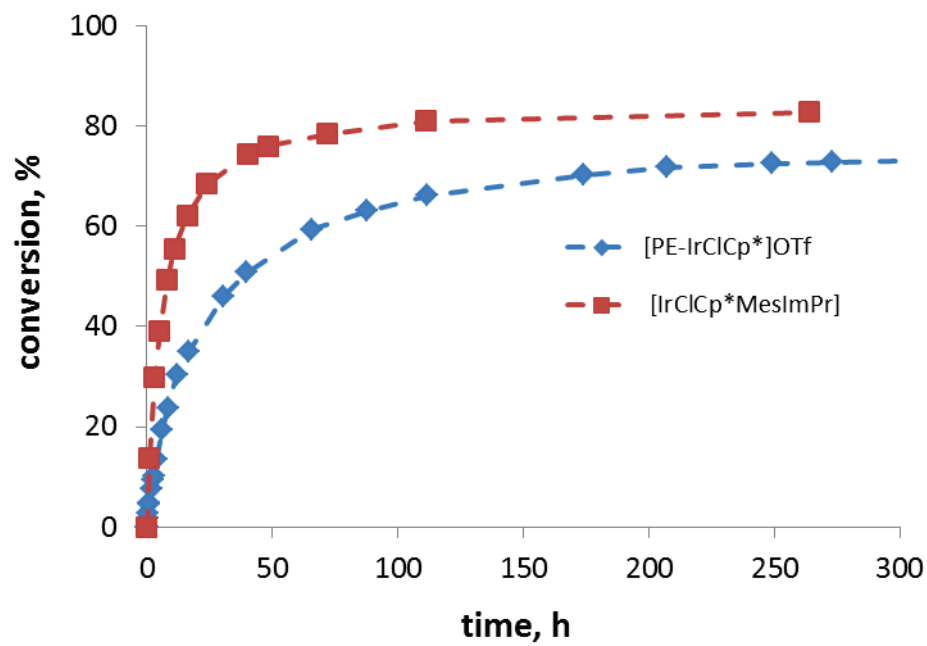
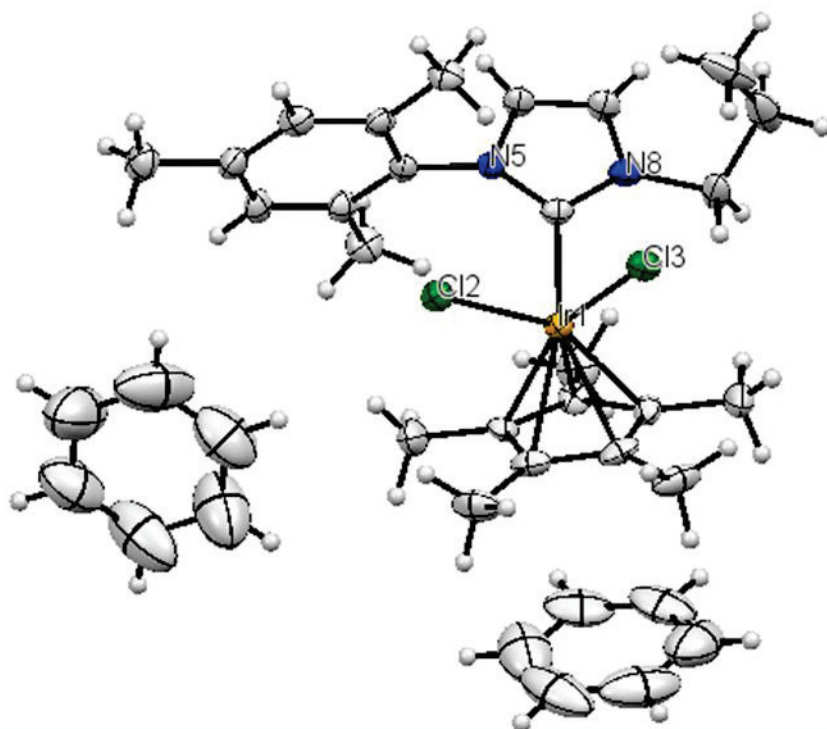


Figure A8. Catalytic activity of [PE-IrCp*Cl]OTf and [IrCp*(MesImPr)Cl]OTf in acetophenone deuteration carried out in toluene at 100 oC with 0.02 mol% cat (R=5000)

**Table A1.** Crystal data structure refinement for [IrCp*(MesImPr)Cl₂]

$C_{25}H_{35}Cl_2IrN_2 \cdot C_6H_6$	$F(000) = 2815.984$
$M_r = 704.78$	$D_x = 1.575 \text{ Mg m}^{-3}$
Monoclinic, $I2/a$	Mo $K\alpha$ radiation, $\lambda = 0.71073 \text{ \AA}$
Hall symbol: $-I 2/a$	Cell parameters from 21283 reflections
$a = 22.9627 (12) \text{ \AA}$	$\theta = 3.9\text{--}29.6^\circ$
$b = 15.9902 (9) \text{ \AA}$	$\mu = 4.69 \text{ mm}^{-1}$
$c = 16.1901 (8) \text{ \AA}$	$T = 100 \text{ K}$
$\beta = 90.838 (4)^\circ$	Plate, yellow
$V = 5944.0 (5) \text{ \AA}^3$	$0.41 \times 0.39 \times 0.08 \text{ mm}$
$Z = 8$	

Data collection

Xcalibur, Atlas, Gemini ultra diffractometer	7888 independent reflections
Radiation source: Enhance (Mo) X-ray Source	6726 reflections with $I > 2.0\sigma(I)$
Graphite monochromator	$R_{\text{int}} = 0.069$
Detector resolution: $10.4685 \text{ pixels mm}^{-1}$	$\theta_{\text{max}} = 29.7^\circ$, $\theta_{\text{min}} = 3.0^\circ$

ω scans	$h = -31 \rightarrow 31$
Absorption correction: analytical <i>CrysAlis PRO</i> , Agilent Technologies, Version 1.171.37.34 (release 22-05-2014 CrysAlis171.NET) (compiled May 22 2014, 16:03:01) Analytical numeric absorption correction using a multifaceted crystal model based on expressions derived by R.C. Clark & J.S. Reid. (Clark, R. C. & Reid, J. S. (1995). <i>Acta Cryst.</i> A51, 887-897) Empirical absorption correction using spherical harmonics, implemented in SCALE3 ABSPACK scaling algorithm.	$k = -22 \rightarrow 20$
$T_{\min} = 0.177$, $T_{\max} = 0.682$	$l = -22 \rightarrow 20$
77968 measured reflections	

Refinement

Refinement on F^2	Primary atom site location: structure-invariant direct methods
Least-squares matrix: full	Hydrogen site location: difference Fourier map
$R[F^2 > 2\sigma(F^2)] = 0.052$	H-atom parameters constrained
$wR(F^2) = 0.153$	Method, part 1, Chebychev polynomial, (Watkin, 1994, Prince, 1982) [weight] = $1.0/[A_0*T_0(x) + A_1*T_1(x) \cdots + A_{n-1}*T_{n-1}(x)]$ where A_i are the Chebychev coefficients listed below and $x = F/F_{\max}$ Method = Robust Weighting (Prince, 1982) $W = [\text{weight}] * [1 - (\Delta F/6*\sigma F)^2]^2$ A_i are: 0.501E+04 0.809E+04 0.530E+04 0.237E+04 655.
$S = 0.94$	$(\Delta/\sigma)_{\max} = 0.003$
7867 reflections	$\Delta\rho_{\max} = 2.45 \text{ e } \text{\AA}^{-3}$
325 parameters	$\Delta\rho_{\min} = -3.64 \text{ e } \text{\AA}^{-3}$
26 restraints	

Symmetry codes: (i) $-x+1/2, y, -z$; (ii) $-x+1/2, y, -z+1$.

Document origin: *publCIF* [Westrip, S. P. (2010). *J. Apply. Cryst.*, **43**, 920-925].

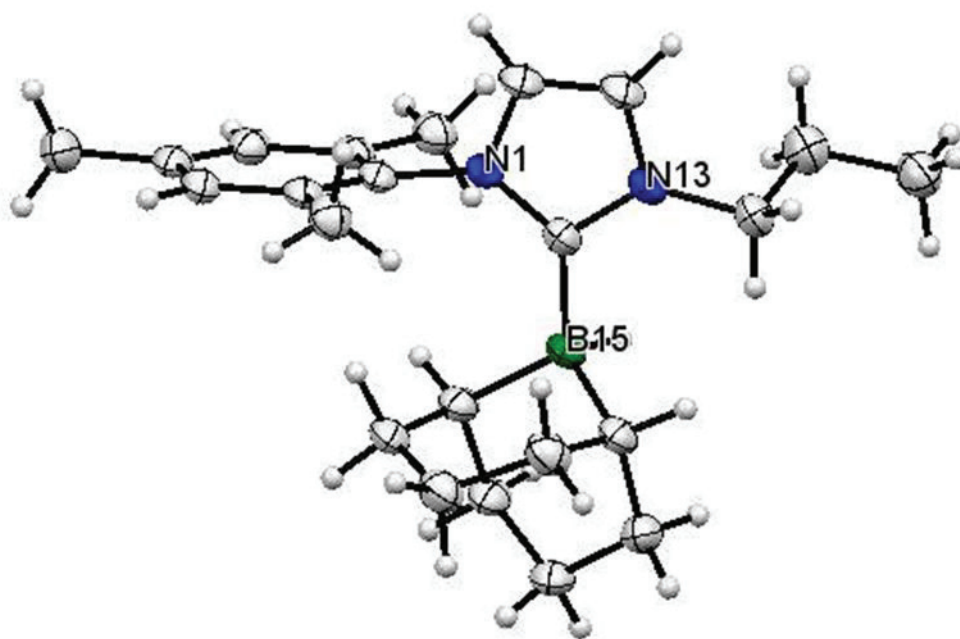


Table A2. Crystal data structure refinement for [MesImPr*BBN]

Crystal data

$C_{23}H_{35}BN_2$	$F(000) = 768$
$M_r = 350.36$	$D_x = 1.151 \text{ Mg m}^{-3}$
Monoclinic, $P2_1/c$	Cu $K\alpha$ radiation, $\lambda = 1.5418 \text{ \AA}$
Hall symbol: -P 2ybc	Cell parameters from 7052 reflections
$a = 12.260 (1) \text{ \AA}$	$\theta = 3.8\text{--}67.1^\circ$
$b = 12.006 (1) \text{ \AA}$	$\mu = 0.49 \text{ mm}^{-1}$
$c = 14.365 (1) \text{ \AA}$	$T = 150 \text{ K}$
$\beta = 107.06 (1)^\circ$	Plate, colorless
$V = 2021.4 (3) \text{ \AA}^3$	$0.54 \times 0.40 \times 0.12 \text{ mm}$
$Z = 4$	

Data collection

Xcalibur, Atlas, Gemini ultra diffractometer	3596 independent reflections
Radiation source: Enhance Ultra (Cu) X-ray Source	2835 reflections with $I > 2.0\sigma(I)$
Mirror monochromator	$R_{\text{int}} = 0.090$
Detector resolution: $10.4678 \text{ pixels mm}^{-1}$	$\theta_{\text{max}} = 68.6^\circ$, $\theta_{\text{min}} = 3.8^\circ$
ω scans	$h = -14 \rightarrow 14$
Absorption correction: analytical <i>CrysAlis PRO</i> , Agilent Technologies, Version 1.171.36.28 (release 01-02-2013 CrysAlis171	$k = -14 \rightarrow 14$

Chapter 4

.NET) (compiled Feb 1 2013,16:14:44) Analytical numeric absorption correction using a multifaceted crystal model based on expressions derived by R.C. Clark & J.S. Reid. (Clark, R. C. & Reid, J. S. (1995). Acta Cryst. A51, 887-897)	
$T_{\min} = 0.846$, $T_{\max} = 0.955$	$l = -17 \rightarrow 17$
28198 measured reflections	

Refinement

Refinement on F^2	Hydrogen site location: difference Fourier map
Least-squares matrix: full	H-atom parameters constrained
$R[F^2 > 2\sigma(F^2)] = 0.056$	Method, part 1, Chebychev polynomial, (Watkin, 1994, Prince, 1982) [weight] = $1.0/[A_0*T_0(x) + A_1*T_1(x) \cdots + A_{n-1}]*T_{n-1}(x)]$ where A_i are the Chebychev coefficients listed below and $x = F/F_{\max}$ Method = Robust Weighting (Prince, 1982) $W = [\text{weight}] * [1 -$ $(\Delta F/6*\sigma F)^2]^2$ A_i are: 0.101E + 04 0.155E + 04 809. 210.
$wR(F^2) = 0.136$	$(\Delta/\sigma)_{\max} = 0.0002$
$S = 1.02$	$\Delta_{\max} = 0.30 \text{ e } \text{\AA}^{-3}$
3577 reflections	$\Delta_{\min} = -0.26 \text{ e } \text{\AA}^{-3}$
236 parameters	Extinction correction: Larson (1970), Equation 22
0 restraints	Extinction coefficient: 41 (6)
Primary atom site location: structure-invariant direct methods	

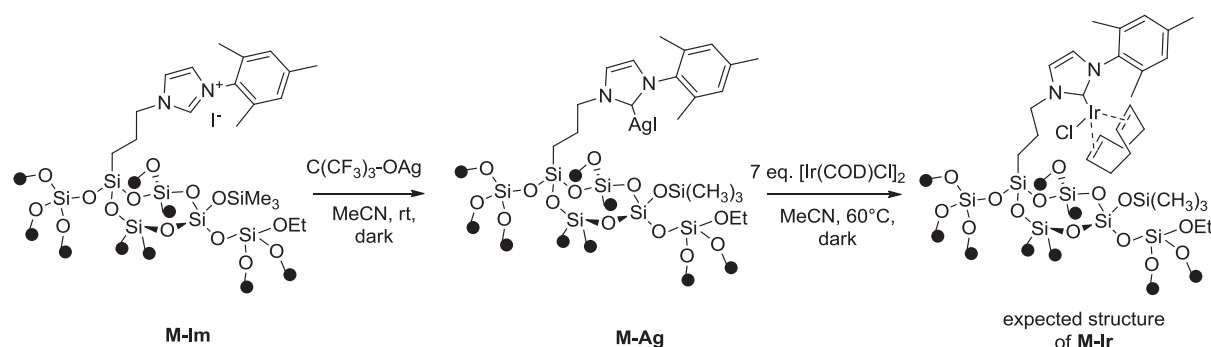
Conclusions and Perspectives

Conclusions and Perspectives

The main objective of this PhD project was to develop a Ir-NHC based heterogeneous catalyst for alkene hydrogenation reactions. The development of such systems in which Ir(I) species can be isolated onto silica surfaces could be of interest to prevent bimolecular processes leading to deactivation of Ir complexes in solution.

The preparation of the catalyst was achieved following a two-step approach. The first step is the preparation of an hybrid mesostructured silica containing regularly distributed L-type ligands via a sol-gel process using a templating route. The surface L-ligand of the parent material is further converted into the targeted supported organometallic complex by Surface OrganoMetallic Chemistry (SOMC).

The final catalyst is obtained through the in-situ formation of a surface Ag-NHC site and its further transformation into an Ir-NHC complex *via* a trans-metallation process. The general synthetic pathway is depicted in the following scheme.



Scheme 1. Preparation of heterogeneous M-Ir catalyst

The elemental analysis of **M-Ir** showed the presence of 2.57% of Ir. The as-obtained material was fully characterized by different advanced solid state NMR techniques, among which ^{13}C and ^{29}Si 2D DNP NMR. All our experimental results indicate the presence of Ir-NHC sites with no COD coordinated to Iridium (only 8% of COD with respect to Ir loading) and the absence of Ir NPs. 2D ^{29}Si - ^1H DNP NMR data also suggested interactions between the Ir surface sites and the silica surface. Based on these observations, we therefore propose the presence of low valent Ir-NHC sites stabilized by Si-O-Si units from silica as shown in the following figure.

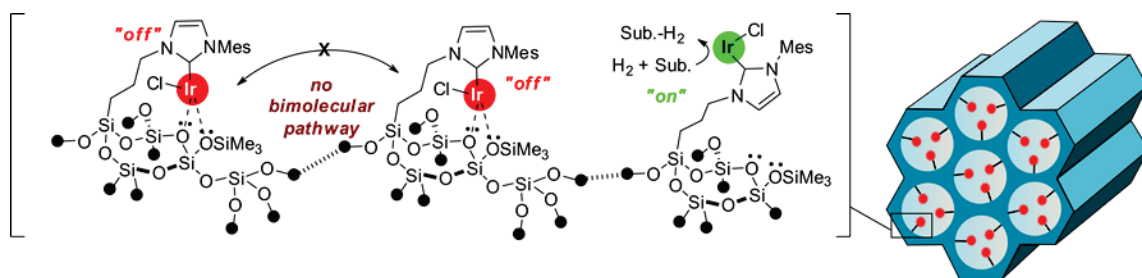


Figure 1. Defined structure of **M-Ir**

The catalytic performance of **M-Ir** and its molecular counterparts, the neutral $[\text{IrCl}(\text{COD})(\text{MesImPr})]$ and cationic $[\text{Ir}(\text{COD})(\text{MesImPr})]\text{BF}_4$, were tested in trans-stilbene hydrogenation under mild conditions (0.1 mol% of cat, 3 bars of H_2 , $T=40^\circ\text{C}$). Surprisingly **M-Ir** showed a 50 times superior activity in comparison with the neutral $[\text{IrCl}(\text{MesImPr})(\text{COD})]$ complex and 15-20 times superior activity than cationic complex $[\text{Ir}(\text{MesImPr})(\text{COD})]\text{BF}_4$. Moreover, using $[\text{IrCl}(\text{MesImPr})(\text{COD})]$ under homogeneous conditions, the hydrogenation reaction fail to reach full conversion after more than 80 days. Cationic iridium species $[\text{Ir}(\text{COD})(\text{MesImPr})]\text{BF}_4$ worked faster than the neutral analogue, but even then the reaction was not complete after 60 days. At the reverse, using **M-Ir**, full conversion was observed after 18 h (Fig3).

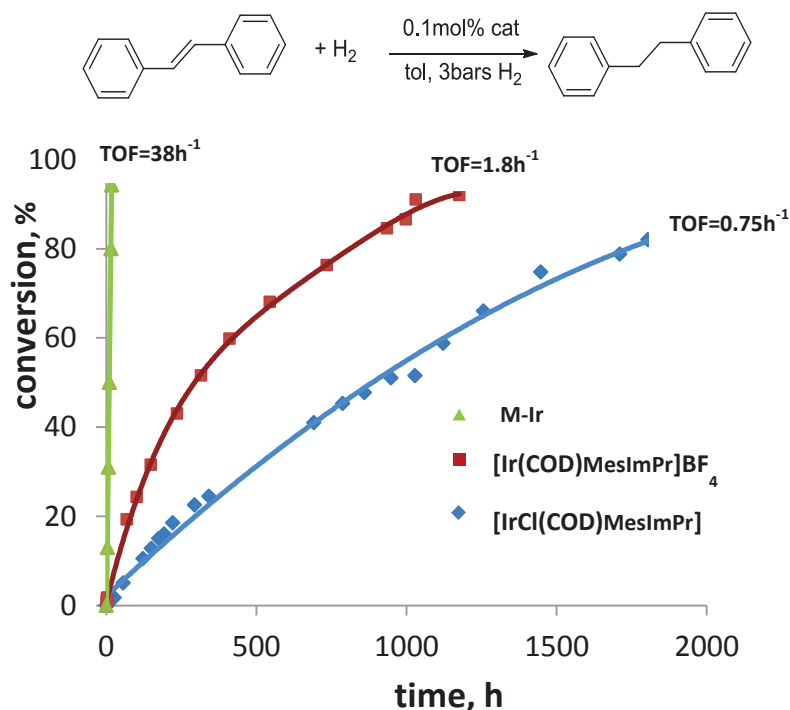


Figure 3. Catalytic performance of neutral $[\text{IrCl}(\text{COD})\text{MesImPr}]$, cationic $[\text{Ir}(\text{COD})(\text{MesImPr})]\text{BF}_4$ and **M-Ir** material in trans-stilbene hydrogenation. The hydrogenation experiments were carried out in toluene at 40°C under 3 bar of H_2 (0.1 mol% of Ir).

Conclusions and Perspectives

Moreover, the **M-Ir** catalyst was found to be very productive, reaching more than 8000 as TON while both homogeneous catalysts hardly reached the value of 1000 as TON. Unfortunately, we were not able to determine the maximum TON for **M-Ir** due to the side poisoning of Ir active sites by trace impurities present in the large quantities of solvent and substrate required for this test. The increase of productivity of **M-Ir** with respect to that of molecular analogues together with the linear profile of hydrogenation suggests the absence of bimolecular deactivation processes in the supported catalyst. Finally, no leaching of Ir was detected in the reaction supernatants by ICP measurements. However, a detailed study of **M-Ir** stability showed that the catalyst undergoes degradation under H₂ pressure in the absence of substrate *via* Ir-NHC bond cleavage with formation of small Ir NPs. As perspectives, the modification of the Ir coordination sphere with for example the replacement of the mono-NHC by a bis-NHC ligand (Fig2, a) could be an option to strengthen the metal-ligand bonding.¹⁵¹ It looks also possible to increase the hydrogenation rate of M-Ir by replacement of Cl with donating ligand like phosphine (Fig2, b). The donating group could facilitate the hydride transfer that is known to be a limiting step in hydrogenation mechanism¹⁵²

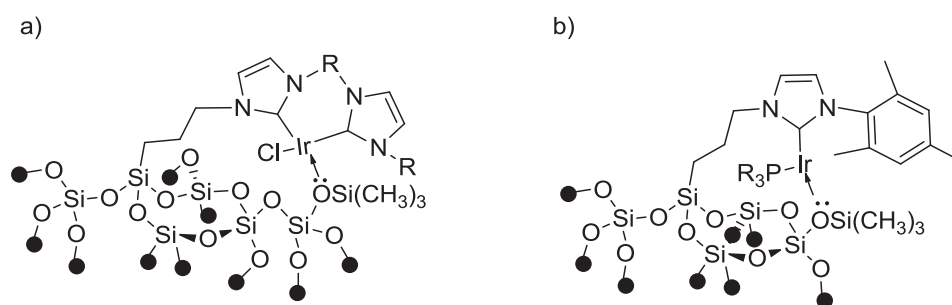


Figure2.

We also studied the catalytic performances of **M-Ir** and neutral [IrCl(MesImPr)(COD)] in the diastereoselective terpinen-4-ol hydrogenation. Despite the low activity of **M-Ir** in terpinen-4-ol hydrogenation (reaching only 35% conversion in 500h.), a high degree of diastereoselectivity (95%) towards the directed product was detected. This level of diastereoselectivity was constant during the hydrogenation process. The homogeneous [IrCl(COD)(MesImPr)] complex was found to be two times less active and showed a slight decrease of diastereoselectivity from 100% to 92%.

¹⁵¹ Sanz, S. ; Azua, A. ; Peris, E. *Organometallics* **2010**, 29, 275-277

¹⁵² Bennie, L. S.; Fraser, C. J.; Irvine, S.; Kerr, W. J.; Andersson, S.; Nilsson, G. N., *Chem. Commun.* **2011**, 47 (42), 11653-11655.

A temperature increase from 40 °C till 80 °C resulted in a 32 fold increase of the hydrogenation rate for **M** $\text{TOF}=38\text{h}^{-1}$ 1 fold increase $\text{TOF}=1.8\text{h}^{-1}$ $[\text{IrCl}(\text{COD})(\text{MesImPr})]$. As expected, this temperature increase resulted in a selectivity decrease. A diastereomer $\text{TOF}=0.75\text{h}^{-1}$ of 90% was obtained with **M-Ir** at 80 °C and this selectivity remains stable during the overall catalytic process. In contrast, with $[\text{IrCl}(\text{COD})(\text{MesImPr})]$, the selectivity dropped dramatically from 100% at 0.2% of conversion to 60% at 80% of conversion. This decrease strongly suggests the formation of Ir NPs, which are known to possess no directing effects and are thus lowering the overall diastereoselectivity (Fig.4).

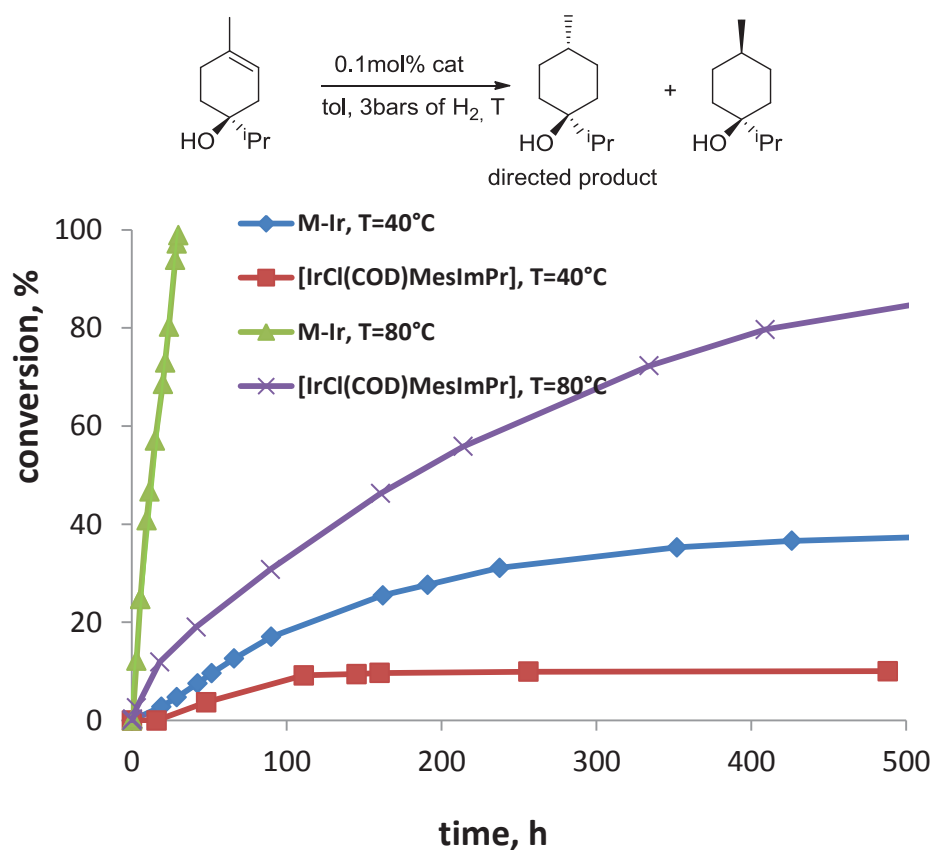


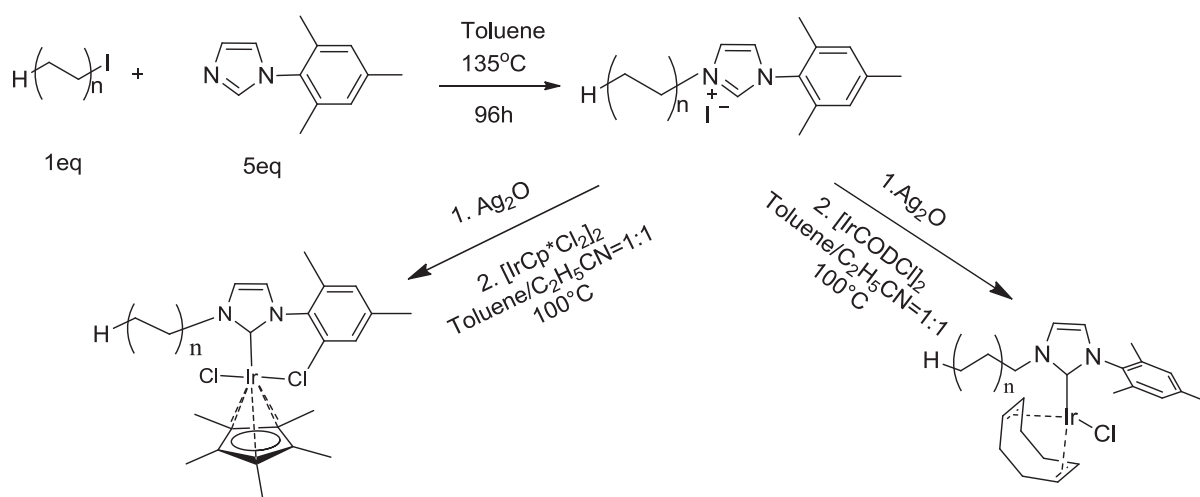
Figure4. Catalytic performance $[\text{IrCl}(\text{COD})\text{MesImPr}]$ and **M-Ir** material in diastereoselective terpinen-4-ol hydrogenation.. The hydrogenation experiments were carried out in toluene at 40 °C and 80 °C under 3 bar of H_2

The catalytic behavior of **M-Ir** and that of neutral molecular analogue were also tested with other functional substrates (styrenes with various substituents, stilbene and limonene). In all cases, **M-Ir** was superior over the homogeneous catalysts. Both catalysts were however able to selectively hydrogenate $\text{C}=\text{C}$ bonds, leaving functional group intact.

Conclusions and Perspectives

We believe that the significant enhancement of **M-Ir** catalytic activity could be explained by two main reasons: 1) the isolation of the Ir species onto the support which resulted in the suppression of bimolecular deactivation processes; 2) the absence of the COD ligand which allows **M-Ir** to be rapidly catalytically active, while the molecular complexes requires an initiation period (COD decooordination) before any activity in hydrogenation.

We also developed in this project a polymer supported Ir-NHC complexe as potential alternative to silica supported homologue. The synthetic method applied to the transformation of the hybrid silica support (containing iodopropyl-groups) to the final silica supported Ir-NHC catalyst was successfully implemented to a telechelic polyethylene containing iodide terminal unit (Scheme2). The as obtained PE-IrCODCl complex was however found to be a poor catalyst for trans-stilbene hydrogenation at both 40°C and 80°C. At elevated temperature, formation of black deposit was observed, as a result of complex decomposition.



Scheme2. Modification of preparation PE-IrCODCl and PE-IrCp*Cl₂

Despite the low catalytic activity of PE-IrCODCl, its Ir(III) analogue, PE-IrCp*Cl₂ showed high catalytic activity in the acetophenone deuteration at 100°C. the polymer supported PE-IrCp*Cl₂ was found to be stable at that temperature and due to its thermomorphic properties, it was successfully recycled 3 times without activity loss. To our knowledge, only very few just a few examples of highly active and recyclable thermomorphic catalysts were reported in the litterature till now. As perspectives, our methodology could be used for the preparation of other thermomorphic NHC-based catalysts.

Conclusions and Perspectives

An other potential research project could be the development of supported Ir-NHC complexes for arene borylation reactions as alternative to supported Ir-phosphine complexes. As an example, Sawamura et al. reported the outstanding catalytic activity of silica-supported iridium phosphine system over its homogeneous analogue in arene borylation (Figure4, structure a). In their publications, the preparation of a supported Ir(COD)(Phosphine)OMe bonded to a silica gel through the compact phosphine ligand (SMAP-silica) was described.¹⁵³ In this particular case, the heterogeneous catalyst was active in ortho borylation of a variety of aromatic substrates at 25°C with 0.005-0.51mol% of catalyst loading while the corresponding homogeneous catalysts afforded only trace conversion.¹⁵⁴ The explanation to this remarkable catalytic performance was not established. From this point of view, it would be interesting to develop supported Ir-NHC homologues with very comparable coordination sphere (-OMe ligand, NHC ligand instead of phosphine homologue) using a flexible or rigid tether (to favor or prevent COD coordinated to the Ir centre) and see how it compared with literature precedents (Figure4).

¹⁵³ (a) Hamasaka, G.; Ochida, A.; Hara, K.; Sawamura, M. *Angew. Chem. Int. Ed.*, **2007**, 46, 5381–5383.

(b) Hamasaka, G.; Kawamorita, S.; Ochida, A.; Akiyama, R.; Hara, K.; Fukuoka, A.; Asakura, K.; Chun, W. J.; Ohmiya, H.; Sawamura, M., *Organometallics* **2008**, 27, 6495–6506.

¹⁵⁴ Kawamorita, S. ; Ohmiya, H. ; Hara, K. ; Fukuoka, A.; Sawamura, M., *J.Am.Chem.Soc.* **2009**, 131(14), 5058-5059.

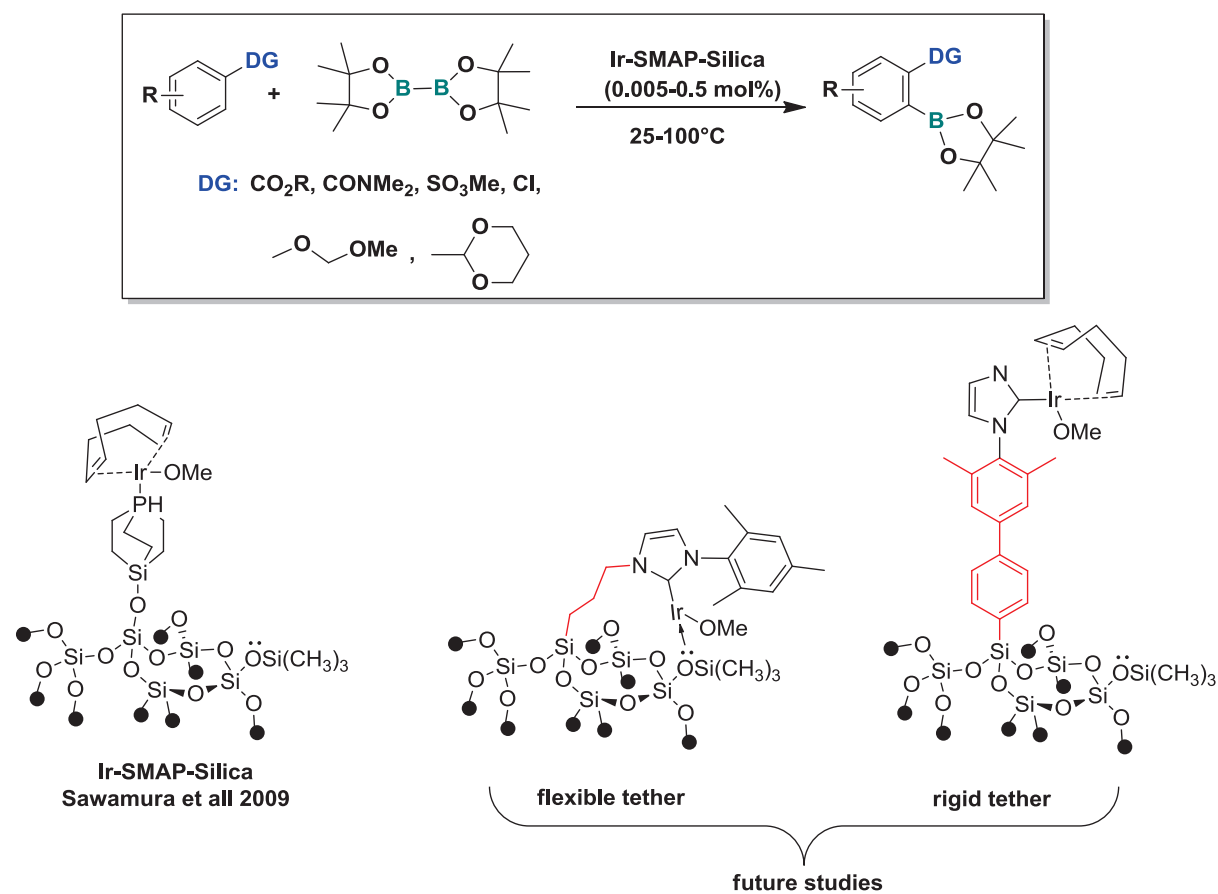


Figure 4. Borylation of arenes catalyzed by silica SMAP-Ir system

Abstract

Alkene hydrogenation is a key in many bulk and fine chemicals production processes. Major efforts were therefore directed towards the preparation of ever more productive and selective catalysts. Among the large number of homogeneous and heterogeneous catalysts, promising Iridium (I) organometallic complexes were prepared since the discovery of the well-known Crabtree's catalyst, $[\text{Ir}(\text{COD})(\text{py})(\text{PCy}_3)]\text{BF}_4$, to address selectivity issues in homogeneous asymmetric hydrogenation or hydrogenation of highly hindered tetrasubstituted olefins. However, the industrial use of Ir organometallic complexes as catalysts is limited by their fast decomposition leading to the formation of highly stable and inactive polynuclear iridium hydride-bridged complexes. The goal of this PhD project was to elaborate supported Ir(I)-NHC catalytic material to prevent such bimolecular deactivation processes. The targeted supported Ir complexes were based on hybrid organic-inorganic material containing regularly distributed imidazolium units along the pore-channels of the silica framework. Beside the Ir-site isolation on the silica support, this catalytic system was also expected to ease catalyst recovery at the end of the hydrogenation. The preparation of the final systems relies on the preparation of supported silver carbenes first, and further transmetallation with an Ir-precursor, namely $[\text{Ir}(\text{COD})\text{Cl}]_2$. The materials were characterized by several techniques as for example advanced solid state NMR using Dynamic Nuclear Polarization to gain insight into the molecular structure of the Ir surface sites. Catalytic performances of the supported Ir-NHC complexes were tested in alkene hydrogenation and compared to those of homogeneous homologues. Several different substrates and reaction conditions were tested. The results showed that the supported catalyst was much more stable and 50 times more active in term of rate and productivity. A polymer supported Ir-complex was also elaborated using a telechelic polyethylene iodide as support. The polymeric materials were fully characterized by NMR and MALDI-TOF experiments and their catalytic performances were compared to those of molecular analogues and those of silica supported systems.

Résumé

La réaction d'hydrogénation des alcènes est une réaction clé dans de nombreux procédés industriels permettant la production de produits de commodité et de spécialité. D'importants efforts de recherche ont donc été réalisés pour développer des systèmes catalytiques de plus en plus productifs et sélectifs. Parmi les nombreux catalyseurs homogènes et hétérogènes développés à ce jour, les complexes organométalliques d'Iridium(I), très prometteurs, ont été préparés depuis la découverte du catalyseur de Crabtree, $[\text{Ir}(\text{COD})(\text{py})(\text{PCy}_3)]\text{BF}_4$, pour répondre à des problèmes de sélectivité dans l'hydrogénation asymétrique ou celle d'oléfines tétrasubstituées fortement encombrées en conditions homogènes. Cependant, l'utilisation industrielle de ce complexe organométallique d'Ir (I) est limité par sa décomposition rapide en solution, qui conduit à la formation de complexes polynucléaires (hydrures pontés d'Iridium) très stables et inactifs en catalyse. Le but de ce travail de thèse a été de développer des matériaux catalytiques contenant des complexes Ir(NHC) isolés à la surface d'une silice contenant des fonctionnalités imidazolium parfaitement distribuées le long de ses canaux poreux. L'isolement des unités Ir(I) sur le support de silice devrait permettre d'empêcher les processus bimoléculaires de désactivation et faciliter la récupération du catalyseur. La préparation des matériaux catalytiques cible se fait grâce à la transformation des unités imidazolium contenues dans le matériau de départ en carbenes d'argent N-hétérocycliques, qui sont ensuite transmétaillés en carbènes d'iridium avec le complexe $[\text{Ir}(\text{COD})\text{Cl}]_2$. Les matériaux obtenus ont été caractérisés par diverses techniques, notamment une technique de RMN très avancée : la RMN de l'état solide utilisant la polarisation nucléaire dynamique. Ceci a permis de mieux comprendre la structure moléculaire des sites de surface iridiés. Les performances catalytiques des complexes Ir-NHC supportés ont été testées dans réaction d'hydrogénation des alcènes et comparées à celles de leurs homologues homogènes. Divers substrats oléfiniques et différentes conditions de réaction ont été testées. Les résultats montrent que le catalyseur supporté est beaucoup plus stable et 50 fois plus actif en terme de vitesse et de productivité. Cette approche a été étendue au développement de catalyseurs d'iridium supportés sur polymère. Le support choisi a été un polyéthylène téléchélique contenant des fonctionnalités iodées terminales. Le solide obtenu après incorporation de l'iridium a été caractérisé par RMN et spectrométrie de masse (MALDI-TOF). Les performances catalytique de ce nouveau système ont été elles aussi comparées à celles de complexes homologues en solution.